Energy-based modelling and control of electric power systems with guaranteed stability properties

Daniele Zonetti

NNT : 2016SACLS118

THÈSE DE DOCTORAT DE
L'UNIVERSITÉ PARIS-SACLAY
PRÉPARÉE À L'UNIVERSITÉ PARIS-SUD

ÉCOLE DOCTORALE N°580
Sciences et Technologies de l'Information et de la Communication (STIC)
Laboratoire des Signaux et Systèmes

Spécialité de doctorat : Automatique

Par

Daniele ZONETTI

Modélisation et commande de systèmes électriques de puissance avec propriétés de stabilité

(Energy-based modeling and control of electric power systems with guaranteed stability properties)

Thèse présentée et soutenue à Gif-sur-Yvette, le 15 Avril 2016 :

Directeur de thèse :	Dr. Romeo ORTEGA	Directeur de recherche	CNRS & L2S
Co-directeur de thèse :	Dr. Abdelkrim BENCHAIB	Ingénieur de recherche	ALSTOM
Président du jury:	Dr. Françoise LAMNABHI-LAGARRIGUE	Directeur de recherche	CNRS & L2S
Rapporteur:	Prof. Florian DÖRFLER	Professeur	ETH Zurich
Rapporteur:	Prof. Claudio DE PERSIS	Professeur	Groningen University
Examinateur:	Dr. Valentin COSTAN	Ingénieur de recherche	EDF

Grazie

One day I will find the right words and will be simple.
(Jack Kerouac)

This dissertation is the result of more than three years work as a PhD student at the Laboratoire des Signaux et Systèmes, under the supervision of Romeo Ortega. First of all, I would like to thank him for the patient guidance and kind advice he has provided throughout my time as his student and for supporting me in the many difficulties I encountered on the path. It was a real privilege to work with someone who share not only his exceptional scientific knowledge, but also his extraordinary human qualities. Thanks to him, I had also the opportunity to meet several researchers during these years, both in the field of control theory and electric power systems, which all had a great impact on my work. I must express then my gratitude to my co–supervisor, Abdelkrim Benchaib, for the constructive suggestions and his full support when I was lost in simulations. A big thanks goes to Johannes Schiffer, for the long emails and Skype sessions discussing on power system and control, maths and physics, theory and application, as well as the long chats on german and italian football. And of course for hosting me during my punctual visits in Berlin. I spent always an amazing time there. Thank you. I also would like to express my gratitude to other researchers that I had the chance to collaborate with, during these years: Aleksandar Stankovic, Iqbal Husain, Arjan van Der Schaft and Jacquelien Scherpen, which all provided major contributions and feedback to my work. I am sincerely grateful to all members of the jury for having accepted to participate in my PhD defense. You have honored me with your presence. I extend my sincere thanks to all members of the Laboratoire des Signaux et Systèmes and all those who contributed directly or indirectly to the dissertation.

Grazie a tutti loro che ci sono stati, per poco o per tanto, in questo lungo viaggio durato tre anni. Grazie a tutte le colocs che hanno condiviso un pezzo di casa in questi anni. Grazie a Giovanni e Nicoló, per le interminabili pause al lab, milioni di caffé, i pranzi insalsati alla francese e le discussioni off–topic sulla *nonlinearitá* del nostro percorso. Grazie a Alice e Marco, per essere finalmente tornati a Parigi ed essere le persone con le quali poter condividere tutto, senza alcun filtro. Parigi o Roma che sia, voi siete sempre lì. Grazie ad Ale, perché resiste con me in questa città, dopo tempo immemore, trasmettendomi la stessa energia di sempre. Gracias a Bob para "estar siempre" aunque viva lejos de Parìs. Siempre quedarà tiempo para hacer planes juntos.

Un grazie infinito, con il cuore, con amore, a Daniela, che mi ha supportato, sopportato, ascoltato ed incoraggiato e mi è stata vicino anche quando mi sono trovato in difficoltà. Non è sempre facile comunicare quanto una persona sia importante, nelle proprie scelte e nel proprio percorso, ma c'è tanto di lei nei piccoli e grandi passi che ho fatto in questi tre anni.

Non credo esista un ringraziamento sufficiente, né parole con cui riesca a spiegare quanto sia grato a mio fratello Simone, a mio padre ed a mia madre per quanto hanno fatto e stanno facendo ancora per me. Per il loro costante sostegno durante questi tre anni e per avermi insegnato che qualsiasi cammino intrapreso è quello giusto, se lo si persegue con passione. Spero che un giorno riesca a trovare parole semplici per esprimere questo sentimento di gratitudine. Che possa essere contenuto in un semplice *grazie*.

Daniele

Contents

List of Figures

List of Tables

Résumé

Introduction

Durant ces dernières années et pour des raisons multiples, nous avons assisté à une véritable révolution dans le monde des systèmes électriques de puissance. Tout d'abord, nous avons pu constater une croissante demande d'énergie liée à la migration de populations des zones rurales vers des centres urbaines à haute densité de population. Ce qui laisse présager, que la demande d'énergie est donc supposée augmenter d'environ le 36% d'ici 2035 [81]. D'autre part, la plus part de la production d'énergie actuelle se base sur l'exploitation des combustibles fossiles, par rapport auxquels deux problèmes fondamentales se posent. Premièrement, il est bien reconnu que l'utilisation massive de ces ressources est un facteur clé intervenant dans les changements climatiques, ceci étant liés aux émissions de dioxyde de carbone (CO_2) qui se produisent avec la combustion [107, 23]. Deuxièmement, l'allure d'utilisation des combustibles fossiles est tel que les réserves actuelles ne seront pas suffisantes pour répondre à la demande d'ici cent ans [107, 47].

À partir de ces considérations, plusieurs économies nationales ont démarré des politiques énergétiques alternatives durant les quinze dernières années, en introduisant dans leur mix énergétique les énergie renouvelables, tels que le solaire, l'éolien et le géothermique, en accord avec le Protocole de Kyoto, signé en 1997 [38, 25]. Par conséquent, on a remarqué une très forte intégration de sources d'énergie renouvelables dans l'infrastructure actuelle des systèmes électriques de puissance. Ces changements, bien évidemment, appellent pour une réflexion sur l'architecture globale des systèmes de production, distribution et utilisation de l'énergie, ainsi que leur modes de fonctionnement. D'un point de vue théorique, une première considération est que des architectures totalement différentes pourraient constituer la meilleure option pour une nouvelle infrastructure des systèmes de puissance, basée uniquement sur la production d'énergie renouvelable. Toutefois, le remplacement intégral de l'infrastructure existante avec un architecture fondée exclusivement sur les énergies renouvelables aurait un coût qui dépasserait largement les avantages inhérents à la nouvelle architecture. Le problème de la conception de nouvelles architectures pour les systèmes électriques modernes devrait donc être formulé de manière progressive: *comment adapter l'infrastructure existante pour une meilleure intégration des énergies renouvelables?*

L'architecture électrique traditionnelle, qui se base sur la génération d'énergie utilisant des générateurs synchrones, implique une claire séparation entre le sous–systèmes de génération et de distribution, ceux–ci opérants à différents niveaux de tension [96, 7]. En effet, la plus part des unités de génération – qui se basent sur des combustibles fossiles et qui sont typiquement de grandes dimensions – nécessitent un mode d'opération en haute tension, tandis que les unités d'utilisation demandent normalement des tensions basses ou moyennes. Les sous–systèmes de génération et de distribution sont alors connectés aux travers

des lignes de transmission et des transformateurs qui permettent d'adapter les différent niveaux de tension. Dans ce contexte, la large diffusion de sources d'énergie renouvelables – qui sont par définition distribuées et de dimensions contenues – pousse inévitablement à concevoir de différents paradigmes conceptuels qui aillent au-delà de la classification standard génération–transmission–distribution. Une des possibilités consiste alors dans la conception de nouvelles architectures électriques à les positionner aux frontières de l'infrastructure déjà existante, plus précisément aux niveaux de haute et basse tension.

Au niveau de haute tension, l'idée principale est de construire un réseau de grand dimension, appelé *global grid* ou *supergrid*, qui se déploie sur tous les cinq continents et qui connecte les plus grandes unités de génération du monde [31, 57]. En utilisant cette architecture, il alors serait possible d'intégrer des sources d'énergie renouvelables, à haut potentiel, situées dans des zones très éloignées des centres urbaines, de manière à fournir l'énergie durable aux réseaux locaux au travers de la transmission en haute tension à courant continu. Quelques exemples de ces sources à haut potentiel sont les réserves d'énergie géothermique en Islande, l'énergie éolienne dans la mer du Nord, l'énergie solaire dans les régions Sahariennes et les sources hydroélectriques en Groenland (voir [31] pour une analyse économique et de faisabilité du projet supergrid). D'un autre côté, au niveau de basse tension, l'objectif principal est de réduire le gaspillage d'énergie qui caractérise la transmission d'énergie sur des distances très longues et de doter le sous–systèmes de distribution de la capacité d'opérer de façon autonome. Une solution potentielle est alors représentée par le concept de *microgrid* [98, 140, 63]. Un microgrid est en effet un réseau de petite dimension qui est constituée par: plusieurs unités de génération, basée principalement sur des sources d'énergie renouvelables, charges résidentielles, batteries et dont le mode de fonctionnement peut être soit autonome, soit en connexion avec le réseau de distribution principal [140].

Ces nouvelles architectures, bien que particulièrement utiles à l'intégration des énergies renouvelables dans l'infrastructure électrique existante, posent des nouveaux problèmes du point de vue opération, ainsi que du contrôle de systèmes de génération, transmission et distribution de l'électricité. Les raisons sont les suivantes. Premièrement, les sources d'énergie renouvelables sont normalement interfacées au réseau principal au travers des convertisseurs de puissance dont la dynamique très différente de celle des générateurs synchrones. En outre, comme on a déjà remarqué et contrairement aux sources d'énergie traditionnelles, les sources d'énergie renouvelables sont généralement distribuées et de dimensions contenue [151]. Il serait donc nécessaire d'avoir plusieurs nouvelles unités de génération assurant la même quantité d'énergie produite par une seule unité de génération traditionnelle. Pour cela il est donc fondamental de déterminer un mode de fonctionnement approprié pour les convertisseurs. En conclusion de ces considérations, il est évident qu'il y a une forte nécessité de méthodes avancées dans la modélisation, l'analyse et la commande de systèmes électriques de puissance modernes.

Contributions principales

Aujourd'hui, on peut constater qu'ils existent des approches très différentes abordant les problèmes de modélisation, analyse et commande de systèmes électriques de puissance. Dans ce contexte, la différence de méthodes et de langage adoptés par la communauté des systèmes électriques de puissance en contraste avec la communauté de contrôle représente sans doute une difficulté majeure. En s'appuyant sur ces considérations, le caractère innovant de ce travail repose sur l'application de nouvelles méthodes, développées récemment par des théoriciens du contrôle – plus précisément des méthodes basées sur la notion d'énergie – aux problèmes de modélisation, analyse et commande de systèmes électriques.

L'objectif principal est de promouvoir une combinaison de la vision pragmatique, typique d'une approche de type ingénieur, avec une vision plus théorique, fondée sur une caractérisation mathématique et physique rigoureuse, conçue à partir de considérations énergétiques. Dans ce travail, les contributions de l'auteur regardent différentes architectures des systèmes électriques de puissance, tels que les systèmes de transmission haute tension en courant continu (hvdc), les microgrids, les systèmes à courant alternatif conventionnel et aussi des classes plus généralisées de systèmes électriques de puissance. Toutefois, les résultats principaux sont développés autour d'une application: les systèmes multi–terminal hvdc. Dans l'opinion de l'auteur, même si la plus part des résultats peuvent être généralisés à des classes plus larges de systèmes et architectures, ceux-ci devraient être analysés au cas par cas, en argumentant les descriptions mathématiques adoptées avec une interprétation technique et spécifique de l'application traitée.

Les contributions principales de ce travail sont les suivantes.

1) **Un approche unifié, basé sur la notion d'énergie, pour la modélisation de systèmes électriques de puissance généralisés, à partir des principes physiques fondamentaux.** (Chapitre 3, Sections 4.3, 5.2, 5.3)

   En littérature, il existe une grande variété des modèles aptes à décrire un système électrique de puissance traditionnelle, basé sur les générateurs synchrones. Typiquement, il est vu comme un système doté de n ports, décrit par des équations algèbro–différentielles, qui souvent ne retiennent pas les identités des composantes et donnent une description cryptique du comportement physique du dit système. Une première contribution – développée dans le Chapitre 3 – est alors la formulation d'un approche généralisée pour la modélisation des systèmes électriques de puissance à partir des principes physiques fondamentaux. Cette formulation se base sur des outils mathématiques, qui permettent de formaliser des importantes notions physiques telles que la passivité, le fluxes énergétiques, les interconnexions et les dissipations. Les outils mathématiques clés sont: la théorie des graphes, utilisée pour la description de l'architecture du système; les systèmes Hamiltoniens à ports, utilisés pour la description individuelle des composantes électriques. Le modèle obtenu a donc l'avantage d'expliciter les caractéristiques physiques du système tout en préservant une formulation mathématique rigoureuse. Il se présente donc comme un *lingua franca* pour des domaines de recherche apparemment différents, avec l'intérêt de faciliter la communication entre théoriciens et ingénieurs. La méthode proposée est appliquée, avec des différences mineures, à la modélisation de systèmes multi–terminal de transmission hvdc (Section 4.3), microgrids (Section 5.2) et à systèmes ac traditionnels (Section 5.3).

2) **Vers une généralisation des procédures de réduction du modèle à partir des principes physiques fondamentaux: quelles sont les hypothèses nécessaires? Le cas des systèmes multi–terminal hvdc et des microgrids.** (Sections 4.8, 5.2)

   Pour l'analyse et la commande de systèmes électriques de puissance traditionnelles, l'utilisation de modèles réduits est largement adoptée en littérature. Toutefois, on peut se demander si les hypothèses sous–jacentes aux procédures de réduction sont encore valides pour des systèmes dont la quantité de sources d'énergie renouvelables est majoritaire. Pour ce type de systèmes en effet, les modèles mathématiques sont souvent présentés sans aucune référence à la procédure de réduction adoptée, ce qui complique la compréhension du comportement physique du système.

Une contribution ultérieure de l'auteur est donc la dérivation – à partir des principes physiques fondamentaux et sous certaines, raisonnables hypothèses – de modèles réduits pour deux classes de systèmes électriques de puissance: les systèmes multi–terminaux de transmission hvdc (Section 4.8) et les microgrids (Section 5.2).

3) **Commande hiérarchisée de systèmes multi–terminaux de transmission hvdc**, (Chapitre 4)

- **a) Modélisation de type énergétique et analyse du système en boucle ouverte** (Sections 4.3–4.5). Un modèle complet d'un système multi–terminal de transmission haute tension à courant continu, en forme Hamiltonienne à ports, est obtenu (Section 4.3), en utilisant l'approche illustré dans le Chapitre 3. Ce modèle constitue le point de départ pour la dérivation des résultats successifs, qui concernent l'équilibre de puissance du système et la définition des solutions admissibles (Section 4.5), ainsi que pour développer une discussion sur l'architecture de contrôle du système (Section 4.4).

- **b) Contrôle de la boucle interne: conception de la lois de commande, stabilité et analyse des performances** (Sections 4.6, 4.7). à partir du modèle Hamiltonien à ports du système, une nouvelle loi de commande, des PIs décentralisés basés sur la notion de passivité (PI–PBC), est dérivée. La stabilité globale du système en boucle fermée est alors garantie sous l'hypothèse que les conditions opératives soient nominales et les gains des PIs soient positifs. Avec l'objectif de placer la loi de commande obtenue dans le contexte de la littérature des systèmes de puissance, une analyse comparative avec les stratégies de contrôle standard est présentée. Premièrement, il est possible de démontrer que des problèmes de stabilité peuvent se vérifier dans le cas des lois de commande standards, *e.g.* vector control, si les gains ne sont pas bien choisis. D'un autre côté, même si le PI–PBC garantit un comportement globalement asymptotiquement stable du système en boucle fermée, on peut constater que les performances sont en–dessous de la moyenne. En effet, on peut vérifier qu'ils existent des limitations de performances claires qui empêche d'obtenir des réponses suffisamment rapides, indépendamment des choix des gains. Pour surmonter ce problème, inspiré de la pratique de rajouter une boucle externe pour optimiser les performances, on détermine une modification du PI–PBC telle que les réponses du système soient améliorées. Les résultats obtenus sont enfin validés avec des simulations et suivis par une discussion sur les avantages et inconvénients du PI–PBC par rapport aux lois de commande standards.

- **c) Contrôle primaire: conception de la lois de commande, stabilité et distribution de puissance** (Section 4.8). Sous certaines, raisonnables, hypothèses on dérive un modèle réduit, non linéaire, d'un système multi-terminal de transmission hvdc. à partir de ce modèle, une classe généralisée de lois de commande primaires, qui comprend le droop control, est formulée. Le modèle obtenu – qui est non linéaire – représente le point de départ pour l'analyse des conditions nécessaires pour l'existence de solutions, la stabilité des équilibres, ainsi qu'une distribution appropriée de puissance parmi les différentes unités. Les résultats obtenus sont validés au travers d'un simple exemple avec des calculs numériques.

Plan de la thèse

Ce travail est structuré en cinq chapitres et il est suivi d'une brève conclusion et une discussion sur les futures lignes de recherche. Note aux lecteurs: avec l'intention d'éviter confusion dans les définitions, tous les chapitres sont auto–contenus et peuvent contenir plusieurs répétitions. Ceci est dû au choix intentionnel de l'auteur afin d'éviter des généralisations erronées des résultats obtenus. Le plan du travail est le suivant.

Dans le Chapitre 2 on rappelle des concepts préliminaires en théorie du contrôle et sur la modélisation des systèmes électriques de puissance. Un approche généralisé pour la modélisation – basé sur les notions d'énergie et graphe – est donc dérivé dans le Chapitre 3. Les principaux résultats sont présentés dans le Chapitre 4, où sont développées des procédures théoriques pour la modélisation, l'analyse et la commande de systèmes multi–terminal de transmission hvdc. Le Chapitre 5 est dédié à aux contributions ultérieures de l'auteur qui peuvent être présentées comme des interprétations alternatives, extensions où applications des résultats obtenus dans les chapitres précédentes. Les conclusions et perspectives futures de recherche sont finalement présentées dans le Chapitre 6.

Chapter 1

Introduction

1.1 Motivation

Since their development at the end of the IX–th century, with the first lighting systems commercialized by Edison and Westinghouse, electric power systems had a powerful impact on society and contributed to a substantial improvement of the quality of everyday life. However, because of their dependence on the nature of the energy resources, as well as of their strict relation with the human needs, they have to be adapted according to the current, rapidly evolving scenario, which has undergone notable changes in recent years. These changes are mainly driven by the following factors:

- New needs naturally arising from the worldwide urbanization processes, the unrelenting growth of the population and of the rising economies, *e.g.* China and India. Hence, a growing energy demand is expected, mainly coming from these developing countries. This is essentially due to people migration from rural areas to densely populated urban centers. The worldwide demand is expected to increase by 36% in the following years until 2035 [81].

- Conventional electric power systems are based on few large–sized, fuel–based generation units constituted by a combination of steam turbines and synchronous generators [151]. The steam is typically obtained by combustion of fossil fuels, *e.g.* oil, coal, natural gas, that are the traditional primary resources employed for electricity supply. Unfortunately, the massive utilization of these resources has the following drawbacks.

    - It has been widely acknowledged by the scientific community that fossil fuels are key contributors to climate change and global warming, because of the greenhouse emission of carbon dioxide (CO_2) that follows the combustion [107, 23].
    - With the current exploitation, reserves of fossil fuels are expected to run out in less than a century. Moreover, since they are a valuable resource, useful for manufacture of plastics, perhaps this would be a better use than simply setting fire to them [107, 47].
    - Countries with small reserves of fossil fuels risks to be highly dependent from countries with larger reserves, thus rising a problem of security of the supplied energy.

All this considered, although the path of the future electric power system is still somehow uncertain, there is quite a clear consensus on the following point: it is necessary to drastically cut the production of energy based on fossil fuels, in order to reduce the decisive human contribution to changing climate trends and mitigate their economical and geopolitical consequences. Since the increase of the population

and of the energy demand by the emerging economies make likely impossible a reduction of the energy consumption, a viable possibility is to shift (at least partially) the energy production from fossil fuels to renewable energy sources, like solar, wind, hydro and geothermal. In the last fifteen years many developed countries started approving energy policies that agreed with this intention and is expected that other countries follow soon the same guidelines, in accordance with the Kyoto Protocol, signed in 1997 [38, 25].

As a result of these new policies, we have assisted to a widespread penetration of renewable energy sources in the existing electric power systems infrastructure. Obviously, these changes call for a reflection on the overall system architecture, as well as on its conventional operation. A first consideration is that, from a purely theoretical point of view, conceptually different architectures may constitute the best option for the architecture of power systems based on renewable energy sources. Nevertheless, it is unlikely that the current architecture will be fully dismantled, all fuel–based units removed and replaced with renewables. The problem of new architectures for modern electric power system with high penetration of renewables should be then better reformulated as follows: *how to integrate and/or extend the existing architectures to better account for the growing penetration of renewables?*
The traditional electric architecture, founded on synchronous generators, is based on a strong separation between the generation and utilization subsystems, since they operate at a different voltage level [96, 7]. Because of the large size of the fuel–based generation units, generation is indeed mostly operated at high–voltage, while utilization requires in general medium– and low–voltage levels. Generation and utilization subsystems are then connected by means of the transmission subsystem that, starting from an high–voltage level, takes care of stepping down the voltages from the generation until the distribution level. Then, with the penetration of renewable energy sources — which are by definition small–sized and distributed — a new paradigm, that goes beyond the standard generation–transmission–distribution classification is required. One possibility is to conceive new architectures that will take place at the boundary of the existing infrastructure, more precisely at the high– and low–voltage levels, as illustrated in Fig. 1.1. At the high–voltage level, the purpose is to build an high–voltage grid spanning the whole planet and connecting most of the large power plants in the world, the so–called *global grid* or *supergrid* concept [31, 57]. In this scheme it would be likely possible to integrate remotely located, high potential, aggregated renewable energy resources that would be able to provide sustainable energy to the main grids using high–voltage transmission systems. Examples of these large green energy reserves are geothermal energy in Iceland, wind energy in the North Sea, solar energy in the Saharian region and hydro power in Greenland (see [31] for an economical and technical feasibility analysis of the supergrid project). At the low–voltage level, on the other hand, the key idea is to cut drastically the waste of energy due to the losses for transmission over long distances and to endow the distribution level with the capacity of autonomous operation. A potential solution is constituted by the *microgrid* concept [98, 140, 63]. A microgrid consists of a collection of generation units, mostly based on renewable energy sources, residential loads and energy storage elements that can be operated either in grid–connected mode or in islanded mode, *i.e.*, in a completely isolated manner from the main transmission system [140]. We do not dwell any longer on these two concepts, for which the reader is referred to Chapter 4 and Chapter 5.

It is clear that these new architectures, that foster the integration of renewable energy sources in the existing infrastructure, pose new problems for operation and control of the overall system. The reasons are twofold. Firstly, renewable energy sources are usually interfaced to the grid through power switched

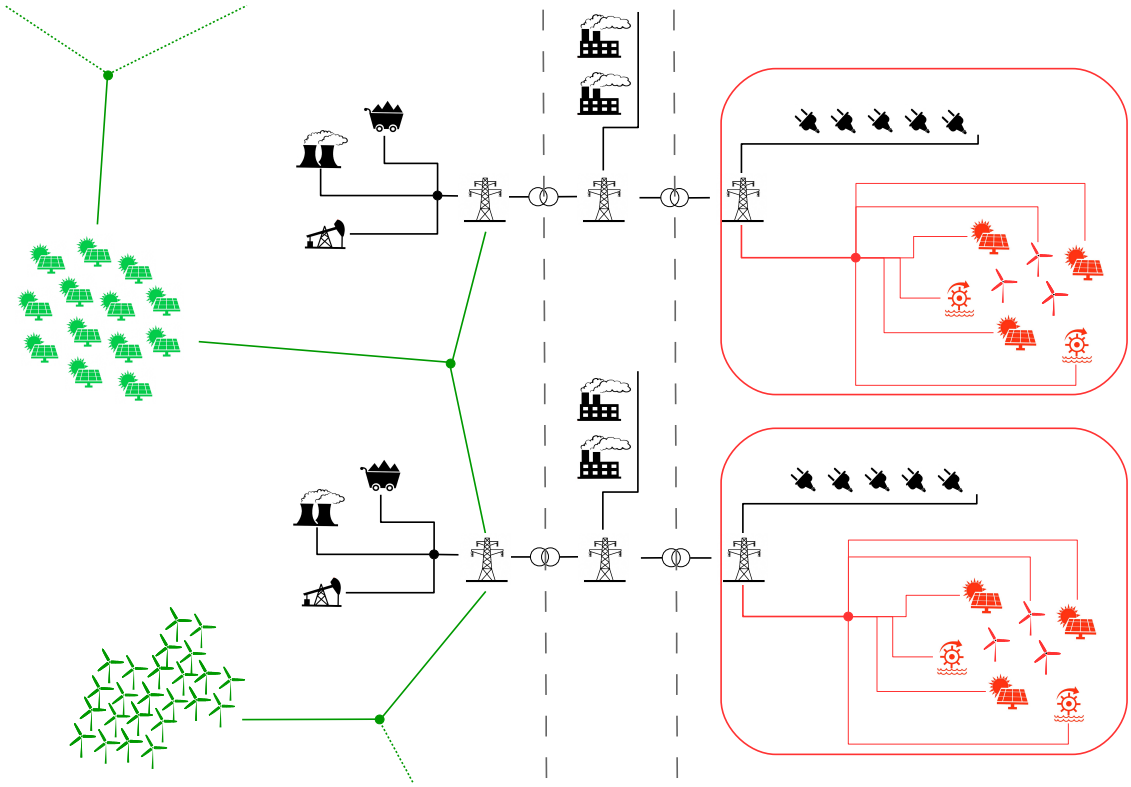

Figure 1.1: Infrastructure of a modern electric power system composed by a *supergrid* (green–colored), conventional power systems based on synchronous generators (black–colored) and *microgrids* (red–colored). Aggregated renewable energy sources are connected to conventional power systems through high–voltage transmission. Distributed renewable energy sources, are interfaced directly at the distribution level.

electronics, the dynamics of which largely differ from standard synchronous generators, which are the traditional generation units in conventional power systems. Secondly, in contrast with traditional power plants, renewable energy sources are small–sized and distributed [151]. Hence, since it will be likely requested for many renewable energy sources to provide the same quantity of energy provided by a single power plant, an appropriate operation of individual switched electronic devices is crucial for a correct and safe operation of the overall system. As a result of these considerations, it is obvious that there is a strong need for advanced methods in modeling, analysis and control of electric power systems, that takes into account the role played by renewable energy sources and by switched power electronics devices.

1.2 Main contributions

Nowadays the gap between power engineer and control theorist approaches is not trivial and far to be closed, and this fact represents in this sense a major shortcoming. Moving from this consideration, the innovative character of the described work relies basically to the applications of emerging approaches recently developed by control theorists — namely energy–based methodologies — to the very topical issue of large–scale electric power systems. The main purpose is then to perform a combination of

a more practical vision, typical of a power system engineering approach with a more theoretical one, characterized by classical mathematical and physical formalism, conceived starting from energy–based considerations. As detailed below, contributions of the author concern various architectures of power systems, ranging from hvdc transmission systems, microgrids, conventional ac systems to generalized classes of electric power systems. Nevertheless, the core of the work is developed around one specific application: multi–terminal high–voltage direct–current (hvdc) transmission systems. It is indeed the author's belief that, although most of the approaches employed in the present work may be possibly adapted to different architectures and scenarios, these should be discussed case by case, by supporting the theoretical description with a technically–founded, application–specific interpretation of the obtained mathematical results.

The main contributions — that are clearly restated in the related chapters and sections to enhance readability — are the following.

1) **A unified, energy–based modeling approach for generalized electric power systems, starting from fundamental physical principles** (Chapter 3, Sections 4.3, 5.2, 5.3)

   In literature there exists a wide variety of models for the description of traditional electric power systems based on synchronous generators. These usually are well–established, reduced models where the system is viewed as an n–port described by a set of ordinary or algebraic differential equations, which often do not retain the identity of the components and provide a cryptic description of the physics of the system. A first contribution — developed in Chapter 3 — is the formulation of a generalized approach for the modeling of electric power systems starting from first physical principles. This is based on two fundamental mathematical tools: graph theory for the description of the system architecture and the port–Hamiltonian framework for the description of the single components. This kind of formulation naturally leads to a simpler formalization of fundamental physical concepts like passivity, energy flows, physical interconnections and dissipations, which are indeed captured by port–Hamiltonian representations. The obtained model is thus expected to provide a *lingua franca* for two apparently different research areas, facilitating communication between control theorists and power systems engineers, due to the incorporating of a priori knowledge and providing more intuitive physical interpretations of classical mathematical frameworks. The proposed method is applied, with some minor differences, to the modeling of multi–terminal hvdc transmission systems (Section 4.3), ac microgrids (Section 5.2) and a simplified model of traditional ac system (Section 5.3). The obtained models are instrumental for the next contributions.

2) **Towards a generalization of model reduction procedures starting from first principles models: under which underlying assumptions? The case of multi–terminal hvdc transmission systems and ac microgrids** (Sections 4.8, 5.2)

   Reduced models are largely employed for analysis and control of traditional electric power systems. However, it may be questioned whether the assumptions underlying these reduction procedures, are still valid for power systems with an high penetration of renewable energy sources and, consequently, of switched power electronics. With respect to this modified scenario, reduced models are in fact typically presented without any reference to the reduction procedure, hampering the understanding of the physical phenomena behind them. Hence, another contribution of this work

consists in the establishment — starting from the previously obtained first principles models, and under some physically motivated assumptions — of the reduced models for two specific class of electric power systems: multi–terminal hvdc transmission systems (Section 4.8) and ac microgrids (Section 5.2). Interestingly, while for the case of ac microgrids the standard model commonly employed in practice is recovered, in the case of hvdc transmission system a new (nonlinear) model is obtained.

3) **Hierarchical control of multi–terminal hvdc transmission systems** (Chapter 4).

- **a) Energy–based modeling & analysis of the open–loop system** (Sections 4.3–4.5). A full model of a multi–terminal, meshely connected, hvdc transmission system, based on port–Hamiltonian representation, is established (Section 4.3), using the modeling approach developed in Chapter 3. The obtained model constitutes the backbone that is necessary for obtaining the next theoretical results (Section 4.5), as well as for developing a discussion on the hierarchical control architecture of the system (Section 4.4).
- **b) Inner–loop control: design, stability & performance analysis** (Sections 4.6, 4.7). Moving from the full port–Hamiltonian model the multi–terminal hvdc transmission system, a new decentralized PI controller, based on passivity arguments (PI–PBC) is derived. It is shown that the obtained controller ensures — under the assumption of nominal operating conditions — global asymptotic stability of the desired set point for any positive gain. In order to place the proposed controller in context, a comparative analysis with inner–loop control strategies commonly employed in practice is presented, thus leading to the following two main contributions. First, it is shown that instability may arise in standard controllers, *e.g.* vector control, if controller gains are not properly tuned. On the other hand, although the PI–PBC ensures a globally asymptotically stable behavior of the system, it is shown to have clear performance limitations. Hence, fast transient responses can not be achieved, independently from the choice of the gains. To cope with this problem, inspired by the engineering pratice of adding an outer–loop for improving performances, we determine a modification of the PI–PBC that effectively overcome the mentioned performance limitations. The mentioned contributions are validated via simulations. A discussion on advantages and disadvantages of the PI–PBC with respect to standard controllers is further presented.
- **c) Primary control: design, stability & power sharing** (Section 4.8). Under some reasonable, physically–motivated assumption, a reduced *nonlinear* model of multi–terminal hvdc transmission system, in closed–loop with standard inner–loop controllers is derived. A generalized class of primary controllers — that includes the ubiquitous voltage droop control — is further formulated. Moving from the obtained model — that should be contrasted with standard linear models employed in literature — necessary conditions for existence, stability and power sharing of equilibria are established and verified via numerical calculations.

1.3 Publications

Main contents of this thesis are based on the following publications, that are listed in chronological order.

Contributed chapter

D. Zonetti, R. Ortega, *"Control of HVDC Transmission Systems: From Theory to Practice and Back"*. In M.K. Camlibel, A.A. Julius, R. Pasumarthy, J. Scherpen (eds.), Mathematical Control Theory I, Springer, pp. 153-177.

Journal papers

J. Schiffer, D. Zonetti, R. Ortega, A. Stankovic, T. Sezi, J. Raisch, *"A survey on modeling of microgrids – From fundamental physics fo phasors and voltage sources"*, Automatica, submitted — [140].

D. Zonetti, R. Ortega, A. Benchaib, *"Modeling and control of HVDC transmission systems: from theory to practice and back"*, Control Engineering Practice, Volume 45, December 2015, Pages 133-146, ISSN 0967-0661, http://dx.doi.org/10.1016/j.conengprac.2015.09.012 — [182].

S. Fiaz, D. Zonetti, R. Ortega, J. Scherpen, A. van der Schaft, *"A port-Hamiltonian approach to power network modeling and analysis"*, European Journal of Control, Volume 19, Issue 6, December 2013, Pages 477-485, ISSN 0947-3580, http://dx.doi.org/10.1016/-j.ejcon.2013.09.002 — [53].

Conference proceedings

D. Zonetti, R. Ortega, *"A tool for stability and power sharing analysis of a class of generalized droop control for high–voltage direct–current transmission systems"*. Decision and Control, Conference on, Las Vegas, US, Dec 2016, submitted.

D. Zonetti, R. Ortega, A. Benchaib, *"A Globally Asimptotically Stable decentralized PI control of multi–terminal High–Voltage DC transmission systems"*. European Control Conference, Strasbourg, France, Jun 2014 — [181].

S. Fiaz, D. Zonetti, R. Ortega., J. Scherpen, A. van der Schaft, *"On port-Hamiltonian modeling of the Synchronous Generator and Ultimate Boundedness of its solutions"*. Proceedings of the conference on Lagrangian and Hamiltonian Methods in Nonlinear Control, Bertinoro, Italy, Aug 2012 — [52].

S. Fiaz, D. Zonetti, R. Ortega., J. Scherpen, A. van der Schaft, *"Port Hamiltonian modeling of Power Networks"*. MTNS 2012 Proceedings, Melbourne, Australia, Jul 2012.

D. Zonetti, S. Fiaz, R. Ortega, A. van der Schaft, D. Langarica, J. Scherpen, *"Du Bond Graph au modèle Hamiltonien à Ports d'un Système de Puissance"*. CIFA 2012 Proceedings, Grenoble, France, Jul 2012 — [180].

1.4 Outline

This work is structured in five chapters and is wrapped–up with some conclusions and guidelines for future research. We bring to the attention of the reader that, in order to avoid *barking up the wrong tree*, chapters are self–contained and repetitions may occur. This is justified by intentional choice of the author to avoid misleading generalization of the obtained results. The outline of this work is as follows.

Chapter 2 is dedicated to recall some preliminary concepts in control theory and modeling of electric power systems. The formulation of a generalized approach for the modeling — based on the notions of energy and graph — is derived in Chapter 3. The main body of the thesis is presented in Chapter 4, where we develop a general, theoretically–founded procedure for the modeling, analysis and control of multi–terminal hvdc transmission systems. Chapter 5 is devoted to further contributions of the author, that can be presented as alternative interpretations, extensions or applications of the results obtained in the previous chapters. Conclusions and future works are finally discussed in Chapter 6.

Chapter 2

Preliminaries

In this chapter, structured in two main sections, we recall some fundamental notions, well–established in literature, that are relevant for this work. Section 2.1 is then dedicated to illustrate preliminary concepts and definitions on modeling, analysis and control of nonlinear dynamical systems, while Section 2.2 is devoted to discuss prevailing signal architectures employed for generation, transmission and distribution of electricity and to introduce standard tools for the description of the electrical behavior.

2.1 Control theory

2.1.1 Notation

The symbols $\mathbb{R}$ and $\mathbb{C}$ denote the sets of real and complex numbers. The real part of a complex number p is denoted by $\mathfrak{Re}(p)$, while its imaginary part is denoted by $\mathfrak{Im}(p)$. For a set $\mathcal{N} = \{l, k, \dots, n\}$ of, possibly unordered, elements, we denote with $i \sim \mathcal{N}$ the elements $i = l, k, \dots, n$. All vectors are column vectors. Given positive integers n, m, the symbol $0_n \in \mathbb{R}^n$ denotes the vector of all zeros, $0_{n\times m}$ the $n \times m$ column matrix of all zeros, $1_n \in \mathbb{R}^n$ the vector with all ones, $\mathbb{I}_n$ the $n \times n$ identity matrix. When clear from the context dimensions are omitted and vectors and matrix are simply denoted by the symbols 0, 1 or $\mathbb{I}$. The matrix J_2 is defined as

$$J_2 := \begin{bmatrix} 0 & 1 \\ -1 & 0 \end{bmatrix} \in \mathbb{R}^{2\times 2}.$$

For a given matrix A, the i-th column is denoted by A_i. $\mathrm{diag}\{a_i\}$ is a diagonal matrix with entries $a_i \in \mathbb{R}$ and $\mathrm{bdiag}\{A_i\}$ denotes a block diagonal matrix with entries the matrices A_i. $x := \mathrm{col}(x_1, \dots, x_n) \in \mathbb{R}^n$ denotes a vector with entries $x_i \in \mathbb{R}$, when clear from the context it is simply referred as $x := \mathrm{col}(x_i)$. For a function $f : \mathbb{R}^n \to \mathbb{R}$, ∇f denotes the transpose of its gradient. The symbol $\otimes$ denots the Kronecker product. The subindex i, preceded by a comma when necessary, denotes elements corresponding to the i-th subsystem or element.

2.1.2 Elements of linear graph theory

Linear graph theory provides a very useful conceptual framework for the modeling of physical and non physical network. The interested reader is referred to [21, 60] for further details on mathematical graph theory and to [168] for an application to physical systems. We define a weighted directed graph an ordered tuple $\mathcal{G} := (\mathcal{N}, \mathcal{E}, \pi, \rho)$ consisting of a finite set of vertices (nodes) $\mathcal{N}$, a finite set of directed

edges $\mathcal{E}$, a mapping π from $\mathcal{E}$ to the set of ordered pairs of $\mathcal{N}$, where no self–loops are allowed, and a weight function $\rho : \mathcal{E} \to \mathbb{R}_+$. Therefore to every edge $e \in \mathcal{E}$, there corresponds an ordered pair $(v, w) \in (\mathcal{N}, \mathcal{N})$, $v \neq w$, representing the tail vertex v and the head vertex w of this edge, and a weight $\rho(e)$. A graph is said to be unweighted if $\rho(e) = 1$ for any $e \in \mathcal{E}$. Otherwise it is said weighted. An undirected graph is the one in which edeges have no orientation and are not ordered in pairs, i.e. the edge (v, w) is identical to the edge (w, v). In an undirected graph $\mathcal{G}$, two vertices v and w are called connected if $\mathcal{G}$ contains a path (i.e. a series of undirected edges) from v to w, Otherwise, they are called disconnected. A graph is said to be connected if every pair of vertices in the graph is connected. We call a graph $\mathcal{G}' := (\mathcal{N}', \mathcal{E}', \pi', \rho')$ a subgraph of $\mathcal{G} := (\mathcal{N}, \mathcal{E}, \pi, \rho)$, if $\mathcal{N} \subset \mathcal{N}'$ and $\mathcal{E} \subset \mathcal{E}'$.

Let v the number of vertices (or nodes), and e the number of edges of the weighted graph $\mathcal{G} = (\mathcal{N}, \mathcal{E}, \pi, \rho)$. We provide fundamental properties of the graph that are captured by the following matrices.

- The *incidence matrix* $\mathcal{M}(\mathcal{G}) \in \mathbb{R}^{\mathsf{v} \times \mathsf{e}}$ is a matrix with element (i, j) equals to $-\rho(e_j)$ if e_j is an edge towards i, equals to $\rho(e_j)$ if it is an edge originating from i, and 0 otherwise.

- The *adjacency matrix* $\mathcal{A}(\mathcal{G}) \in \mathbb{R}^{\mathsf{v} \times \mathsf{v}}$ is a matrix with element (i, j) equals to $\rho(e)$ if there exists an edge e connecting vertices i, j, including self–loops, and 0 otherwise.

- The *degree matrix* $\mathcal{D}(\mathcal{G}) \in \mathbb{R}^{\mathsf{v} \times \mathsf{v}}$ is a diagonal matrix with entry (i, i) equals to the sum of the weight of the edges towards and originating from vertex i.

- The *Laplacian matrix* $\mathcal{L}(\mathcal{G}) \in \mathbb{R}^{\mathsf{v} \times \mathsf{v}}$ is a matrix $\mathcal{L}(\mathcal{G}) := \mathcal{D}(\mathcal{G}) - \mathcal{A}(\mathcal{G})$. The Laplacian matrix of a directed graph is nonnegative, its off–diagonal entries are nonpositive and its row sums are zero. If the graph is undirected it is symmetric and positive semidefinite.

2.1.3 Port–Hamiltonian systems

Conceiving subsystems as vehicles of energy is a very appealing approach for the modeling of complex physical systems. Indeed, energy transfer can be seen as a process in which subsystems energy is exchanged by means of injections/ejections with respect to some ports (so–called *energy ports*) and correspondent variables (so–called *port variables*). In particular, the act of delivering energy can be associated with one variable giving the flux of energy flow, that is called *effort (e)* variable, and a variable giving the pitch of energy flow, that is called *flow* (f) variable [168, 109]. Thus, an energy port can be represented by a pair of terminals with a pair (e, f) of generalized variables, which together represent the energy transfer mechanism, and whose by–product is a power, see Fig. 2.1. In this context, port–Hamiltonian (pH) systems provide a particularly interesting paradigm for modeling, analysis and control of complex nonlinear systems using the notion of energy and port. There are two reasons for their appeal: first, that they can be used to represent a wide class of multiphysical systems, including (but not limited to), systems described by Euler–Lagrange equations. Second, they directly reveal the fundamental role of the physical concepts of energy, dissipation and interconnection. For a wide overview on this subject, see the excellent books [161, 159, 43].

We introduce the following definitions.

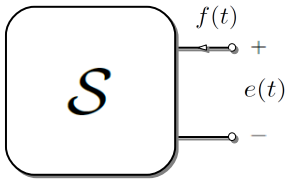

Figure 2.1: Port representation of a generalized subsystem with effort and flow variables.

Nonlinear port–Hamiltonian systems. We define a time–invariant, port–controlled Hamiltonian system $\mathcal{S}$ with dissipation, the following stationary, differential algebraic equations (DAEs):

$$\mathcal{S}: \begin{cases} \dot{x} & = [\mathcal{J}(x) - \mathcal{R}(x)]\, \nabla_x \mathcal{H}(x) + g(x)u + G(x)\sigma + G_0(x)\sigma_0 \\ y & = G^\top(x)\nabla_x \mathcal{H}(x) \\ y_0 & = G_0^\top(x)\nabla_x \mathcal{H}(x) \\ 0 & = w(\sigma_0, y_0), \end{cases} \tag{2.1.1}$$

where $x : \mathbb{R}_+ \to \mathcal{X} \subseteq \mathbb{R}^n$ denotes the state vector, $u : \mathbb{R}_+ \to \mathcal{U} \in \mathbb{R}^m$ the control input,$(\sigma_0, y_0) \in \Sigma_0 \times \mathcal{Y}_0$, with $\Sigma_0, \mathcal{Y}_0 \in \mathbb{R}^{p_0}$ the conjugated algebraic port–variables, $(\sigma, y) \in \Sigma \times \mathcal{Y}$, with $\Sigma, \mathcal{Y} \in \mathbb{R}^p$, the conjugated interaction port–variables, $\mathcal{H} : \mathbb{R}^n \to \mathbb{R}$, the Hamiltonian (energy) function, $w : \mathbb{R}^{p_0} \times \mathbb{R}^{p_0} \to \mathbb{R}^{p_0}$, the characteristic function. Matrices are further defined as follows: interconnection matrix $\mathcal{J}(x) = \mathcal{J}(x)^\top \in \mathbb{R}^{n\times n}$, positive semi–definite dissipation matrix $\mathcal{R}(x) = \mathcal{R}^\top \in \mathbb{R}^{n\times n}$, input matrix $g(x) \in \mathbb{R}^{n\times m}$, algebraic–port matrix $G_0(x) \in \mathbb{R}^{n\times p_0}$, interaction–port matrix $G(x) \in \mathbb{R}^{n\times p}$. In some cases, it may be also convenient to introduce a reference output

$$y_r := h(x, u), \tag{2.1.2}$$

with $y_r : \mathbb{R}^+ \to \mathcal{Y}_r \subseteq \mathbb{R}^q$. The vector x of state variables describes the capacity of the system to store information related to its past history. The control input u is a set of m exogenous signals that usually correspond to variables that can be directly manipulated by the user. The Hamiltonian function $\mathcal{H}$ accounts for the total energy stored by the system, the matrix $\mathcal{J}$ specifies the internal interconnection and $\mathcal{R}$ the dissipation structure of the system. The conjugated port variables (σ_0, y_0) are a set of p_0 pairs of variables that are related by an algebraic characteristic w. The conjugated port–variables (σ, y) are a set of p pairs of variables that describe the interaction of the system with the external environment and are called the interaction port–input and port–ouput variables. The product of port variables has the dimension of a power. The energy flowing through the ports at time T is indeed given by:

$$E(T) = E(t_0) + \int_{t_0}^{T} y^\top(t)\sigma(t)\mathrm{d}t. \tag{2.1.3}$$

The reference output y_r is a set of q variables that are of particular interest for analysis and/or control purposes. For example it may consist of a (sub)set of the state variables that are available for measurement (measured output) or that are of some interest for performance analysis.
Whenever no characteristic function is defined, the system is said to be an ordinary differential equa-

tions (ODEs) port–Hamiltonian system. Otherwise, it is said to be a differential algebraic equations (DAEs) port–Hamiltonian system. Special subclasses of the system (2.1.1) can be further obtained by: assuming that the system is energetically isolated from the external environment, that corresponds to take $G(x) = 0$; or assuming the absence of any control action, that corresponds to take $g(x) = 0$. In the sequel we refer to these subclasses as *isolated* and *uncontrolled* port–Hamiltonian systems respectively.

Power preserving interconnection laws. To introduce the notion of power preserving interconnection laws we consider two port–Hamiltonian systems $\mathcal{S}_1$, $\mathcal{S}_2$ of dimension n_1, n_2 and assume that the correspondent ports have the same dimension, as depicted in Fig. 2.2. Then we define a time–invariant power preserving interconnection law any relation

$$\mathcal{I}_{12}: \quad \begin{bmatrix} \sigma_1 \\ \sigma_2 \end{bmatrix} = \begin{bmatrix} 0 & \beta(x_1, x_2) \\ -\beta^\top(x_1, x_2) & 0 \end{bmatrix} \begin{bmatrix} y_1 \\ y_2 \end{bmatrix}, \tag{2.1.4}$$

with $\beta : \mathbb{R}^{n_1} \times \mathbb{R}^{n_2} \to \mathbb{R}^p$, that verifies:

$$y_1^\top \sigma_1 + y_2^\top \sigma_2 = 0. \tag{2.1.5}$$

Recalling that the by–product of the port variables is a power, it is easy to see that (2.1.5) expresses the fact that power is preserved by the interconnection between $\mathcal{S}_1$ and $\mathcal{S}_2$.

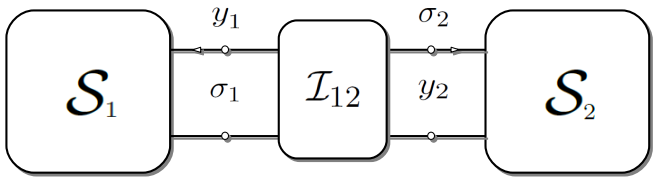

Figure 2.2: Power–preserving interconnection laws.

2.1.4 Equilibria Analysis

We consider the following general DAEs nonlinear system[1]:

$$\begin{aligned} \dot{x} &= f(x, \sigma_0) + g(x)u \\ 0 &= \mu(x, \sigma_0), \end{aligned} \tag{2.1.6}$$

with f, g, μ sufficiently differentiable functions. Let $x(t_0; x_0)$ the correspondent evolution in time of the state vector, moving at time t_0 from an initial point $x_0 \in \mathcal{X}$. A special situation is when the trajectory is constant for some constant control input, that is equivalent to determine a constant $\bar{x} = x_0$ that verifies:

$$0_n = f(\bar{x}, \bar{\sigma}_0) + g(\bar{x})\bar{u}, \qquad 0_{p_0} = \mu(\bar{x}, \bar{\sigma}_0) \tag{2.1.7}$$

[1] An isolated DAEs port–Hamiltonian system can be always rewritten as a general nonlinear system in input–affine form with appropriate functions f, g, μ.

for some $\bar{u} \in \mathcal{U}$, $\bar{\sigma}_0 \in \Sigma_0$. The pair $(\bar{x}, \bar{u}) \in \mathbb{R}^n \times \mathbb{R}^m$ is usually referred as an equilibrium pair of the system (2.1.1), while (2.1.7) as the *equilibria equation*. We further refer to $\bar{x}$ as a *(state) equilibrium point*, and to $\bar{u}$ as the *equilibrium control*. Obviously, in general (2.1.7) does not admit a solution for *any* constant $\bar{x} \in \mathbb{R}^n$. Hence, we find convenient to define the *set of admissible equilibria*:

$$\mathcal{E}^\star := \{\bar{x} \in \mathbb{R}^n \ : \ 0_n = g^\perp(\bar{x}) f(\bar{x}, \bar{\sigma}_0), \ \ 0_{p_0} = \mu(\bar{x}, \bar{\sigma}_0)\}, \tag{2.1.8}$$

where $g^\perp(x)$ is a full–rank left annihilator of $g(x)$, *i.e.* it verifies $g^\perp(x)g(x) = 0$. Moreover, given $\bar{x}$, it is easy to see that the corresponding equilibrium control $\bar{u}$ is determined by:

$$\bar{u} = -\left[(g^\top g)^{-1} g^\top f\right](\bar{x}, \bar{\sigma}_0), \qquad 0_{p_0} = \mu(\bar{x}, \bar{\sigma}_0). \tag{2.1.9}$$

2.1.5 Stability in the sense of Lyapunov

Though stability is widely acknowledged as a fundamental property in systems and control theory, there exist many definitions available in literature. Roughly speaking, stability of a given trajectory means that the system motion can be kept arbitrarily close to this trajectory by starting sufficiently close to it [147]. For a precise definition we consider an isolated nonlinear system described by ODEs. This situation arises when there are no algebraic constraints or, if they are, they can be solved with respect to σ_0 and included in the ODEs of (2.1.6). Moreover, we assume that the nonlinear system is uncontrolled, *i.e.* $g(x) = 0$ in (2.1.6). This case may represent, for example, a system in closed–loop with some designed controller or for which no control action is allowed. Under these assumptions the dynamical system (2.1.6) reduces to:

$$\dot{x} = f(x), \tag{2.1.10}$$

the equilibria of which are determined by the equilibria equation:

$$0 = f(\bar{x}). \tag{2.1.11}$$

We are now in the position to define the notion of stability of an equilibrium point for the system (2.1.10), similarly to [92].

Definition 2.1.1 (Stability)**.** *Let $\bar{x}$, $x_0 \in \mathcal{X}$, where $\bar{x}$ is an equilibrium point for the system* (2.1.10)*, i.e. it verifies* (2.1.11)*. Then, $\bar{x}$ is said to be:*

- *stable if, for any scalar $\epsilon > 0$, there exist $\delta(\epsilon) > 0$ such that*

$$\|x_0 - \bar{x}\| < \delta, \quad \Rightarrow \quad \|x(t; x_0) - \bar{x}\| < \epsilon, \quad \forall t \geq 0; \tag{2.1.12}$$

- *unstable if it is not stable;*

- *asymptotically stable if it is stable and δ can be chosen such that*

$$\|x_0 - \bar{x}\| < \delta, \quad \Rightarrow \quad \lim_{t \to \infty} \|x(t; x_0) - \bar{x}\| = 0; \tag{2.1.13}$$

- *globally asymptotically stable, if it is stable and $x(t; x_0) \to \bar{x}$ as t goes to infinity for any $x_0 \in \mathcal{X}$.*

It is clear that it is in general difficult to verify the stability of an equilibrium point using the mentioned definitions, because they are tantamount to calculate the solution of the n differential equations

describing the dynamical system (2.1.10). A well–established theory for investigating stability without explicit calculation of the solutions is the Lyapunov theory. At the end of the XIX century, the Russian mathematician Lyapunov showed indeed that particular classes of functions can be used to determine the stability properties of an equilibrium point. In order to introduce this fundamental result, we provide the following useful definitions.

Definition 2.1.2. *Consider a neighborhood of a point $\bar{x} \in \Omega \subseteq \mathbb{R}^n$. A continously differentiable function $\mathcal{V} : \Omega \to \mathbb{R}$ is said to be:*

- *positive definite with respect to $\bar{x}$, if*

$$\mathcal{V}(\bar{x}) = 0, \qquad \mathcal{V}(x) > 0, \ \ \forall x \in \Omega - \{\bar{x}\};$$

- *positive semidefinite with respect to $\bar{x}$, if*

$$\mathcal{V}(\bar{x}) = 0, \qquad \mathcal{V}(x) \geq 0, \ \ \forall x \in \Omega;$$

- *negative definite with respect to $\bar{x}$, if $-\mathcal{V}(x)$ is positive definite;*

- *negative semidefinite with respect to $\bar{x}$, if $-\mathcal{V}(x)$ is positive semidefinite;*

- *indefinite, if $\mathcal{V}(x)$ does not have a definite sign as per one of the cases above.*

We are now ready to state the Lyapunov's stability theorem.

Theorem 2.1.3. *Let $\mathcal{V} : \Omega \to \mathbb{R}$ a positive definite function with respect to the point $\bar{x} \in \Omega \subseteq \mathcal{X}$, that is an equilibrium point for* (2.1.10)*. Then, if its derivative along the trajectories $\dot{\mathcal{V}}(x)$ of the system* (2.1.10) *is:*

- *negative semidefinite with respect to $\bar{x}$, i.e.*

$$\dot{\mathcal{V}}(x) \leq 0, \ \ \forall x \in \Omega, \tag{2.1.14}$$

  the equilibrium point $\bar{x}$ is stable;

- *negative definite with respect to $\bar{x}$, i.e.*

$$\dot{\mathcal{V}}(x) < 0, \ \ \forall x \in \Omega - \{\bar{x}\}, \tag{2.1.15}$$

  the equilibrium point $\bar{x}$ is asymptotically stable.

The positive definite function $\mathcal{V}$ that satisfies the properties (2.1.14) is usually called a *Lyapunov function*. Because stability and asymptotic stability in the sense of (2.1.12), (2.1.13), are concerned only with a subset of the state space $\mathcal{X}$, it is of interest to determine global stability conditions. We have then the following theorem.

Theorem 2.1.4. *Let $\mathcal{V} : \mathbb{R}^n \to \mathbb{R}$ a positive definite function with respect to the point $\bar{x} \in \Omega \subseteq \mathcal{X}$, that is an equilibrium point for* (2.1.10)*. Then, if its derivative along the trajectories $\dot{\mathcal{V}}(x)$ of the system* (2.1.10) *is negative definite, i.e.:*

$$\dot{\mathcal{V}}(x) < 0, \ \ \forall x \in \Omega - \{\bar{x}\}, \tag{2.1.16}$$

and

$$\mathcal{V}(x) \to \infty \quad as \quad \|x\| \to \infty, \tag{2.1.17}$$

the equilibrium point $\bar{x}$ is globally asymptotically stable.

A function that verifies the property (2.1.17) is said to be *radially unbounded*.

In many situations it may be difficult to determine a positive definite function for the system (2.1.10) that verifies (2.1.15), thus stimying the application of Theorem 2.1.3 or Theorem 2.1.4 for the establishment of asymptotic stability. However asymptotic stability can be still inferred with the help of the LaSalle's invariance principle. We first introduce the following definition.

Definition 2.1.5. *The set $\Omega \subseteq \mathcal{X}$ is said to to be positively invariant with respect to* (2.1.10) *if for any $x_0 \in \Omega$, $x(t; x_0) \in \Omega$ for any $t \geq 0$.*

Theorem 2.1.6. *Let $\omega \subset \mathcal{X}$ be a positively invariant, compact set with respect to* (2.1.10)*. Let $\mathcal{V} : \mathcal{X} \to \mathbb{R}$ be a continuously differentiable function that verifies $\dot{\mathcal{V}}(x) \leq 0$ in Ω. Let M the largest invariant set contained in the subset of Ω such that $\dot{\mathcal{V}}(x) = 0$. Then everyy solution starting in Ω approaches M as $t \to \infty$.*

We have then the following corollary, that extend Theorem 2.1.3 and Theorem 2.1.4 to the case where $\mathcal{V}(x)$ is not positive definite.

Corollary 2.1.7. *Let $\bar{x}$ an equilibrium point for* (2.1.10)*. Let $\mathcal{V} : \mathcal{X} \to \mathbb{R}$ be a continuously differentiable function that is positive definite with respect to $\bar{x}$ and verifies $\dot{\mathcal{V}}(x) \leq 0$ in $\mathcal{X}$. Consider the set $S := \{x \in \mathcal{X} : \dot{\mathcal{V}}(x) = 0\}$ and suppose that no solution can stay identically in S, except the trivial solution $x(t) \equiv \bar{x}$. Then $\bar{x}$ is asymptotically stable. If moreover $\mathcal{X} \equiv \mathbb{R}^n$ and $\mathcal{V}$ is radially unbounded, it is globally asymptotically stable.*

Theorems 2.1.3 and 2.1.4 are usually referred as Lyapunov's second method for checking stability of an equilibrium point, while Theorem 2.1.6 and Corollary 2.1.7 are known as LaSalle's invariance principle and its criterion for asymptotic stability. We next provide a further method that allows to establish local stability properties of a nonlinear system and that is known as Lyapunov's first method.

Theorem 2.1.8. *Let $\bar{x}$ an equilibrium point for* (2.1.10) *and define $J(\bar{x}) := \frac{\partial f}{\partial x}(\bar{x})$. If:*

- *$\mathfrak{Re}\{\lambda_i(J(\bar{x}))\} < 0$ for all eigenvalues λ_i of $J(\bar{x})$, then the equilibrium point is locally asymptotically stable and the matrix $J(\bar{x})$ is said to be an Hurwitz or stability matrix;*
- *$\mathfrak{Re}\{\lambda_i(J(\bar{x}))\} > 0$ for at least one eigenvalue λ_i of $J(\bar{x})$, then the equilibrium point is unstable.*

2.1.6 Zero Dynamics

Some important properties of general nonlinear systems can be characterized using the concept of zero dynamics. For this purpose, we briefly introduce the fundamental notions of *relative degree* and *normal form*. For more rigourous definitions, the reader is referred to [82, 27].

Let consider an ODEs nonlinear system in input–affine form expressed by:

$$\begin{aligned} \dot{x} &= f(x) + g(x)u \\ y_r &= h(x, u), \end{aligned} \tag{2.1.18}$$

where input and output vectors have the same dimension $m = q$. Such a (multi–input multi–output) system is said to have *relative degree* $\{1, 1, \ldots, 1\}$ at a point x_0 if the matrix

$$A(x_0) := \left[\frac{\partial h}{\partial x} \cdot g(x)\right]_{x=x_0}$$

is nonsingular. If this is the case, under a further controllability condition[2], there exist $n - m$ functions $z_1(x), \ldots, z_{n-m}(x)$, defined in a neighborhood of x_0 and vanishing at x_0, which, together with the m components of the output map $y_r = h(x)$, qualify as a new set of local coordinates. Hence, the system can be represented in new coordinates (z, y) as follows [27]:

$$\begin{aligned} \dot{z} &= q(z, y) \\ \dot{y} &= b(z, y) + a(z, y)u, \end{aligned} \tag{2.1.19}$$

that is called the *normal form* of the system (2.1.18).

Moving from these definitions, the *zero dynamics* is defined as the internal dynamics of the system that are induced by *zeroing the output*, *i.e.* by constraining the system to:

$$y(t) \equiv 0, \qquad \forall t \geq t_0.$$

If a system has relative degree $\{1, 1, \ldots, 1\}$ at $x = x_0$, its zero dynamics locally exist in a neighborhood $\mathcal{I}$ of x_0, evolve on the smooth $(n - m)$– dimensional submanifold:

$$\mathcal{Z}^\star = \{x \in \mathcal{I}(x_0) \ : \ h(x) = 0\}, \tag{2.1.20}$$

that is called the *zero dynamics manifold*. Moreover it is described by a differential equation of the form:

$$\dot{z} = q(z, 0), \tag{2.1.21}$$

while the input is given by $u = -\left[a(z, 0)\right]^{-1} b(z, 0)$. Such dynamics can be equivalently rewritten in the original coordinates as:

$$\dot{x} = f^\star(x), \qquad x \in \mathcal{Z}^\star, \tag{2.1.22}$$

that is the restriction to $\mathcal{Z}^\star$ of the system (2.1.18).

Depending on the stability property of the zero dynamics of the system, we have the following definitions [27]. The system (2.1.18) is said to be: *minimum phase*, if its zero dynamics is asymptotically stable; *weakly minimum phase*, if its zero dynamics is stable; *non–minimum phase* if its zero dynamics is unstable.

2.1.7 Passivity

Passivity is a notion widely diffused to describe the input–output behavior of a system, see [169, 159, 27] for an overview from a control theory perspective. For a precise definition we consider the ODEs nonlinear system in input–affine expressed by (2.1.18), where input and output vectors are of the same dimension, that is $m = q$. Consider the function $s : \mathcal{U} \times \mathcal{Y}_r \to \mathbb{R}$, that is called the *supply rate* of the

[2]The controllability condition consists in that the distribution spanned by the columns of $g(x)$ is involutive [82, 117].

system and assume that for any $u \in \mathcal{U}$ and initial condition $x_0 = x(t_0)$, the output trajectory $y_r(t)$ is such that:

$$\left| \int_{t_0}^{t} s(u(\tau), y_r(\tau)) \mathrm{d}\tau \right| < \infty. \tag{2.1.23}$$

We have then the following definitions.

Definition 2.1.9 (Dissipativity)**.** *The system* (2.1.18) *is said to be dissipative with respect to the supply rate s if there exists a function $\mathcal{V} : \mathcal{X} \to \mathbb{R}^+$, called the storage function, such that for all $x_0 \in \mathcal{X}$, all $t_1 \geq t_0$ and all input functions $u \in \mathcal{U}$, we have:*

$$\mathcal{V}(x(t_1; x_0)) \leq \mathcal{V}(x_0) + \int_{t_0}^{t_1} s(u(t), y_r(t)), \mathrm{d}t. \tag{2.1.24}$$

If (2.1.24) *holds with equality, then the system is said to be lossless.*

The inequality is called *dissipation inequality*. A special case of the dissipativity inequality (2.1.24) arises when the supply rate is defined as:

$$s(u, y_r) := u^\top y_r, \tag{2.1.25}$$

from which follow the next definitions.

Definition 2.1.10 (Passivity)**.** *The system* (2.1.18) *is said to be:*

- *passive (conservative), if it is dissipative (lossless) with respect to the supply rate* (2.1.25)*;*
- *input strictly passive, if there exists a scalar $\delta > 0$ such that the system is dissipative with respect to the supply rate:*
$$s(u, y_r) = u^\top y_r - \delta \|u\|^2;$$
- *output strictly passive, if there exists a scalar $\epsilon > 0$ such that the system is dissipative with respect to the supply rate:*
$$s(u, y) = \sigma^\top y_r - \epsilon \|y_r\|^2.$$

We now provide a characterization of the zero dynamics of passive systems recalling the following theorem, formulated in [27].

Theorem 2.1.11. *Suppose that the system* (2.1.18) *is passive with a positive definite storage function $\mathcal{V}$. Suppose that either:*

$$x^\star := \arg\min \mathcal{V}$$

is a point of regularity for the system or that $\mathcal{V}$ is nondegenerate. Then the zero dynamics of the system locally exist at $x = x^\star$ and the system is weakly minimum phase.

For the special case of port–Hamiltonian systems we have the following passivity property [159].

Lemma 2.1.12. *Let consider the system* (2.1.1) *with input and output signals given by:*

$$\hat{u} := \mathrm{col}(u, \sigma, \sigma_0), \qquad \hat{y} := \mathrm{col}(y_r, y, y_0). \tag{2.1.26}$$

with $y_r := g^\top(x) \nabla \mathcal{H}$. Then the system is passive with storage function given by $\mathcal{H}$.

Proof. For the proof it suffices to calculate the derivative of $\mathcal{H}$ along the trajectories, thus giving:

$$\begin{aligned}\dot{\mathcal{H}} &= -(\nabla\mathcal{H})^\top \mathcal{R}\nabla\mathcal{H} + (\nabla\mathcal{H})^\top gu + (\nabla\mathcal{H})^\top G\sigma + (\nabla\mathcal{H})^\top G_0\sigma_0 \\ &= -(\nabla\mathcal{H})^\top \mathcal{R}\nabla\mathcal{H} + \hat{y}^\top\hat{u} \leq \hat{y}^\top\hat{u},\end{aligned} \tag{2.1.27}$$

that proves passivity.

□□□

2.2 Electric systems

2.2.1 Lumped parameters assumption

An electric system can be viewed as the composition of smaller electric subsystems — that from now on we call *power units* — that are interconnected according to an appropriate circuit topology. All along this thesis we make the following assumption.

Assumption 2.2.1. *All power units composing an electric system can be represented by lumped parameters models.*

This assumption implies that all electric subsystems (power units) can be described as the composition of a certain number of ideal elements with no geometrical dimension. This is equivalent to assume that such elements have negligible physical dimension with respect to the generated electromagnetic field [109].

Under the limits of validity of the lumped parameter assumption a power unit can be characterized by a pair of generalized port variables, effort and flow, that correspond to the fundamental electric quantities of *voltage* $v(t)$ and *current* $i(t)$. These two quantities are then related by some mathematical expressions that can be of different type (differential, algebraic, differential–algebraic) and that describe the physical characteristics of the power unit [43, 168, 109]. The simplest power units are: ideal generators, resistors, inductors and capacitors, transformers and gyrators, that correspond indeed to elementary energy behaviors expressed by source and sink, dissipation, storage and transformation elements. Standard description of elementary power units can be found in any basic textbook of electric circuits, see for example [109], and is for this reason omitted. For more details about fundamental energy element, see [85] for the electric domain, or [43, 168] for generalized multiphysics systems. The positive and negative signs of voltage and current are arbitrary. However, to avoid confusion, we adopt the sign convention for which their by product, that is a power, is equivalent to the power *absorbed* by the power units from the environment. For a precise definition of power, the reader is referred to Subsection 2.2.5.

2.2.2 Dc and ac signals

Electric systems employ two alternatives way of generating, transmitting and utilizing power: direct–current (dc) and alternating–current (ac). The denomination refers explicitly to current signals, but usually the abbreviations ac and dc stands for general time–varying electric signal. Dc and ac signals play an important role in electric power systems. As a matter of fact, for single–phase and three–phase systems — that are the most diffused architectures — it is often of practical interest that, in steady–state operation, electric signals waveform are of dc or ac type. Hence, it is usual to refer to such systems as dc and ac systems. Both ac and dc describe types of current flow in a circuit, but there are some

differences. Indeed, in dc, the electric charges moves only in one direction, from which follows that the voltage is also unipolar, thus meaning that one pole is always at an higher voltage than the other. Electric charges in ac, on the other hand, periodically reverse their direction [40, 109]. As a result, the voltage reverses polarity along with the current. We then introduce the following definitions — based on [140, 109] — for an electric time–varying signal $x(t)$, that can either represents a current or a voltage.

Definition 2.2.2. *A real (time–varying) electric signal $x : \mathbb{R}_+ \to \mathbb{R}$ is said to be a dc signal if it is constant in time, that is*

$$x(t) = \bar{x}.$$

Definition 2.2.3. *A real (time–varying) electric signal $x : \mathbb{R}_+ \to \mathbb{R}$ is said to be a single–phase T–periodic ac signal if:*

- *it is periodic, with period $T \in \mathbb{R}_+$, that is*

$$x(t) = x(t + kT), \qquad k \in \mathbb{N};$$

- *it has zero arithmetic mean over the period, that is*

$$\int_{T,i}^{t+T} x(\tau)\mathrm{d}\tau = 0.$$

Note that from these definitions it follows that a dc signal can be interpreted as a single–phase ac signal with period $T = \infty$. An appropriate composition of three single–phase ac signals leads to the following definitions.

Definition 2.2.4. *A real (time–varying) electric signal $x_{3\phi} : \mathbb{R}_+ \to \mathbb{R}^3$ is said to be a three–phase T–periodic ac signal if any of its components is a single–phase T–periodic ac signal for a unique $T \in \mathbb{R}_+$.*

Definition 2.2.5. *Consider a three–phase T–periodic ac signal $x_{3\phi} : \mathbb{R}_+ \to \mathbb{R}^3$. It is said to be balanced if:*

$$x_{3\phi}(t) := \begin{bmatrix} x_a(t) \\ x_b(t) \\ x_c(t) \end{bmatrix} = X(t) \begin{bmatrix} \sin(\alpha(t)) \\ \sin(\alpha(t) - \frac{2}{3}\pi) \\ \sin(\alpha(t) + \frac{2}{3}\pi) \end{bmatrix}. \tag{2.2.1}$$

Moreover, $X : \mathbb{R}_+ \to \mathbb{R}$ is referred as the amplitude and $\alpha : \mathbb{R}_+ \to \mathbb{S}$ as the phase angle of the three–phase ac signal.

Note that three–phase T–periodic ac signals are completely described by the pair (X, α) and can be alternatively represented using these two quantities, that are called *polar coordinates* of the three–phase ac signal, in contrast with the *abc coordinates* expressed by (2.2.1).

2.2.3 Dq0–transformation

While considering three–phase signals, in many situations it may be convenient to adopt a reference frame that does not coincide with the *abc*–reference frame in which the signal is usually expressed. It is then possible to perform a transformation of coordinates so that the transformed waveform is represented in a more suitable form for the purpose of analysis. It is common to employ the following transformation, that was originally formulated by Robert H. Park, in 1929 [118].

Definition 2.2.6. *Let $\vartheta : \mathbb{R}_+ \to \mathbb{S}$. The mapping $T_{dq0} : \mathbb{S} \to \mathbb{R}^{3\times 3}$, with*

$$T_{dq0}(\vartheta) := \sqrt{\frac{2}{3}} \begin{bmatrix} \cos(\vartheta) & \cos(\vartheta - \frac{2}{3}\pi) & \cos(\vartheta + \frac{2}{3}\pi) \\ \sin(\vartheta) & \sin(\vartheta - \frac{2}{3}\pi) & \sin(\vartheta + \frac{2}{3}\pi) \\ \frac{\sqrt{2}}{2} & \frac{\sqrt{2}}{2} & \frac{\sqrt{2}}{2} \end{bmatrix},$$

is called a $dq0$–transformation with angle ϑ. Moreover

$$x_{dq0}(\vartheta(t), x_{3\phi}(t)) := \begin{bmatrix} X_d(t) \\ X_q(t) \\ X_0(t) \end{bmatrix} = T_{dq0}(\vartheta(t)) x_{3\phi}(t),$$

is called the correspondent $dq0$–transformed signal, where $X_d(t)$, $X_q(t)$, $X_0(t)$ are named respectively its direct, quadrature and 0–components.

$Dq0$–transformations are widely employed to obtain an alternative representation of balanced three–phase ac signals [7, 96]. The frame in which the signal is represented is usually called $dq0$–frame, in contrast with the abc–frame, that is the natural frame for three–phase ac signals. By applying the transformation to (2.2.1), we have:

$$\begin{aligned} x_{dq0} &= T_{dq0}(\vartheta) x_{3\phi} \\ &= \sqrt{\frac{2}{3}} X \begin{bmatrix} \cos(\vartheta)\sin(\alpha) + \cos(\vartheta - \frac{2}{3}\pi)\sin(\alpha - \frac{2}{3}\pi) + \cos(\vartheta + \frac{2}{3}\pi)\sin(\alpha + \frac{2}{3}\pi) \\ \sin(\vartheta)\sin(\alpha) + \sin(\vartheta - \frac{2}{3}\pi)\sin(\alpha - \frac{2}{3}\pi) + \sin(\vartheta + \frac{2}{3}\pi)\sin(\alpha + \frac{2}{3}\pi) \\ \frac{\sqrt{2}}{2}\sin(\alpha) + \frac{\sqrt{2}}{2}\sin(\alpha - \frac{2}{3}\pi) + \frac{\sqrt{2}}{2}\sin(\alpha + \frac{2}{3}\pi) \end{bmatrix} \\ &= \sqrt{\frac{3}{2}} X \begin{bmatrix} \sin(\alpha - \vartheta) \\ \cos(\alpha - \vartheta) \\ 0 \end{bmatrix}, \end{aligned}$$

where the last equivalence follows by standard trigonometric formulas. Because of the 0–component is always zero, it is shown that any three–phase balanced ac signal can be mapped into a two dimensional space by means of a $dq0$–transformation. Let then:

$$\vartheta(t) = \alpha(t) - \varphi_0,$$

where φ_0 is constant. With this choice the $dq0$–transformed signal is given by:

$$x_{dq0} = \begin{bmatrix} \bar{X}_d \\ \bar{X}_q \\ \bar{X}_0 \end{bmatrix} = \sqrt{\frac{3}{2}} X \begin{bmatrix} \sin(\varphi_0) \\ \cos(\varphi_0) \\ 0 \end{bmatrix},$$

that is also constant. Recalling then Definition 2.2.2, it this easy to see that the original three–phase ac signal can be transformed into a two–dimensional signal, where both components are of dc–type.

Because in this work we focus exclusively on system driven by balanced three–phase ac and dc signals, we find convenient to define the following transformation $T_{dq} : \mathbb{S} \to \mathbb{R}^{2\times 3}$, with:

$$T_{dq}(\vartheta) := \sqrt{\frac{2}{3}} \begin{bmatrix} \cos(\vartheta) & \cos(\vartheta - \frac{2}{3}\pi) & \cos(\vartheta + \frac{2}{3}\pi) \\ \sin(\vartheta) & \sin(\vartheta - \frac{2}{3}\pi) & \sin(\vartheta + \frac{2}{3}\pi) \end{bmatrix},$$

that applied to a balanced three–phase ac signal $x_{3\phi}$, gives the following dq–transformed signal

$$x_{dq} = \begin{bmatrix} X_d \\ X_q \end{bmatrix} = T_{dq}(\vartheta) x_{3\phi} = \sqrt{\frac{3}{2}} X \begin{bmatrix} \sin(\alpha - \vartheta) \\ \cos(\alpha - \vartheta) \end{bmatrix}.$$

2.2.4 Representation of ac signals in the complex domain

We now recall some fundamental notions about representation of ac signals in the complex domain. A very common waveform for electric ac signals, single–phase or three–phase, is of sinusoidal type of the following form[3]:

$$x(t) = X \cos(\omega t + \varphi), \tag{2.2.2}$$

where X, ω, φ are respectively the amplitude, the (costant) frequency and the phase shift of the sinusoidal ac signal. If we consider X and φ as the polar coordinates of a point p in a two–dimensional plane, it is obvious that there is a one–to–one mapping between the function (2.2.2) and the point p. Such a plane is usually called *phasor (complex) domain* and the quantity:

$$\mathbf{X} = X e^{j\varphi}, \tag{2.2.3}$$

is called the *phasor* of the function (2.2.2).
It is possible to determine a clear relationship between the function $x(t)$ and the correspondent phasor $\mathbf{X}$. Using Euler's formula we have indeed:

$$x(t) = X \cos(\omega t + \varphi) = X \frac{e^{j(\omega t + \varphi)} + e^{-j(\omega t + \varphi)}}{2}, \tag{2.2.4}$$

from which follows

$$x(t) = \frac{\mathbf{X} e^{j\omega t} + \mathbf{X}^\star e^{-j\omega t}}{2} = \mathfrak{Re}\{\mathbf{X} e^{j\omega t}\}. \tag{2.2.5}$$

We next provide voltage–current characteristics for resistive, inductive and capacitive elements in the phasors domain, as available in basic textbooks of electrotechnics, see for example [109].

Resistive. The voltage-current time-domain relation of a purely resistive element is given by Ohm's law

$$v(t) = Ri(t) \qquad \text{or} \qquad i(t) = Gv(t), \quad G := \frac{1}{R}, \tag{2.2.6}$$

with R, G called respectively the resistance and the conductance of the element. The correspondent voltage-current phasors–domain relation is given by

$$\mathbf{V} = R\mathbf{I}. \tag{2.2.7}$$

Inductive. The voltage-current time-domain relation of a purely inductive element is given by the ordinary differential equation

$$L\dot{i}(t) = v(t), \tag{2.2.8}$$

with L called the inductance of the element. The correspondent voltage-current phasors-domain relation is given by

$$\mathbf{V} = jX_L\mathbf{I}, \qquad X_L := \omega L,$$

[3] A purely sinusoidal signal can be always rewritten as a cosinusoidal signal.

where X_L is called *inductive reactance*.

Capacitive. The voltage-current time-domain relation of a purely capacitive element is given by the ordinary differential equation

$$C\dot{v}(t) = i(t), \tag{2.2.9}$$

with L called the inductance of the element. The correspondent voltage-current phasors-domain relation is given by

$$\mathbf{V} = jX_C\mathbf{I}, \qquad X_C := -\frac{1}{\omega C}$$

where X_C is called *capacitive reactance*.

Generalized impedance. The complex number:

$$Z := R + jX, \tag{2.2.10}$$

where R is a resistance and X is a sum of reactances, that is

$$X := \sum_{i=1}^{n_C} X_{C,i} + \sum_{k=1}^{n_L} X_{L,k},$$

is called a *generalized impedance*. The complex number

$$Y := \frac{1}{Z}, \tag{2.2.11}$$

is called a *generalized admittance*. Noting that Y is also a complex number, it can be rewritten as:

$$Y = G + jB, \tag{2.2.12}$$

where G, B are called respectively *conductance* and *susceptance* of the generalized admittance.

2.2.5 Power definitions

Consider a power unit with voltage–current generalized variables pair $(v(t), i(t))$. The power, in a strict physical sense, is defined as the rate of absorbing work W through the port, that is:

$$P(t) := \frac{dW(t)}{dt} = \frac{dW}{dq}\frac{dq}{dt} = v(t) \cdot i(t), \tag{2.2.13}$$

where q represent the electrical charge. This signal in general a time-varying signal and is usually called *instantaneous power*.

However, it is well–known that instantaneous power is not sufficient to describe the power behavior of three–phase power units, because of the existence of terms representing the *nonactive power*, due to the oscillations associated to storage elements [109]. Hence, we introduce the following definitions of instantaneous active, reactive and apparent power under balanced, but not necessarily steady-state,

conditions. Let the following pair of balanced three–phase voltage and current:

$$v_{3\phi}(t) = \sqrt{2}V(t)\begin{bmatrix}\sin(\alpha_V(t))\\ \sin(\alpha_V(t)-\frac{2}{3}\pi)\\ \sin(\alpha_V(t)+\frac{2}{3}\pi)\end{bmatrix}, \quad i_{3\phi}(t) = \sqrt{2}I(t)\begin{bmatrix}\sin(\alpha_I(t))\\ \sin(\alpha_I(t)-\frac{2}{3}\pi)\\ \sin(\alpha_I(t)+\frac{2}{3}\pi)\end{bmatrix}, \tag{2.2.14}$$

where $\alpha_V : \mathbb{R}_+ \to \mathbb{S}$, $\alpha_I : \mathbb{R}_+ \to \mathbb{S}$ are the phase angles, and $\sqrt{2}V : \mathbb{R}_+ \to \mathbb{R}_+$, $\sqrt{2}I : \mathbb{R}_+ \to \mathbb{R}$ the amplitude of the voltage and current signals. Using the dq–transformation introduced in Subsection 2.2.3, it is easy to obtain the dq–transformed signals:

$$v_{dq} = \begin{bmatrix}V_d\\ V_q\end{bmatrix} = \sqrt{3}V(t)\begin{bmatrix}\sin(\alpha_V(t)-\vartheta(t))\\ \sin(\alpha_V(t)-\vartheta(t))\end{bmatrix}, \quad v_{dq} = \begin{bmatrix}I_d\\ I_q\end{bmatrix} = \sqrt{3}I(t)\begin{bmatrix}\sin(\alpha_I(t)-\vartheta(t))\\ \sin(\alpha_I(t)-\vartheta(t))\end{bmatrix}. \tag{2.2.15}$$

We now introduce the following definition, that are based on [6, 140].

Definition 2.2.7. *Let $v_{dq}(t)$ and $i_{dq}(t)$ be given by* (2.2.15)*. The instantaneous three-phase active power is defined as*

$$P(t) := v_{dq}^\top(t) i_{dq}(t) = V_d(t)I_d(t) + V_q(t)I_q(t). \tag{2.2.16}$$

The instantaneous three-phase reactive power is defined as

$$Q(t) := v_{dq}^\top(t) J_2 i_{dq}(t) = V_d(t)I_q(t) - V_q(t)I_d(t). \tag{2.2.17}$$

Finally, the instantaneous three-phase (complex) apparent power is defined as

$$S(t) := P(t) + jQ(t). \tag{2.2.18}$$

Chapter 3

Modeling of electric power systems

3.1 Introduction

3.1.1 Motivation

Market liberalization and the ever increasing electricity demand have forced the power systems to operate under highly stressed conditions. This situation has led to the need to revisit the existing modeling, analysis and control techniques that enable the power system to withstand unexpected contingencies without experiencing voltage or transient instabilities. At the network level power engineers used reduced network models (RNM) where the system is viewed as an n–port described by a set of ordinary differential equations. RNMs do not retain the identity of the network components and induces non–negligible values to the conductances which hinders present energy–like functions for stability analysis and also complicates controller design. Even for constant impedance loads terminated to ground at the load buses the analysis becomes quite difficult with RNMs due to transfer conductances appearing in reduced admittance matrices. The concept of energy functions in the presence of transfer conductances is not clear. In order to overcome the aforementioned difficulties in RNMs, structure preserving models (SPM) were first proposed in [16], and later refined in [157] (for a review see [162]). In SPMs the structure remains intact and complete with load buses paving the way for easy inclusion of nonlinear loads [77]. SPMs foster the approach to view the entire network as the power–preserving interconnections of its components such as generators, transmission lines and loads whose dissipativity–based properties may be added to study the overall system's stability. The SPMs consists of differential algebraic equations (DAEs). In [73] SPM with nonlinear loads have been used with the singular perturbation approach, in which the algebraic equations are considered as a limit of fast dynamics to calculate an $\mathcal{L}_2$–gain disturbance attenuation control. The network was assumed to be lossless. The approach of fast dynamics is used in order to circumvent the singular properties in the nonlinear differential algebraic system. In [39] SPM is used to design a globally convergent controller for the transient stability of multi–machine power systems. At the synchronous generator level, power engineers used simplified, reduced order, models that neglect some fast transients and losses (see [41]). In particular, it is assumed that the electrical magnitudes can be represented via (first harmonic) phasors, and the generator dynamics is reduced to a second or a third order model. On the other hand, these reductions may result in loss of physical structure, leading to some approximate rationalizations of the new quantities, *e.g.*, the concept of "voltage behind the reactance". The urge to develop a complete nonlinear, structure preserving model which is useful for studying power system stability still exists. Furthermore, with

the recent developments in various types of renewable energy–sources and energy–storing devices there is a strong need for a unifying modeling framework which can treat different components on an equal footing.

3.1.2 Main contributions

This chapter is dedicated to introduce a novel, generalized approach for the modeling of electric power systems, that is based on two main mathematical tools that have been introduced in the previous chapter: graph theory for the description of the *circuit topology* and the port–Hamiltonian framework for the description of the *power units*. The remainder of the chapter is organized as follows. First of all, in Section 3.2, a qualitative classification of components constituting an electric power system is provided. In Section 3.3 we then present a procedure for the description of the power system topology, based on linear graph theory. The generalized port–Hamiltonian models of the power units are introduced in Section 3.4. The overall model, that is obtained by combining the mentioned graph description and the individual port–Hamiltonian models of the power units, is finally presented in Section 3.5.

3.2 Classification

An electric power system is a complex physical system that is employed for generation, transmission and utilization of electricity. It is traditionally defined as the interconnection of smaller subsystems that belong to the following macro categories [96, 7]:

- generation
- transmission, sub–transmission and distribution
- utilization.

An example of such a classification is illustrated in Fig. 3.1. It is also common to refer to the transmission, sub–transmission and distribution category as the network subsystem. This classification stems from the traditional architecture of electric power systems, that has been for a long time dominated by a few type of components: large–size fuel–based ac synchronous generators for the generation, passive loads for the utilization, lossy transmission lines and passive transformers for the network. However, because of the unrelenting penetration of renewable energy sources, the recent advancements in switched power electronics and the diversification of modern power loads, this scenario is rapidly mutating [151, 50]. This fact adds particular value to the modeling approach that we propose in the next sections, since it provides a unifying framework which can treat different components on an equal footing. All this considered, the purpose of this chapter is not to give an overarching collection of specific models for any subsystem that may constitute a modern power system — this being burdensome considering the wide variety of scenarios — but more likely to provide a generalized approach for the description of power systems using the fundamental notions of *energy* and *port*. To simplify the presentation of our results, we make the following assumption.

Assumption 3.2.1. *Interactions between subsystems occur through ports of the same dimension p and are fully determined by power preserving interconnection laws.*

This assumption is equivalent to assume that all interconnections between power units occur through the same number of phases p and that no power is dissipated through them, *i.e.* any interconnection law between two subsystems need to verify (2.1.5). Standard architectures are typically cosntituted by

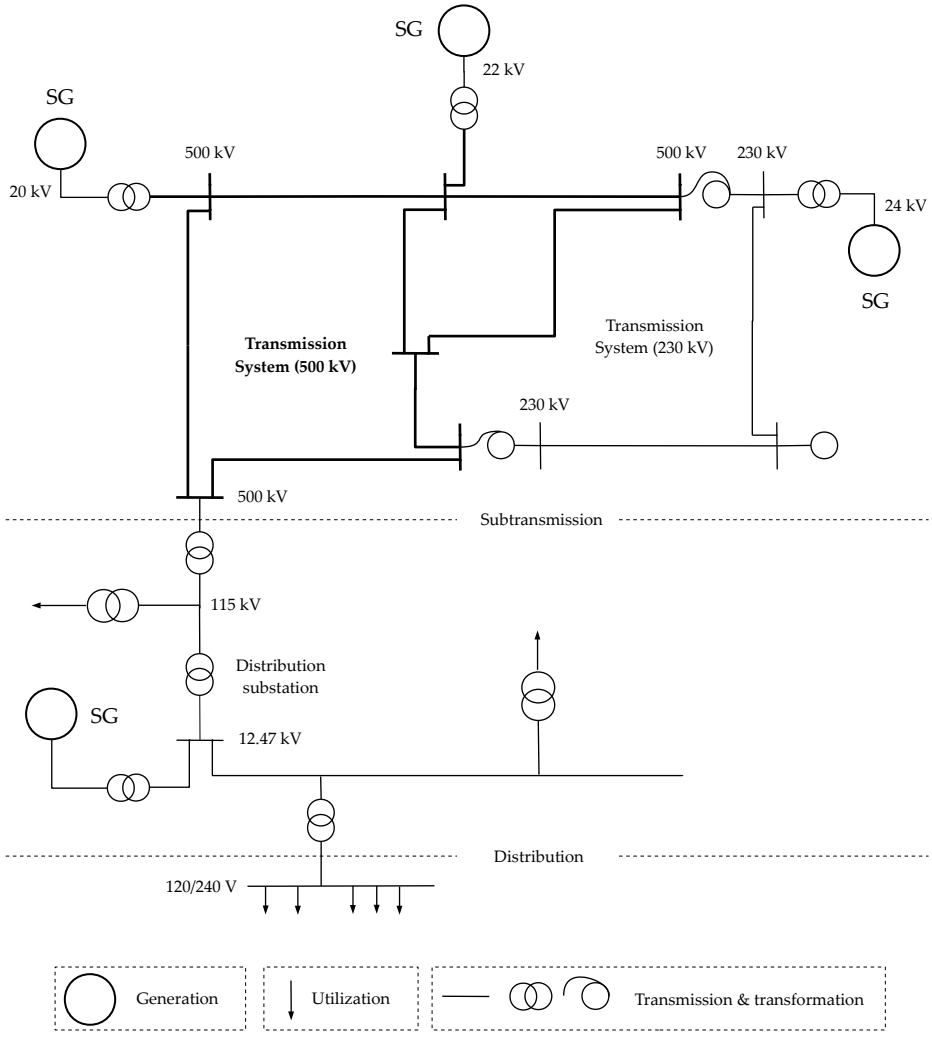

Figure 3.1: Standard classification of a traditional electric power system [96].

three–phase ($p = 3$), single–phase ($p = 1$), or a mix of three–phase and single–phase interconnections, the last implying that the value of p may change depending on the point of interconnection considered. Although we consider only the case in which p is the same at all interconnection points, it will result clear from the next subsections that the modeling procedure can be easily extended to the mixed general case with no loss of generality.

We propose to classify power units according to the traditional paradigm generation–transmission–utilization. Hence, we assume that units can be *generation* or *utilization units*, that correspond respectively to units injecting a relevant amount of power into the environment or absorbing a relevant power from the environment — over a given period of time. If the amount of power injected or absorbed is little compared with the amount injected or absorbed by the other generation and utilization units, such units are referred as *transmission units*.

Remark 3.2.2. It is obvious that the adopted classification provides only a qualitative characterization of the power units. As a matter of fact — when a mode of operation is not a priori fixed — a power unit may operate alternatively as a generation or as an utilization unit. Different classifications can be then considered, depending on the purpose of the analysis. For instance, units can be classified in terms of their controllability or regrouped according to analogous modes of operation.

3.3 Circuit topology: a graph description

An electric power system can be viewed as an unweighted directed graph $\mathcal{G}^{\uparrow}$ where power units correspond to edges and buses correspond to nodes. Based on the mentioned classification we call a bus: a *generation bus* when a generation unit is connected to it; an *utilization bus* when an utilization unit is connected to it; a *transmission bus* when nor generation nor utilization units are connected to it. All buses associate a potential and we call a bus a *reference bus* when all the potential of the buses in the power system are measured with respect to it. The reference bus is assumed to be at ground potential. The generation, utilization and reference buses are boundary buses, while the transmission buses are interior buses. Because it is always possible to eliminate these interior buses through a process, that is called Kron–reduction [42, 160], we make the following assumption.

Assumption 3.3.1. *The graph $\mathcal{G}^{\uparrow}$ has no interior nodes.*

Let there be g generation buses and r utilization buses and one reference bus. Then the total number of buses (nodes) of the power system (graph) is $\mathsf{n}+1$, with $\mathsf{n}=\mathsf{g}+\mathsf{r}$. Without loss of generality we assume that the set of nodes $\mathcal{N}$ can be partitioned into three ordered subsets called $\mathcal{N}_G$, $\mathcal{N}_R$ and the one–element set $\mathcal{N}_0$ associated to generation, utilization nodes and the reference node respectively. We call $\mathcal{V}\in\mathbb{R}^{\mathsf{n}+1}$ the vector of node potentials. There is a *generation edge* — associated to a generation unit — between every generation node and the reference node and there is an *utilization edge* — associated to an utilization unit — between the utilization node and the reference node. It is a standard practice to define power units such that their interaction with the environment is modeled by a voltage capacitor at the given bus of interconnection. Nevertheless, as there might be several power units attached at the same bus, this will result in the parallel connection of a certain number of capacitors at the bus. For simplicity then, and with no loss of generality, we make the following assumption.

Assumption 3.3.2. *All (possibly lossy) capacitors in parallel connection at a given bus are replaced by an equivalent capacitor, whose dynamics are fully described by a capacitor edge.*

Consequently, all capacitors that are shared by power units at their point of interconnection can be safely neglected and there is an equivalent *capacitor edge* between every generation or utilization node and the reference node. Therefore there are in total g generation, r utilization and $\mathsf{g}+\mathsf{r}$ capacitor edges. Let there be t the number of *transmission edges* — associated to transmission units — that connect generation and utilization buses. Hence there are in total $\mathsf{m}=2\mathsf{g}+2\mathsf{r}+\mathsf{t}$ edges. Without loss of generality we assume that the set of edges $\mathcal{E}$ can be partitioned into four ordered subsets called $\mathcal{E}_G$, $\mathcal{E}_R$, $\mathcal{E}_T$, $\mathcal{E}_C$, associated to generation, utilization, transmission and capacitor edges respectively. We call $(V_e, I_e)\in\mathbb{R}^{\mathsf{m}}\times\mathbb{R}^{\mathsf{m}}$ the vectors pair associated to edge voltages and currents respectively. Note that because of Assumption 3.2.1 implies that all power units share a port of the same dimension p, each node/edge defined above corresponds to p nodes/edges representing the different phases. Hence, all the definitions provided hold *modulo* p, where p is the (uniform) number of phases. Then, under Assumption 3.2.1, Assumption 3.3.1 and Assumption 3.3.2, the topology of the electric power system

is fully described by a directed graph $\mathcal{G}^{\uparrow}$ to which are associated the vectors $\mathcal{V}$, V_e, I_e and the following one–phase incidence matrix:

$$\mathcal{B} = \begin{bmatrix} \mathbb{I}_{\mathsf{g}} & 0 & \mathcal{B}_G & \mathbb{I}_{\mathsf{g}} & 0 \\ 0 & \mathbb{I}_{\mathsf{r}} & \mathcal{B}_R & 0 & \mathbb{I}_{\mathsf{r}} \\ -1_{\mathsf{g}}^{\top} & -1_{\mathsf{g}}^{\top} & 0 & -1_{\mathsf{r}}^{\top} & -1_{\mathsf{r}}^{\top} \end{bmatrix} \in \mathbb{R}^{(\mathsf{n}+1)\times \mathsf{m}}. \tag{3.3.1}$$

The submatrix

$$\mathcal{B}_{net} = \mathcal{B}(\mathcal{G}^{\uparrow}_{net}) = \begin{bmatrix} \mathcal{B}_G \\ \mathcal{B}_R \end{bmatrix} \in \mathbb{R}^{\mathsf{n}\times \mathsf{t}}, \tag{3.3.2}$$

represents the one–phase incidence matrix of the sub–graph $\mathcal{G}^{\uparrow}_{net}$, that is obtained by eliminating the reference node and edges that are connected to it. The incidence matrix $\mathcal{B}_{net}$ thus captures the information about the interconnection structure of generation and utilization units, *i.e.* the interconnection structure of the network. To avoid confusion, in the sequel we refer to: $\mathcal{G}$ and $\mathcal{B}$ as the *power system graph* and the *power system incidence matrix*; to $\mathcal{G}_{net}$ and $\mathcal{B}_{net}$ as the *network graph* and the *network incidence matrix*. The latter in particular plays a significant role in the construction of network reduced models, see for example Section 4.8 in Chapter 4, where this is investigated for the specific case of high–voltage direct current transmission systems. An example of graph, that corresponds to the power system depicted in Fig. 3.1 is provided in Fig. 3.2.

Remark 3.3.3. *A similar graph–based description can be obtained using bond graph theory, as developed in [180]. This has the interesting feature to lead naturally to the formulation of a port–Hamiltonian representation of the power units [43].*

3.4 Power units as edges: a port–Hamiltonian representation

3.4.1 Generation edge

According to the mentioned classification we call a generation unit i a power unit that injects a *relevant* amount of power into the network to which it is connected through a port of dimension p_i. Using Assumption 3.2.1 we have $p_i = p$. There are g generation units, the totality of which constitutes the *generation subsystem*. In order to describe the dynamics of the generation edges we consider a port–Hamiltonian system of the form (2.1.1), that is

$$\mathcal{S}_i : \quad i \sim \mathcal{E}_G \quad \begin{cases} \dot{x}_i = (\mathcal{J}_i - \mathcal{R}_i)\nabla\mathcal{H}_i(x_i) + g_i u_i + G_i v_i + G_{0,i}\sigma_{0,i} \\ i_i = G_i^{\top}\nabla\mathcal{H}_i(x_i) \\ y_{0,i} = G_{0,i}^{\top}\nabla\mathcal{H}_i(x_i) \\ 0 = w_i(\sigma_{0,i}, y_{0,i}), \end{cases} \tag{3.4.1}$$

with: state space vector $x_i \in \mathbb{R}^{n_i}$; Hamiltonian energy function $\mathcal{H}_i : \mathbb{R}^{n_i} \to \mathbb{R}$; control input vector $u_i \in \mathbb{R}^{m_i}$; conjugated interaction port variables $(v_i, i_i) \in \mathbb{R}^p \times \mathbb{R}^p$; conjugated generation port variables $(\sigma_{0,i}, y_{0,i}) \in \mathbb{R}^{p_{0,i}} \times \mathbb{R}^{p_{0,i}}$ and generation characteristic function $w_i : \mathbb{R}^{p_{0,i}} \times \mathbb{R}^{p_{0,i}} \to \mathbb{R}^{p_{0,i}}$. Matrices can be state–dependent and are defined as follows: interconnection, dissipation matrices $\mathcal{J}_i, \mathcal{R}_i \in \mathbb{R}^{n_i\times n_i}$; control matrix $g_i \in \mathbb{R}^{n_i\times m_i}$, interaction port matrix $G_i \in \mathbb{R}^{n_i\times p}$ and generation port matrix $G_{0,i} \in \mathbb{R}^{n_i\times p_{0,i}}$.

Generation characteristic is usually a complex, possibly time–varying, function of the generation

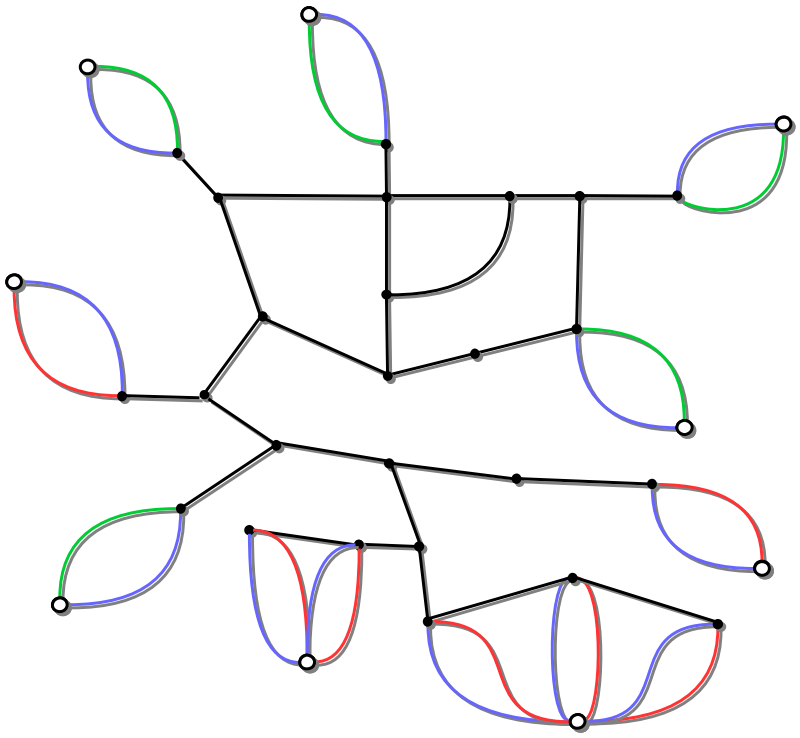

Figure 3.2: Graph of the power system depicted in Fig. 3.1. Nodes are represented by circles and edges are represented by lines. Unfilled circles represent the reference node, that is shown multiple time for aesthetic reasons. Green, red, black and blue lines denote respectively generation, utilization, transmission and capacitor edges. The network graph can be simply obtained by removing the colored edges and the unfilled circles.

port variables $\sigma_{0,i}$, $y_{0,i}$, see for example Fig. 3.3, where characteristic functions of a wind energy system and a solar cell are illustrated. Nevertheless, in many cases some simplifications can be made and assumed that the generation characteristic function is simply defined as a constant source, that is equivalent to have:

$$w_i(\sigma_{0,i}, y_{0,i}) = \sigma_{0,i} - E_{0,i},$$

where $E_{0,i} \in \mathbb{R}^p$ is a p–phases source. In literature there exists many examples of generation units that can be represented by (3.4.1) and include multiphysics three–phase ac, purely dc, or hybrid dc/ac systems [182, 53], see for example [11], [52] for synchronous generators, [49] for a generalized class of power converters, [12], [174] for induction machines and the excellent book [43] for an overview on different generation models.

3.4.2 Utilization edge

We call a utilization unit i a power unit that absorbs a *relevant* amount of power from the network to which it is connected through a port of dimension p_i. Using Assumption 3.2.1 we have $p_i = p$. There

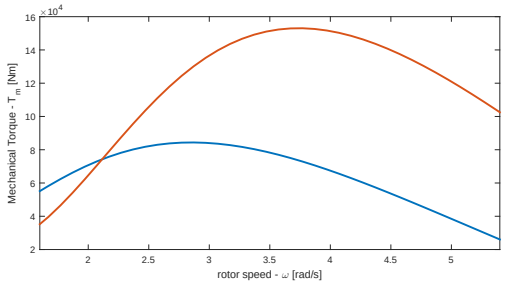

(a) Torque–speed characteristic of a wind turbine with $(\sigma_0, y_0) = (T, \omega)$.

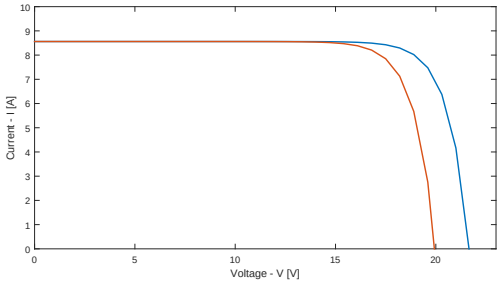

(b) Current–voltage characteristic of a solar cell with $(\sigma_0, y_0) = (i, v)$.

Figure 3.3: Examples of generation characteristic functions.

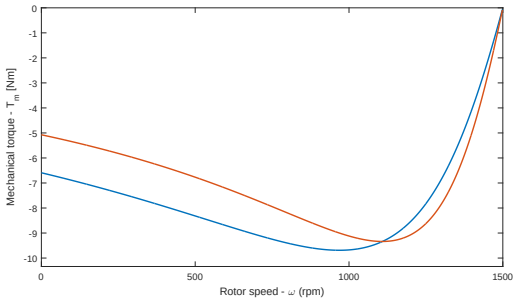

(a) Torque–speed characteristic of a motor with $(\sigma_0, y_0) = (T, \omega)$.

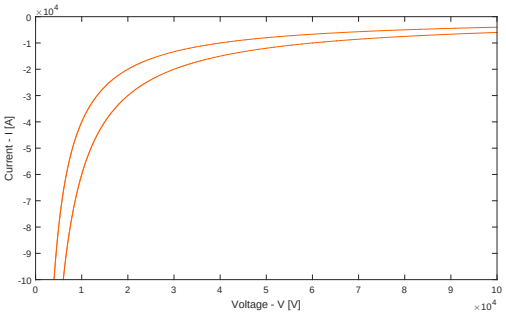

(b) Current–voltage characteristic of an active load with $(\sigma_0, y_0) = (i, v)$.

Figure 3.4: Examples of utilization characteristic functions.

are r utilization units, the totality of which constitutes the *utilization subsystem*. In order to describe the dynamics of the utilization edges we consider a port–Hamiltonian system of the form (2.1.1), that is

$$\mathcal{S}_i : \quad i \sim \mathcal{E}_R \quad \begin{cases} \dot{x}_i = (\mathcal{J}_i - \mathcal{R}_i)\nabla\mathcal{H}_i(x_i) + g_i u_i + G_i v_i + G_{0,i}\sigma_{0,i}, \\ i_i = G_i^\top \nabla\mathcal{H}_i(x_i) \\ y_{0,i} = G_{0,i}^\top \nabla\mathcal{H}_i(x_i) \\ 0 = w_i(\sigma_{0,i}, y_{0,i}), \end{cases} \tag{3.4.2}$$

with: state space vector $x_i \in \mathbb{R}^{n_i}$; Hamiltonian energy function $\mathcal{H}_i : \mathbb{R}^{n_i} \to \mathbb{R}$; control input vector $u_i \in \mathbb{R}^{m_i}$; conjugated interaction port variables $(v_i, i_i) \in \mathbb{R}^p \times \mathbb{R}^p$; conjugated utilization port variables $(\sigma_{0,i}, y_{0,i}) \in \mathbb{R}^{p_{0,i}} \times \mathbb{R}^{p_{0,i}}$ and utilization characteristic function $w_i : \mathbb{R}^{p_{0,i}} \times \mathbb{R}^{p_{0,i}} \to \mathbb{R}^{p_{0,i}}$. Matrices can be state–dependent and are defined as follows: interconnection, dissipation matrices $\mathcal{J}_i, \mathcal{R}_i \in \mathbb{R}^{n_i \times n_i}$; control matrix $g_i \in \mathbb{R}^{n_i \times m_i}$, interaction port matrix $G_i \in \mathbb{R}^{n_i \times p}$ and utilization port matrix $G_{0,i} \in \mathbb{R}^{n_i \times p_{0,i}}$.

Similarly to generation, utilization characteristic is usually a complex, possibly time–varying, function of the utilization port variables $\sigma_{0,i}$, $y_{0,i}$, see for example Fig. 3.4, where the utlization characteristic of a motor and a constant power load, are illustrated. This generalized model is well–suited to represent passive loads ($g_i = 0$), either three–phase ac or purely dc, static or dynamic, among which the ubiquitous ZIP models [96], see for example Chapter 4, where the latter are employed for the (reduced) modeling of voltage–controlled units in hvdc transmission systems. On the other hand, the inclusion of a control input vector ($g_i \neq 0$) further allows to encompass models of active loads.

3.4.3 Transmission edge

We call a transmission unit i is a power unit that absorbs or inject a *little* amount of power — compared to generation and utilization units — from the network to which it is connected through a port of dimension p_i. Using Assumption 3.2.1 we have $p_i = p$. There are $\mathtt{t}$ transmission units, the totality of which, together with the bus capacitors, constitute the *network subsystem*. In order to describe the dynamics of the transmission edges we consider a port–Hamiltonian system of the form (2.1.1), that is

$$\mathcal{S}_i : \quad i \sim \mathcal{E}_T \quad \begin{cases} \dot{x}_i = (\mathcal{J}_i - \mathcal{R}_i)\nabla\mathcal{H}_i(x_i) + g_i u_i + G_i v_i \\ i_i = G_i^\top \nabla\mathcal{H}_i(x_i), \end{cases} \tag{3.4.3}$$

with: state space vector $x_i \in \mathbb{R}^{n_i}$; Hamiltonian energy function $\mathcal{H}_i : \mathbb{R}^{n_i} \to \mathbb{R}$; control input vector $u_i \in \mathbb{R}^{m_i}$ and conjugated interaction port variables $(\sigma_i, y_i) \in \mathbb{R}^p \times \mathbb{R}^p$. Matrices can be state–dependent and are defined as follows: interconnection, dissipation matrices $\mathcal{J}_i, \mathcal{R}_i \in \mathbb{R}^{n_i \times n_i}$; control matrix $g_i \in \mathbb{R}^{n_i \times m_i}$ and interaction port matrix $G_i \in \mathbb{R}^{n_i \times p}$.

This generalized model is well–suited to represent standard lumped models of transmission lines — including multi–cell lines — conventional transformers, either three–phase ac or purely dc [43, 53]. The inclusion of a control input vector ($g_i \neq 0$) further allows to model flexible transmission devices [108] and controllable transformers. Nevertheless, although there exists a great variety of transmission units, the majority of transmission units composing a power system are power transmission lines. For their modeling, π–models are largely diffused in literature [7]. We then make the following assumption.

Assumption 3.4.1. *All transmission units are power transmission lines that can be described by single–cell π–models.*

A circuit representation of standard, single–cell, lossy π–model is illustrated in Fig. 3.5. The model consists in the interconnection of elementary (linear) power units: an RL unit (resistance connected in series with an inductor) in parallel connection with shunt RC units (resistance connected in parallel with a capacitor). Recalling Assumption 3.3.2, we can build the model of the correspondent edge by

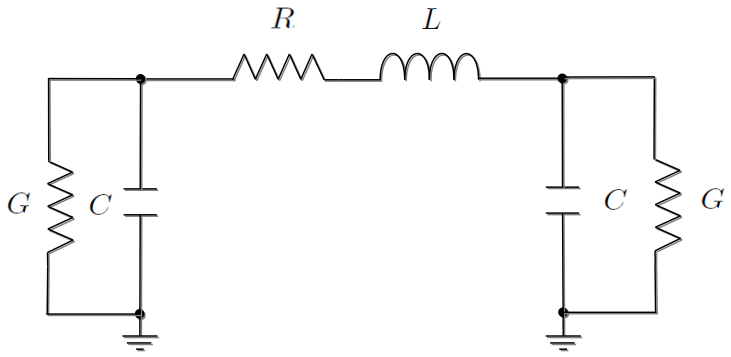

Figure 3.5: π–model of a transmission unit.

removing the lossy capacitors situated at both end of the π–model — that are included in the capacitor edges — so that the model reduces to a simple RL unit. At this point, the model of the i–th RL unit

is simply given by the following port–Hamiltonian system:

$$\mathcal{S}_i : \quad i \sim \mathcal{E}_T \quad \begin{cases} \dot{\psi}_i = -(R_i \otimes \mathbb{I}_p)\nabla\mathcal{H}_i(\psi_i) + v_i \\ i_i = \nabla\mathcal{H}_i(\psi_i), \end{cases} \tag{3.4.4}$$

with Hamiltonian energy function $\mathcal{H}_i : \mathbb{R}^p \to \mathbb{R}$:

$$\mathcal{H}_i(\psi_i) := \frac{1}{2}\psi_i^\top (L_i \otimes \mathbb{I}_p)^{-1}\psi_i, \tag{3.4.5}$$

where L_i, $R_i \in \mathbb{R}^{p\times p}$ are phase inductance, resistance respectively, the state $\psi_i \in \mathbb{R}^p$ is the magnetic flux in the inductor, the conjugated interaction port variables $(v_i, i_i) \in \mathbb{R}^p \times \mathbb{R}^p$ are respectively the voltages across and the current through the inductor.

3.4.4 Capacitor edge

A lossy capacitor i characterizes the dynamics at the bus that interfaces a generation or utilization unit to the network through a port of dimension $p_i = n_i$. Using Assumption 3.2.1 we have $n_i = p$. There are $\mathtt{g}+\mathtt{r}$ bus capacitors of which $\mathtt{g}$ are associated to generation buses and $\mathtt{r}$ are associated to utilization buses. As already noted, the totality of bus capacitors, together with the transmission units, constitute the *network susbsystem*. The model of a single bus capacitor is given by the following port–Hamiltonian system $\mathcal{S}_i$ of the form

$$\mathcal{S}_i : \quad i \sim \mathcal{E}_C \quad \begin{cases} \dot{q}_i = -(G_i \otimes \mathbb{I}_p)\nabla\mathcal{H}_i(q_i) + i_i \\ v_i = \nabla\mathcal{H}_i(q_i), \end{cases} \tag{3.4.6}$$

with Hamiltonian energy function $\mathcal{H}_i : \mathbb{R}^p \to \mathbb{R}$:

$$\mathcal{H}_i(q_i) := \frac{1}{2}q_i^\top (C_i \otimes \mathbb{I}_p)^{-1}q_i, \tag{3.4.7}$$

where C_i, $G_i \in \mathbb{R}^{p\times p}$ are p–phases capacitance, conductance respectively, the state $q_i \in \mathbb{R}^p$ are the electric charges in the capacitor, the conjugated interaction port variables $(i_i, v_i) \in \mathbb{R}^p \times \mathbb{R}^p$ are respectively the current through and voltage across the capacitor.

3.5 Overall system

3.5.1 Aggregated models

To obtain a full model of the interconnected system we consider a directed graph $\mathcal{G}^\uparrow$ and the associated p–phases incidence matrix $\mathcal{B} \otimes \mathbb{I}_p$, that is defined by (3.3.1). Then, we need the aggregated models of the edges, that are the aggregated models of the generation, utilization, transmission units and of the bus capacitors.

Generation edges

The aggregated model of the generation edges can be obtained collecting the port–Hamiltonian systems $\mathcal{S}_i$ with $i \sim \mathcal{E}_G$ given by (3.4.1). Let the numbers

$$n_{\mathtt{g}} := \sum_{i=1}^{\mathtt{g}} n_i, \quad m_{\mathtt{g}} := \sum_{i=1}^{\mathtt{g}} m_i, \quad p_{\mathtt{g}_0} := \sum_{i=1}^{\mathtt{g}} p_{G,i},$$

the aggregated vectors

$$x_G := \mathrm{col}(x_i) \in \mathbb{R}^{n_{\mathsf{g}}}, \quad v_G := \mathrm{col}(\sigma_i) \in \mathbb{R}^{p\mathsf{g}}, \quad i_G := \mathrm{col}(y_i) \in \mathbb{R}^{p\mathsf{g}}$$
$$u_G := \mathrm{col}(u_i) \in \mathbb{R}^{m_{\mathsf{g}}}, \quad \sigma_{G_0} := \mathrm{col}(\sigma_{0,i}) \in \mathbb{R}^{p_{\mathsf{g}_0}}, \quad y_{G_0} := \mathrm{col}(y_{0,i}) \in \mathbb{R}^{p_{\mathsf{g}_0}},$$

the interconnection and dissipation matrices

$$\mathcal{J}_G := \mathrm{bdiag}\{\mathcal{J}_i\} \in \mathbb{R}^{n_{\mathsf{g}} \times n_{\mathsf{g}}}, \quad \mathcal{R}_G := \mathrm{bdiag}\{\mathcal{R}_i\} \in \mathbb{R}^{n_{\mathsf{g}} \times n_{\mathsf{g}}},$$

the control input and interaction port matrices

$$g_G := \mathrm{bdiag}\{g_i\} \in \mathbb{R}^{n_{\mathsf{g}} \times m_{\mathsf{g}}}, \quad G_G := \mathrm{bdiag}\{G_i\} \in \mathbb{R}^{n_{\mathsf{g}} \times p\mathsf{g}}, \quad G_{G_0} := \mathrm{bdiag}\{G_i\} \in \mathbb{R}^{n_{\mathsf{g}} \times p_{\mathsf{g}_0}}$$

and the total Hamiltonian function $\mathcal{H}_G : \mathbb{R}^{n_{\mathsf{g}}} \to \mathbb{R}$ and the generation characteristic function $w_G : \mathbb{R}^{p_{\mathsf{g}_0}} \times \mathbb{R}^{p_{\mathsf{g}_0}} \to \mathbb{R}^{p_{\mathsf{g}_0}}$:

$$\mathcal{H}_G(x_G) := \sum_{i=1}^{\mathsf{g}} \mathcal{H}_i(x_i), \qquad w_G := \mathrm{col}(w_i). \tag{3.5.1}$$

The aggregated model of the generation edges can be then written as

$$\mathcal{S}_G : \begin{cases} \dot{x}_G = (\mathcal{J}_G - \mathcal{R}_G)\nabla\mathcal{H}_G(x_G) + g_G u_G + G_G v_G + G_{G_0}\sigma_{G_0} \\ i_G = G_G^\top \nabla\mathcal{H}_G(x_G) \\ y_{G_0} = G_{G_0}^\top \nabla\mathcal{H}_G(x_G) \\ 0 = w_G(\sigma_{G_0}, y_{G_0}). \end{cases} \tag{3.5.2}$$

Utilization edges

The aggregated model of the utilization edges can be obtained collecting the port–Hamiltonian systems $\mathcal{S}_i$ with $i \sim \mathcal{E}_R$ given by (3.4.2). Let the numbers

$$n_{\mathsf{r}} := \sum_{i=\mathsf{g}+1}^{\mathsf{g}+\mathsf{r}} n_i, \quad m_{\mathsf{r}} := \sum_{i=\mathsf{g}+1}^{\mathsf{g}+\mathsf{r}} m_i, \quad p_{\mathrm{r}_0} := \sum_{i=\mathsf{g}+1}^{\mathsf{g}+\mathsf{r}} p_{0,i},$$

the aggregated vectors

$$x_R := \mathrm{col}(x_i) \in \mathbb{R}^{n_{\mathsf{r}}}, \quad v_R := \mathrm{col}(\sigma_i) \in \mathbb{R}^{p\mathsf{r}}, \quad i_R := \mathrm{col}(y_i) \in \mathbb{R}^{p\mathsf{g}}$$
$$u_R := \mathrm{col}(u_i) \in \mathbb{R}^{m_{\mathsf{r}}}, \quad \sigma_{R_0} := \mathrm{col}(\sigma_{0,i}) \in \mathbb{R}^{p_{\mathrm{r}_0}}, \quad y_{R_0} := \mathrm{col}(y_{0,i}) \in \mathbb{R}^{p_{\mathrm{r}_0}},$$

the interconnection and dissipation matrices

$$\mathcal{J}_R := \mathrm{bdiag}\{\mathcal{J}_i\} \in \mathbb{R}^{n_{\mathsf{r}} \times n_{\mathsf{r}}}, \quad \mathcal{R}_R := \mathrm{bdiag}\{\mathcal{R}_i\} \in \mathbb{R}^{n_{\mathsf{r}} \times n_{\mathsf{r}}},$$

the control input and interaction port matrices

$$g_R := \mathrm{bdiag}\{g_i\} \in \mathbb{R}^{n_{\mathsf{r}} \times m_{\mathsf{r}}}, \quad G_R := \mathrm{bdiag}\{G_i\} \in \mathbb{R}^{n_{\mathsf{r}} \times p\mathsf{r}}, \quad G_{R_0} := \mathrm{bdiag}\{G_i\} \in \mathbb{R}^{n_{\mathsf{g}} \times p_{\mathrm{r}_0}}$$

and the total Hamiltonian function $\mathcal{H}_R : \mathbb{R}^{n_{\mathsf{r}}} \to \mathbb{R}$ and the utilization characteristic function w_G :

$\mathbb{R}^{p_{r_0}} \times \mathbb{R}^{p_{r_0}} \to \mathbb{R}^{p_{r_0}}$:

$$\mathcal{H}_R(x_R) := \sum_{i=\mathsf{g}+1}^{\mathsf{g}+\mathsf{r}} \mathcal{H}_i(x_i), \qquad w_R := \mathrm{col}(w_i) \tag{3.5.3}$$

The aggregated model of the utilization edges can be then written as

$$\mathcal{S}_R : \begin{cases} \dot{x}_R = (\mathcal{J}_R - \mathcal{R}_R)\nabla\mathcal{H}_R(x_R) + g_R u_R + G_R v_R + G_{G_0}\sigma_{G_0} \\ i_R = G_R^\top \nabla\mathcal{H}_R(x_R) \\ y_{R_0} = G_{R_0}^\top \nabla\mathcal{H}_R(x_R) \\ 0 = w_R(\sigma_{R_0}, y_{R_0}). \end{cases} \tag{3.5.4}$$

Transmission edges

Under Assumption 3.4.1, the aggregated model of the transmission edges can be thus obtained collecting the port–Hamiltonian systems $\mathcal{S}_i$ with $i \sim \mathcal{E}_T$ given by (3.4.4). Let the aggregated vectors

$$\psi_T := \mathrm{col}(\psi_i) \in \mathbb{R}^{p\mathsf{t}}, \quad v_T := \mathrm{col}(v_i) \in \mathbb{R}^{p\mathsf{t}}, \quad i_T := \mathrm{col}(i_i) \in \mathbb{R}^{p\mathsf{t}},$$

the dissipation matrix

$$\mathcal{R}_T := \mathrm{bdiag}\{R_i \otimes \mathbb{I}_p\} \in \mathbb{R}^{p\mathsf{t}\times p\mathsf{t}}$$

and the total Hamiltonian function $\mathcal{H}_T : \mathbb{R}^{p\mathsf{t}} \to \mathbb{R}$:

$$\mathcal{H}_T(\psi_T) := \sum_{i=\mathsf{g}+\mathsf{r}+1}^{\mathsf{g}+\mathsf{r}+\mathsf{t}} \mathcal{H}_i(\psi_i). \tag{3.5.5}$$

The aggregated model of the transmission edges can be then written as

$$\mathcal{S}_T : \begin{cases} \dot{\psi}_T = -\mathcal{R}_T\nabla\mathcal{H}_T(\psi_T) + v_T \\ i_T = \nabla\mathcal{H}_T(x_T). \end{cases} \tag{3.5.6}$$

Capacitor edges

Recalling that capacitors can be connected either to generation either to utilization buses, let partition the set of edges $\mathcal{E}_C$ in two ordered subsets $\mathcal{E}_{Cg}$, $\mathcal{E}_{Cr}$. Hence, the aggregated models can be obtained collecting the port–Hamiltonian systems (3.4.6). Let $i \sim \mathcal{E}_{Cg}$, $k \sim \mathcal{E}_{Cr}$, the aggregated vectors

$$\begin{aligned} q_g &:= \mathrm{col}(q_i) \in \mathbb{R}^{p\mathsf{g}}, \quad i_g := \mathrm{col}(v_i) \in \mathbb{R}^{p\mathsf{g}}, \quad v_g := \mathrm{col}(i_i) \in \mathbb{R}^{p\mathsf{g}} \\ q_r &:= \mathrm{col}(q_k) \in \mathbb{R}^{p\mathsf{r}}, \quad i_r := \mathrm{col}(v_k) \in \mathbb{R}^{p\mathsf{r}}, \quad v_r := \mathrm{col}(i_k) \in \mathbb{R}^{p\mathsf{r}} \end{aligned}$$

the dissipation matrices

$$\mathcal{R}_g := \mathrm{bdiag}\{R_i \otimes \mathbb{I}_p\} \in \mathbb{R}^{p\mathsf{g}\times p\mathsf{g}}, \qquad \mathcal{R}_r := \mathrm{bdiag}\{R_k \otimes \mathbb{I}_p\} \in \mathbb{R}^{p\mathsf{r}\times p\mathsf{r}}, \tag{3.5.7}$$

and the total Hamiltonian functions $\mathcal{H}_g : \mathbb{R}^{p\mathsf{g}} \to \mathbb{R}$, $\mathcal{H}_r : \mathbb{R}^{p\mathsf{r}} \to \mathbb{R}$:

$$\mathcal{H}_g := \sum_{i=\mathsf{g}+\mathsf{r}+\mathsf{t}+1}^{2\mathsf{g}+\mathsf{r}+\mathsf{t}} \mathcal{H}_i(q_i), \qquad \mathcal{H}_r := \sum_{k=2\mathsf{g}+\mathsf{r}+\mathsf{t}+1}^{\mathsf{m}} \mathcal{H}_k(q_k). \tag{3.5.8}$$

The aggregated model of the capacitor edges can be then written as

$$\mathcal{S}_C : \begin{cases} \dot{q}_g = -\mathcal{R}_g \nabla \mathcal{H}_g(q_g) + i_g \\ \dot{q}_r = -\mathcal{R}_r \nabla \mathcal{H}_r(q_r) + i_r \\ v_g = \nabla \mathcal{H}_g(q_g) \\ v_r = \nabla \mathcal{H}_r(q_r). \end{cases} \tag{3.5.9}$$

3.5.2 Interconnected model

Collecting the aggregated models (3.5.2), (3.5.4), (3.5.6) and (3.5.9), we get then:[1]

$$\dot{x}_G = (\mathcal{J}_G - \mathcal{R}_G)\nabla \mathcal{H}_G + g_G u_G + G_G v_G + G_{G_0}\sigma_{G_0} \tag{3.5.10}$$
$$\dot{x}_R = (\mathcal{J}_R - \mathcal{R}_R)\nabla \mathcal{H}_R + g_R u_R + G_R v_R + G_{R_0}\sigma_{R_0} \tag{3.5.11}$$
$$\dot{\psi}_T = -\mathcal{R}_T \nabla \mathcal{H}_T + v_T \tag{3.5.12}$$
$$\dot{q}_g = -\mathcal{R}_g \nabla \mathcal{H}_g + i_g \tag{3.5.13}$$
$$\dot{q}_r = -\mathcal{R}_r \nabla \mathcal{H}_r + i_r \tag{3.5.14}$$
$$i_G = G_G^\top \nabla \mathcal{H}_G \tag{3.5.15}$$
$$i_R = G_R^\top \nabla \mathcal{H}_R \tag{3.5.16}$$
$$i_T = \nabla \mathcal{H}_T \tag{3.5.17}$$
$$v_g = \nabla \mathcal{H}_g \tag{3.5.18}$$
$$v_r = \nabla \mathcal{H}_r \tag{3.5.19}$$
$$y_{G_0} = G_{G_0}^\top \nabla \mathcal{H}_G \tag{3.5.20}$$
$$y_{R_0} = G_{R_0}^\top \nabla \mathcal{H}_R \tag{3.5.21}$$
$$0 = w_G(\sigma_{G_0}, y_{G_0}) \tag{3.5.22}$$
$$0 = w_R(\sigma_{R_0}, y_{R_0}). \tag{3.5.23}$$

Let the numbers

$$n := n_{\mathsf{g}} + n_{\mathsf{r}} + p(\mathsf{g} + \mathsf{r} + \mathsf{t}), \quad m := m_{\mathsf{g}} + m_{\mathsf{r}}, \quad p_0 := p_{\mathsf{g}_0} + p_{\mathsf{r}_0}.$$

Then (3.5.10)–(3.5.23) can be rewritten in compact form as

$$\begin{aligned} \dot{x} &= (\mathcal{J} - \mathcal{R})\nabla \mathcal{H}(x) + gu + G\sigma + G_0\sigma_0 \\ y &= G^\top \nabla \mathcal{H}(x) \\ y_0 &= G_0^\top \nabla \mathcal{H}(x) \\ 0 &= w(\sigma_0, y_0), \end{aligned} \tag{3.5.24}$$

with state vector $x := \mathrm{col}(x_G, x_R, \psi_T, q_g, q_r) \in \mathbb{R}^n$, control input vector $u := \mathrm{col}(u_G, u_R) \in \mathbb{R}^m$, conjugated interaction port variables $(\sigma, y) \in \mathbb{R}^{p\mathsf{m}} \times \mathbb{R}^{p\mathsf{m}}$, with $\sigma := \mathrm{col}(v_G, v_R, v_T, i_g, i_r)$, $y := \mathrm{col}(i_G, i_R, i_T, v_g, v_r)$, counjugated generation/utilization port variables $(\sigma_0, y_0) \in \mathbb{R}^{p_0} \times \mathbb{R}^{p_0}$, with $\sigma_0 := \mathrm{col}(\sigma_{G_0}, \sigma_{R_0})$, $y_0 := \mathrm{col}(y_{G_0}, y_{R_0})$, interconnection and dissipation matrices

$$\mathcal{J} := \mathrm{bdiag}\{\mathcal{J}_G, \mathcal{J}_R, 0, 0, 0\}, \quad \mathcal{R} := \mathrm{bdiag}\{\mathcal{R}_G, \mathcal{R}_R, \mathcal{R}_T, \mathcal{R}_g, \mathcal{R}_r\},$$

[1] The dependence of the Hamiltonian functions from the state is here omitted to enhance readability.

the control input and interaction port matrices

$$g := \begin{bmatrix} g_G & 0 \\ 0 & g_R \\ 0 & 0 \\ 0 & 0 \\ 0 & 0 \end{bmatrix}, \quad G := \begin{bmatrix} G_G & 0 & 0 & 0 & 0 \\ 0 & G_R & 0 & 0 & 0 \\ 0 & 0 & \mathbb{I} & 0 & 0 \\ 0 & 0 & 0 & \mathbb{I} & 0 \\ 0 & 0 & 0 & 0 & \mathbb{I} \end{bmatrix}, \quad G_0 := \begin{bmatrix} G_{G_0} & 0 \\ 0 & G_{R_0} \\ 0 & 0 \\ 0 & 0 \\ 0 & 0 \end{bmatrix}$$

of appropriate dimension, the total Hamiltonian energy function $\mathcal{H} : \mathbb{R}^n \to \mathbb{R}$, with:

$$\mathcal{H}(x) := \mathcal{H}_G + \mathcal{H}_R + \mathcal{H}_T + \mathcal{H}_g + \mathcal{H}_r \tag{3.5.25}$$

and the function $w := \mathrm{col}(w_G, w_R)$.

From Assumption 3.3.2, we have that all the capacitors that are shared by power units at their port are removed and included in the bus capacitors dynamics, from which follows that the ouputs of the power units have the physical dimension of a current, while the outputs of the bus capacitors have the dimension of a voltage. Hence, clearly v_G, v_R, v_T, v_g and v_r have the dimension of a voltage, while i_G, i_R, i_T, i_g and i_r have the dimension of a current. Also, recalling Assumption 3.2.1, all ports have the same dimension. We consider the reference node to be at ground potential and define the node and edge vectors:

$$V := \begin{bmatrix} \mathcal{V}_G \\ \mathcal{V}_R \\ 0 \end{bmatrix} \in \mathbb{R}^{\mathsf{n}+1}, \quad V_e := \begin{bmatrix} v_G \\ v_R \\ v_T \\ v_g \\ v_r \end{bmatrix} \in \mathbb{R}^{\mathsf{m}}, \quad I_e := \begin{bmatrix} i_G \\ i_R \\ i_T \\ i_g \\ i_r \end{bmatrix} \in \mathbb{R}^{\mathsf{m}}. \tag{3.5.26}$$

Using Kirckhhoff's current and voltage laws we get then [160]:

$$[\mathbf{KCL}] \quad 0_{\mathsf{n}+1} = (\mathcal{B} \otimes \mathbb{I}_p) I_e, \qquad [\mathbf{KVL}] \quad V_e = (\mathcal{B} \otimes \mathbb{I}_p)^\top V. \tag{3.5.27}$$

Then, recalling the definition of incidence matrix given in (3.3.1), we have

$$\begin{aligned} [\mathbf{KCL}] \quad & \begin{cases} 0 &= i_G + (\mathcal{B}_G \otimes \mathbb{I}_p) i_T + i_g \\ 0 &= i_R + (\mathcal{B}_R \otimes \mathbb{I}_p) i_T + i_r \\ 0 &= \mathbf{1}_{\mathsf{g}p}^\top i_G + \mathbf{1}_{\mathsf{r}p}^\top i_R + \mathbf{1}_{\mathsf{g}p}^\top i_g + \mathbf{1}_{\mathsf{r}p}^\top i_r \end{cases} \\ \hline [\mathbf{KVL}] \quad & \begin{cases} v_G &= \mathcal{V}_G \\ v_R &= \mathcal{V}_R \\ v_T &= (\mathcal{B}_G \otimes \mathbb{I}_p)^\top \mathcal{V}_G + (\mathcal{B}_R \otimes \mathbb{I}_p)^\top \mathcal{V}_R \\ v_g &= \mathcal{V}_G \\ v_r &= \mathcal{V}_R \end{cases} \end{aligned} \tag{3.5.28}$$

After some manipulations, we obtain the overall interconnection laws

$$\sigma = \mathcal{I} y, \tag{3.5.29}$$

with

$$\mathcal{I} := \begin{bmatrix} 0 & 0 & 0 & \mathbb{I}_{\mathsf{g}} & 0 \\ 0 & 0 & 0 & 0 & \mathbb{I}_{\mathsf{r}} \\ 0 & 0 & 0 & \mathcal{B}_G^\top & \mathcal{B}_R^\top \\ -\mathbb{I}_{\mathsf{g}} & 0 & -\mathcal{B}_G & 0 & 0 \\ 0 & -\mathbb{I}_{\mathsf{r}} & -\mathcal{B}_R & 0 & 0 \end{bmatrix} \otimes \mathbb{I}_p \in \mathbb{R}^{p\mathsf{m}\times p\mathsf{m}}. \tag{3.5.30}$$

Note that the obtained interconnection laws are power preserving. In fact

$$\sigma^\top y = y^\top \mathcal{I}^\top y = 0, \tag{3.5.31}$$

where the second equivalence follows from skew–symmetry of $\mathcal{I}$. It now suffices to replace (3.5.29) into (3.5.24) to obtain:

$$\boxed{\begin{aligned} \dot{x} &= (\mathcal{J} - \mathcal{R} + G\mathcal{I}G^\top)\nabla\mathcal{H}(x) + gu + G_0\sigma_0 \\ y_0 &= G_0^\top \nabla\mathcal{H}(x) \\ 0 &= w(\sigma_0, y_0), \end{aligned}} \tag{3.5.32}$$

that is the overall interconnected port–Hamiltonian model of the electric power system.

Remark 3.5.1. Noting that $\mathcal{I}$ is a skew–symmetric matrix, it follows that also $\mathcal{J}_0 := G\mathcal{I}G^\top$ is skew–symmetric. Hence, with this new definition the system can be written in the standard port–Hamiltonian form (2.1.1).

Remark 3.5.2. The overall system satisfies the power balance equation

$$\dot{\mathcal{H}} = -(\nabla\mathcal{H})^\top \mathcal{R}\nabla\mathcal{H} + (\nabla\mathcal{H})^\top gu + (\nabla\mathcal{H})^\top G_0\sigma_0, \tag{3.5.33}$$

with $0 = w(\sigma_0, y_0)$, where the term:

- $\dot{\mathcal{H}}$ accounts for the stored power;
- $(\nabla\mathcal{H})^\top \mathcal{R}\nabla\mathcal{H}$ represents the dissipated power;
- $(\nabla\mathcal{H})^\top gu$ represents the controlled power;
- $(\nabla\mathcal{H})^\top G_0\sigma_0$ represents the difference between supplied and absorbed power.

Remark 3.5.3. Although a port–Hamiltonian representation of the individual power units is in general more suitable for an energy–based analysis of the electric power system, a standard state–space representation can be obtained with no loss of generality. For, it suffices to calculate an explicit expression of the gradient of the Hamiltonian function, while preserving the same interaction ports characterization. The invidual units can be then interconnected using the same modeling procedure.

Chapter 4

Hvdc transmission systems

4.1 Introduction

4.1.1 Motivation

As is well known, ac systems are overwhelmingly dominant over the alternative dc option in the electrical power industry. See [57] for a vivid account of this debate, which stretches back to the famous Edison–Tesla "war of the current", and [71] for a more technical discussion. However, this configuration is rapidly changing in the XXI–st century with dc systems playing an ever increasing role in the overall power systems scenario. The reasons for this change are manifold.

i) A widespread utilization of renewable energy sources (RES), mainly based on wind and solar power [50, 151, 83, 31]. These sources will be deployed either as small-scale sources in low-voltage residential distribution networks [71, 80], either as aggregated sources located in remote areas [57, 31].

ii) Improved efficiency due to decreased losses between dc sources and loads. Moreover, since dc are rapidly replacing ac loads in residential distribution networks, dc networks becomes attractive because they require less conversion stages [151, 71, 165].

iii) High–voltage dc transmission has significantly less (heat) losses than an equivalent ac system for long distances and specially for submarine connections [165, 152].

All this considered, two architectural paradigms have recently attracted the attention of the research community: dc microgrids [87, 128] and multi–terminal hvdc transmission systems [86, 61]. These new architectures pose new challenging control problems, which significantly differ from the ones appearing in traditional ac systems for the following reasons.

- The key building block of these architectures is the power converter, which is a highly *nonlinear* device [130, 29, 90, 49] for which standard linear PI controllers yield below par performances [76].

- In traditional (large–scale, centralized, fuel–based) ac power systems there is a clear time–scale separation between generation and transmission–distribution of power that considerably simplifies the control task [131]. This property is absent in RES, which are small–sized and distributed. The control problem is further complicated by the intermittent nature of RES.

- Traditional ac generation units can be practically considered to have an "infinite impedance", diminishing the effect of the loads, and allowing us to treat them as "closed systems" [96]. The

loading effect in RES cannot be neglected leading to the problem of controlling a highly interconnected nonlinear system.

- The ever increasing presence of nonlinear, *e.g.*, constant power, loads invalidates the standard assumption of linear impedance loads and poses new control theoretical questions [14, 97, 9].

4.1.2 Main contributions

Although many of the treated arguments have validity for generalized dc grids, this chapter focuses exclusively on high–voltage direct–current (hvdc) transmission systems. The main objective is to contribute, if modestly, towards the development of a general, theoretically–founded procedure for the modeling, analysis and control of these systems. With the intention to bridge the gap between theory and applications, one of the main concerns is to establish connections between existing engineering solutions, usually derived via *ad–hoc* considerations, and the solutions stemming from theoretical analysis. The main contributions are the following.

(C1) To propose a unified, physically motivated, modeling framework for hvdc transmission systems. This framework is based on port–Hamiltonian models of the system components combined with a suitable graph theoretic representation of their interconnection, as illustrated in Chapter 3.

(C2) In the spirit of [76, 84, 130] it is proved that the incremental model of the hvdc transmission system defines a *passive* map with respect to some suitably designed output. A consequence of this fundamental property is that a decentralized PI passivity–based controller (PBC) *globally asymptotically stabilizes* (GAS) any *assignable* equilibrium, with no restriction imposed on the (positive) gains of the PI–PBC. It is also shown that the proposed PI–PBC is closely related with Akagi's PQ instantaneous power method [5] that was derived (without a stability analysis) invoking power balance considerations and is standard in applications.

(C3) It is well–known that passive systems are minimum phase and have relative degree one [27, 159]. Consequently, the attainable performance of a PI–PBC is limited by its associated zero dynamics. Another contribution of the paper is the proof that, in hvdc systems, the zero dynamics is "extremely slow", stymying the achievement of fast transient responses. On the other hand, it is also shown that standard inner–loop controllers reported in the literature may exhibit unstable behavior because the zero dynamics associated to the corresponding outputs are *non–minimum phase*.

(C4) Inspired by common engineering practice, an outer–loop that determines the PI–PBC reference signals is added to improve the transient performance. This consists in a modification of the standard PI–PBC, for which it is shown that the intrinsic performance limitation are overcome, further preserving global asymptotic stability.

(C5) Under a reasonable time–scale separation assumption, a reduced (nonlinear) model of the hvdc transmission system — suitable for primary control analysis and design — is obtained. The obtained model — that includes the model of the widely diffused *voltage droop control* [123, 70, 142, 65] — should be contrasted with linear models usually employed for primary control analysis and design [8, 177].

(C6) A final contribution consists in the analysis of equilibria and stability of the reduced model. More

precisely, conditions on existence of equilibria, power sharing and stability of an (assumed existent) equilibrium point — dependent from the free primary control parameters — are established, thus determining an appropriate procedure for the choice of the gains of the controller.

The remainder of the chapter is structured as follows. First of all, the hvdc transmission concept is introduced in Section 4.2. The physical modeling of a wide class of hvdc systems — under some reasonable assumptions — is developed in Section 4.3. The hierarchical control architecture is then presented in Section 4.4, thus illustrating the four–layered structure of the control system. In Section 4.5 we provide a characterization of the assignable behavior of the system, that is instrumental for the formulation of the tertiary control and the centralized reference calculator, also called secondary control. Section 4.6 and Section 4.7 are then dedicated to the analysis and design of the "innermost level" of control, that is called inner–loop control. A reduced model, suitable for primary control design, followed by an analysis on existence of equilibria, power sharing and stability is presented in Section 4.8.

4.2 The hvdc transmission concept

Although the existing power systems architecture is dominantly ac, hvdc transmission systems are one of the few dc options that always received great attention from the industry and the research community. This is motivated by the clear disadvantages of ac transmission in terms of heat losses, when power is transmitted over long distances. Ac transmission is indeed typically realized using overhead lines, the inductive and capacitive elements of which puts limits to the transmission capacity and the transmission distance [152]. Since ac cable usually have a maximum distance of 50 to 100 km, for longer distances the hvdc transmission is then the only available option. On the other hand, for what concern costs, it should be noted that ac systems usually employ a three–phase architecture, while in dc systems only two conductors are necessary. Hence, for the transmission only a narrow power corridor is required. Several applications make use of hvdc transmission technologies, among wich the most relevant are the following.

- Integration — with small losses — of remotely located energy sources, such as hydro, off–shore wind and solar power that are typically situated at hundreds or thousands of kilometers from load centers [31, 61].
- Interconnection of ac grids, thus allowing for easy transfer of power between grids operating at different frequencies and giving the possibility to tap into the line at intermediate points [57].
- Connection of densely populated urban centers with no need of overhead lines or connection of islands via submarine connection [86, 57, 31].

Since the first prototypes, many technologies have been employed in hvdc transmission systems, ranging from mercury arc valves, thyristors (also called current source converters) until the more recent voltage source and multimodular converter technologies — that are based on IGBTs. In this work, we focus on hvdc based on voltage source converters [173, 54]. There are many advantages in using this new technology with respect to the traditional hvdc transmission systems based on line–commutated thyristors [2]:

- Since the voltage source converter does not depend on line–commutation, all the four quadrants of the PQ operating plane are possible.

- Power reversal can be realized without changing polarity of the dc voltage.
- No need of an external voltage source for commutation.
- Improved controllability of active, reactive power and ac, dc voltages, thus giving a strong dynamic enhancement to transient stability.

For more informations about development of hvdc during this last century and for a technical discussion on the advantages voltage source converters with respect to other technologies, the interested reader is referred to [173, 152, 2, 54].

An example of a multi–terminal hvdc transmission system based on voltage source converters is illustrated in Fig. 4.1. Ac subsystems are interfaced to the dc network through ac/dc voltage source

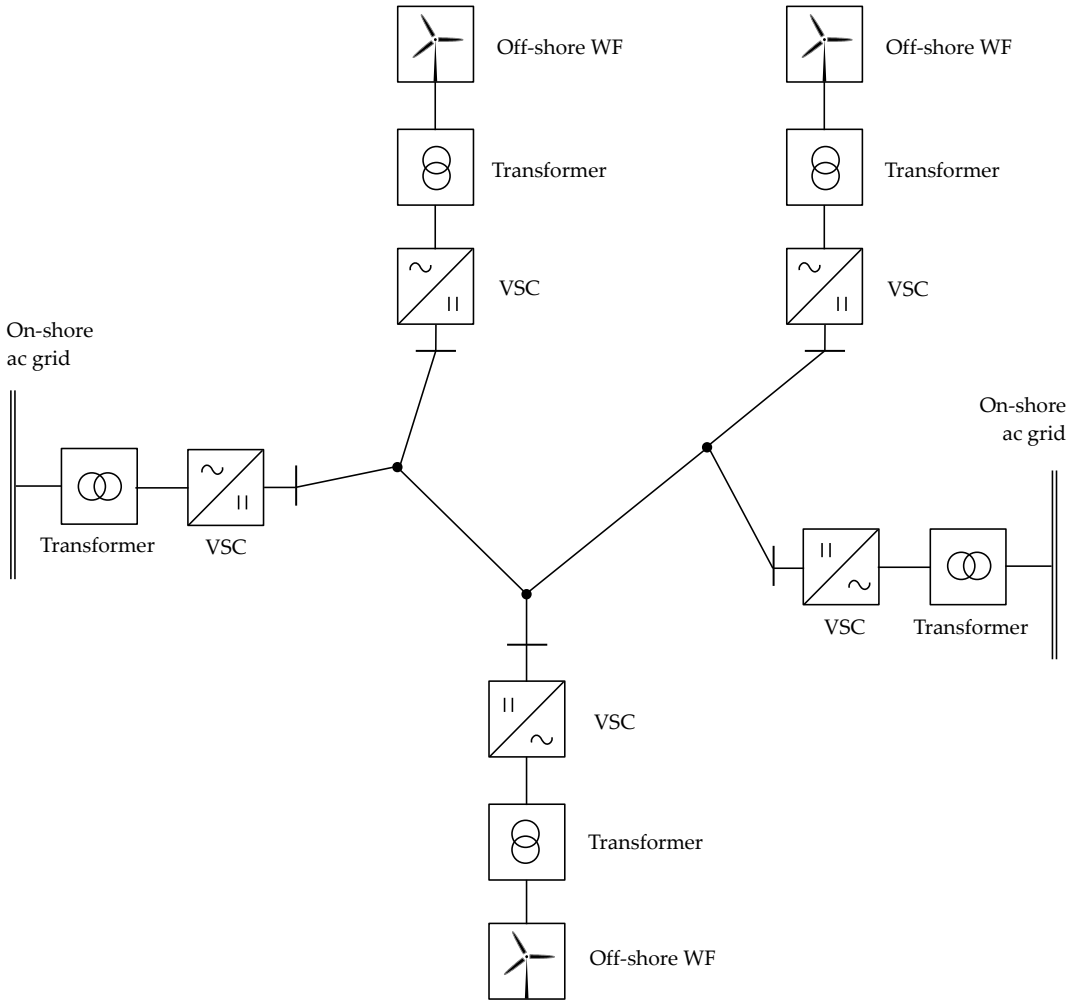

Figure 4.1: Circuit scheme of a five–terminal hvdc transmission system.

converters, that are in their turn connected by dc transmission lines. Typical ac subsystem interfaced via hdvc can be medium/high–voltage ac grids or renewable energy sources based on wind, hydro or solar power. Converters are preceded by a transformer that step–up the voltage, a phase reactor and

further equipped with filters on both ac and dc sides to mitigate harmonics propagation [37, 54, 96]. According to the traditional nomenclature [54, 93, 133], the converter subsystem, including transformer, phase reactor and filters, is said an *hvdc station* or *terminal*, while the ensemble of dc tranmission lines — called *dc links* — constitutes the *hvdc network*.

Terminals can be classified according to the characteristics of the associated ac subsystem. Then an hvdc terminal is said to be: *strongly connected*, if the ac voltage at the point of interconnection remains constant regardless of the power flowing through that point; *weakly connected*, if the ac voltage depends on the power flowing through that point [1]. Ac systems can be defined as weak from two aspects: if their impedance is high relative to their point of interconnection and if the mechanical inertia is inadequate relative to the dc power infeed [175]. Example of weak ac systems are large ac system connected to hvdc at a weak point of interconnection or systems with a few numbers of rotating machines.

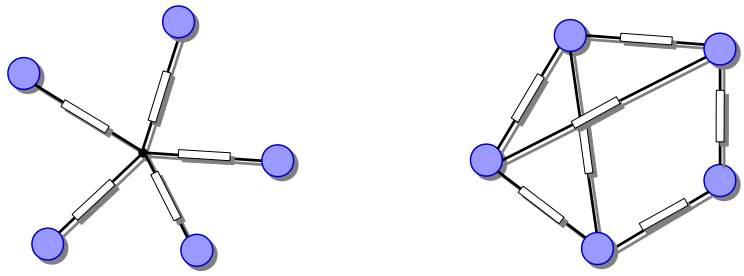

Figure 4.2: Radial and meshed topology of a multi–terminal hvdc transmission system.

There exist two possible schemes for the interconnection of terminals through the hvdc network. Converters can be indeed parallel–connected, from which follows that they operate at the same voltage. Or they can be series–connected, from which follows that the same current is flowing through the dc links. Parallel scheme is the most popular and for this reason is the one considered in this work [96]. It is typically characterized by a *radial* or a *meshed* topology [54, 26, 61], which are illustrated in Fig. 4.2. The radial topology provides a common point of interconnection to which all terminals are connected. This is the case for example of on–shore stations situated on opposite seacoasts while the off–shore stations are placed in their middle [26, 94, 152, 181]. Nevertheless, in a radial topology any fault occurring at a given tranmission line implies the total service interruption to the associated terminal. In this work we consider the more suitable architecture in which the stations are directly connected with lines, that corresponds to a meshed topology. In such a case it is in general possible to guarantee no interruption of service because of the existence of different paths connecting the various terminals [26].

4.3 Physical modeling

In Chapter 3 it was shown that generalized electric power systems can be represented by a directed graph, where the power units correspond to edges and the buses correspond to nodes. Moreover, to underscore the physical structure of the power units, it was employed a generalized port–Hamiltonian representation. In this section the same procedure is applied to describe the dynamics of a multi–

terminal hvdc transmission system based on voltage source converters. According to such a procedure and in particular — under Assumption 3.4.1 — we consider only two types of power units: voltage source converters and their attached ac subsystem (terminals) — that we call *converter units* — and dc transmission lines — that are *transmission units*. We next provide a graph description of the system topology and appropriate port–Hamiltonian models of the individual units.

4.3.1 Graph description

An hvdc transmission system can be viewed as an unweighted directed graph $\mathcal{G}^{\uparrow}$ where power converters and dc lines correspond to edges and buses correspond to nodes. We call a bus a *converter bus* when a converter unit is connected to it and a *transmission bus* when no converter units are connected to it. All buses associates a potential and we call a bus a *reference bus* when all buses potentials are measured with respect to it. The reference bus is assumed to be at ground potential. Converter and reference buses are boundary buses, while the transmission buses are interior buses. We further assume, as in Chapter 3, that transmission (interior) buses are eliminated via Kron–reduction [42, 160], from which follows that if c is the number of converter buses, then the total number of buses (nodes) is $\mathsf{c}+1$. Without loss of generality we assume that the set of nodes $\mathcal{N}$ can be partitioned into two ordered subsets called $\mathcal{N}_{VSC}$ and the one–element set $\mathcal{N}_0$, associated to converter nodes and the reference node respectively. We call $\mathcal{V} \in \mathbb{R}^{\mathsf{c}+1}$ the vector of node potentials. We also mentioned that is common practice to define power units such that their interaction with the environment is modeled by a voltage capacitor at their interaction port. In the case of hvdc systems it is easy to see that both converters and tranmission units share a capacitor at the converter buses to which they are attached. For simplicity then, we make the following assumption.

Assumption 4.3.1. *All (possibly lossy) capacitors in parallel connection at a given bus are replaced by an equivalent capacitor, whose dynamics is included in the power converter dynamics.*

Consequently, all capacitors shared by tranmission units at their ports can be safely neglected, while capacitors shared by voltage source converters need to be replaced by equivalent capacitors. Let t the number of *transmission edges* — associated to transmission units — that connect converter buses. Since, there is a *converter edge* between every converter bus and the reference bus, there are in total $\mathsf{m} = \mathsf{c}+\mathsf{t}$ edges. Without loss of generality we assume that the set of edges $\mathcal{E}$ can be partitioned into two ordered subsets called $\mathcal{E}_{VSC}$ and $\mathcal{E}_T$ associated to converter edges and transmission edges respectively. We call $(V_e, I_e) \in \mathbb{R}^{\mathsf{m}} \times \mathbb{R}^{\mathsf{m}}$ the vectors pair associated to edge voltages and currents respecitvely. The topology of the hvdc transmission system is fully described by the directed graph $\mathcal{G}^{\uparrow}$ to which are associated the vectors $\mathcal{V}$, V_e, I_e and the following incidence matrix

$$\mathcal{B} = \begin{bmatrix} \mathbb{I}_{\mathsf{c}} & \mathcal{B}_{net} \\ -1_{\mathsf{c}}^{\top} & 0 \end{bmatrix} \in \mathbb{R}^{(\mathsf{c}+1)\times \mathsf{m}}. \tag{4.3.1}$$

The submatrix $\mathcal{B}_{net} \in \mathbb{R}^{\mathsf{c}\times\mathsf{t}}$, represents the incidence matrix of the sub–graph $\mathcal{G}^{\uparrow}_{net}$, that is obtained by eliminating the reference node and edges that are connected to it. The incidence matrix $\mathcal{B}_{net}$ thus fully captures the topology of the hvdc network. To avoid confusion we refer to $\mathcal{G}^{\uparrow}$ as the *hvdc transmission system graph* and to $\mathcal{G}^{\uparrow}_{net}$ as the *hvdc network graph*.

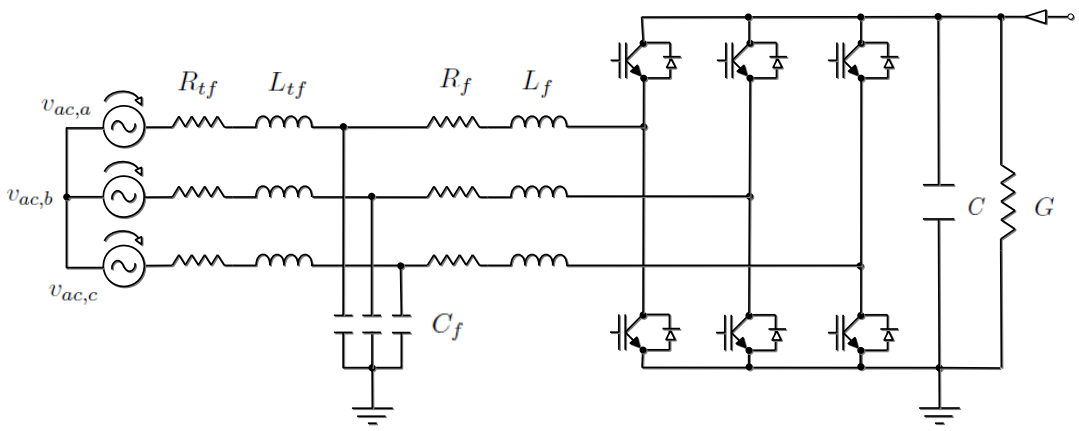

Figure 4.3: Circuit scheme of a three–phase voltage source converter, in *abc* coordinates.

4.3.2 Converter edges

From the switched to the averaged model

The circuit scheme of a three–phase two–level voltage source converter is depicted in Fig. 4.3. The voltage source converter is characterized by six switches — that are supposed to be ideal (diodes nonlinear dynamic neglected), bidirectional and mutually synchronized — and is connected to the ac subsystem through a phase reactor and a transformer. Converters are further equipped with purely capacitive filter on the ac side — located between the phase reactor and the transformer — and on the dc side, see Fig. 4.3. These are usually provided to minimize ripples generated respectively in ac currents and dc voltage. Nevertheless, several models proposed in literature do not consider the filter bus on the ac side. In [37] it is shown that, although the value of the capacitance largely affects the ac voltage amplitude, this has little effect on the values of active and reactive power. Hence, neglecting the filter leads to slightly different results in stability studies. Another assumption is that three–phase line voltages are balanced and that the neutral connection is neglected. While considering a bidirectional power flow — an important requirement in hvdc transmission systems — the converter can operate in two different modes: *rectifier mode* (turning ac energy into dc energy) and *inverter mode* (turning dc energy into ac energy). To obtain the full model, we refer to the equivalent single phase circuit given in Fig. 4.4, that consists in mutually coupled ac and dc circuits [170, 171, 156].

By direct application of Kirchhoff's current and voltage laws we obtain the following differential equations in *abc* coordinates:

$$\begin{aligned} L_i \mathbb{I}_3 \dot{i}_i &= -R_i \mathbb{I}_3 i_i + v_{ac,i} - v_{1,i} \\ C_i \dot{v}_{C,i} &= -G_i v_{C,i} + i_{2,i} + i_{C,i}. \end{aligned} \tag{4.3.2}$$

For the ac circuit, $i_i \in \mathbb{R}^3$ is the three–phase vector of inductor currents, $v_{ac,i} \in \mathbb{R}^3$ the three–phase vector of input voltages, $L_i, R_i \in \mathbb{R}$ respectively the (balanced) inductance and resistance. For the dc circuit, $v_{C,i} \in \mathbb{R}$ is the capacitor voltage, $i_{C,i} \in \mathbb{R}$ the input current, $C_i, G_i \in \mathbb{R}$ respectively the capacitance and conductance. The vector $v_{1,i} \in \mathbb{R}^3$ and the scalar $i_{2,i} \in \mathbb{R}$ are three–phase voltages and dc current sources, mutually controlled, that describe the behavior of the switches. They are related to inductor currents and capacitor voltage through the three–phase modulating variables $m_i =$

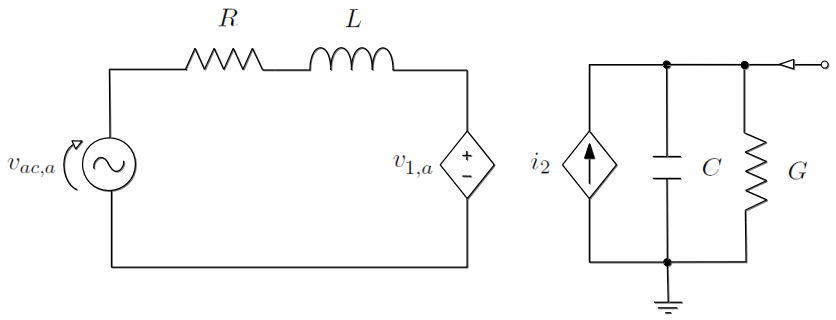

Figure 4.4: Equivalent circuit scheme of the a–phase — with $R := R_{tf} + R_f$, $L := L_{tf} + L_f$ — and of the dc side of the three–phase voltage source converter.

$\mathrm{col}(m_{a,i}, m_{b,i}, m_{c,i})$ by means of the following relation [155, 156]:

$$v_{1,i} = [\Upsilon m_i]\, v_{C,i}, \qquad i_{2,i} = m_i^\top i_i \tag{4.3.3}$$

with

$$\Upsilon = \frac{1}{3}\begin{bmatrix} 2 & -1 & -1 \\ -1 & 2 & -1 \\ -1 & -1 & 2 \end{bmatrix}. \tag{4.3.4}$$

Now by replacing (4.3.3) in (4.3.2) we obtain:

$$\begin{aligned} L_i \mathbb{I}_3 \dot{i}_i &= -R_i \mathbb{I}_3 i_i - \Upsilon m_i v_{C,i} + v_{ac,i} \\ C_i \dot{v}_{C,i} &= -G_i v_{C,i} + m_i^\top i_i + i_{C,i}. \end{aligned} \tag{4.3.5}$$

Note that the variables $m_{a,i}$, $m_{b,i}$, $m_{c,i}$ determine the status of the switches and are defined on a binary set. Hence they can be either 0 (closed switch) or 1 (open switch). The system (4.3.5) is usually called the *switched model* of the voltage source converter [173].

Voltage source converters, like all power converters, are indeed switching electronic devices. Switches are usually controlled by means of pulse width modulation (PWM) techniques [170, 2], in order to regulate the power supplied to the attached electrical devices. The underlying philoshopy of such a technique consists in turning on and off the switches as fast as practically possible to minimize the switching transition time and the associated switching losses. For an overview of PWM techniques, the reader is referred to [78]. In the frequency range much lower than the switching frequency, the modulating (binary) variables m_i can be thus replaced in the model (4.3.5) by their average value (or *duty ratio*) $u_i \in \mathbb{R}^3$ in that switching period [170]. Such a modified model is called the *averaged model* of the voltage source converter [173]. We now make the following assumptions.

Assumption 4.3.2. *The three–phase input of the voltage source converter is instantaneously synchronized to the attached ac subsystem.*

Assumption 4.3.3. *All terminals constituting the hvdc transmission system are strongly connected.*

Assumption 4.3.2 is justified by the introduction of a phase–locked–loop (PLL) circuit that detects the latching phase [173]. A PLL circuit is a circuit that synchronizes an oscillator with a reference

sinusoidal input, see [17] for more details on this topic. Hence, the PLL is locked to the a–phase of the ac voltage $v_{ac,i}$ at the point of interconnection between the power converter and the attached ac subsystem.

Assumption 4.3.3 is equivalent to assume that the dynamics of the attached ac subsystems evolve at a time–scale much slower than the time–scale in which the power converter is operated. Since the rates of change of amplitude $V_i(t)$ and frequency $\omega_i(t)$ of the three–phase ac voltage are very slow, the PLL circuit allows then to latch the input voltage of the converter to a purely sinsouidal three–phase voltage source.

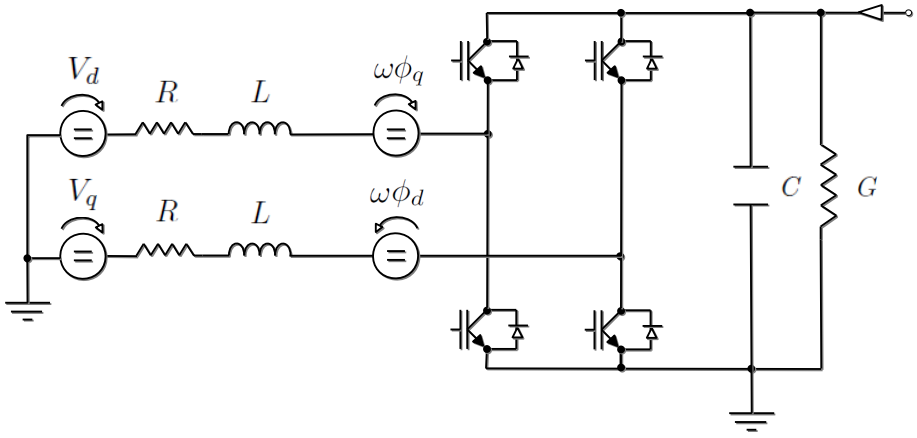

Figure 4.5: Equivalent circuit scheme of a three–phase voltage source converter, in dq coordinates.

Let $v_{ac,a,i} = \sqrt{2}V_i \sin(\omega_i + \varphi_i)$ the a–phase of the ac voltage. First of all, it is easy to see that the averaged version of the system (4.3.5) is a nonlinear time–varying system. Hence, it is convenient to transform it in an appropriate rotating frame by means of the dq–transformation introduced in Subsection 2.2.3, picking as transformation angle the phase $\vartheta_i(t) = \omega_i t + \varphi_i - \pi/2$. Because the system is balanced, it is possible to reduce the three–phase system into a two–phase system, thus leading to the following model of the voltage source converter in dq–frame [20], the circuit equivalent of which is illustrated in Fig. 4.5:

$$\begin{aligned} L_i \mathbb{I}_2 \dot{i}_{dq,i} &= (J_2 L_i \omega_i - R_i \mathbb{I}_2) i_{dq,i} - u_{dq,i} v_{C,i} + v_{dq,i} \\ C_i \dot{v}_{C,i} &= -G_i v_{C,i} + u_{dq,i}^\top i_{dq,i} + i_{C,i}, \end{aligned} \tag{4.3.6}$$

where $i_{dq,i} := T_{dq}(\vartheta) i_i \in \mathbb{R}^2$, $v_{dq,i} := T_{dq}(\vartheta) v_{C,i} \in \mathbb{R}^2$ are the dq vector of inductor currents and input voltage respectively, and $u_{dq,i} := T_{dq}(\vartheta) u_i \in \mathbb{R}^2$ are the dq–transformed duty ratios. Note that for this particular choice of ϑ_i we have:

$$v_{dq,i} = \begin{bmatrix} V_{d,i} \\ V_{q,i} \end{bmatrix} = \sqrt{3} V_i \begin{bmatrix} \sin(\frac{\pi}{2}) \\ \cos(\frac{\pi}{2}) \end{bmatrix} = \begin{bmatrix} \sqrt{3} V_i \\ 0 \end{bmatrix}, \tag{4.3.7}$$

from which follows that the transformed system (4.3.6) is now time–invariant.

Port–Hamiltonian model

It is now easy to see that (4.3.6) admits the following port–Hamiltonian representation [49, 119]:

$$\mathcal{S}_i: \ \ i \sim \mathcal{E}_{VSC} \ \begin{cases} \dot{x}_i & = [\mathcal{J}_i(u_i) - \mathcal{R}_i]\,\nabla\mathcal{H}_i + e_1 V_{d,i} + e_3 i_{C,i} \\ v_{C,i} & = \nabla\mathcal{H}_i, \end{cases} \tag{4.3.8}$$

with state space vector $x_i := \mathrm{col}(\phi_{d,i}, \phi_{q,i}, q_{C,i}) \in \mathbb{R}^3$, duty cycles $u_i := \mathrm{col}(u_{d,i}, u_{q,i}) \in \mathbb{R}^2$, external source $V_{d,i} \in \mathbb{R}$, port variables $(i_{C,i}, v_{C,i}) \in \mathbb{R} \times \mathbb{R}$, interconnection and dissipation matrices

$$\mathcal{J}_i(u,i) := \mathcal{J}_{0,i} L_i \omega_i + \mathcal{J}_{d,i} u_{d,i} + \mathcal{J}_{q,i} u_{q,i}, \quad \mathcal{R}_i := \mathrm{diag}\{R_i, R_i, G_i\} \tag{4.3.9}$$

with:

$$\mathcal{J}_{0,i} := \begin{bmatrix} 0 & 1 & 0 \\ -1 & 0 & 0 \\ 0 & 0 & 0 \end{bmatrix}, \quad \mathcal{J}_{d,i} := \begin{bmatrix} 0 & 0 & -1 \\ 0 & 0 & 0 \\ 1 & 0 & 0 \end{bmatrix}, \quad \mathcal{J}_{1,i} := \begin{bmatrix} 0 & 0 & 0 \\ 0 & 0 & -1 \\ 0 & 1 & 0 \end{bmatrix},$$

port matrices $e_1 := \mathrm{col}(1,0,0)$, $e_3 := \mathrm{col}(0,0,1) \in \mathbb{R}^3$, Hamiltonian energy function

$$\mathcal{H}_i(x_C) := \frac{1}{2} x_i^\top Q_i x_i, \quad Q_i := \mathrm{diag}\{\frac{1}{L_i}, \frac{1}{L_i}, \frac{1}{C_i}\}. \tag{4.3.10}$$

Remark 4.3.4. Note that, in view of the skew–symmetry of $\mathcal{J}_i(u_i)$, the i–th converter satisfies the power balance equation

$$\underbrace{\dot{\mathcal{H}}_i}_{\text{stored power}} = - \underbrace{x_i^\top Q_i \mathcal{R}_i Q_i x_i}_{\text{dissipated power}} + \underbrace{x_i^\top Q_i e_1 V_{d,i} + x_i^\top Q_i e_3 i_{C,i}}_{\text{supplied power}} \tag{4.3.11}$$

Recalling that c is the number of converter units (edges) composing the hvdc transmission, we now formulate the correspondent aggregated model. We have then:

$$\mathcal{S}_{VSC}: \ \begin{cases} \dot{x}_C & = [\mathcal{J}_C(u) - \mathcal{R}_C]\nabla\mathcal{H}_C + E_3 i_C \\ v_C & = E_3^\top \nabla\mathcal{H}_C, \end{cases} \tag{4.3.12}$$

with the following definitions.

- State space vector $x_C := \mathrm{col}(\mathrm{col}(\phi_{d,i}), \mathrm{col}(\phi_{q,i}), \mathrm{col}(q_{C,i})) \in \mathbb{R}^{3\mathsf{c}}$.

- Energy function

$$\mathcal{H}_C(x_C) := \frac{1}{2} x_C^\top Q_C x_C, \quad Q_C := \mathrm{bdiag}\{L_C^{-1}, L_C^{-1}, C_C^{-1}\},$$

  with $L_C := \mathrm{diag}\{L_i\}$, $C_C := \mathrm{diag}\{C_i\}$.

- Duty cycles $u := \mathrm{col}(u_{Cd}, u_{Cq}) \in \mathbb{R}^{2\mathsf{c}}$, where $u_{Cd} := \mathrm{col}(u_{d,i})$ and $u_{Cq} := \mathrm{col}(u_{q,i})$.

- External sources $V := \mathrm{col}(V_{d,i}) \in \mathbb{R}^{\mathsf{c}}$.

- Port variables $i_C := \mathrm{col}(i_{C,i}) \in \mathbb{R}^{\mathsf{c}}$ and $v_C := \mathrm{col}(v_{C,i}) \in \mathbb{R}^{\mathsf{c}}$.

- Interconnection matrix

$$\mathcal{J}_C(u) := \sum_{i=1}^{\mathsf{c}} (\mathcal{J}_{C0,i} L_i \omega_i + \mathcal{J}_{Cd,i} u_{d,i} + \mathcal{J}_{Cq,i} u_{q,i}) \tag{4.3.13}$$

where:

$$\mathcal{J}_{C0,i} := \begin{cases} -1 \text{ in } _{(i,\mathsf{c}+i)} \\ 1 \text{ in } _{(\mathsf{c}+i,i)} \\ 0 \text{ elsewhere} \end{cases} \quad \mathcal{J}_{Cd,i} := \begin{cases} 1 \text{ in } _{(i,2\mathsf{c}+i)} \\ -1 \text{ in } _{(2\mathsf{c}+i,i)} \\ 0 \text{ elsewhere} \end{cases} \quad \mathcal{J}_{Cq,i} := \begin{cases} -1 \text{ in } _{(\mathsf{c}+i,2\mathsf{c}+i)} \\ 1 \text{ in } _{(2\mathsf{c}+i,\mathsf{c}+i)} \\ 0 \text{ elsewhere} \end{cases}$$

- Dissipation matrix $\mathcal{R}_C := \text{bdiag}\{R_C, R_C, G_C\}$, where $R_C := \text{diag}\{R_i\}$ and $G_C := \text{diag}\{G_i\}$.

- Port matrices $E_1 := [\mathbb{I}_{\mathsf{c}}\ 0\ 0]^\top$, $E_3 := [0\ 0\ \mathbb{I}_{\mathsf{c}}]^\top \in \mathbb{R}^{3\mathsf{c}\times\mathsf{c}}$.

Remark 4.3.5. Note that, in view of the skew–symmetry of $\mathcal{J}_C(u)$, the set of converters satisfy the aggregated power balance equation

$$\underbrace{\dot{\mathcal{H}}_C}_{\text{stored power}} = -\underbrace{x_C^\top Q_C \mathcal{R}_C Q_C x_C}_{\text{dissipated power}} + \underbrace{x_C^\top Q_C E_1 V + x_C^\top Q_C E_3 i_C}_{\text{supplied power}}. \tag{4.3.14}$$

4.3.3 Transmission line edges

In order to describe the dynamics of a transmission line, a π–model — that consists of the parallel connection of two capacitors by means of an RL–series impedance — has been considered in Chapter 3. However, under Assumption 4.3.1, dc lines reduces to a more simple RL–series impedance. This is justified, as explained before, by the definition of an equivalent capacitor at the output of each converter. Hence, a set of t dc transmission lines can be represented by the port–Hamiltonian system:

$$\mathcal{S}_T : \begin{cases} \dot{x}_T &= -\mathcal{R}_T \nabla \mathcal{H}_T + v_T \\ i_T &= -\nabla \mathcal{H}_T, \end{cases} \tag{4.3.15}$$

with the following definitions.

- State space variables the collection of lines inductor fluxes $x_T := \text{col}(\phi_{T,i}) \in \mathbb{R}^{\mathsf{t}}$.

- Energy function

$$\mathcal{H}_T(x_T) := \frac{1}{2} x_T^\top Q_T x_T, \qquad Q_T := \text{diag}\{\frac{1}{L_{T,i}}\},$$

where $L_{T,i}$ is the inductance of the line.

- Port variables the voltages at the terminals $v_T := col(v_{T,i}) \in \mathbb{R}^{\mathsf{t}}$ and the inductors currents $i_T := \text{col}(i_{T,i}) \in \mathbb{R}^{\mathsf{t}}$.

- Dissipation $\mathcal{R}_T = \text{diag}\{R_{T,i}\}$, with $R_{T,i}$ the resistance of the line.

4.3.4 Interconnected model

The interconnection laws can be obtained following the same approach used in Chapter 3, where Kirchhoff's current and voltage laws are expressed in relation to the incidence matrix $\mathcal{B}$. We first define the

node and edge vectors:

$$V := \begin{bmatrix} \mathcal{V}_C \\ 0 \end{bmatrix} \in \mathbb{R}^{\mathsf{c}+1}, \quad V_e := \begin{bmatrix} v_C \\ v_T \end{bmatrix} \in \mathbb{R}^{\mathsf{m}}, \quad I_e := \begin{bmatrix} i_C \\ i_T \end{bmatrix} \in \mathbb{R}^{\mathsf{m}}. \tag{4.3.16}$$

Using the definition of the incidence matrix (4.3.1) and the Kirchhoff's currents and voltages laws expressed by (3.5.27), we have:

$$0_{\mathsf{c}} = i_C + \mathcal{B}_{net} i_T, \quad -1_n^\top i_C = 0, \quad \mathcal{V}_C = v_C, \quad \mathcal{B}_{net}^\top \mathcal{V}_C = v_T, \tag{4.3.17}$$

Recalling the expression for i_L from (4.3.12) and v_C from (4.3.15) it is easy to get:

$$i_C = -\mathcal{B}_{net} \nabla \mathcal{H}_T, \qquad v_T = \mathcal{B}_{net}^\top E_3^\top \nabla \mathcal{H}_C, \tag{4.3.18}$$

so that in order to obtain the overall port–Hamiltonian representation it is sufficient to combine (4.3.12), (4.3.15) and (4.3.18), thus leading to

$$\dot{x} = [\mathcal{J}(u) - \mathcal{R}] \nabla \mathcal{H} + EV, \tag{4.3.19}$$

with the following definitions.

- State space variables $x := \mathrm{col}(x_C, x_T) \in \mathbb{R}^{3\mathsf{c}+\mathsf{t}}$.
- Energy function $\mathcal{H}(x) := \mathcal{H}_C(x) + \mathcal{H}_T(x)$.
- Duty cycles (controls) $u := \mathrm{col}(u_{Cd}, u_{Cq}) \in \mathbb{R}^{2\mathsf{c}}$.
- Interconnection matrix
$$\mathcal{J}(u) := \begin{bmatrix} J_C(u) & -E_3 \mathcal{B}_{net} \\ \mathcal{B}_{net}^\top E_3^\top & 0 \end{bmatrix}, \tag{4.3.20}$$
- Dissipation matrix
$$\mathcal{R} := \mathrm{bdiag}\{\mathcal{R}_C, \mathcal{R}_T\} > 0. \tag{4.3.21}$$
- Input matrix $E := \begin{bmatrix} E_1^\top & 0 \end{bmatrix}^\top$.

Remark 4.3.6. It is easy to see that it is possible to rewrite (4.3.19) in the standard port–Hamiltonian form (2.1.1). In fact, after some manipulations we can obtain:

$$\mathcal{J}(u) \nabla \mathcal{H} = \mathcal{J}_0 \nabla \mathcal{H} + g(x) u, \tag{4.3.22}$$

with the following definitions

$$\mathcal{J}_0 := \begin{bmatrix} \sum_{i=1}^n (\mathcal{J}_{C0,i} L_i \omega_i) & -E_3 \mathcal{B}_{net} \\ \mathcal{B}_{net}^\top E_3^\top & 0 \end{bmatrix}, \quad g(x) := \begin{bmatrix} g_{Cd}(x_C) & g_{Cq}(x_C) \\ 0 & 0 \end{bmatrix},$$

where

$$\begin{aligned} g_{Cd}(x_C) :&= \begin{bmatrix} \mathcal{J}_{Cd,1} Q_C x_C & \dots & \mathcal{J}_{Cd,n} Q_C x_C \end{bmatrix} \\ g_{Cq}(x_C) :&= \begin{bmatrix} \mathcal{J}_{Cq,1} Q_C x_C & \dots & \mathcal{J}_{Cq,n} Q_C x_C \end{bmatrix}. \end{aligned}$$

Remark 4.3.7. To simplify the notation in the port–Hamiltonian representation it is selected a state representation of the system using energy variables, that is, inductor fluxes and capacitor charges, instead of the more commonly used co–energy variables, *i.e.*, inductor currents and capacitor voltages. The coordinates are indeed related by

$$i_{d,i} = \frac{\phi_{d,i}}{L_i}, \quad i_{q,i} = \frac{\phi_{q,i}}{L_i}, \quad v_{C,i} = \frac{q_{C,i}}{C_i}, \quad i_L = \frac{\phi_T}{L_{T,i}}. \tag{4.3.23}$$

Remark 4.3.8. For ease of presentation it is assumed that the state of the system lives in $\mathbb{R}^{3\mathsf{c}+\mathsf{t}}$. Due to physical and technological constraints it is actually only defined in a subset of $\mathbb{R}^{3\mathsf{c}+\mathsf{t}}$. In particular, the voltages of the dc links are strictly bounded away from zero.

4.4 Control goals & architecture

For its correct operation, hvdc systems — like all electrical power systems — must satisfy a large set of different regulation objectives that are, typically, associated to the multiple time–scale behavior of the system. One way to deal with this issue, that prevails in practice, is the use of hierarchical architectures. These are nested control loops, at different time scales, each one providing references for an inner controller [173, 90, 46, 65]. The control architecture — that mimicks the well–established control architecture of ac systems [7, 96] — is illustrated in Fig. 4.6.

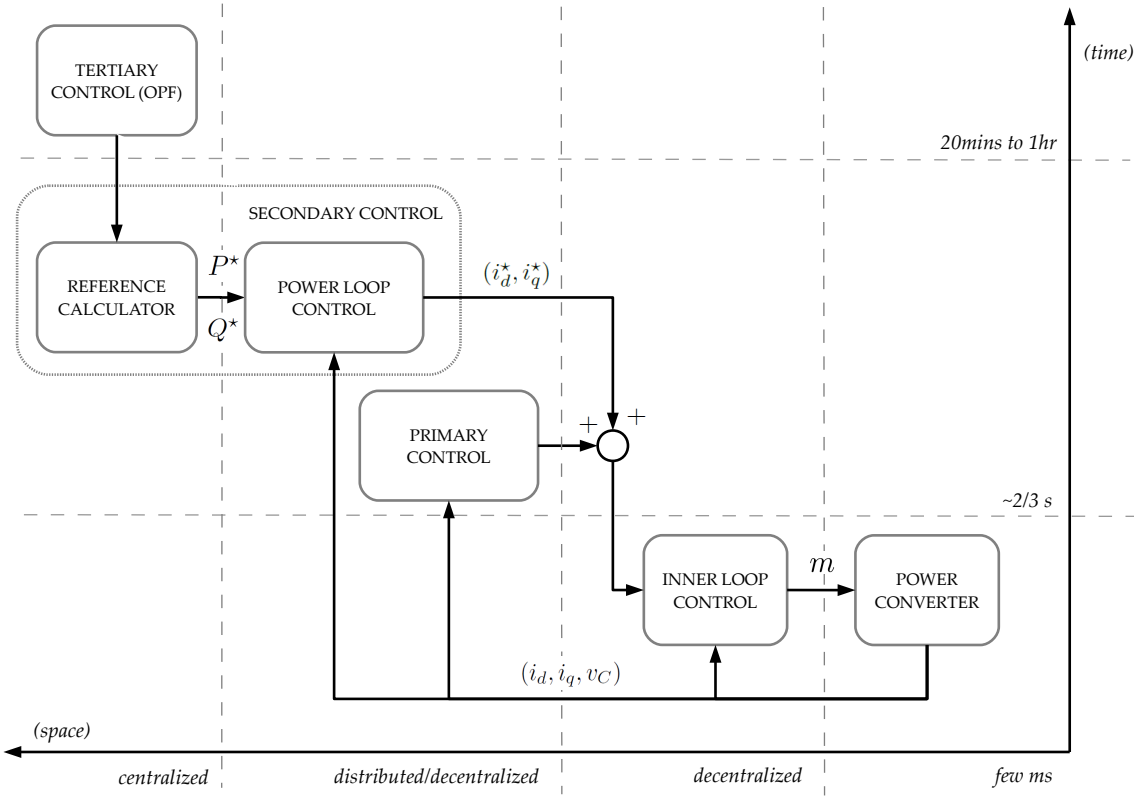

Figure 4.6: Control architecture of multi–terminal hvdc transmission systems.

Tertiary control. For a precise description, it is convenient to start from the "outermost" level of control, that is called *tertiary control* [46, 152, 15]. This takes as input the desired behavior specified

by each terminal operator and provides as output a set of power references, that are the solution of an appropriate *centralized* optimization problem. Such references play the role of operating conditions of the hvdc system — and are obtained by solving a minimization problem, that takes economics and technical aspects into account, as well as their constraints, *e.g.* the power balance. Tertiary control is usually based on algorithms for optimization of the power flow (OPF) [45, 116]. If the tertiary control has an exact knowledge of such constraints and of the desired operation of all terminals, then it is able to formulate a nominal optimization problem and allows the lower levels of control to operate in *nominal conditions*. Otherwise, the tertiary control will formulate a perturbed optimization problem and the system will be operating in *perturbed conditions*. Perturbed conditions may arise because of uncertainty on system parameters and references or whereas one or more terminals provide erroneous information about its current operation. The time–scale in which this layer of control takes action ranges from 20 minutes to an hour [45].

Inner–loop control. We call *inner–loop control* the "innermost" level of control, that is control at the power converter level. The objective of the inner–loop control is to asymptotically drive the hvdc transmission system, if possible, towards the desired steady–state regime specified by the reference input. This steady–state regime is usually expressed in terms of currents and/or voltage, that are determined by the immediately higher level of control or energy–management system [173, 90, 148]. If the desired behavior is not feasible, *i.e.* in perturbed conditions, convergence to an arbitrary steady–state regime is in general required. Regulation should be achieved selecting a suitable switching policy for the converters. A major practical constraint is that the control should be *decentralized*. That is, the controller of each power converter has only available for measurement its corresponding coordinates, with no exchange of information between them. The time–scale in which this layer of control takes action is of a few ms [171, 152, 148]. The design of a new inner–loop controller and an analysis of standard inner–loop control scheme is carried out in Section 4.6 and Section 4.7.

Primary control. It is of fundamental importance — when a perturbation occurs — that the control system takes action adjusting promptly the references to be provided to the inner–loop control in order to preserve properties that are essential for the correct and safe operation of the system. First of all, as for all power systems, stability should be mantained. Furthermore, two fundamental properties must be preserved irrespective of the perturbation: a prespecified power distribution (the so–called *power sharing*); vicinity of the terminals voltage near their nominal value [13, 152, 8]. These are usually achieved by an appropriate control of the dc voltage of one or more terminals at their point of interconnection with the hvdc network [164, 142, 13]. Note that in nominal conditions, the sent power references match those given by the tertiary control and no reference modifications are required. This layer of control — that can be either *distributed* or *decentralized* — is called *primary control*. Several primary controls have been proposed in literature, see [164, 142, 120] for an overview of traditional control methods. The most diffused design is however the *droop control* [18, 123, 69], that takes action by properly modifying the references to be provided to the lower level of control. The time–scale in which this layer of control should take action is — at the best of author's knwoledge — a controversial point. Indeed, although in many practical cases simulated in literature it is assumed a time–scale of ms [46, 45, 18, 152], stability analysis is usually carried out under the assumption that the primary control takes action at a time scale of s, that is the same time–scale adopted in primary control of ac systems [65, 177]. modeling and analysis of an hvdc system under such slower droop controllers is carried out in Section 4.8.

Secondary control. Since the objectives of the *secondary control* are twofold, it is convenient to separate such a control layer in two stages, similarly to [46]. A first stage is devoted to calculate currents and/or voltage references to be provided to the inner–loop control, starting from the measured power and power references obtained by the tertiary control. This stage is usually known as *power control* and has a decentralized architecture. On the other hand, the second stage takes care of recalculating power references whereas a contingency occurs. This stage is known as *reference calculator* and is based on power flow equations. Hence, it requires a centralized architecture to exchange information with the terminals. The outputs of the reference calculator are the sent new power references, that are transformed in currents and/or voltage by the power control. In nominal conditions the sent power references match those given by the tertiary control and no reference modifications are required. A typical example is when a terminal is disconnected, from which follows that previous references cannot be maintained. In this case the secondary control tries to restore the power balance [45].

4.5 Open–loop analysis: assignable equilibria

A first step towards the development of a control strategy for the system (4.3.19) is the definition of its achievable, steady–state behavior, which is determined by the assignable equilibria, as defined in Subsection 2.1.4. To identify this set the following lemmata are established.

Lemma 4.5.1. The equilibria of the transmission line coordinates are given by

$$x_T^\star = (\mathcal{R}_T Q_T)^{-1} \mathcal{B}_{net}^\top E_3^\top Q_C x_C^\star. \tag{4.5.1}$$

Proof. Setting to zero the left–hand side of (4.3.15), calculated at $x_T^\star$, gives

$$0_{\mathsf{t}} = -\mathcal{R}_T Q_T x_T^\star + v_T^\star \quad \Rightarrow \quad x_T^\star = (\mathcal{R}_T Q_T)^{-1} v_T^\star.$$

Moreover, from (4.3.18) it follows that $v_T^\star = \mathcal{B}_{net}^\top E_3^\top Q_C x_C^\star$, that replaced in the equation above completes the proof. □□□

Lemma 4.5.2. The equilibria of the converters coordinates are the solution of the following c quadratic equations:

$$-\frac{R_i}{L_{c,i}^2}\left[(\phi_{d,i}^\star)^2 + (\phi_{q,i}^\star)^2\right] - \frac{G_i}{C_{c,i}^2}(q_{C,i}^\star)^2 + \frac{v_{d,i}}{L_{c,i}}\phi_{d,i}^\star + \frac{1}{C_{c,i}} q_{C,i}^\star i_{C,i}^\star = 0, \tag{4.5.2}$$

with $\mathrm{col}(i_{C,i}^\star) = \mathcal{B}_{net}\mathcal{R}_T^{-1}\mathcal{B}_{net}^\top Q_C \mathrm{col}(q_{C,i}^\star)$, $i \sim \mathcal{E}_{VSC}$.

Proof. In [129] it is shown that the set of admissible equilibria of a voltage source converter is obtained by setting equal to zero its power balance, that for c converters is equivalent to (4.5.2). To complete the proof, it is now sufficient to recall definitions

$$\mathrm{col}(i_{dc,i}^\star) = i_C^\star, \qquad E_3^\top Q_C x_C^\star = \mathrm{col}(q_{C,i}^\star),$$

together with (4.3.18), (4.5.1). □□□

The main result of the section is now presented, the proof of which follows immediately from the lemmata above.

Proposition 4.5.3. The set of assignable equilibria of the system (4.3.19) is given by

$$\mathcal{E}^\star := \{x^\star \in \mathbb{R}^{3\mathsf{c}+\mathsf{t}} \mid (4.5.1) \text{ and } (4.5.2) \text{ hold}\}. \tag{4.5.3}$$

Remark 4.5.4. From the derivations above it is clear that the equilibria of the network are univocally determined by the equilibria of the converters. Moreover, the latter should satisfy the quadratic equations (4.5.2), which are called the *power flow (steady–state) equations* (PFSSE) of the individual converter subsystems. In contrast with standard power flow equations reported in literature [116], that are indeed expressed using power variables, the PFSSE (4.5.2) are expressed in terms of currents and voltages of the power converters. A question of interest is how system operators should select from this set the equilibrium points that correspond to some *desired behavior*. In the latter there are many practical considerations to be taken into account, including technical and economical aspects. The layer of control in charge of this task is the tertiary control.

Remark 4.5.5. Differently from the single converter case, the set of assignable equilibria does not coincide, but is strictly contained, in the set where the power of the system is balanced, that is

$$\mathcal{E}^\star \subset \mathcal{P}^\star, \qquad \mathcal{P}^\star := \{x^\star \in \mathbb{R}^{3\mathsf{c}+\mathsf{t}} \mid \dot{\mathcal{H}} = 0\}.$$

This fact is clearly explained in [129], where it is proved that a necessary condition for $\mathcal{E}^\star \equiv \mathcal{P}^\star$, is the system to be of co-dimension one.

4.6 Inner–loop control: design

4.6.1 Control objectives & standard controllers

For an appropriate design of the inner–loop control, the control problem should be first established. This is done briefly reviewing some of the inner–loop controllers for converters reported in the literature, that are implicitly determined by the correspondent control objectives. The vast majority of the papers reported on this topic — and, in general, of control of power converters [90, 173, 112, 48] — uses the description of the dynamics of the single converter in co–energy variables, that is the one given by (4.3.6). Since we focus on the model of a single voltage source converter the subindex i — when clear from the context — is omitted. The total energy of the single converter expressed by (4.3.10) can be then rewritten in co–energy variables as:

$$\mathcal{H}_C(i_d, i_q, v_C) := \frac{1}{2}\left(Li_d^2 + Li_q^2 + Cv_C^2\right),$$

and the power balance is

$$\dot{\mathcal{H}}_C = -R(i_d^2 + i_q^2) - Gv_C^2 + P + P_{dc}. \tag{4.6.1}$$

Note, that in the last equation we used the fact that $V_q = 0$ and the definitions of power provided in Subsection 2.2.5, from which follows:

$$P = V_d i_d, \qquad Q = V_d i_q, \qquad P_{dc} = v_C i_{dc}. \tag{4.6.2}$$

Because under Assumption 4.3.3 V_d is constant, it is clear that the regulation of P and Q is equivalent to the regulation of i_d and i_q respectively. Since two variables among the three can be controlled, we have three possible combinations: active/reactive power, active power/dc voltage and reactive power/dc

voltage. In practice however, because of the small losses of the converter, the value of P slightly differs from P_{dc}, and consequently there is no interest in regulating the pair P and v_C at the same time. It is thus common to distinguish two modes of operation:

i) *PQ (also: active/reactive power) control mode*, when the converter is required to control the active and reactive power. This is achieved regulating to zero the output

$$y_I = \begin{bmatrix} i_d - i_d^\star \\ i_q - i_q^\star \end{bmatrix}. \tag{4.6.3}$$

The converter is operated as power source, *i.e.*, it provides a pre-specified amount of active and reactive power. The inner control loop is a current control the feedback signal of which is the current through the filter inductance. Current references are determined by an outer power controller — based on (4.6.2) — that takes measured active and reactive powers and their references $P^\star, Q^\star$ as input and provides as output $i_d^\star$ and $i_q^\star$. This layer of control is referred as *power control* and is usually considered to be part of the secondary control, while the overall scheme is also called *direct current control* [100, 143].

ii) *$Q - v_C$ (also: reactive power/dc voltage) control mode*, when the converter is required to control reactive power and dc voltage. In this case, the regulated output is

$$y_V = \begin{bmatrix} v_C - v_C^\star \\ i_q - i_q^\star \end{bmatrix}. \tag{4.6.4}$$

The converter is controlled in such way that reactive power and dc voltage can be specified by the designer. This can be achieved either by an inner quadrature current/dc voltage control or via a cascaded control scheme consisting of an inner current control and an outer voltage control [100, 143, 120]. The latter control architecture is sometimes preferred since it improves the control performance. These kind of schemes are also called *direct* and *undirect output voltage control* respectively. The quadrature current reference — as for the case of PQ control — is determined by an outer (reactive) power controller — based on (4.6.2) — that takes the measured reactive power and its reference $Q^\star$ as input and provides as output $i_q^\star$. This layer of control takes the name of *reactive power control*.

In the recent years many innovative control strategies have been proposed to regulate the outputs (4.6.3) and (4.6.4), based on H_∞ theory [176, 102], Lyapunov theory [101], sliding–modes control [126] or complex feedback linearization schemes [155, 32, 33, 15]. However, such new control strategies often lead to complicate (nonlinear) controllers and are in general difficult to implement. More conservative control strategies are indeed used in real applications [148]. The control strategy most used is vector control [171, 20, 100] and consists in an appropriate combination of a feedback linearization and a PI control scheme, see Fig. 4.7, where such a scheme is illustrated with respect to the equivalent circuit of the power converter, in dq coordinates. An invariably local analysis is usually carried out to justify these control schemes [171, 152] and suitable tuning procedures are adopted to ensure the stability of the system [150, 172]. In Section 4.7 it is proved that y_I and y_V with respect to which the feedback linearization is performed, have *unstable zero dynamics*. Consequently, applying high gains in the PIs will induce instability and the internal behavior of the feedback linearizing schemes will be unstable.

This well–known phenomenon of nonlinear systems [82] is akin to cancellation of unstable zeros of the plant with the unstable poles of the controller in linear systems.

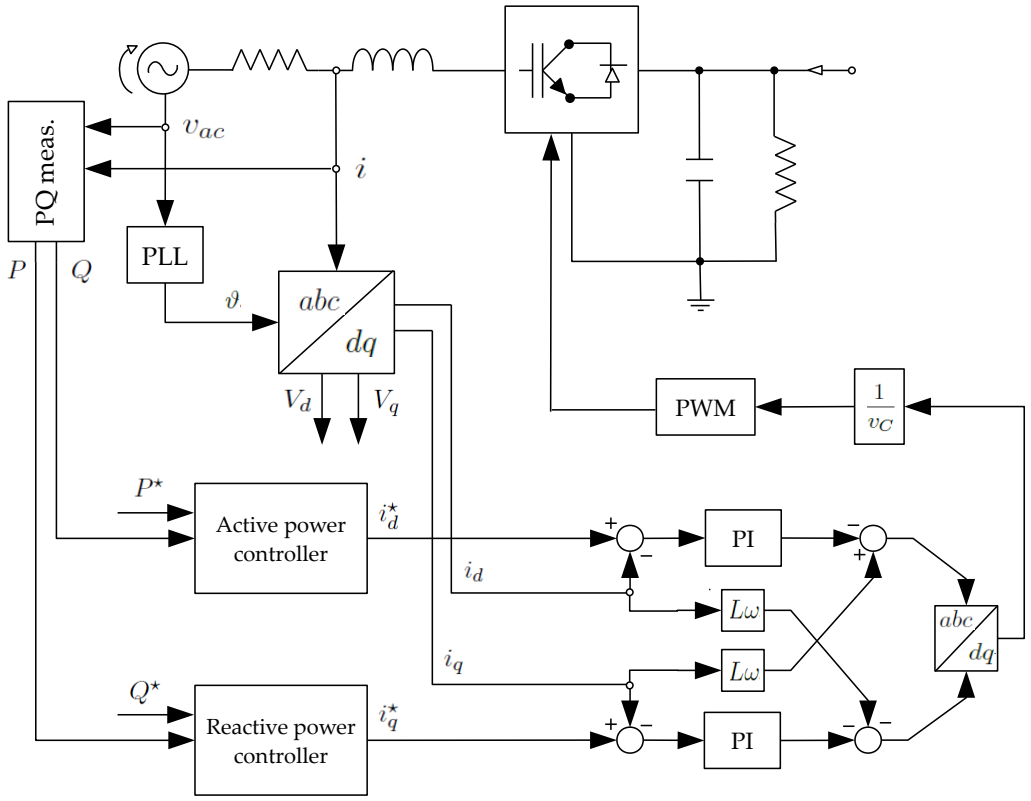

Figure 4.7: Vector control as a combination of a feedback linearization and a PI control scheme.

Remark 4.6.1. For weakly connected terminals, the ac voltage is a controllable variable and further modes of operation have to be considered, namely for the control of the ac/dc voltages and of the active power/ac voltage, for which the interested reader is referred to [68].

Remark 4.6.2. An important observation is that any arbitrary pair $(i_d^\star, i_q^\star)$ or $(i_q^\star, v_C^\star)$ always, univocally, determines an assignable equilibrium point $x^\star = (i_d^\star, i_q^\star, v_C^\star) \in \mathcal{E}^\star$. Hence a steady–state that verfies $y_I = 0$ (or $y_V = 0$) is always achievable.

4.6.2 PI–passivity based control

In this section it is presented a decentralized, globally asymptotically stabilizing, PI controller based on passivity arguments (PI–PBC) for the system (4.3.19). The construction of the controller is inspired by previous works on passivity–based control of power converters [119, 76, 84], which exploit the property of passivity of the *incremental model*. For, the following assumption, that is equivalent to assume the system operating in nominal conditions, is made.

Assumption 4.6.3. *The desired operating point belongs to the set of assignable equilibria, that is* $x^\star \in \mathcal{E}^\star$.

Along the lines of Proposition 1 in [76], it is possible to establish passivity of the incremental model of the overall hvdc transmission system (4.3.19) with respect to a suitable defined output. As is well–known, global regulation of a passive output can be achieved with a simple PI controller [27]. Regulation of the state to the desired equilibrium then follows provided a suitable detectability assumption is satisfied [159].

Proposition 4.6.4. Consider the hvdc transmission system (4.3.19). Let $x^\star \in \mathcal{E}^\star$ be the desired equilibrium with corresponding (univocally defined) control $u^\star \in \mathbb{R}^{2\mathsf{c}}$. Define the error signals

$$\tilde{x} = x - x^\star, \quad \tilde{u} = u - u^\star \tag{4.6.5}$$

and the output signal

$$y := \begin{bmatrix} \mathrm{col}(y_{d,i}) \\ \mathrm{col}(y_{q,i}) \end{bmatrix} \in \mathbb{R}^{2\mathsf{c}}, \tag{4.6.6}$$

with

$$y_{d,i} := x_C^{*\top} Q_C \mathcal{J}_{Cd,i} Q_C x_C, \qquad y_{q,i} := x_C^{*\top} Q_C \mathcal{J}_{Cq,i} Q_C x_C.$$

The mapping $\tilde{u} \to y$ is *passive*. More precisely, the system verifies the dissipation inequality

$$\dot{\mathcal{H}}_d \leq y^\top \tilde{u}, \tag{4.6.7}$$

with storage function $\mathcal{H}_d(\tilde{x}) = \frac{1}{2}\tilde{x}^\top Q \tilde{x}$.

Proof. The proof mimics the proof of Proposition 1 in [76]. First of all, recalling the relation (4.3.22) in Remark 4.3.6, it is possible to rewrite (4.3.19) in the alternative form:

$$\begin{aligned} \dot{x} &= (\mathcal{J}_0 - \mathcal{R})Qx + EV + g(x)u \\ &= (\mathcal{J}_0 - \mathcal{R})Q(\tilde{x} + x^\star) + EV + g(\tilde{x} + x^\star)(\tilde{u} + u^\star) \\ &= (\mathcal{J}_0 - \mathcal{R})Q\tilde{x} + g(\tilde{x})(\tilde{u} + u^\star) + g(x^\star)\tilde{u}, \end{aligned} \tag{4.6.8}$$

where definitions (4.6.5) have been used to get the second equation and the fact that the assignable equilibria $x^\star$ and corresponding (constant) control $u^\star$ satisfy

$$(\mathcal{J}_0 - \mathcal{R})Qx^\star + EV + g(x^\star)u^\star = 0,$$

are used to obtain the third equation.

The derivative of $\mathcal{H}_d$ along the trajectories of the incremental model (4.6.8) yields

$$\dot{\mathcal{H}}_d = -\tilde{x}^\top Q\mathcal{R}Q\tilde{x} + \tilde{x}^\top Q g(x^\star)\tilde{u} = -\tilde{x}^\top Q\mathcal{R}Q\tilde{x} + y^\top \tilde{u},$$

where the skew–symmetry of $\mathcal{J}_0$, $\mathcal{J}_{Rd,i}$ and $\mathcal{J}_{Rq,i}$ is used in the first equation, and the fact that the output signal can be rewritten as

$$y = g^\top(x^\star)Qx = g^\top(x^\star)Q\tilde{x}$$

is used to obtain the second identity. The proof is completed recalling that the dissipation matrix verifies $\mathcal{R} > 0$ to obtain the bound (4.6.7). □□□

We have then the following result.

Proposition 4.6.5. Consider the hvdc transmission system (4.3.19), with a desired steady–state $x^\star \in \mathcal{E}^\star$, in closed–loop with the decentralized PI control

$$u = -K_P y + K_I \zeta, \quad \dot{\zeta} = -y, \tag{4.6.9}$$

with y given in (4.6.6) and positive definite gain matrices

$$K_P = \begin{bmatrix} K_{Pd} & 0 \\ 0 & K_{Pq} \end{bmatrix} \in \mathbb{R}^{2\mathsf{c}\times 2\mathsf{c}}, \quad K_I = \begin{bmatrix} K_{Id} & 0 \\ 0 & K_{Iq} \end{bmatrix} \in \mathbb{R}^{2\mathsf{c}\times 2\mathsf{c}}, \tag{4.6.10}$$

where $K_{Pd} = \text{diag}\{k_{Pd,i}\}$, $K_{Pq} = \text{diag}\{k_{Pq,i}\}$, $K_{Id} = \text{diag}\{k_{Id,i}\}$, $K_{Iq} = \text{diag}\{k_{Iq,i}\}$. The equilibrium point $(x^\star, K_I^{-1}u^\star)$ is globally asymptotically stable (GAS).

Proof. Define the Lyapunov function candidate

$$W(\tilde{x}, \tilde{\zeta}) := \mathcal{H}_d(\tilde{x}) + \frac{1}{2}\tilde{\zeta}^\top K_I \tilde{\zeta}, \tag{4.6.11}$$

where $\tilde{\zeta} := \zeta - K_I^{-1}u^\star$. The derivative of $W(x, \zeta)$ along the trajectories of the closed–loop system (4.3.19)-(4.6.9) is given by

$$\begin{aligned} \dot{W} &= -\tilde{x}^\top Q\mathcal{R}Q\tilde{x} + y^\top \tilde{u} + \tilde{\zeta}^\top K_I y \\ &= -\tilde{x}^\top Q\mathcal{R}Q\tilde{x} + y^\top \tilde{u} - (\tilde{u}^\top + y^\top K_P)y \\ &= -\tilde{x}^\top Q\mathcal{R}Q\tilde{x} - y^\top K_P y \leq 0, \end{aligned}$$

which proves global stability. Asymptotic stability follows, as done in [76], using LaSalle's arguments. Indeed, from the inequality above and the definition of $\mathcal{R}$ in (4.3.21) it is clear that all components of the error state vector $\tilde{x}$ tend asymptotically to zero. □□□

Remark 4.6.6. The proposed PI–PBC is decentralized in the sense that, for its implementation, the controller requires only the measurement of the inductor currents and capacitor voltage of the associated terminal. Guaranteeing this property motivates the choice of block diagonal gain matrices (4.6.10).

Remark 4.6.7. The PI–PBC requires the selection of the desired values for the inductor currents and capacitor voltages that, clearly, cannot all be chosen arbitrarily. Instead, they have to be selected from the set of assignable equilibrium points $\mathcal{E}$, that is determined by the PFSSE. This set has a rather simple structure: the quadratic equation (4.5.2) defines the converters variables from which it is possible to *univocally* determine the transmission lines coordinates via (4.5.1).

Remark 4.6.8. The PI–PBC is *universal*, in the sense that it can operate either in PQ or $Q{-}v_C$ *control mode*, depending on which components of the equilibrium point are assigned as desired references, and which ones are consequently determined via the PFSSE.

4.6.3 Relation of PI–PBC with Akagi's PQ method

A dominant approach for the design of controllers for reactive power compensation using active filters (for three–phase circuits) is the PQ instantaneous power method proposed by Akagi, *et al.* in [5]. It consists of an outer–loop that generates references for the inner PI loops. The references are selected

in order to satisfy a very simple heuristic: the ac active power P has to be equal to the dc power P_{dc}, thus ensuring the maximal power transfer from the ac to the dc side, and the reactive power should take a desired value. For the sake of comparison the passive output (4.6.6) in co–energy variables, for a single converter, is provided:

$$y = \begin{bmatrix} v_C^\star i_d - i_d^\star v_C \\ v_C^\star i_q - i_q^\star v_C \end{bmatrix}, \tag{4.6.12}$$

where $(i_d^\star, i_q^\star, v_C^\star) \in \mathcal{E}^\star$, that is, they belong to the assignable equilibrium set. Now, using (4.6.2) define the active ac and dc powers at the equilibrium as

$$P^\star = V_d i_d^\star, \quad P_{dc}^\star = v_C^\star i_C.$$

Consider then the following equivalences

$$P^\star P_{dc} = P_{dc}^\star P \quad \Leftrightarrow \quad v_C^\star i_d = i_d^\star v_C \quad \Leftrightarrow \quad y_1 = 0,$$

with y_1 the first component of the passive output (4.6.12). Similarly, for the reactive power

$$Q^\star P_{dc} = P_{dc}^\star Q_i \quad \Leftrightarrow \quad v_C^\star i_q = i_q^\star v_C \quad \Leftrightarrow \quad y_2 = 0,$$

with y_2 the second component of the passive output (4.6.12). In other words, the objective of the PI–PBC to drive the passive output y to zero can be reinterpreted as a power equalization objective identical to the one used in Akagi's PQ method.

4.7 Inner–loop control: performance & stability analysis

Quality assessment of control algorithms is a difficult task — epitomized by the classical performance versus robustness tradeoff, neatly captured by the stability margins in linear designs. The situation for nonlinear systems, where the notions of (dominant) poles and frequency response are specious, is far more complicated. In any case, it is well–known that the achievable performance in control systems is limited by the presence of minimum phase zeros [55, 125, 141]. In this section an attempt is made to evaluate stability properties and performance limitations of the inner–loop controllers discussed in the previous sections, namely the PI–PBC introduced in Section 4.6.2 and the vector control schemes described in Section 4.6.1.

4.7.1 Zero dynamics analysis

The zero dynamics of the converter system (4.3.6) for the outputs y (4.6.6), y_I (4.6.3) and y_V (4.6.4) are computed. All three outputs have relative degrees $\{1, 1\}$, hence their zero dynamics is of order one but, while it is exponentially stable for the passive output y it turns out that — for normal operating regimes of the converter — it is *unstable* for y_I and y_V. If the zero dynamics is *unstable* cranking up the controller gains yields an unstable behavior. This should be contrasted with the passive output y that, as shown in Proposition 4.6.5 yields an asymptotically stable closed–loop system for all positive gains.[1]

[1] This discussion pertains only to the behavior of the adopted mathematical model of the converter. In practice, other dynamical phenomena and unmodeled effects may trigger instability even for the PI–PBC.

A caveat regarding the subsequent analysis is, however, necessary. When the converters are connected to the transmission lines the currents i_C are linked to the currents on the line via (4.3.17), which are clearly nonconstant. However, to simplify the analysis, it is assumed that they are *constant*. This assumption is standard for the inner control of power converters [90, 173, 112] and can be justified by exploiting the fact that their rate of change is slow (with respect to the converter dynamics). Under this assumption the assignable equilibrium set of (4.3.6) is given by:

$$\mathcal{E}^\star = \{x \in \mathbb{R}^3 \mid R(i_d^2 + i_q^2) - V_d i_d + G v_C^2 - i_C v_C = 0\}. \tag{4.7.1}$$

To simplify the derivations only the case of $i_q^\star = 0$ is considered. This assumption is justified since it corresponds to fix to zero the desired value of the reactive power, which is a common operating mode of converters. Moreover, this is done without loss of generality because it is possible to show — alas, with messier calculations — that the stability of the zero dynamics is the same for the case of $i_q^\star \neq 0$. This situation may arise when the converter is associated to an ac grid and not to a renewable energy source. In this section, it is possible to prove that the (first order) zero dynamics associated to (4.6.6), is "extremely slow" — with respect to the overall bandwidth of the converter. Since this zero "attracts" one of the poles of the closed–loop system, it stymies the achievement of fast transient responses. This situation motivates the inclusion of an outer–loop controller that generates the references to the inner–loop PI. This modification is presented in Section 4.7.3.

Before presenting the main result, an important observation is done: the zero dynamics of the converter model (4.3.6) and of its corresponding incremental version are the same. Indeed, the zero dynamics describes the behavior of the dynamical system restricted to the set where the output is zero. Since the incremental model dynamics is the *same* as the original model dynamics — simply adding and substracting a constant — their zero dynamics coincide.

Zero dynamics analysis of the passive output y

Proposition 4.7.1. Fix $(i_d^\star, i_q^\star, v_C^\star) \in \mathcal{E}^\star$ with $i_q^\star = 0$. The zero dynamics[2] of the converter (4.3.6) with respect to the output (4.6.12) is *exponentially stable* and is given by

$$\dot{v}_C = -\lambda v_C + \lambda v_C^\star, \qquad \lambda := \frac{R(i_d^\star)^2 + G(v_C^\star)^2}{L(i_d^\star)^2 + C(v_C^\star)^2}. \tag{4.7.2}$$

Proof. By setting the output (4.6.12) identically to zero and using the fact that $i_q^\star = 0$, it is easy to get

$$i_d = \frac{i_d^\star}{v_C^\star} v_C, \qquad i_q = \frac{i_q^\star}{v_C^\star} v_C = 0. \tag{4.7.3}$$

Replacing (4.7.3) into (4.3.6) gives

$$L\frac{i_d^\star}{v_C^\star}\dot{v}_C = -R\frac{i_d^\star}{v_C^\star} v_C - v_C u_1 + V_d, \tag{4.7.4}$$

$$0 = -L\omega\frac{i_d^\star}{v_C^\star} v_C - v_C u_2, \tag{4.7.5}$$

$$C\dot{v}_C = \frac{i_d^\star}{v_C^\star} v_C u_1 - G v_C + i_{dc}. \tag{4.7.6}$$

[2]With some abuse of notation, the zero dynamics is represented using the same symbols of the system dynamics.

To eliminate u_1 it suffices to multiply (4.7.6) by $\frac{v_C^\star}{i_d^\star}$ and add it to (4.7.4), yielding

$$\left(\frac{Cv_C^\star}{i_d^\star}+\frac{Li_d^\star}{v_C^\star}\right)\dot{v}_C=-\left(\frac{Ri_d^\star}{v_C^\star}+\frac{Gv_C^\star}{i_d^\star}\right)v_C+V_d+\frac{v_C^\star}{i_d^\star}i_C.$$

The proof is completed by noting from (4.7.1) that, for $(i_d^\star, i_q^\star, v_C^\star)\in\mathcal{E}^\star$ with $i_q^\star=0$, it follows that

$$V_d+\frac{v_C^\star}{i_d^\star}i_C=\frac{R(i_d^\star)^2+G(v_C^\star)^2}{i_d^\star}$$

and by pulling out the common factor $\frac{1}{i_d^\star v_C^\star}$. □□□

Remark 4.7.2. The parameters R and G, that represent the losses in the converter, are usually small — compared to L and C. Consequently, λ will also be a small value, placing the pole of the zero dynamics very close to the origin and inducing slow convergence.

Remark 4.7.3. It is interesting to note that the rate of exponential convergence of the zero dynamics can be rewritten as

$$\lambda=\frac{1}{2}\frac{R(i_d^\star)^2+G(v_C^\star)^2}{\mathcal{H}(i_d^\star,i_q^\star,v_C^\star)},$$

that is equivalent to half the ratio between the steady–state dissipated power and the steady–state energy of the system. This relation holds true also for the case $i_q^\star\neq 0$.

Zero dynamics analysis of y_I

Before analyzing the zero dynamics of the PQ and dc voltage control outputs, (4.6.3) and (4.6.4), respectively, it is important to recall that their references necessarily belong to the assignable equilibrium set, see Remark 4.6.2. Moreover, similarly to the case of the passive output, it is assumed that $i_q^\star=0$.

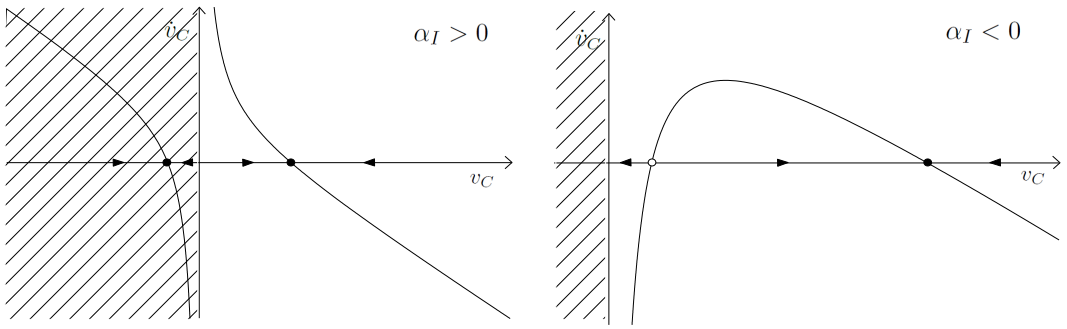

Figure 4.8: Plot of $\dot{v}_C$ versus v_C for the cases of (a) $\alpha_I>0$ and (b) $\alpha_I<0$. The arrows in the horizontal axis indicate the direction of the flow of the zero dynamics.

Proposition 4.7.4. Fix $i_d^\star\in\mathbb{R}$, $i_q^\star=0$. The zero dynamics of the converter (4.3.6) with respect to the output (4.6.3) is given by

$$C\dot{v}_C=-Gv_C+\frac{\alpha_I}{v_C}+i_C^\star,\qquad \alpha_I:=V_di_d^\star-R(i_d^\star)^2 \tag{4.7.7}$$

where $i_C^\star$ is a constant value for i_C satisfying

$$(i_C^\star)^2 > -4G\alpha_I. \tag{4.7.8}$$

- If $\alpha_I > 0$ the zero dynamics has one equilibrium and it is *stable*.
- If $\alpha_I < 0$ the zero dynamics has two equilibria one stable and one unstable.
- If $\alpha_I = 0$ the zero dynamics is a linear asymptotically *stable* system.

Proof. Setting the output (4.6.3) equal to zero with $i_q^* = 0$ and replacing into (4.3.6) gives

$$0 = -Ri_d^\star - v_C u_1 + V_d \tag{4.7.9}$$
$$0 = -L\omega i_d^\star - v_C u_2 \tag{4.7.10}$$
$$C\dot{v}_C = i_d^\star u_1 - Gv_C + i_C^\star, \tag{4.7.11}$$

where the superscript $(\cdot)^\star$ has been added to i_C. Replacing u_1 obtained from (4.7.9) into (4.7.11) yields directly (4.7.7). Condition (4.7.8) is then necessary and sufficient for the existence of a (real) equilibrium of (4.7.7). If $\alpha_I = 0$ the dynamics reduces to

$$C\dot{v}_C = -Gv_C + i_C^\star.$$

The proof is completed by recalling that $v_C > 0$ and looking at the plots of the right hand side of (4.7.7) for α_I positive and negative in Fig. 4.8. □□□

Remark 4.7.5. From Fig. 4.8, if $\alpha_I < 0$, it is easy to see that the stable equilibrium point is the largest one. For standard values of the system parameters it turns out that this equilibrium is located beyond the physical operating regime of the system, hence it is of no practical interest.

Remark 4.7.6. The parameters R and G are usually very small and $i_C^\star$ can take positive or negative values in standard operation. Then condition (4.7.8) is always verified while α_I can take positive or negative values.

Remark 4.7.7. The situation $\alpha_I = 0$, when the zero dynamics is linear and asymptotically stable, is unattainable in applications. Indeed, assuming that in steady–state all signals converge to their reference values, it can be shown that $\alpha_I = 0$ if and only if $Gv_C - i_C = 0$ that, given the small values of G is not realistic in practice.

Zero dynamics analysis of y_V

Proposition 4.7.8. Fix $v_C^\star \in \mathbb{R}$, $i_q^\star = 0$. The zero dynamics of the converter (4.3.6) with respect to the output (4.6.4) is given by

$$L\frac{di_d}{dt} = -Ri_d + \frac{\alpha_V}{i_d} + V_d, \qquad \alpha_V := i_C^\star v_C^\star - G(v_C^\star)^2 \tag{4.7.12}$$

where $i_C^\star$ is a constant value for i_C satisfying

$$V_d^2 > -4R\alpha_V. \tag{4.7.13}$$

- If $\alpha_V > 0$ the zero dynamics has two equilibria and they are both *stable*.

- If $\alpha_V < 0$ the zero dynamics has two equilibria one stable and one unstable.

- If $\alpha_V = 0$ the zero dynamics is a linear asymptotically *stable* system.

Proof. Setting the output (4.6.4) equal to zero with $i_q^* = 0$ and replacing into (4.3.6) gives

$$L\frac{di_d}{dt} = -Ri_d - v_C^\star u_1 + V_d, \tag{4.7.14}$$

$$0 = -L\omega i_d - v_C^\star u_2, \tag{4.7.15}$$

$$0 = i_d u_1 - G v_C^\star + i_C. \tag{4.7.16}$$

Replacing u_1 obtained from (4.7.16) into (4.7.14) yields directly (4.7.12). Condition (4.7.13) is necessary and sufficient for the existence of a (real) equilibrium of (4.7.12). The proof is completed invoking the same arguments used in the proof of Proposition 4.7.4 and are omitted for brevity. □□□

Remark 4.7.9. Remarks 4.7.5, 4.7.6 and 4.7.7 apply *verbatim* to (4.7.12) and α_V of Proposition 4.7.8.

4.7.2 An illustrative example

Although Proposition 4.7.1 proves that the zero dynamics for the passive output y is exponentially stable, it turns out that, for the components used in standard hvdc transmission system, the convergence rate is $\lambda \approx 0.04$, which is extremely slow. As indicated above this dominating dynamics stymies the achievement of fast transient responses — a situation that is shown in the following simulations. Also, simulated evidence of the unstable behavior of the vector control inner–loops using the outputs (4.6.3) and (4.6.4) is presented.

A three–terminals hvdc transmission system with a simple *meshed* topology is considered, as illustrated in Fig. 4.9, where the corresponding graph is also given. The model of the system is given by (4.3.19), that is a system of dimension $3\mathsf{c} + \mathsf{t} = 11$ with $2\mathsf{c} = 6$ inputs. Parameters of the converters and of the transmission lines are given in Table 1.

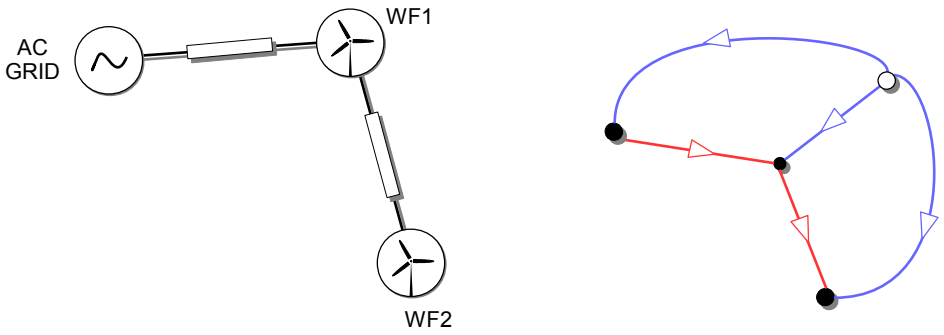

Figure 4.9: Schematic representation of a multi–terminal hvdc transmission system constituted by three terminals, associated to two wind farms (WFs) and an ac grid, with associated graph. The graph is represented by filled circles for the *converter buses* and the unfilled circle for the *ground* node. Blue and red edges characterize converters and lines, respectively.

Table 4.1: Three-terminal hvdc transmission system parameters.

	Value		Value
$R_{r,i}$	0.01 Ω	$G_{r,i}$	0 Ω^{-1}
$L_{r,i}$	40 mH	$C_{r,i}$	20 μF
V_i	130 kV	ω_i	50 Hz
$R_{\ell,12}$	26 Ω	$L_{\ell,12}$	3.76 mH
$R_{\ell,23}$	20 Ω	$L_{\ell,23}$	2.54 mH

Table 4.2: Three-terminal hvdc transmission system references.

	SB	WF_1	WF_2	SB	WF_1	WF_2
0	-1260	900	1000	100	142.595	158.951
T	-1588	900	1800	100	153.650	179.691
$2T$	-266	500	-200	100	109.004	104.004
$3T$	905	-400	-200	100	69.419	60.877
$4T$	-849	1300	-200	100	128.708	124.532

Consider then the following *control objectives*: all the terminals are required to regulate the reactive power to zero; the terminals associated to the wind farms (WF1, WF2) are required to regulate the active power to desired (constant) values; the remaining terminal, called *slack bus* (SB), must regulate the voltage around its nominal value. The corresponding references of direct current and dc voltages are then selected by the operator of each terminal and the corresponding assignable equilibria are determined by the PFSSE defined by (4.5.3). Changes in references occur every T s over a time interval of $5T$ s and are described in Table 2[3]. From 0 to $2T$ s both WFs are injecting (active) power into the hvdc transmission system so that the SB is absorbing power. At $2T$ s, WF1 is reducing the amount of injected power, while at the same time WF2 becomes unable to provide enough power to supply local loads. Thus, the power flow at WF2 is reversed, but the required power can be still matched by the power injected by WF1. At $3T$ s, also WF1 becomes unable to supply its local loads, from which follows that the power flow is fully reversed and the SB is now demanded to contribute for the missing power. Finally, at $4T$ s WF1 regain the ability of supplying local loads, reversing again the power flow and contributing to feed both WF2 and the SB.

PI–PBC

In this subsection the simulations on the three–terminals benchmark example of the decentralized PI–PBC defined in Section 4.6.2 are presented, illustrating the stability properties and performance limitations previously discussed. Setting $T = 2000$ s the controllers (4.6.9) are designed with identical parameters and diagonal matrices $k_{P,i} = \text{diag}\{1, 1\}$, $k_{I,i} = \text{diag}\{10, 10\}$. Some considerations before an analysis of the simulations are, however, necessary. Recalling Remark 4.6.7, since the PI–PBC requires, for its implementation, the knowledge of the equilibrium point, this needs to be computed beforehand by a centralized calculator via the PFSSE defined by (4.5.3). A correct computation of such equilibrium is thus possible in practice *only if* information about selected references and terminal parameters is correctly and instantaneously transferred from the terminals to such a calculator, *i.e.* the system is operated in *nominal conditions*.

[3]It is worth mentioning that such a strongly changing scenario is not frequently experienced in practice and it is here employed only for validation purposes.

The behavior of the converters — in *nominal conditions* — is depicted in Fig. 4.10. As expected, the direct currents of each station attain the assignable equilibria defined in Table 2, while the quadrature currents are always kept to zero after a very short transient. Moreover, the dc voltage at the slack bus is maintained near the nominal value of 100 kV, as required, while the dc voltage variation at the wind farms stations, balances the fluctuation of power demand. Even though the desired steady–state is attained for all practical purposes, the convergence time of direct currents and dc voltages is extremely slow. This poor transient performance behavior is independent of the controller gains. Indeed, extensive simulations show that the system maintains the same slow convergence time even with larger gains, thus validating the performance limitations analysis realized in Subsection 4.7.1.

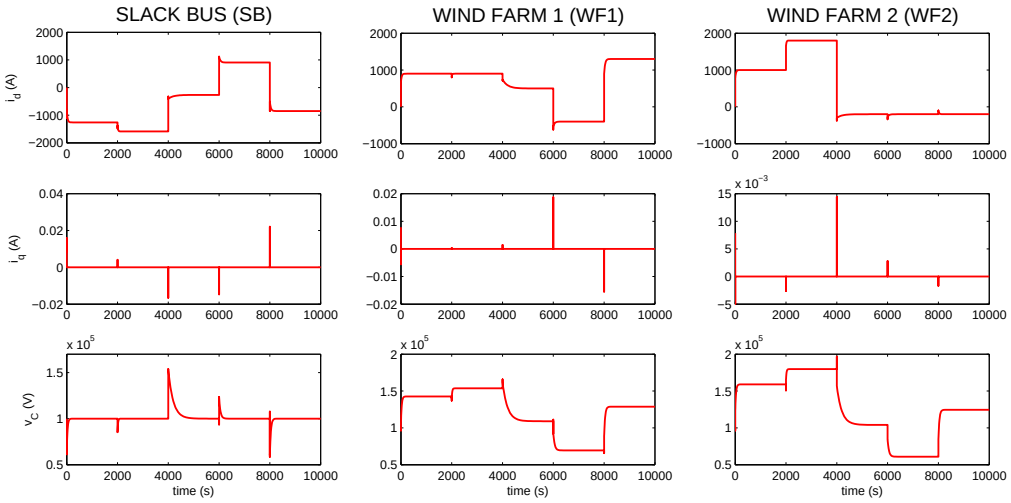

Figure 4.10: Responses of converters variables under the decentralized PI–PBC — in *nominal conditions.*

Unfortunately if we suppose that at perturbation occurs, *e.g.* in the form of a change of active power references provided by a terminal to its PI–PBC, although the responses of the converters still converge to a steady–state, this may be not suitable for pratical operation of the hvdc system. It can be indeed shown that the responses stay close the nominal operating condition only for very small perturbations. For larger perturbations on the other hand, the system is driven to a steady–state regime with a large drop of the dc voltages from the nominal value and active powers almost zero at all terminals — this being clearly unsuitable in practice.

Remark 4.7.10. From Fig. 4.10, it is noted that dc voltages exhibit significant overshoots at $2T$, $3T$, $4T$ s. This behavior is due to the highly stressed scenario and the essential benchmark employed for the simulations. A more realistic scenario would include more terminals — some of which would be operated as *slack buses* — and less significant reference changes. Hence, any reference change in terms of active power is supposed to be better absorbed by the slack buses, thus reducing the amplitude of the overshoots.

PQ and $Q - v_C$ controllers

The behavior of the system under the standard PQ and $Q - v_C$ controllers of Subsection 4.6.1, is next analyzed. In agreement with the control requirements described above, two PQ controllers are designed to regulate direct and quadrature currents of the wind farm stations and one $Q-v_C$ controller is designed

to regulate dc voltage and quadrature current of the slack bus. Vector controllers defined over the outputs (4.6.3), (4.6.4) are considered, designed with identical controller gains $k_{P,i}$, $k_{I,i}$. The behavior of the converters in *nominal conditions* are depicted in Fig. 4.11, while responses in *perturbed conditions* are omitted. This is justified by the fact that PQ and $Q - v_C$ controllers are not directly affected by perturbed conditions, since no additional references calculation is required for their implementation and references are always assignable, see also Remark 4.6.2. We take $T = 4\ s$, in contrast with the value ($T = 2000\ s$) used for the PI–PBC. It is easy to see that the PQ and $Q - v_C$ controllers correctly (and rapidly) regulate the station at the desired references between 0 and 8 s. This good behavior is not surprising, since PQ controllers applied to converters that are injecting power, and the $Q - v_C$ controller applied to converters that is absorbing power, have associated globally asymptotically stable zero dynamics, as proved in Subsection 4.7.1. On the other hand, as shown in the figures, when at stations $WF1$ and $WF2$ the power flow is reversed (respectively at $t = 12\ s$ and $t = 8\ s$), the correspondent dc voltages go unstable, because in these cases the zero dynamics is unstable. Similar unstable behavior appears also at the slack bus station. A tuning procedure of the controllers gains is thus usually adopted to ensure boundedness of the uncontrolled variable [150, 172]. Note however that such a procedure is not independent from the provided references and may fail for perturbed operating conditions.

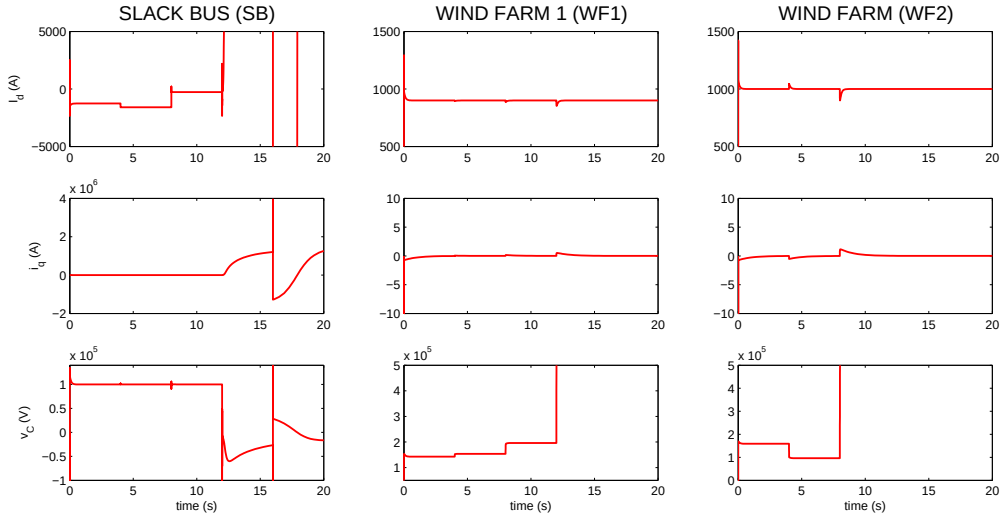

Figure 4.11: Responses of converters variables under the decentralized PQ and $Q - v_C$ controllers — in *nominal conditions*.

4.7.3 Adding an outer–loop to the PI–PBC

To overcome the transient performance limitations of the PI–PBC exhibited in Subsection 4.7.2, in this subsection it is proposed to add an outer–loop that takes as input some desired references — indicated with $(\cdot)^{\text{ref}}$ — and generates as output the references $(\cdot)^\star$ to the inner–loop scheme — see Fig. 4.12.

The latter will replace the desired equilibria in the definition of the passive output (4.6.12), associated to each converter and, if properly designed, allows to overcome the performance limitations of the passive output, while preserving global asymptotic stability of the closed–loop system. Since the objective is to improve performances of the PI–PBC in nominal conditions, the following assumption is made.

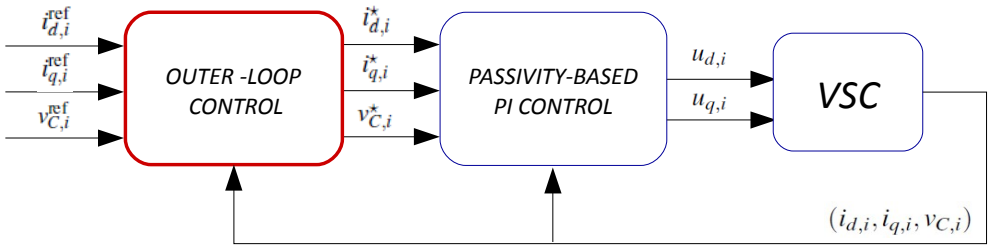

Figure 4.12: Proposed architecture for improving performance limitations of the PI–PBC. The new outer–loop is located behind the PI–PBC .

Assumption 4.7.11. *The input references* $(\cdot)^{\text{ref}}$ *of the outer–loop control belong to the set of assignable equilibria* $\mathcal{E}^{\star}$.

The proposed modification of the PI–PBC consists of an additional linear feedback that affects only the proportional part. The following proposition is then presented.

Proposition 4.7.12. Consider the hvdc transmission system (4.3.19), with a desired steady–state $x^{\star} \in \mathcal{E}^{\star}$, in closed–loop with the PI control

$$u = -K_P y + K_I \zeta - K_L Q \tilde{x}, \quad \dot{\zeta} = -y, \tag{4.7.17}$$

with y given in (4.6.6), gain matrices K_P, K_I as in (4.6.10) and $K_L \in \mathbb{R}^{2\times(3\mathtt{c}+\mathtt{t})}$ verifying

$$\mathcal{R}_0 := \mathcal{R} + g(x^{\star})K_P g^{\top}(x^{\star}) + \frac{1}{2}\left[g(x^{\star})K_L + K_L^{\top} g^{\top}(x^{\star})\right] > 0. \tag{4.7.18}$$

Then, the equilibrium point $(x^{\star}, K_I^{-1}u^{\star})$ is globally asymptotically stable (GAS).

Proof. Using the same Lyapunov function (4.6.11) employed in the proof of Proposition 4.6.5, the derivative along the trajectories of the closed–loop system (4.3.19)–(4.7.17) is given by

$$\begin{aligned}
\dot{W} &= -\tilde{x}^{\top} Q\mathcal{R}Q\tilde{x} + y^{\top}\tilde{u} + \tilde{\zeta}^{\top} K_I y \\
&= -\tilde{x}^{\top} Q\mathcal{R}Q\tilde{x} + y^{\top}\tilde{u} - (\tilde{u}^{\top} + y^{\top}K_P + \tilde{x}^{\top}QK_L^{\top})y \\
&= -\tilde{x}^{\top} Q\mathcal{R}Q\tilde{x} - \tilde{x}^{\top} Qg(x^{\star})K_P g^{\top}(x^{\star})Q\tilde{x} - \tilde{x}^{\top}QK_L^{\top} g^{\top}(x^{\star})Q\tilde{x} \\
&= -\tilde{x}^{\top} Q\mathcal{R}_0 Q\tilde{x} < 0,
\end{aligned}$$

where in the third equivalence the output definition $y = g^{\top}(x^{\star})Q\tilde{x}$ is used, while the last equivalence follows from condition (4.7.18). □□□

Loosely speaking, the Proposition 4.7.17 states that the property of global asymptotic stability of the closed–loop system (4.3.19)–(4.6.9) — that is the hvdc transmission system controlled via PI–PBC — is preserved for any additional linear feedback that affects only the proportional part of the controller and any gain matrix K_L which verifies condition (4.7.18). However, beside this stability

result, Proposition 4.7.12 does not provide any hint on how to select the controller gains in order to overcome the performance limitations of the PI–PBC, nor how to preserve the decentralization property that — for some inappropriate choice of the gain matrix — can be even lost.

4.7.4 Relation of the outer–loop with droop control

A commonly used outer–loop control is the so–called *droop control* [142, 69], which replaces — at the i–th converter — the direct current $i^\star_{d,i}$ with its desired reference $i^{\text{ref}}_{d,i}$ plus a deviation (droop) term proportional to the voltage error, leaving some constant references for $i^\star_{q,i}$ and $v^\star_{C,i}$. Inspired by this controller, the following assignment is made:

$$K_L := \begin{bmatrix} 0 & 0 & K_D & 0 \\ 0 & 0 & 0 & 0 \end{bmatrix},$$

where $K_D := \text{diag}\{k_{D,i}\} \in \mathbb{R}^{\mathsf{c}\times\mathsf{c}}$ is a positive matrix to be defined. With this choice it is easy to see that the controller (4.7.17) can be decomposed in c decentralized controllers of the form

$$\begin{bmatrix} u_{d,i} \\ u_{q,i} \end{bmatrix} = \begin{bmatrix} -k_{Pd,i}y_{d,i} + k_{Id,i}z_{d,i} - k_{D,i}(v_{C,i} - v^\star_{C,i}) \\ -k_{Pq,i}y_{q,i} + k_{Iq,i}z_{q,i}. \end{bmatrix}, \quad \begin{bmatrix} \dot{z}_{d,i} \\ \dot{z}_{q,i} \end{bmatrix} = \begin{bmatrix} -y_{d,i} \\ -y_{q,i} \end{bmatrix}, \tag{4.7.19}$$

that correspond to c PI–PBC plus an additional linear feedback in the local dc voltage error. Straightforward calculations — here omitted for brevity — show that it is always possible to determine a gain matrix K_D, such that (4.7.18) is verified, thus guaranteeing global asymptotic stability of the closed–loop system.

The modified PI–PBC (4.7.19) can be indeed interpreted, similarly to a droop controller, as an outer–loop providing references for the the standard PI–PBC, *but only* affecting its proportional part. It is indeed easy to see that it corresponds to assume the following inner–loop control scheme

$$\begin{bmatrix} u_{d,i} \\ u_{q,i} \end{bmatrix} = \begin{bmatrix} k_{Pd,i}(v^{\star P}_{C,i}i_{d,i} - i^{\star P}_{d,i}v_{C,i}) + k_{Id,i}z_{d,i} \\ k_{Pq,i}(v^{\star P}_{C,i}i_{q,i} - i^{\star P}_{q,i}v_{C,i}) + k_{Iq,i}z_{q,i} \end{bmatrix}, \quad \begin{bmatrix} \dot{z}_{d,i} \\ \dot{z}_{q,i} \end{bmatrix} = \begin{bmatrix} v^{\star I}_{C,i}i_{d,i} - i^{\star I}_{d,i}v_{C,i} \\ v^{\star I}_{C,i}i_{q,i} - i^{\star I}_{q,i}v_{C,i} \end{bmatrix},$$

together with the following outer–loop assignments of the proportional and integral references

$$\begin{aligned} &i^{\star,P}_{d,i} \leftarrow i^{\text{ref}}_{d,i} + k_{D,i}\frac{v_{C,i} - v^{\text{ref}}_{C,i}}{v_{C,i}}, \quad i^{\star,P}_{q,i} \leftarrow i^{\text{ref}}_{q,i}, \quad v^{\star,P}_{C,i} \leftarrow v^{\text{ref}}_{C,i} \\ &i^{\star,I}_{d,i} \leftarrow i^{\text{ref}}_{d,i}, \quad i^{\star,I}_{q,i} \leftarrow i^{\text{ref}}_{q,i}, \quad v^{\star,I}_{C,i} \leftarrow v^{\text{ref}}_{C,i}, \end{aligned} \tag{4.7.20}$$

where, as done before, the notation $(\cdot)^{\text{ref}}$ indicates the (assignable) references of the outer–loop.

The behavior of the converters under PI–PBC plus outer GAS control — in *nominal conditions* — are illustrated in Fig. 4.13. In contrast to the simulations of the basic PI–PBC of Subsection 4.7.2 when the references change every $T = 2000\ s$, now they are a *thousand times faster* that is, every $T = 2\ s$. It is easy to see that, compared to Fig. 4.10, the responses maintain the same shape while the convergence occurs with a rate $\approx 10^3$ faster. Unfortunately, in *perturbed conditions* the controller presents the same problems of the simple PI–PBC, from which follows that unsuitable steady–states are usually achieved also by the modified PI–PBC.

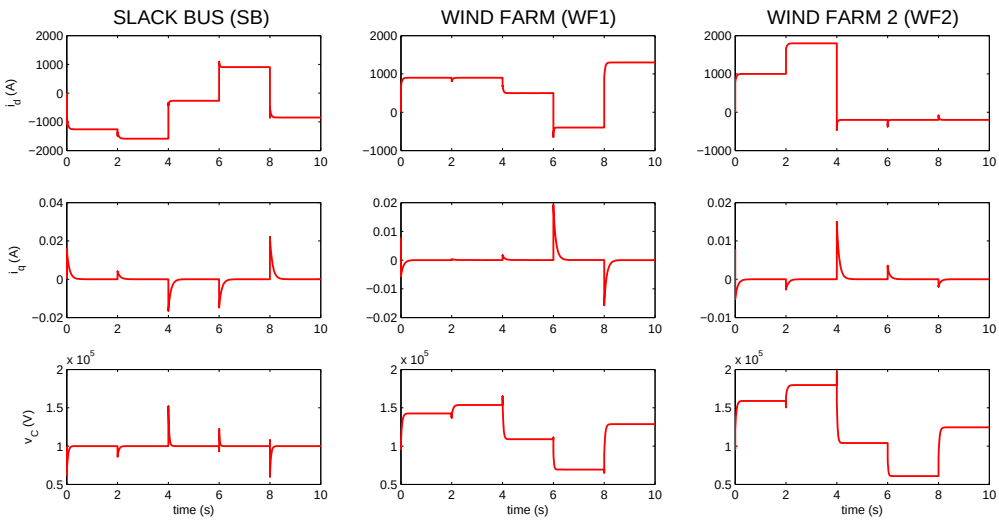

Figure 4.13: Responses of converters variables with the decentralized PI–PBC plus GAS outer controller — in *nominal conditions*.

4.7.5 Some conclusions on inner–loop control

Sections 4.6 and 4.7 have been dedicated to analysis and design of inner–loop controllers for the hvdc transmission system described by (4.3.19). We have proposed a globally stable inner–loop decentralized PI–PBC controller and made a comparative analysis with standard vector controllers employed in practice. For the hvdc transmission system in closed–loop with these controllers we can then draw the following conclusions, see also Table 4.3.

- Under the assumption of nominal operating condition, the PI–PBCs are able to guarantee global asymptotic stability of any *known* operating point, for any positive controller gain.

- PI–PBC are *universal*, in the sense that they can operate either in PQ or $Q - v_C$ *control mode*, see also Remark 4.6.8. One important advantage of this universal feature is that there is *no need to switch* between different controllers when the converters are requested to change their mode of operation — this is in contrast with other inner–loop schemes that require switching between controllers, which is clearly undesirable in practice.

- The system controlled via PI–PBC has clear performance limitations that cannot be overcome by appropriate tuning of the controller gains.

- The addition of a further loop of control to the PI–PBC allows to overcome the performance limitation, preserving global asymptotic stability of the closed–loop system.

- Although simulations show that a stable behavior is preserved, in presence of large perturbations the system may converge to unpractical steady–states. An appropriate tuning of the controller gains is thus required to ensure convergence to reasonable steady–state regimes.

On the other hand, for standard vector controllers, we can draw the following conclusions.

- The hvdc transmission system in closed–loop with standard vector controllers may exhibit an unstable behavior of the uncontrolled variables, independently from the operating conditions.

Table 4.3: Comparison of inner–loop controllers.

	Nominal conditions	**Perturbed conditions**
PI	*stable for some gains, tuning required, good performances*	*stable for some gains, tuning required (hard), fair performances*
PI – PBC	*stable for any gain (nonlinear proof), poor performances*	*stable (simulations), unsuitable steady–state*
PI – PBC + outer loop	*stable for a defined set of gain (nonlinear proof), best performances*	*stable (simulations), unsuitable steady-state*

Hence, a tuning procedure is required not only to improve transient performance, but also to guarantee stability of the controlled system.

- Switches between different controllers are required, when a terminal is requested to change its mode of operation.

4.8 Primary control: modeling & design

4.8.1 Graph description

A first step towards the construction of a suitable model for primary control analysis and design is the definition of an appropriate graph description of the system topology. Since the action of primary control has to be taken into account, this description slightly differs from the one presented in Section 4.3. As before, we consider an hvdc transmission system described by a graph $\mathcal{G}^{\uparrow}$ where $\mathsf{c}+1$ is the number of graph nodes, and $\mathsf{m}=\mathsf{c}+\mathsf{t}$ the number of graph edges, with c and t the number of converters and transmission units respectively. Furthemore, we define p the number of converter units not equipped with primary control — that we call *PQ units* — and v the number of converter units equipped with primary control — that we call *voltage–controlled units*. Without loss of generality we assume that the set of converter nodes $\mathcal{N}_{VSC}$ (respectively edges $\mathcal{E}_{VSC}$) can be partitioned into two ordered subsets called $\mathcal{N}_P$ and $\mathcal{N}_V$ (respectively $\mathcal{E}_P$ and $\mathcal{E}_V$) associated to *PQ* and *voltage–controlled* units. Hence, the incidence matrix (4.3.1) can be decomposed as:

$$\mathcal{B}=\begin{bmatrix} \mathbb{I}_{\mathsf{p}} & 0 & \mathcal{B}_P \\ 0 & \mathbb{I}_{\mathsf{v}} & \mathcal{B}_V \\ -1_{\mathsf{p}}^{\top} & -1_{\mathsf{v}}^{\top} & 0 \end{bmatrix} \in \mathbb{R}^{(\mathsf{c}+1)\times\mathsf{m}}, \tag{4.8.1}$$

where the submatrices $\mathcal{B}_P$, $\mathcal{B}_V$ fully captures the interconnection topology of *PQ* and *voltage–controlled units.*

4.8.2 Internally controlled voltage source converters

We next assume that any hvdc terminal is internally controlled via fast direct current control schemes. These can be implemented, for example, via vector control, see Subsection 4.6.1 for more details on this control strategy. The combined architecture of the vector control inner–loop scheme plus primary control is illustrated in Fig. 4.14. The assumption can be formalized as follows.

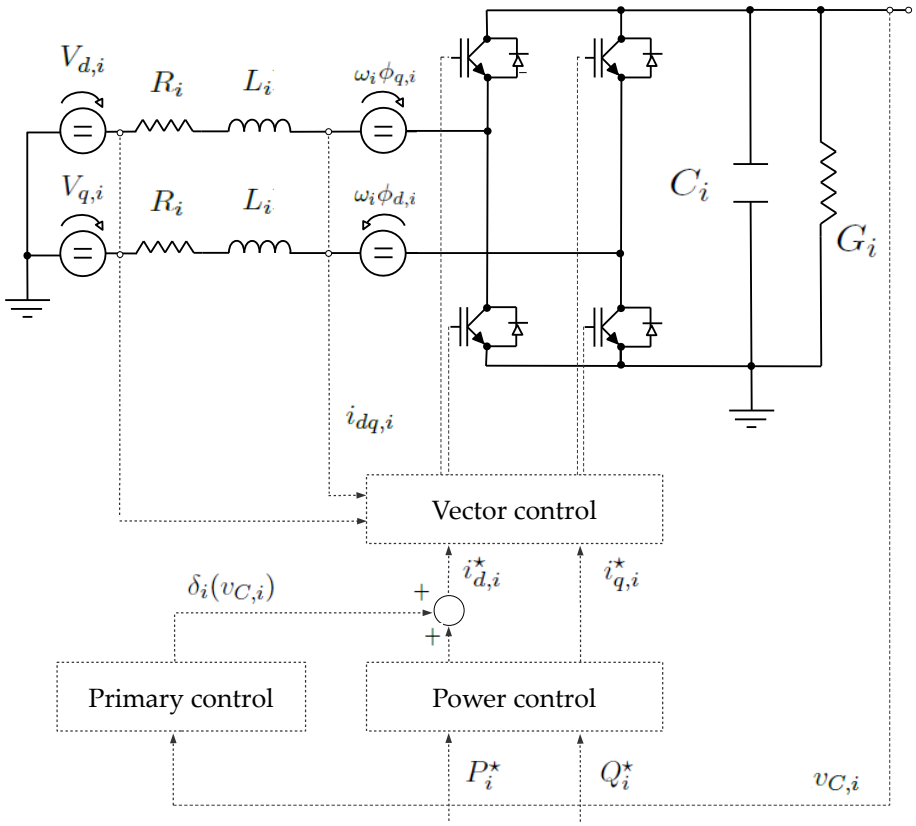

Figure 4.14: Primary and inner–loop control architecture of an hvdc terminal, where the inner–loop direct current scheme is implemented via vector control. The primary control takes action — for the units that are equipped with — by properly modifying the direct current reference.

Assumption 4.8.1. *All voltage source converters are controlled via stable direct current control schemes. Moreover, such schemes guarantee instantaneous and exact tracking of the desired currents.*

This assumption can be justified by an appropriate design of the inner–loop control scheme so that the resulting closed–loop system is internally stable and has a very large bandwidth compared to the primary control. As already discussed, this is usually achieved using tuning procedures. If stability is guaranteed and this time–scale separation is followed in the design of the system, the assumption can be mathematically formalized by invoking singular perturbation theory [92, 140].

We now determine implications of the aforementioned assumption for the dynamics of the PQ and *voltage–controlled units*. Since the vector control allows perfect tracking of the references and converters are instantaneously synchronized to the attached ac voltage sources through the PLL, the controlled ac–side can be approximated by a power source:

$$\hat{P}_i = V_{d,i}(i^\star_{d,i} + i^\star_{q,i}). \tag{4.8.2}$$

If the converter unit is a *PQ unit* the references are established by the outer power loop:

$$i^\star_{d,i} = \frac{P^\star_i}{V_{d,i}}, \quad i^\star_{q,i} = \frac{Q^\star_i}{V_{d,i}}, \qquad i \sim \mathcal{E}_P. \tag{4.8.3}$$

Hence, the ac side can be approximated by a constant power device, as illustrated in Fig. 4.15. This is equivalent to a current source u_i constrained by the following relation:

$$P^\star_{P,i} := P^\star_i + Q^\star_i = v_{C,i} u_i, \qquad i \sim \mathcal{E}_P. \tag{4.8.4}$$

On the other hand, if the converter unit is a *voltage–controlled unit*, the references are defined according to the primary control strategy. A common approach is to introduce an additional deviation in the direct current reference — obtained from the outer power loop — as a function of the dc voltage, keeping unchanged the reference of the quadrature current. Then, we can write:

$$i^\star_{d,k} = \frac{P^\star_k}{V_{d,k}} + \delta_k(v_{C,k}), \quad i^\star_{q,k} = \frac{Q^\star_k}{V_{d,k}}, \qquad k \sim \mathcal{E}_V, \tag{4.8.5}$$

where $\delta_k(v_{C,k})$ represents the state–dependent contribution provided by the primary control. We propose to take:

$$\delta_k(v_{C,k}) = -\frac{1}{V_{d,k}}(\mu_{P,k} + \mu_{I,k} v_{C,k} + \mu_{Z,k} v^2_{C,k}), \qquad k \sim \mathcal{E}_V, \tag{4.8.6}$$

where $\mu_{P,k}, \mu_{I,k}, \mu_{Z,k} \in \mathbb{R}$ are free control parameters. With this choice, the ac side can be approximated by a ZIP model, *i.e.* by the parallel connection of a constant impedance (Z), a constant current source (I) and a constant power device (P), see Fig. 4.15. The injected power (4.8.2) is thus given by:

$$\hat{P}_k(v_{C,k}) = P^\star_{V,k} - \mu_{I,k} v_{C,k} - \mu_{Z,k} v^2_{C,k}, \qquad k \sim \mathcal{E}_V, \tag{4.8.7}$$

with $P^\star_{V,k} := P^\star_k + Q^\star_k - \mu_{P,k}$. Then the parameters $P^\star_{V,k}$, $\mu_{I,k}$, $\mu_{Z,k}$ represent respectively the constant absorbed power, absorbed current and impedance of the equivalent ZIP model. Note that consistency with a ZIP loads simply follows by taking all parameters strictly positive. The dynamics of the *PQ* and

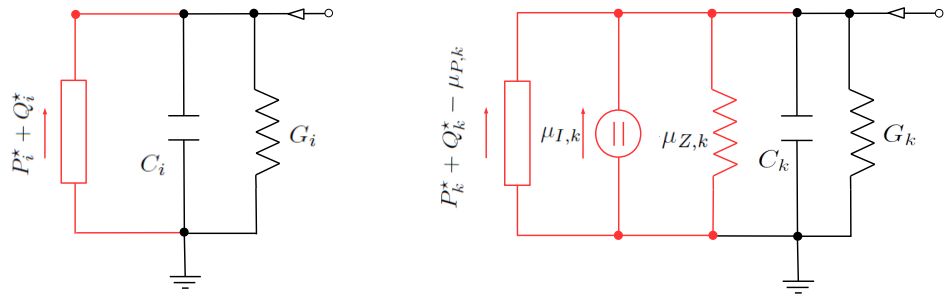

Figure 4.15: Circuit equivalent for *PQ units* (left) and *voltage–controlled units* (right).

voltage–controlled units can be finally represented by the following scalar port–Hamiltonian systems $\mathcal{S}_i$:

$$i \sim \mathcal{E}_P \begin{cases} \dot{q}_{C,i} &= -G_i \nabla \mathcal{H}_i + u_i + i_{C,i} \\ v_{C,i} &= \nabla \mathcal{H}_i \\ 0 &= P^\star_{P,i} - v_{C,i} i_{0,i} \end{cases} \qquad k \sim \mathcal{E}_V \begin{cases} \dot{q}_{C,k} &= -(G_k + \mu_{Z,k}) \nabla \mathcal{H}_k - \mu_{I,k} + u_k + i_{C,k} \\ v_{C,k} &= \nabla \mathcal{H}_k \\ 0 &= P^\star_{V,k} - v_{C,k} i_{0,k} \end{cases} \tag{4.8.8}$$

with scalar states the electric charges in the capacitors $q_{C,i}, q_{C,k}$, scalar port variables $v_{C,i}, v_{C,k}$ the capacitors voltages, u_i, u_k the converters currents, $i_{C,i}, i_{C,k}$ the network currents, G_i, G_k the capacitor conductances and the Hamiltonian energy functions

$$\mathcal{H}_i(q_{C,i}) = \frac{1}{2C_i} q^2_{C,i}, \qquad \mathcal{H}_k(q_{C,k}) = \frac{1}{2C_k} q^2_{C,k}.$$

The aggregated model is then given by:

$$\begin{aligned} \begin{bmatrix} \dot{q}_P \\ \dot{q}_V \end{bmatrix} &= \begin{bmatrix} -G_P & 0 \\ 0 & -(G_V + G_Z) \end{bmatrix} \begin{bmatrix} \nabla \mathcal{H}_P \\ \nabla \mathcal{H}_V \end{bmatrix} + \begin{bmatrix} u_P \\ u_V \end{bmatrix} - \begin{bmatrix} 0 \\ \bar{u}_I \end{bmatrix} + \begin{bmatrix} i_P \\ i_V \end{bmatrix} \\ \begin{bmatrix} v_P \\ v_V \end{bmatrix} &= \begin{bmatrix} \nabla \mathcal{H}_P \\ \nabla \mathcal{H}_V \end{bmatrix} \end{aligned} \tag{4.8.9}$$

constrained by:

$$P^\star_{P,i} = v_{P,i} u_{P,i}, \quad i \sim \mathcal{E}_P, \qquad P^\star_{V,k} = v_{V,k} u_{V,k}, \quad k \sim \mathcal{E}_V \tag{4.8.10}$$

with the following definitions.

- State space vectors $q_P := \mathrm{col}(q_{C,i}) \in \mathbb{R}^{\mathsf{p}}$, $q_V := \mathrm{col}(q_{C,k}) \in \mathbb{R}^{\mathsf{v}}$.
- Energy functions

$$\mathcal{H}_P(q_P) := \sum_{i=1}^{\mathsf{p}} \mathcal{H}_i(q_{C,i}), \qquad \mathcal{H}_V(q_V) := \sum_{k=\mathsf{c}+1}^{\mathsf{v}} \mathcal{H}_k(q_{C,k}).$$

- External sources $\bar{u}_I := \mathrm{col}(\mu_{I,i}) \in \mathbb{R}^{\mathsf{v}}$.
- Port variables $i_P := \mathrm{col}(i_{C,i}) \in \mathbb{R}^{\mathsf{p}}$, $i_V := \mathrm{col}(i_{C,k}) \in \mathbb{R}^{\mathsf{v}}$, $u_P := \mathrm{col}(u_i) \in \mathbb{R}^{\mathsf{p}}$, $u_V := \mathrm{col}(u_k) \in \mathbb{R}^{\mathsf{v}}$ and $v_P := \mathrm{col}(v_{C,i}) \in \mathbb{R}^{\mathsf{p}}$, $v_V := \mathrm{col}(v_{C,k}) \in \mathbb{R}^{\mathsf{v}}$.
- Dissipation matrices $G_P := \mathrm{diag}\{G_i\}$, $G_V := \mathrm{diag}\{G_k\}$, $G_Z := \mathrm{diag}\{\mu_{Z,k}\}$.

Remark 4.8.2. With the following choice of the control parameters:

$$\mu_{P,k} = -d_k V_{d,k} v_C^{\mathrm{nom}}, \quad \mu_{I,k} = d_k V_{d,k}, \quad \mu_{Z,k} = 0, \tag{4.8.11}$$

the primary control (4.8.6) reduces to:

$$\delta_k(v_{C,k}) = -d_k (v_{C,k} - v_C^{\mathrm{nom}}), \tag{4.8.12}$$

that is the widely diffused voltage droop control [69, 142, 123], where d_k is called droop coefficient and v_C^{nom} is the nominal voltage of the hvdc system. Hence, the droop control can be interpreted as an appropriate parallel connection of a current sink with a constant power device. This should

be contrasted with the model provided in [8, 13], where it is modeled as a current source in parallel connection with an impedance.

4.8.3 Fast dc transmission lines

We consider the aggregated model of the dc transmission lines established in Section 4.3, whose expression is recalled to enhance readability. The model is given by:

$$\mathcal{S}_T : \begin{cases} \dot{x}_T &= -\mathcal{R}_T \nabla \mathcal{H}_T + v_T \\ i_T &= \nabla \mathcal{H}_T. \end{cases} \tag{4.8.13}$$

The following assumption is made.

Assumption 4.8.3. *The dynamics of the dc transmission lines evolve on a time–scale that is much faster than the time–scale at which the capacitors dynamics evolve.*

This assumption is a generalization of a fairly standard assumption in traditional power systems, where this typically holds because of the very slow dynamics of generation and utilization units compared to transmission units [131, 7]. From (4.8.13) it is easy to obtain:

$$i_T^\star = G_T v_T, \tag{4.8.14}$$

where $i_T^\star$ is the steady–state vector of line currents and $G_T := \mathcal{R}_T^{-1}$ the conductance matrix of the transmission lines.

Remark 4.8.4. *Note that Assumption 4.8.3 may not hold anymore while considering very long dc transmission lines, for which a slower dynamics is expected. However, as it will be clear from the next analysis, since line dynamics* (4.8.13) *are linear, analogous results can be obtained by removing the mentioned assumption.*

4.8.4 Interconnected model

In order to obtain the reduced, interconnected model of the hvdc transmission system under Assumption 4.8.1, Assumption 4.8.3, we need to consider the interconnection laws determined by the incidence matrix (4.8.1). Let define the node and edge vectors:

$$V := \begin{bmatrix} \mathcal{V}_P \\ \mathcal{V}_V \\ 0 \end{bmatrix} \in \mathbb{R}^{\mathsf{c}+1}, \quad V_e := \begin{bmatrix} v_P \\ v_V \\ v_T \end{bmatrix} \in \mathbb{R}^{\mathsf{m}}, \quad I_e := \begin{bmatrix} i_P \\ i_V \\ i_T \end{bmatrix} \in \mathbb{R}^{\mathsf{m}}. \tag{4.8.15}$$

Using the definition of the incidence matrix (4.8.1) and the Kirchhoff's currents and voltages laws expressed by (3.5.27), we have:

$$\begin{aligned} &[\mathbf{KCL}] \qquad 0_{\mathsf{p}} = i_P + \mathcal{B}_P i_T^\star, \quad 0_{\mathsf{v}} = i_V + \mathcal{B}_V i_T^\star, \quad -1_n^\top i_P - 1_n^\top i_V = 0, \\ &[\mathbf{KVL}] \qquad \mathcal{V}_P = v_P, \quad \mathcal{V}_V = v_V, \quad v_T = \mathcal{B}_P^\top \mathcal{V}_P + \mathcal{B}_V^\top \mathcal{V}_V \end{aligned} \tag{4.8.16}$$

Recalling (4.8.14), it is easy to obtain:

$$\begin{aligned} i_P &= -\mathcal{B}_P G_T \mathcal{B}_P^\top v_P - \mathcal{B}_P G_T \mathcal{B}_V^\top v_V \\ i_V &= -\mathcal{B}_V G_T \mathcal{B}_P^\top v_P - \mathcal{B}_V G_T \mathcal{B}_V^\top v_V, \end{aligned} \tag{4.8.17}$$

that can be rewritten as:

$$\begin{bmatrix} i_P \\ i_V \end{bmatrix} = - \begin{bmatrix} \mathcal{L}_P & \mathcal{L}_m \\ \mathcal{L}_m^\top & \mathcal{L}_V \end{bmatrix} \begin{bmatrix} v_P \\ v_V \end{bmatrix}, \tag{4.8.18}$$

with

$$\mathcal{L}_P := \mathcal{B}_P G_T \mathcal{B}_P^\top, \quad \mathcal{L}_V := \mathcal{B}_V G_T \mathcal{B}_V^\top, \quad \mathcal{L}_m := \mathcal{B}_P G_T \mathcal{B}_V^\top. \tag{4.8.19}$$

Now, it suffices to replace (4.8.18) into (4.8.9), to obtain the overall (reduced) interconnected model:

$$\begin{aligned} \begin{bmatrix} \dot{q}_P \\ \dot{q}_V \end{bmatrix} &= - \begin{bmatrix} \mathcal{L}_P + G_P & \mathcal{L}_m \\ \mathcal{L}_m^\top & \mathcal{L}_V + G_V + G_Z \end{bmatrix} \begin{bmatrix} \nabla \mathcal{H}_P \\ \nabla \mathcal{H}_V \end{bmatrix} + \begin{bmatrix} u_P \\ u_V \end{bmatrix} + \begin{bmatrix} 0 \\ \bar{u}_I \end{bmatrix} \\ \begin{bmatrix} v_P \\ v_V \end{bmatrix} &= \begin{bmatrix} \nabla \mathcal{H}_P \\ \nabla \mathcal{H}_V \end{bmatrix} \end{aligned} \tag{4.8.20}$$

constrained by:

$$P^\star_{P,i} = v_{P,i} u_{P,i}, \quad i \sim \mathcal{E}_P, \qquad P^\star_{V,k} = v_{V,k} u_{V,k}, \quad k \sim \mathcal{E}_V. \tag{4.8.21}$$

Remark 4.8.5. Since hvdc transmission systems are usually employed for transmitting power from remote areas and/or to connect ac networks at different frequencies, their peculiarity with respect to generalized dc grids is the absence of loads, in the sense that they act as pure transmission systems. Nevertheless, the model (4.8.20) can be employed for the modeling of dc grids with loads without loss of generality. Loads can be in fact represented either by *PQ units* (constant power loads) or by *voltage–controlled units* with assigned parameters (ZIP loads). This model – which is nonlinear because of the constraints (4.8.21) – should be contrasted with standard linear models adopted in literature, where loads are supposed to be modeled as constant current sources, see for example [8, 177].

Remark 4.8.6. It is interesting to note that the matrix:

$$\mathcal{L} := \begin{bmatrix} \mathcal{L}_P & \mathcal{L}_m \\ \mathcal{L}_m^\top & \mathcal{L}_V \end{bmatrix} \in \mathbb{R}^{\mathsf{c} \times \mathsf{c}} \tag{4.8.22}$$

can be interpreted as the Laplacian matrix associated to the weighted undirected graph $\bar{\mathcal{G}}^w$, obtained from the hvdc transmission system (unweighted directed) graph $\mathcal{G}^\uparrow$ by: 1) eliminating the reference node and edges connected to it; 2) assigning as weights of the transmission edges the value of their conductances. Similar definitions are also encountered in [8, 177].

4.8.5 Conditions for existence of an equilibrium point

From an electrical point of view, the reduced system (4.8.20) is a linear capacitive–resistive circuit, where at each node a constant power device is attached. It has been observed in experiments and simulations that the presence of constant power devices may seriously affect the dynamics of linear *RLC* circuits hindering the achievement of a stable behavior of the state variables — the dc voltages in the present case [14, 97, 9, 129]. A first objective is thus to determine conditions on free control parameters of the system (4.8.20) that guarantee the existence of an equilibrium point and that this is at least locally asymptotically stable.

In order to present the main result on existence of equilibria for the system (4.8.20), we first introduce the following Lemma, that is reported in [9] and that we recall here fore sake of completeness.

Lemma 4.8.7. *Consider m quadratic equations of the form $f_i : \mathbb{R}^n \to \mathbb{R}$,*

$$f_i(x) := \frac{1}{2} x^\top \mathcal{A}_i x + x^\top \mathcal{B}_i, \qquad i \in [1, m], \tag{4.8.23}$$

where $\mathcal{A}_i = \mathcal{A}_i^\top \in \mathbb{R}^{n\times n}$, $\mathcal{B}_i \in \mathbb{R}^n$ and define:

$$\mathcal{A}(T) := \sum_{i=1}^m t_i \mathcal{A}_i, \quad \mathcal{B}(T) := \sum_{i=1}^m t_i \mathcal{B}_i, \quad \mathcal{P}(T) := \sum_{i=1}^m t_i P_i. \tag{4.8.24}$$

If the following LMI

$$\begin{bmatrix} \mathcal{A}(T) & \mathcal{B}(T) \\ \mathcal{B}^\top(T) & 2\mathcal{P}(T) \end{bmatrix} > 0, \tag{4.8.25}$$

is feasible, then equations

$$f_i(x) = -P_i, \qquad i \in [1, m] \tag{4.8.26}$$

have no solution.

Proof. Write equations (4.8.26) in vector form as $f(x) = -P$ and define the set

$$F := \{f(x) : x \in \mathbb{R}^n\}, \tag{4.8.27}$$

that is the image of $\mathbb{R}^n$ under the quadratic map $f : \mathbb{R}^n \to \mathbb{R}^m$. Let us minimize a linear function $\sum_{i-1}^m t_i z_i$ on F provided that $\mathcal{A}(T) > 0$:

$$\alpha := \min_{z\in F} \sum_{i=1}^m t_i z_i = \min_x \sum_{i=1}^m t_i f_i(x) = -\frac{1}{2}\mathcal{B}(T)\mathcal{A}(T)^{-1}\mathcal{B}(T). \tag{4.8.28}$$

On the other hand, using the definition of $\mathcal{P}(T)$ and if

$$-\mathcal{P}(T) < \min_{z\in F} \sum_{i=1}^m t_i z_i, \tag{4.8.29}$$

it means that the hyperplane

$$\sum_{i=1}^m t_i z_i = \frac{1}{2}\left[\alpha - \mathcal{P}(T)\right] \tag{4.8.30}$$

strictly separates $-\mathcal{P}$ and F, hence equations (4.8.26) have no solution. Finally, using Schur's complement, the inequalities

$$\mathcal{A}(T) > 0, \quad \mathcal{P}(T) > \frac{1}{2}\mathcal{B}^\top(T)\mathcal{A}(T)^{-1}\mathcal{B}(T) \tag{4.8.31}$$

are equivalent to (4.8.25), thus completing the proof. □□□

We are now ready to formulate the following proposition, that establishes necessary, control parameters–dependent, conditions for the existence of equilibria of the system (4.8.20).

Proposition 4.8.8. *Consider the system* (4.8.20)–(4.8.21)*, for some given $P_P^\star := \mathrm{col}(P_{P,i}^\star) \in \mathbb{R}^{\mathsf{p}}$, $P_V^\star := \mathrm{col}(P_{V,i}^\star) \in \mathbb{R}^{\mathsf{v}}$. If there exist two diagonal matrices $T_P \in \mathbb{R}^{\mathsf{p}\times\mathsf{p}}$, $T_V \in \mathbb{R}^{\mathsf{v}\times\mathsf{v}}$ such that:*

$$\Upsilon(T_P, T_V) > 0, \tag{4.8.32}$$

with

$$\Upsilon(T_P,T_V):=\begin{bmatrix} T_P(\mathcal{L}_P+G_P)+(\mathcal{L}_P+G_P)T_P & T_P\mathcal{L}_m+\mathcal{L}_m^\top T_V & 0\\ \mathcal{L}_m^\top T_P+T_V\mathcal{L}_m & T_V(\mathcal{L}_V+G_V+G_Z)+(\mathcal{L}_V+G_V+G_Z)T_V & T_V\bar{u}_V\\ 0 & \bar{u}_V^\top T_V & -2(1^\top T_P P_P^\star+1^\top T_V P_V^\star)\end{bmatrix}, \tag{4.8.33}$$

the system does not admit an equilibrium point.

Proof. Setting the left–hand of the differential equations in (4.8.20) to zero, we have:

$$\begin{aligned} 0 &= -(\mathcal{L}_P+G_P)v_P^\star-\mathcal{L}_m v_V^\star+u_P^\star,\\ 0 &= -\mathcal{L}_m^\top v_P^\star-(\mathcal{L}_V+G_V+G_Z)v_V^\star+u_V^\star-\bar{u}_V.\end{aligned}$$

Left–multiplying the first and second set of equations by $v_{P,i}^\star$ and $v_{V,k}^\star$ respectively, with $i\sim\mathcal{E}_P$, $k\sim\mathcal{E}_V$, we get

$$\begin{aligned} P_{P,i}^\star &= v_{P,i}^\star(\mathcal{L}_{P,i}^\top+G_{P,i})v_P^\star+v_{P,i}^\star\mathcal{L}_{m,i}^\top v_V^\star,\\ P_{V,k}^\star &= v_{V,k}^\star\mathcal{L}_{m,k}v_P^\star+v_{V,k}^\star(\mathcal{L}_{V,k}^\top+G_{V,k}+G_{Z,k})v_V^\star+v_{V,k}^\star\bar{u}_{V,k}.\end{aligned}$$

After some manipulations it is easy to rewrite

$$p_i^\star=\frac{1}{2}(v^\star)^\top\mathcal{A}_i v^\star,\qquad i\sim\mathcal{E}_P\cup\mathcal{E}_V, \tag{4.8.34}$$

with

$$\begin{aligned} \mathcal{A}_i &:= e_ie_i^\top\begin{bmatrix}\mathcal{L}_P+G_P & \mathcal{L}_m\\ \mathcal{L}_m^\top & \mathcal{L}_V+G_V+G_Z\end{bmatrix}+\begin{bmatrix}\mathcal{L}_P+G_P & \mathcal{L}_m\\ \mathcal{L}_m^\top & \mathcal{L}_V+G_V+G_Z\end{bmatrix}e_ie_i^\top,\\ \mathcal{B}_i &:= e_ie_i^\top\begin{bmatrix}0\\ \bar{u}_V\end{bmatrix},\qquad p_i^\star:=e_i^\top\begin{bmatrix}P_P^\star\\ P_V^\star\end{bmatrix},\end{aligned}$$

where $e_i\in\mathbb{R}^{\mathsf{c}}$ is the i-th Euclidean basis vector and $v^\star:=\mathrm{col}(v_P^\star,v_V^\star)\in\mathbb{R}^{\mathsf{c}}$. Let consider the map $f(v^\star):\mathbb{R}^{\mathsf{c}}\to\mathbb{R}^{\mathsf{c}}$ with components

$$f_i(v^\star)=\frac{1}{2}(v^\star)^\top\mathcal{A}_i v^\star,\qquad i\sim\mathcal{E}_P\cup\mathcal{E}_V$$

and denote F the image of $\mathbb{R}^{\mathsf{c}}$ under this map. The problem of solvability of such equations can be formulated using Lemma 4.8.7, *i.e.* if the LMI (4.8.32) holds, then $p^\star$ is not in F, that completes the proof. □□□

The LMI (4.8.32) implicitly determines a necessary condition for the existence of an equilibrium point for (4.8.20). This can be formulated with the following corollary.

Corollary 4.8.9. *Consider the system* (4.8.20)–(4.8.21)*, for some given* $P_P^\star:=\mathrm{col}(P_{P,i}^\star)\in\mathbb{R}^{\mathsf{p}}$*,* $P_V^\star:=\mathrm{col}(P_{V,i}^\star)\in\mathbb{R}^{\mathsf{v}}$*. Then the system admits an equilibrium point only if there are no diagonal matrices* $T_P\in\mathbb{R}^{\mathsf{p}\times\mathsf{p}}$*,* $T_V\in\mathbb{R}^{\mathsf{v}\times\mathsf{v}}$ *that verify* (4.8.32)*.*

Remark 4.8.10. Note that the feasibility of the LMI (4.8.32) depends from system parameters, among which G_Z, $\bar{u}_V$ and $P_V^\star$ are free (primary) control parameters. Since the feasibility condition is only necessary for the existence of equilibria for (4.8.20), it is of interest to determine regions for these parameters that implies non–existence of an equilibrium point.

4.8.6 Conditions for power sharing

As already discussed in Section 4.4, in practice one may be interested in determining conditions for the existence of equilibria that possess two suitable properties: a proportional distribution of power among the terminals and vicinity of the voltages near the nominal value [13, 8]. In this subsection we address the first problem, while the latter is left for future investigation. More precisely, using the same approach adopted for the problem of existence of equilibria, we determine additional conditions for the existence of equilibria that possess the power sharing property, that we define as follows.

Definition 4.8.11. *Let $v^\star := (v_P^\star, v_V^\star)$ an equilibrium point for (4.8.20)–(4.8.21), $\hat{P}_V(v^\star) := \mathrm{col}(\hat{P}_k(v_{C,k}^\star)) \in \mathbb{R}^{\mathsf{v}}$, i.e. the collection of power injected by voltage–controlled units, as defined by (4.8.7), and $\Gamma := \mathrm{diag}\{\gamma_k\} \in \mathbb{R}^{\mathsf{v}\times\mathsf{v}}$, a positive definite matrix. Then $v^\star$ is said to possess the power sharing property with respect to Γ if:*

$$\Gamma \hat{P}_V(v^\star) = 1_{\mathsf{v}}. \tag{4.8.35}$$

This property consists in having guaranteed an appropriate (proportional) power distribution among the terminals. A typical choice for the weights γ_k is the nominal power ratings of the hvdc terminals. We next show, through the following lemma, that is possible to reformulate such a control objective as a set of quadratic constraints on the (assumed existent) equilibrium point.

Lemma 4.8.12. *Let $v^\star = (v_P^\star, v_V^\star)$ an equilibrium point for (4.8.20)–(4.8.21), $\Gamma := \mathrm{diag}\{\gamma_k\} \in \mathbb{R}^{\mathsf{v}\times\mathsf{v}}$, a positive definite matrix. Then $v^\star$ possesses the power sharing property with respect to Γ if an only if the quadratic equations*

$$\frac{1}{2}(v^\star)^\top \mathcal{A}_k^{\mathrm{ps}} v^\star + (\mathcal{B}_k^{\mathrm{ps}})^\top v^\star = p_k^{\mathrm{ps}}, \qquad k \sim \mathcal{E}_V, \tag{4.8.36}$$

with:

$$\mathcal{A}_k^{\mathrm{ps}} := -2 \begin{bmatrix} 0 & 0 \\ 0 & \Gamma G_Z \end{bmatrix} e_k e_k^\top, \quad \mathcal{B}_k^{\mathrm{ps}} := -e_k e_k^\top \begin{bmatrix} 0 \\ \Gamma \bar{u}_V \end{bmatrix}, \quad p_k^{\mathrm{ps}} := e_k^\top \begin{bmatrix} 0 \\ \Gamma P_V^\star \end{bmatrix},$$

admit a solution.

Proof. From the definition (4.8.35) we have:

$$\gamma_k \hat{P}_k(v_{C,k}) = 1, \qquad k \sim \mathcal{E}_V, \tag{4.8.37}$$

that, recalling (4.8.7), is equivalent to:

$$\gamma_k (P_{V,k}^\star - \mu_{I,k} v_{C,k} - \mu_{Z,k} v_{C,k}^2) = 1. \tag{4.8.38}$$

After some straightforward manipulations, it is easy to see that these can be rewritten as (4.8.36), completing the proof. □□□

An immediate implication of this lemma is given in the following proposition, that establishes necessary conditions for the existence of an equilibrium point that possesses the power sharing property.

Proposition 4.8.13. *Consider the system (4.8.20)–(4.8.21), for some given $P_P^\star$, $P_V^\star$, Γ. If there exist three diagonal matrices $T_P \in \mathbb{R}^{\mathsf{p}\times\mathsf{p}}$, $T_V, T_V^{\mathrm{ps}} \in \mathbb{R}^{\mathsf{v}\times\mathsf{v}}$, such that:*

$$\Upsilon(T_P, T_V) + \Upsilon_{\mathrm{ps}}(T_V^{\mathrm{ps}}) > 0, \tag{4.8.39}$$

with

$$\Upsilon_{\text{ps}} := -\begin{bmatrix} 0 & 0 & 0 \\ 0 & 2T_V^{\text{ps}}\Gamma G_Z & T_V^{\text{ps}}\Gamma\bar{u}_V \\ 0 & T_V^{\text{ps}}\Gamma\bar{u}_V & 2T_V^{\text{ps}}(\mathbf{1}_{\mathsf{v}} - \Gamma P_V^\star) \end{bmatrix} \tag{4.8.40}$$

and $\Upsilon(T_P, T_V)$ *defined as in* (4.8.33)*, the system does not admit an equilibrium point.*

Proof. The proof is similar to the proof of Proposition 4.8.8. Using Lemma 4.8.12 the power sharing constraints can be indeed rewritten as quadratic equations, similarly to (4.8.34). Hence, it suffices to apply Lemma 4.8.7 to the quadratic equations (4.8.34), (4.8.36) to complete the proof. □□□

4.8.7 Conditions for local stability of a given equilibrium point

We now present a result on stability of a given equilibrium point, that is obtained by straghtforward application of Lyapunov's first method.

Proposition 4.8.14. *Consider the system* (4.8.20)–(4.8.21) *and assume that* $v^\star = (v_P^\star, v_V^\star)$ *is an equilibrium point. Define*

$$G_P^\star := \text{diag}\left\{\frac{P_{P,i}^\star}{(v_{P,i}^\star)^2}\right\}, \quad G_V^\star := \text{diag}\left\{\frac{P_{V,i}^\star}{(v_{V,i}^\star)^2}\right\} \tag{4.8.41}$$

and the matrix:

$$J(v^\star) := -\begin{bmatrix} C_P^{-1}(\mathcal{L}_P + G_P + G_P^\star) & C_P^{-1}\mathcal{L}_m \\ C_V^{-1}\mathcal{L}_m^\top & C_V^{-1}(\mathcal{L}_V + G_V + G_Z + G_V^\star) \end{bmatrix}. \tag{4.8.42}$$

Then if:

- *all eigenvalues* λ_i *of* J *are such that* $\mathfrak{Re}\{\lambda_i\,[J(v^\star)]\} < 0$*, the equilibrium point* $v^\star$ *is locally asymptotically stable;*

- *there exist an eigenvalue* λ_i *of* J *such that* $\mathfrak{Re}\{\lambda_i\,[J(v^\star)]\} > 0$*, the equilibrium point* $v^\star$ *is unstable.*

Proof. A first–order approximation of the state matrix around $v^\star$ is given by:

$$\begin{bmatrix} C_P\dot{v}_P \\ C_V\dot{v}_V \end{bmatrix} = -\begin{bmatrix} \mathcal{L}_P + G_P & \mathcal{L}_m \\ \mathcal{L}_m^\top & \mathcal{L}_V + G_V + G_Z \end{bmatrix}\begin{bmatrix} v_P \\ v_V \end{bmatrix} + \begin{bmatrix} \frac{\partial i_P}{\partial v_P} & \frac{\partial i_P}{\partial v_V} \\ \frac{\partial i_V}{\partial v_P} & \frac{\partial i_V}{\partial v_V} \end{bmatrix}_{(v_P^\star, v_V^\star)}. \tag{4.8.43}$$

Differentiating (4.8.21) with respect to v_P, v_V, it is easy to obtain:

$$0_{\mathsf{p}\times\mathsf{p}} = \frac{\partial i_P}{\partial v_P}\cdot\text{diag}\{v_{P,i}\} + \text{diag}\{i_{P,i}\}, \quad 0_{\mathsf{v}\times\mathsf{v}} = \frac{\partial i_V}{\partial v_V}\cdot\text{diag}\{v_{V,i}\} + \text{diag}\{i_{V,i}\}, \tag{4.8.44}$$

from which, using definitions (4.8.41), follows

$$\frac{\partial i_P}{\partial v_P}(v_P^\star) = -G_P^\star v_P^\star, \qquad \frac{\partial i_V}{\partial v_V}(v_V^\star) = -G_V^\star v_V^\star. \tag{4.8.45}$$

The proof is then completed replacing into (4.8.43) and using Lyapunov's first method. □□□

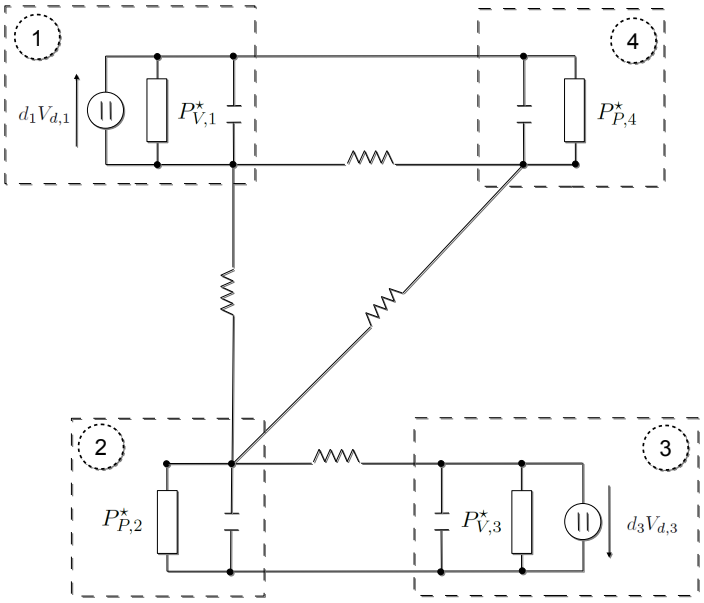

Figure 4.16: Four–terminal hvdc transmission system.

Table 4.4: Four–terminal hvdc transmission system parameters.

	Value		Value		Value		Value		Value
G_i	0 Ω^{-1}	$P^\star_{V,1}$	180 MW	$P^\star_{P,2}$	-200 MW	$P^\star_{V,3}$	90 MW	$P^\star_{P,4}$	-240 MW
C_i	20 μF	G_{12}	0.1 Ω^{-1}	G_{14}	0.04 Ω^{-1}	G_{23}	0.41 Ω^{-1}	G_{24}	0.2 Ω^{-1}

4.8.8 An illustrative example

In order to validate the result on existence of equilibria and power sharing for the system (4.8.20)–(4.8.21) we next provide an illustrative, simple, example. We consider the four–terminal hvdc transmission system depicted in Fig. 4.16, the parameters of which are given in Table 4.4. Since $\mathsf{c} = 4$, $\mathsf{t} = 5$, the graph associated to the hvdc system has $\mathsf{n} = 4 + 1 = 5$ nodes and $\mathsf{m} = \mathsf{c} + \mathsf{t} = 4 + 5 = 9$ edges. We then make the following assumptions.

- Terminal 1 (T1) and terminal 3 (T3) are equipped with primary control, from which follows that there are $\mathsf{p} = 2$ PQ units and $\mathsf{v} = 2$ voltage–controlled units. More precisely we consider the following primary control:

$$\delta_k(v_{C,k}) = -d_k(v_{C,k} - v_C^{\text{nom}}), \quad k = \{1, 3\} \tag{4.8.46}$$

  that is the well–known *voltage droop control*, where d_k is a free control parameter, while v_C^{nom} is the nominal voltage of the hvdc system, see also Remark 4.8.2.

- Power has to be equally shared among terminal 1 and terminal 3, from which follows $\Gamma = \mathbb{I}_2$ in Definition 4.8.11.

The next results are obtained investigating feasibility of the LMIs (4.8.32), (4.8.39) as a function of the free control parameters d_1, d_3. For this purpose, CVX, a package for specifying and solving convex programs, has been used to solve the semidefinite programming feasibility problem. In Fig. 4.17 it is shown — using a gridding approach — the regions of the (positive) parameters d_1, d_3 that

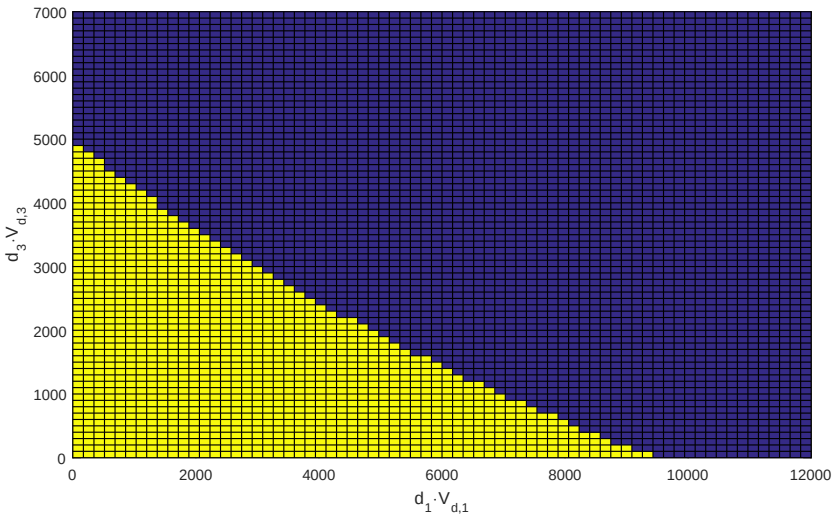

Figure 4.17: Feasibility regions of the LMI (4.8.8) on the plane $(V_{d,1}d_1, V_{d,3}d_3)$ of droop control parameters. Regions are yellow-coloured if the LMI is feasible and blue–coloured if the LMI is unfeasible.

guarantee feasibility (yellow) and unfeasibility (blue) of the LMI (4.8.32), while in Fig. 4.18 the same is done with respect to the LMI (4.8.39). We deduce that a necessary condition for the existence of an equilibrium point is that control parameters are chosen inside the blue region of Fig. 4.17, while a necessary conditions for the existence of an equilibrium point that further possesses the power sharing property is that control parameters are chosen inside the blue region of Fig. 4.18.

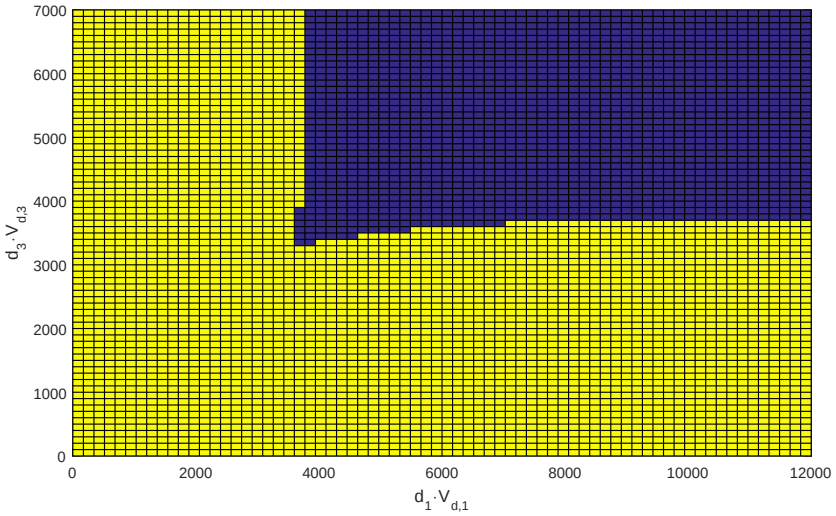

Figure 4.18: Feasibility regions of the LMI (4.8.39) on the plane $(V_{d,1}d_1, V_{d,3}d_3)$ of droop control parameters. Regions are yellow–coloured if the LMI is feasible and blue–coloured if the LMI is unfeasible.

Chapter 5

Related works

5.1 Introduction

This chapter is devoted to further contributions of the author, that can be presented as alternative interpretations, extensions or applications of the results obtained in the previous chapters. The purpose is to show the generality of the proposed methods as well as to provide some guidelines for future research. The sections that are here presented constitute abridged version of papers and reports of the author, as detailed below.

Section 5.2, see also [140], focuses on modeling of ac microgrids, using an approach similar to the one illustrated in Chapter 3. The main objective is to provide a guideline for control engineers attracted by this fundamental application for Smart Grids to assess the importance of the main dynamical components of a three-phase inverter-based microgrid as well as the validity of different models used in the power literature. For this purpose, we present the microgrid concept, discuss its main components, their modes of operation, as well as corresponding control schemes. This paves the path for —starting from fundamental physics — presenting detailed dynamical models of the individual microgrid components and clearly stating the underlying assumptions which lead to the standard reduced model representation.

Section 5.3, see also [53, 52, 180] is dedicated to modeling and analysis of an extremely simplified model of an electric power system, that is constituted by a synchronous generator connected to a resistive load. The same (but simplified) approach used in Chapter 3 is employed. Under some assumptions preliminary stability results of the generator when it is fed by constant mechanical torque and constant electrical field excitation are given. Although the result is not particularly interesting *per se*, it is the authour belief that it provides an insightful starting point for extending the methodology to larger power networks containing, *e.g.*, multiple generators.

5.2 Ac microgrids: modeling

5.2.1 Motivation & contributions

We have witnessed in the recent years a significant increase in the use of renewable energies worldwide [154]. Unlike fossil-fueled thermal power plants, most renewable power plants are relatively small in

terms of their generation power. An important consequence of this smaller size is that most renewable power plants are connected to the low voltage (LV) and medium voltage (MV) levels. Such generation units are commonly denoted as distributed generation (DG) units [3]. In addition, most renewable DG units are interfaced to the network via ac inverters. The physical characteristics of such power electronic devices largely differ from the characteristics of synchronous generators (SGs), which are the standard generating units in existing power systems. Hence, different control and operation strategies are needed in networks with a large amount of renewable DG units [63, 163, 154].

One potential solution to facilitate the integration of large shares of renewable DG units are microgrids [98, 74, 63, 89, 35, 149]. A microgrid gathers a combination of generation units, loads and energy storage elements at distribution or sub-transmission level into a locally controllable system, which can be operated either in grid-connected mode or in islanded mode, *i.e.*, in a completely isolated manner from the main transmission system. The microgrid concept has been identified as a key component in future electrical networks [35, 51, 99, 149].

Many new control problems arise for this type of networks. Their satisfactory solution requires the development of advanced model-based controller design techniques that often go beyond the classical linearization-based nested-loop proportional-integral (PI) schemes. This situation has, naturally, attracted the attention of the control community as it is confronted with some new challenging control problems of great practical interest.

It is clear that to carry out this task it is necessary to develop a procedure for assembling mathematical models of a microgrid that reliably capture the fundamental aspects of the problem. Such models have been developed by the power systems and electronics communities and their pertinence has been widely validated in simulations and applications [36, 88, 122, 111]. However, these are reduced or simplified, *i.e.*, linearized, models that are typically presented without any reference to the reduction procedure—hampering the understanding of the physical phenomena behind them.

We focus on purely inverter–based networks, since inverter-interfaced units are the main new elements in microgrids compared to traditional power systems. For modeling of traditional electromechanical SG-based DG units, the reader is referred to standard textbooks on power systems [96, 106, 7]. The main contributions are summarized as follows.

(C1) Provide a detailed comprehensive model derivation of a microgrid based on fundamental physics and combined with detailed reviews of the microgrid concept, its components and their main operation modes.

(C2) Answer the question, when an inverter can be modeled as a controllable ac voltage source and depict the necessary underlying model assumptions.

(C3) Show that the usual power flow equations can be obtained from a network with dynamic line models via a suitable coordinate transformation (called dq-transformation) together with a singular perturbation argument.

(C4) By combining the two latter contributions, recover the reduced-order microgrid model currently widely used in the literature.

We emphasize that the aim of the present section is not to give an overarching justification for the

final (simplified) model, but to provide a comprehensive overview of the modeling procedure for main microgrid components together with their dynamics, as well as of the main necessary assumptions, which allow the reduction of model complexity. Which of the presented models (if any) is appropriate for a specific control design and analysis cannot be established in general, but has to be decided by the user. Any model used in simulation and analysis necessarily involves certain assumptions. Therefore, it is of great importance that the user is aware of the pertinence of the employed model to appropriately assess the implications of a model-based analysis.

The remainder of the section is structured as follows. The microgrid concept is reviewed in Subsection 5.2.2. A detailed dynamical model of a microgrid is derived in Subsection 5.2.3. In particular, common operation modes of inverter-interfaced units are discussed therein. The model reduction yielding models of inverters as ac voltage sources and phasorial power flow equations is conducted in Subsection 5.2.4.

5.2.2 The microgrid concept

Microgrids have attracted a wide interest in different research and application communities over the last decade [144, 74, 122, 149]. However, the term "microgrid" is not uniformly defined in the literature [98, 74, 63, 89, 35, 59, 149]. Based on [63, 74, 149], the following definition of an ac microgrid is employed in this survey paper.

Definition 5.2.1. *An ac electrical network is said to be an ac microgrid if it satisfies the following conditions.*

i) It is a connected subset of the LV or MW distribution system of an ac electrical power system.

ii) It possesses a single point of connection to the remaining electrical power system. This point of connection is called point of common coupling (PCC).

iii) It gathers a combination of generation units, loads and energy storage elements.

iv) It possesses enough generation and storage capacity to supply most of its loads autonomously during at least some period of time.

v) It can be operated either connected to the remaining electrical network or as an independent island network. The first operation mode is called grid-connected mode and the second operation mode is called islanded, stand-alone or autonomous mode.

vi) In grid-connected mode, it behaves as a single controllable generator or load from the viewpoint of the remaining electrical system.

vii) In islanded mode, it is a locally controllable system, that is frequency, voltage and power can be actively controlled within the microgrid.

According to Definition 5.2.1, the main components in a microgrid are DG units, loads and energy storage elements. Typical DG units in microgrids are renewable DG units, such as photovoltaic (PV) units, wind turbines, fuel cells (FCs), as well as microturbines or reciprocating engines in combination with SGs. The latter two can either be powered with biofuels or fossil fuels [103, 59].

Typical loads in a microgrid are residential, commercial and industrial loads [98, 89, 103]. It is also foreseen to categorize the loads in a microgrid with respect to their priorities, *e.g.*, critical and non-critical loads. This enables load shedding as a possible operation option in islanded mode [98, 103].

Finally, storage elements play a key-role in microgrid operation [103, 59]. They are especially useful in balancing the power fluctuations of intermittent renewable sources and, hence, to contribute to network control. Possible storage elements are, *e.g.*, batteries, flywheels or supercapacitors. The combination of renewable DGs and storage elements is also an important assumption for the inverter models derived in this paper. An illustration of an exemplary microgrid is given in Fig. 5.1.

Most of the named DG and storage units are either dc sources (PV, FC, batteries) or are often operated at variable or high-speed frequency (wind turbines, microturbines, flywheels). Therefore, they have to be connected to an ac network via ac or dc-ac inverters [63, 154]. For ease of notation, such devices are simply called "inverters" in the following. Overviews on existing test-sites and experimental microgrids around the globe are provided in the survey papers [74, 10, 103, 121, 67]. As a consequence, fundamental network control actions, such as frequency or voltage control, have to be performed by inverter-interfaced units. This fact represents a fundamental difference to the operation of conventional power systems, where mainly SG units are responsible for network control. Therefore and since the modeling of SGs is a well-covered topic in the literature [96, 7, 106], we focus in the following on microgrids with purely inverter-interfaced DG and storage units. Also, it is straight-forward to incorporate SG-based units into the microgrid model presented hereafter.

5.2.3 Physical modeling & inner–loop control

In Chapter 3 it was shown that generalized electric power systems can be represented by a directed graph, where the power units correspond to edges and the buses correspond to nodes. In this section a similar procedure is applied to describe the dynamics of an ac inverter–based microgrid. According to such a procedure and in particular — under Assumption 3.4.1 — we consider only two types of power units: inverters — that we call *converter units* — and *transmission units*. We next provide a graph description of the system topology and appropriate models of the individual units.

Graph description

In line with this approach, an inverter-based microgrid can be represented by an unweighted directed graph $\mathcal{G}^{\uparrow}$ where inverters and transmission lines correspond to edges and buses correspond to nodes. We call a bus an *converter bus* when a inverter unit is connected to it and a *load bus* when a load is connected to it. Moreover, we call a bus a *transmission bus* when no inverter units or loads are connected to it. All buses associates a potential and we call a bus a *reference bus* when all buses potentials are measured with respect to it. The reference bus is assumed to be at ground potential. Converter, load and reference buses are boundary buses, while the transmission buses are interior buses. We further assume, as in Chapter 3, that transmission (interior) buses are eliminated via Kron–reduction [160], from which follows that if c is the number of three–phase converter buses and r is the number of three–phase load buses, then the total number of buses (nodes) is $\mathsf{n}+1 = 3\mathsf{c}+3\mathsf{r}+1$. Without loss of generality we assume that the set of nodes $\mathcal{N}$ can be partitioned into three ordered subsets called $\mathcal{N}_I$, $\mathcal{N}_R$ and the one–element set $\mathcal{N}_0$, associated to inverter, load nodes and the reference node respectively. We call $\mathcal{V} \in \mathbb{R}^{\mathsf{n}+1}$ the vector of node potentials. We also mentioned that is common practice to define power units such that their interaction with the environment is modeled by a voltage capacitor at their interaction port. In the case of ac microgrids it is easy to see that both inverters, loads and tranmission units share a capacitor at the converter buses to which they are attached. For simplicity then, we make the following assumption.

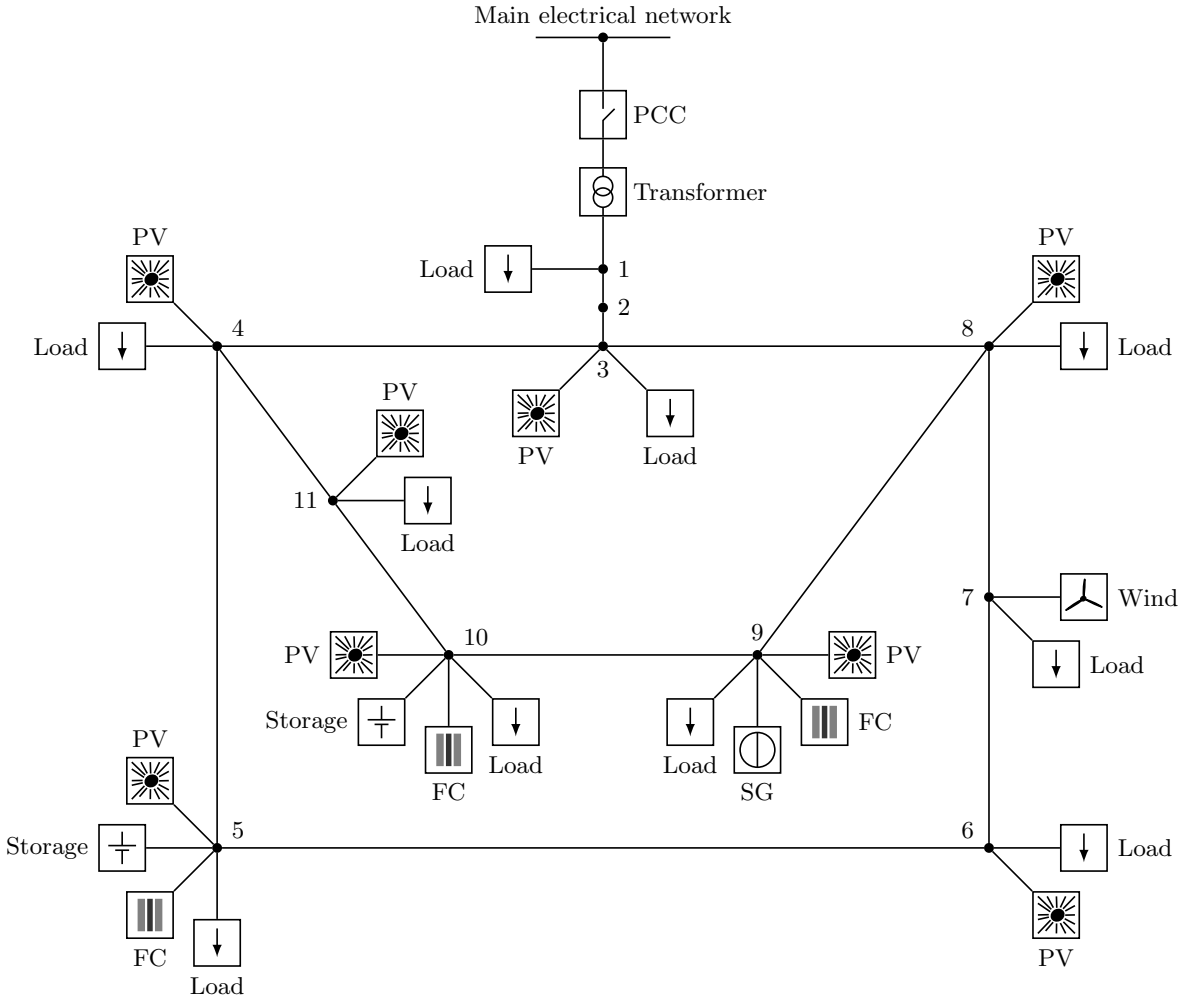

Figure 5.1: Schematic representation of a microgrid. The microgrid is composed of several DG units, loads and storage devices. The DG units are inverter-interfaced photovoltaic (PV), fuel cell (FC) and wind power plants. In addition, a power generation unit is connected to the network via a synchronous generator (SG). The point of connection of the microgrid to the main network is called point of common coupling (PCC).

Assumption 5.2.2. *All (possibly lossy) capacitors in parallel connection at a given bus are replaced by an equivalent capacitor, whose dynamics is included in the inverter dynamics.*

Consequently, all capacitors shared by tranmission units at their ports can be safely neglected, while capacitors shared by inverters need to be replaced by equivalent capacitors. Let $3\mathsf{t}$ the number of *transmission edges* — associated to the t three–phase transmission units — that connect converter buses. Since, there is a *converter edge* between every converter bus and the reference bus, there are in total $\mathsf{m} = 3\mathsf{c} + 3\mathsf{t}$ edges. Without loss of generality we assume that the set of edges $\mathcal{E}$ can be partitioned into three ordered subsets called $\mathcal{E}_I$, $\mathcal{E}_R$ and $\mathcal{E}_T$ associated to converter, load and transmission edges respectively. We call $(V_e, I_e) \in \mathbb{R}^{\mathsf{m}} \times \mathbb{R}^{\mathsf{m}}$ the vectors pair associated to edge voltages and currents respectively. The topology of the ac microgrids is fully described by the directed graph $\mathcal{G}^{\uparrow}$ to which are associated the vectors $\mathcal{V}$, V_e, I_e and the following incidence matrix

$$\mathcal{B} = \begin{bmatrix} \mathbb{I}_{\mathsf{c}+\mathsf{r}} & \mathcal{B}_{net} \\ -\mathbb{1}_{\mathsf{c}+\mathsf{r}}^{\top} & 0 \end{bmatrix} \otimes \mathbb{I}_3 \in \mathbb{R}^{(\mathsf{n}+1)\times \mathsf{m}}. \tag{5.2.1}$$

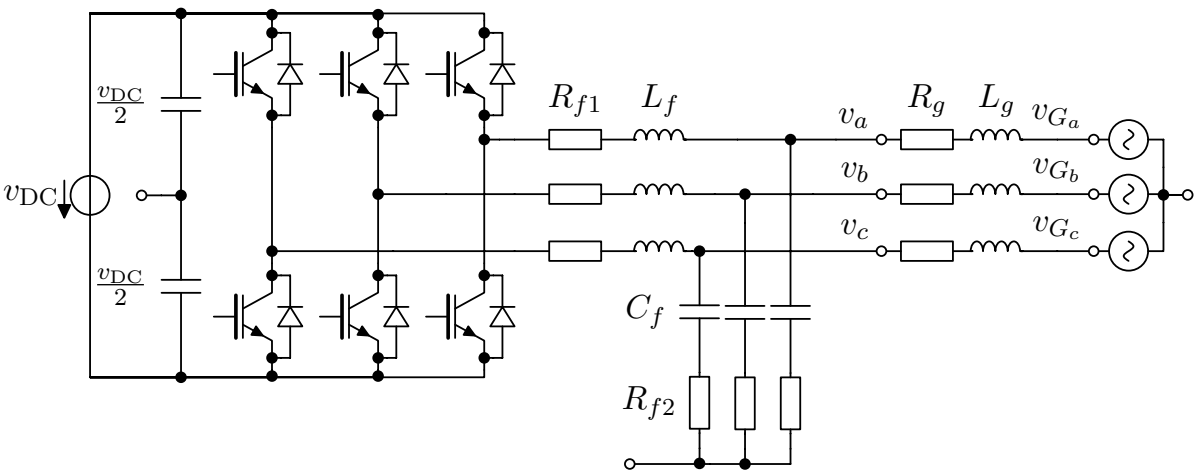

Figure 5.2: Typical circuit of a two-level three-phase inverter with LC output filter to convert a dc into a three-phase ac voltage. The inverter is constructed with insulated-gate bipolar transistors (IGBTs) and antiparallel diodes. The dc voltage is denoted by $v_{\mathrm{DC}} \in \mathbb{R}$, the three-phase ac voltage generated by the inverter with $v_{abc} \in \mathbb{R}^3$, $v_{abc} = \mathrm{col}(v_a, v_b, v_c)$ and the three-phase grid-side ac voltage by $v_G \in \mathbb{R}^3$, $v_G = \mathrm{col}(v_{G_a} v_{G_b}, v_{G_c})$. The components of the output filter are an inductance L_f, a capacitance C_f and two resistances R_{f_1}, respectively R_{f_2}. Typically, the resistance R_g and the inductance L_g represent a transformer or an output impedance. At the open connectors denoted by "$\mathbf{o}$" the circuit can be grounded if desired.

The submatrix $\mathcal{B}_{net} \otimes \mathbb{I}_3 \in \mathbb{R}^{\mathrm{n} \times 3\mathrm{t}}$, represents the incidence matrix of the sub–graph $\mathcal{G}_{net}^{\uparrow}$, that is obtained by eliminating the reference node and edges that are connected to it. The incidence matrix $\mathcal{B}_{net}$ thus fully captures the topology of the ac microgrid network. To avoid confusion we refer to $\mathcal{G}^{\uparrow}$ as the *ac microgrid graph* and to $\mathcal{G}_{net}^{\uparrow}$ as the *ac network graph*.

Inverters

Recall that inverters are key components of microgrids. The main elements of inverters are power semiconductor devices [48, 112]. An exemplary basic hardware topology of the electric circuit of a two-level three-phase inverter constructed with insulated-gate bipolar transistors (IGBTs) and antiparallel diodes is shown in Fig. 5.2. The conversion process from dc to ac is usually achieved by adjusting the on- and off-times of the transistors. These on- and off-time sequences are typically determined via a modulation technique, such as pulse-width-modulation [48, 112]. To improve the quality of the ac waveform, *e.g.*, to reduce the harmonics, the generated ac signal is typically processed through a low-pass filter constructed with LC elements. Further information on the hardware design of inverters and related controls is given in [48, 112, 178].

In microgrids, two main operation modes for inverters can be distinguished [166, 127]: grid-forming and grid-feeding mode. The latter is sometimes also called grid-following mode [89] or PQ control [105], whereas the first is also referred to as voltage source inverter (VSI) control [105]. The main characteristics of these two different operation modes are as follows [105, 89, 166, 127].

i) Grid-forming mode (also: VSI control).

   The inverter is controlled in such way that its output voltage can be specified by the designer. This is typically achieved via a cascaded control scheme consisting of an inner current control and an outer voltage control as shown in Fig. 5.3, based on [127]. The feedback signal of the current

control loop is the current through the filter inductance, while the feedback signal of the voltage control loop is the inverter output voltage $v_{abc} : \mathbb{R}_+ \to \mathbb{R}^3$. The inner loop of the control cascade is not necessary to control the output voltage of the inverter and can hence also be omitted. Nevertheless, it is often included to improve the control performance.

ii) Grid-feeding mode (also: grid-following mode, PQ control).

The inverter is operated as power source, *i.e.*, it provides a pre-specified amount of active and reactive power to the grid. The active and reactive power setpoints are typically provided by a higher-level control or energy management system, see [127, 22, 72]. Also in this case, a cascaded control scheme is usually implemented to achieve the desired closed-loop behavior of the inverter, as illustrated in Fig. 5.4. As in the case of a grid-forming inverter, the inner control loop is a current control the feedback signal of which is the current through the filter inductance. However, the outer control loop is not a voltage, but rather a power (or, sometimes, a current) control. The feedback signals of the power control are the active and reactive power provided by the inverter.

In both aforementioned operation modes, the current and voltage control loops are, in general, designed with the objectives of rejecting high frequency disturbances, enhancing the damping of the output $LC(L)$ filter and providing harmonic compensation [124, 19, 111, 122]. Furthermore, nowadays, most inverter-based DG units, such as PV or wind plants, are operated in grid-feeding mode [127]. However, grid-forming units are essential components in ac power systems, since they are responsible for frequency and voltage regulation in the network. Therefore, in microgrids with a large share of renewable inverter-based DG units, grid-forming capabilities often also have to be provided by inverter-interfaced sources [105, 89]. It is convenient to partition the set $\mathcal{E}_I$ into two subsets, *i.e.*, $\mathcal{E}_I = \mathcal{E}_F \cup \mathcal{E}_P$, such that $\mathcal{E}_F$ contains f edges associated to grid-forming inverters — that we call *grid–forming edges* — and $\mathcal{E}_P$ contains $\mathsf{p} = \mathsf{c} - \mathsf{f}$ edges associated to grid-feeding inverters — that we call *grid–feeding edges.*

Grid–forming edges

A suitable model of a grid-forming inverter for the purpose of control design and stability analysis of microgrids is derived. There are many control schemes available to operate an inverter in grid-forming mode, such as PI control in *dq*-coordinates [122], proportional resonant control [56, 153] or repetitive control [167, 79] among others. An overview of the most common control schemes with an emphasis on H_∞ repetitive control is given in [178]. For a comparison of different control schemes, the reader is referred to [104]. The assumption below is key for the subsequent model derivation.

Assumption 5.2.3. *Whenever an inverter operated in grid-forming mode connects an intermittent renewable generation source, it is equipped with a fast-reacting storage.*

Assumption 5.2.3 implies that the inverter can increase and decrease its power output within a certain range. This is necessary if the inverter should be capable of providing a fully controllable voltage also when interfacing an intermittent renewable DG unit to the network. Furthermore, since the storage element is assumed to be fast-reacting, the dc-side dynamics can be neglected in the model. The capacity of the required dc storage element depends on the specific source at hand. Generally, the standard capacitive elements of an inverter don't provide sufficient energy storage capacity and an additional storage component, *e.g.*, a battery or flywheel, is required if an inverter is operated in grid-forming mode [154] See [30] for a survey of energy storage technologies in the context of power electronic systems and renewable energy sources.

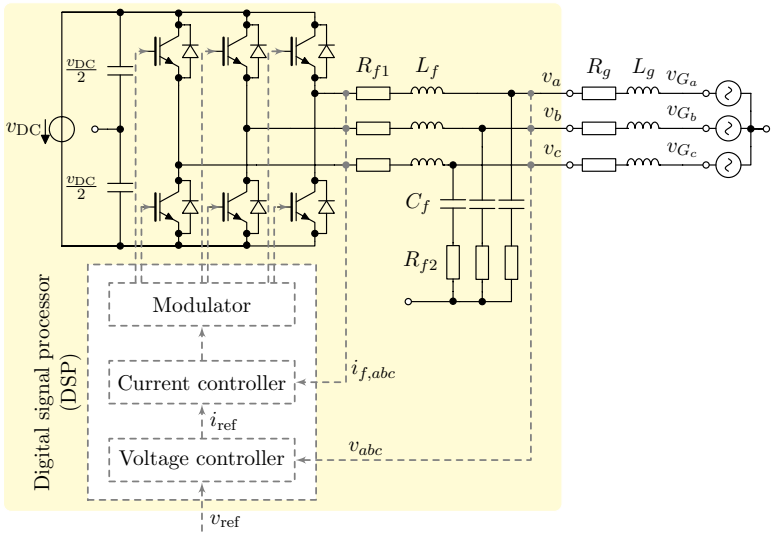

Figure 5.3: Schematic representation of an inverter operated in grid-forming mode based on [127]. Bold lines represent electrical connections, while dashed lines represent signal connections. The current through the filter inductance is denoted by $i_{f,abc} \in \mathbb{R}^3$ and the inverter output voltage by $v_{abc} \in \mathbb{R}^3$. Both quantities are fed back to a cascaded control consisting of an outer voltage and an inner current control. The reference signal $v_{\text{ref}} \in \mathbb{R}^3$ for the voltage controller is set by the designer, respectively a higher-level control. The IGBTs of the inverter are then controlled via signals generated by a modulator. The control structure can also be reduced to a pure voltage control.

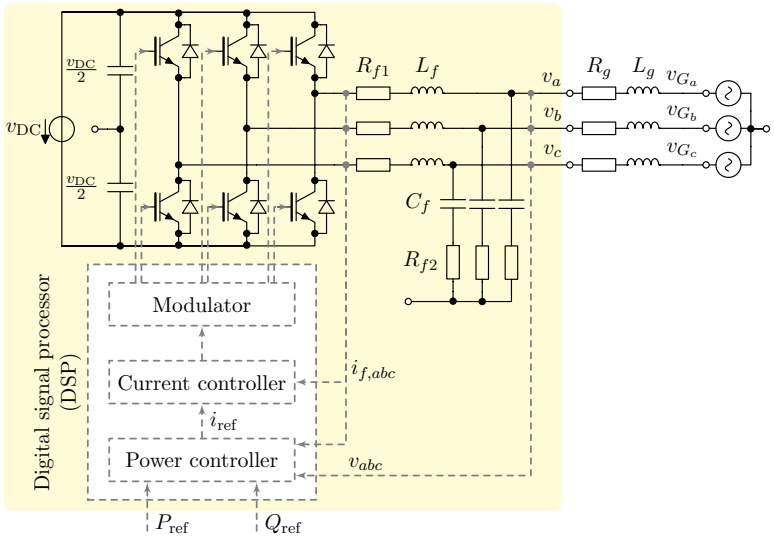

Figure 5.4: Schematic representation of an inverter operated in grid-feeding mode based on [127]. Bold lines represent electrical connections, while dashed lines represent signal connections. As in Fig. 5.3, the current through the filter inductance is denoted by $i_{f,abc} \in \mathbb{R}^3$ and the inverter output voltage by $v_{abc} :\in \mathbb{R}^3$. In grid-feeding mode, both quantities are fed back to a cascaded control consisting of an outer power and an inner current controller. The reference active and reactive powers $P_{\text{ref}} \in \mathbb{R}$, respectively $Q_{\text{ref}} \in \mathbb{R}$, are set by the designer or a higher-level control.

Due to the large variety of available control schemes, it is difficult to determine a standard closed-loop model of an inverter operated in grid-forming mode together with its inner control and output filter. Therefore, the approach taken in this work is to represent such a system as a generic dynamical system. Note that the operation of the IGBTs of an inverter occurs typically at very high switching frequencies (2-20 kHz) compared to the network frequency (45-65 Hz). It is therefore common practice [105, 63, 122, 111, 34] to model an inverter in network studies with continuous dynamics by using the so-called averaged switch modeling technique [48, 34], *i.e.*, by averaging the internal inverter voltage and current over a suitably chosen time interval such as one switching period.

Consider a grid-forming inverter located at the i-th node of a given microgrid, *i.e.*, $i \in \mathcal{E}_F$. Denote its three-phase symmetric output voltage by $v_{abc,i} : \mathbb{R}_+ \to \mathbb{R}^3$ with phase angle $\alpha_i : \mathbb{R}_+ \to \mathbb{S}$ and amplitude $\sqrt{\frac{2}{3}}V_i : \mathbb{R}_+ \to \mathbb{R}_+$, *i.e.*,

$$v_{abc,i} = \sqrt{\frac{2}{3}}V_i \begin{bmatrix} \sin(\alpha_i) \\ \sin(\alpha_i - \frac{2}{3}\pi) \\ \sin(\alpha_i + \frac{2}{3}\pi) \end{bmatrix}.$$

Furthermore, denote by $\omega_i := \dot{\alpha}_i$ the frequency of the voltage $v_{abc,i}$. Denote the state vector of the inverter with its inner control and output filter by $x_i \in \mathbb{R}^m$, its input vector by $v_{\mathrm{ref},i} \in \mathbb{R}^3$ and its conjugated interacion port variables by $(v_{abc,i}, i_{abc,i}) \in \mathbb{R}^3 \times \mathbb{R}^3$, see Fig. 5.3. Let $f_i : \mathbb{R}^m \times \mathbb{R}^3 \times \mathbb{R}^3 \to \mathbb{R}^m$ and $h_i : \mathbb{R}^m \times \mathbb{R}^3 \to \mathbb{R}^3$ denote continuously differentiable functions and ν_i denote a nonnegative real constant. Then, the closed-loop inverter dynamics with inner control and output filter can be represented in a generic manner as

$$\begin{aligned} \nu_i\gamma_i\dot{x}_i &= f_i(x_i, v_{\mathrm{ref},i}, i_{abc,i}), \\ v_{abc,i} &= h_i(x_i, v_{\mathrm{ref},i}), \end{aligned} \tag{5.2.2}$$

where the positive real constant γ_i denotes the time-drift due to the clock drift of the processor used to operate the inverter, see [137] for further details.

One key objective in microgrid applications is to design suitable higher-level controls to provide a reference voltage $v_{\mathrm{ref},i}$ for the system (5.2.2) [64]. Within the hierarchical control scheme discussed, *e.g.*, in [66, 64] this next higher control level corresponds to the primary control layer of a microgrid. Let $z_i \in \mathbb{R}^p$ denote the state vector of this higher-level control system, $u_i \in \mathbb{R}^q$ its control input vector and $v_{\mathrm{ref},i}$ its output vector. Furthermore, let $g_i : \mathbb{R}^p \times \mathbb{R}^q \to \mathbb{R}^p$ and $w_i : \mathbb{R}^p \times \mathbb{R}^q \to \mathbb{R}^3$ be continuously differentiable functions. Then, the outer control system of the inverter can be described by

$$\begin{aligned} \gamma_i\dot{z}_i &= g_i(z_i, u_i), \\ v_{\mathrm{ref},i} &= w_i(z_i, u_i). \end{aligned} \tag{5.2.3}$$

Combining (5.2.2) and (5.2.3) yields the overall inverter dynamics:

$$\mathcal{S}_i : \quad i \sim \mathcal{E}_F \quad \begin{cases} \gamma_i\dot{z}_i = g_i(z_i, u_i), \\ \nu_i\gamma_i\dot{x}_i = f_i(x_i, w_i(z_i, u_i), i_{abc,i}), \\ v_{abc,i} = h_i(x_i, w_i(z_i, u_i)). \end{cases} \tag{5.2.4}$$

Let define the state vectors $z := \mathrm{col}(z_i) \in \mathbb{R}^{p\mathsf{f}}$, $x : \mathrm{col}(x_i) \in \mathbb{R}^{m\mathsf{f}}$, the control input vector $u :=$

$\mathrm{col}(u_i) \in \mathbb{R}^{q\mathsf{f}}$, with $i \sim \mathcal{E}_F$ and the matrices

$$\Gamma := \mathrm{diag}(\gamma_i) \in \mathbb{R}^{\mathsf{f}\times\mathsf{f}}, \quad V := \mathrm{diag}(\nu_i) \in \mathbb{R}^{\mathsf{f}\times\mathsf{f}},$$

Hence the aggregated model of grid–forming edges can be obtained collecting the dynamical systems $\mathcal{S}_i$ with $i \sim \mathcal{E}_F$, thus giving:

$$\mathcal{S}_F : \begin{cases} [\Gamma \otimes \mathbb{I}_{p\mathsf{f}}]\, \dot{z} = g(z,u) \\ [V\Gamma \otimes \mathbb{I}_{m\mathsf{f}}]\, \dot{x} = f(x, w(z,u), i_{abc}) \\ \qquad v_{abc,i} = h_i(x_i, w_i(z_i,u_i)), \qquad i \sim \mathcal{E}_F. \end{cases} \tag{5.2.5}$$

Grid–feeding and load edges

As already discussed in Subsection 5.2.3, grid-feeding inverters are typically operated as current or power sources. In order to achieve such behavior, the control methods employed to design the inner control loops of grid-forming inverters (see Subsection 5.2.3) can equivalently be applied to operate inverters in grid-feeding mode. The current or power reference values are typically provided by a higher-level control, *e.g.*, a maximum power point tracker (MPPT) [127].

We define the sets $\mathcal{N}_L := \mathcal{N}_P \cup \mathcal{N}_R$, $\mathcal{E}_L := \mathcal{E}_P \cup \mathcal{E}_R$ the sets that contain the nodes, respectively the eddges, associated to grid-feeding inverters and loads and let $\mathsf{l} := \mathsf{p} + \mathsf{r}$. As done for the model of a grid-forming inverter in (5.2.4), let $x_i \in \mathbb{R}^\ell$ denote the state vector, $(v_{abc,i}, i_{abc,i}) \in \mathbb{R}^3 \times \mathbb{R}^3$ denote the conjugated interaction port variables, $f_i : \mathbb{R}^\ell \times \mathbb{R}^3 \to \mathbb{R}^\ell$ and $h_i : \mathbb{R}^\ell \times \mathbb{R}^3 \to \mathbb{R}^3$ denote continuously differentiable functions and κ_i denote a nonnegative real constant. We assume then a generic dynamic model of the form

$$\mathcal{S}_i : \ \ i \sim \mathcal{E}_L \ \begin{cases} \kappa_i \dot{x}_i = f_i(x_i, i_{abc,i}), \\ v_{abc,i} = h_i(x_i, i_{abc,i}). \end{cases} \tag{5.2.6}$$

In addition to grid-feeding inverters, the model (5.2.6) can equivalently represent impedance (*e.g.*, R parallel to L), current- or power-controlled loads. Furthermore, a large variety of other load behaviors can be modeled by (5.2.6). We refer the reader to [96, 158] for further details on load modeling. Let define the state vector $x_L := \mathrm{col}(x_i) \in \mathbb{R}^{r\mathsf{l}}$, with $i \sim \mathcal{E}_L$ and the matrix

$$K := \mathrm{diag}(\kappa_i) \in \mathbb{R}^{\ell\mathsf{l}\times\ell\mathsf{l}}.$$

Hence the aggregated model of grid–feeding and load edges can be obtained collecting the dynamical systems $\mathcal{S}_i$ with $i \sim \mathcal{E}_L$, thus giving:

$$\mathcal{S}_L : \begin{cases} [K \otimes \mathbb{I}_{\ell\mathsf{l}}]\, \dot{x}_L = f_L(x_L, i_{abc}) \\ \qquad v_{abc,i} = h_i(x_i, i_{abc,i}), \qquad i \sim \mathcal{E}_L. \end{cases} \tag{5.2.7}$$

Transmission lines edges

We recall that the set of transmission lines and transformers interconnecting the different network nodes $i \sim \mathcal{N}$ is given by $\mathcal{E}_T$. In order to describe the dynamics of a transmission line, a π–model — that consists of the parallel connection of two capacitors by means of an RL–series impedance — has been considered in Chapter 3. However, under Assumption 5.2.2, dc lines reduces to a more simple RL–series impedance. This is justified, as explained before, by the definition of an equivalent capacitor at the output of each inverter. In light of Assumption 3.4.1 and to ease presentation, we solely use

the term power lines to refer to the network interconnections in the following sections. Also, note that it is straight-forward to extent the modeling approach presented hereafter to more detailed power line models and to DG units interfaced to the network via SGs. Using the model of transmission edges given by (3.5.6), but represented in standard state–space form, the aggregated model of transmission edges can be written as

$$\mathcal{S}_T : \begin{cases} (L_T \otimes \mathbb{I}_3)\dot{x}_T = -(R_T \otimes \mathbb{I}_3)x_T + v_T \\ i_T = x_T. \end{cases} \tag{5.2.8}$$

with state vector $x_T \in \mathbb{R}^{3\mathsf{t}}$ the aggregated line currents, conjugated interaction port variables $(v_T, i_T) \in \mathbb{R}^{3\mathsf{t}} \times \mathbb{R}^{3\mathsf{t}}$ and matrices

$$L_T := \operatorname{diag}(L_i) \in \mathbb{R}^{\mathsf{t}\times\mathsf{t}}, \quad R_T := \operatorname{diag}(R_i) \in \mathbb{R}^{\mathsf{t}\times\mathsf{t}}.$$

The three-phase interconnection laws can be obtained using the incidence matrix $\mathcal{B}\otimes\mathbb{I}_3$ and Kirchhoff's current and voltage laws expressed by (3.5.28), from which it is easy to obtain

$$i_{abc} = (\mathcal{B} \otimes \mathbb{I}_3)i_T, \qquad (\mathcal{B}^\top \otimes \mathbb{I}_3)v_{abc} = v_T.$$

Hence, the dynamical system representing the network is given by

$$\begin{aligned} (L_T \otimes \mathbb{I}_3)\dot{x}_T &= -(R \otimes \mathbb{I}_3)x_T + (\mathcal{B}^\top \otimes \mathbb{I}_3)v_{abc} \\ i_{abc} &= (\mathcal{B} \otimes \mathbb{I}_3)x_T \end{aligned} \tag{5.2.9}$$

Interconnected model

For the construction of the interconnected model, we next transform the model (5.2.9) into dq-coordinates by means of the transformation T_{dq} introduced in Subsection 2.2.3. This coordinate transformation is instrumental for the model reduction carried out in Subsection 5.2.4. Let

$$\vartheta := \operatorname{mod}_{2\pi}(\omega^{\mathrm{com}} t) \in \mathbb{S}, \tag{5.2.10}$$

where the operator[1] $\operatorname{mod}_{2\pi}$ is added to respect the topology of the torus. Applying the transformation T_{dq} with transformation angle ϑ to the signals $v_{abc,i}$ and $i_{abc,i}$, $i \sim \mathcal{E}_I$, gives

$$\hat{v}_{dq,i} := T_{dq}(\vartheta)v_{abc,i} = \begin{bmatrix} \hat{V}_{d,i} \\ \hat{V}_{q,i} \end{bmatrix}, \qquad \hat{i}_{dq,i} := T_{dq}(\vartheta)i_{abc,i} = \begin{bmatrix} \hat{I}_{d,i} \\ \hat{I}_{q,i} \end{bmatrix},$$

where the superscript "$\hat{\cdot}$" is introduced to denote signals in dq-coordinates with respect to the angle ϑ. This notation is used in the subsequent section, where a reduced-order model of a microgrid is derived by using several dq-transformation angles. Furthermore, following standard notation in power systems, the constant $\dot{\vartheta} = \omega^{\mathrm{com}}$ is referred to as the rotational speed of the common reference frame. Likewise, the signal $x_{T,i}$ becomes

$$\hat{x}_{T,dq,i} := T_{dq}(\vartheta)x_{T,abc,i} = \begin{bmatrix} \hat{X}_{T,d,i} \\ \hat{X}_{T,q,i} \end{bmatrix}.$$

[1]The operator $\operatorname{mod}_{2\pi} : \mathbb{R} \to [0, 2\pi)$, is defined as follows: $y = \operatorname{mod}_{2\pi}\{x\}$ yields $y = x - k2\pi$ for some integer k, such that $y \in [0, 2\pi)$.

Note that

$$\dot{\hat{x}}_{T,dq,i} = \dot{T}_{dq}(\vartheta)x_{T,i} + T_{dq}(\vartheta)\dot{x}_{T,i} = \omega^{\text{com}} \begin{bmatrix} -\hat{X}_{T,q,i} \\ \hat{X}_{T,d,i} \end{bmatrix} + T_{dq}(\vartheta)\dot{x}_{T,i}.$$

Hence, the transmission line in dq-coordinates reads as

$$\begin{aligned} L_i\dot{\hat{x}}_{T,dq,i} &= L_i \left(\omega^{\text{com}} \begin{bmatrix} -\hat{X}_{T,q,i} \\ \hat{X}_{T,d,i} \end{bmatrix} + T_{dq}(\vartheta)\dot{x}_{T,i} \right) = -R_i\hat{x}_{T,dq,i} + L_i\omega^{\text{com}} \begin{bmatrix} -\hat{X}_{T,q,i} \\ \hat{X}_{T,d,i} \end{bmatrix} + \hat{v}_{dq,i}, \\ \hat{i}_{T,dq,i} &= \hat{x}_{T,dq,i}. \end{aligned} \tag{5.2.11}$$

Let define the aggregated voltages and currents of the converter edges, in dq-coordinates

$$\hat{v}_{dq} := \text{col}(\hat{v}_{dq,i}) \in \mathbb{R}^{2\mathsf{c}}, \quad \hat{i}_{dq} := \text{col}(\hat{i}_{dq,i}) \in \mathbb{R}^{2\mathsf{c}}. \tag{5.2.12}$$

Similarly, the aggregated voltages and currents of the transmission edges, in dq-coordinates, read:

$$\hat{v}_{T,dq} := \text{col}(\hat{v}_{T,dq,i}) \in \mathbb{R}^{2\mathsf{t}}, \quad \hat{x}_{T,dq} := \text{col}(\hat{x}_{T,dq,i}) \in \mathbb{R}^{2\mathsf{t}}.$$

Bu further introducing the matrix $\mathcal{X} := \text{diag}\{J_2 L_i \omega^{\text{com}}\} \in \mathbb{R}^{2\mathsf{t}\times 2\mathsf{t}}$, the aggregated model (5.2.9) finally becomes:

$$\begin{aligned} (L \otimes \mathbb{I}_2)\dot{\hat{x}}_{T,dq} &= (-R \otimes \mathbb{I}_2 + \mathcal{X})\hat{x}_{T,dq} + (\mathcal{B}^\top \otimes \mathbb{I}_2)\hat{v}_{dq} \\ \hat{i}_{dq} &= (\mathcal{B} \otimes \mathbb{I}_2)\hat{x}_{T,dq}. \end{aligned} \tag{5.2.13}$$

To obtain the interconnected model, it suffices now to combine (5.2.5), (5.2.7) and (5.2.13), thus leading to the following differential equations

$$\begin{aligned} [\Gamma \otimes \mathbb{I}_{pf}]\, \dot{z} &= g(z,u) \\ [V\Gamma \otimes \mathbb{I}_{mf}]\, \dot{x} &= f(x, w(z,u), \mathcal{B} \otimes T_{dq}^\top(\vartheta)\hat{x}_{T,dq}) \\ [K \otimes \mathbb{I}_{\ell l}]\, \dot{x}_L &= f_L(x_L, \mathcal{B} \otimes T_{dq}^\top(\vartheta)\hat{x}_{T,dq}) \\ [L \otimes \mathbb{I}_2]\, \dot{\hat{x}}_{L,dq} &= (-R \otimes \mathbb{I}_2 + \mathcal{X})\hat{x}_{T,dq} + (\mathcal{B}^\top \otimes \mathbb{I}_2)\hat{v}_{dq}, \end{aligned} \tag{5.2.14}$$

Note that the voltage at the nodes are expressed by

$$\hat{v}_{dq} = [\mathbb{I}_{\mathsf{c}} \otimes T_{dq}(\vartheta)]\, v_{abc}, \tag{5.2.15}$$

with

$$v_{abc,i} = h_i(x_i, w_i(z_i, u_i)), \quad i \sim \mathcal{E}_F, \qquad v_{abc,k} = h_k(x_k, i_{abc,k}), \quad k \sim \mathcal{E}_L. \tag{5.2.16}$$

5.2.4 A reduced model for primary control design

For the purpose of deriving a model that is suitable for stability analysis, it is customary to make the following assumptions on (5.2.14), (5.2.15), where ϵ stands for a generic small positive real constant.

Assumption 5.2.4. *$\nu_i < \epsilon$ in (5.2.4), $i \sim \mathcal{E}_F$. Therefore, $\dot{x}_i(t) = 0_m$ for all $t \geq 0$. Furthermore, $v_{abc,i} = w_i(z_i, u_i)$, $i \sim \mathcal{E}_F$.*

Assumption 5.2.5. *$\kappa_k < \epsilon$ in (5.2.6), $k \sim \mathcal{E}_L$. Therefore, $\dot{x}_k(t) = 0_r$ for all $t \geq 0$. Furthermore, the instantaneous power balance at each node $k \in \mathcal{N}_L$ can be described by a ZIP model [96], i.e.,*

$$\begin{aligned} P_k(\hat{v}_{dq,k}, \hat{i}_{dq,k}) &= -\left(a_{P,k}\|\hat{v}_{dq,k}\|_2^2 + b_{P,k}\|\hat{v}_{dq,k}\|_2 + c_{P,k}\right) := P_k^*(\|\hat{v}_{dq,k}\|_2), \\ Q_k(\hat{v}_{dq,k}, \hat{i}_{dq,k}) &= -\left(a_{Q,k}\|\hat{v}_{dq,k}\|_2^2 + b_{Q,k}\|\hat{v}_{dq,k}\|_2 + c_{Q,k}\right) := Q_k^*(\|\hat{v}_{dq,k}\|_2), \end{aligned}$$

where $a_{P,k}$, $b_{P,k}$, $c_{P,k}$, $a_{Q,k}$, $b_{Q,k}$ and $c_{Q,k}$ are real constants and $P_k(\hat{v}_{dq,k}, \hat{i}_{dq,k})$ and $Q_k(\hat{v}_{dq,k}, \hat{i}_{dq,k})$ are power are calculated according to the definition provided in Subsection 2.2.5.

Assumption 5.2.6. *$L < \epsilon \mathbb{I}_{\mathfrak{t}}$ in (5.2.13). Therefore, $\dot{\hat{x}}_{T,dq}(t) = 0_{2\mathfrak{t}}$ for all $t \geq 0$.*

Assumption 5.2.4 is equivalent to the assumption that the inner current and voltage controllers track the voltage and current references instantaneously and exactly. Usually, the current and voltage controllers in (5.2.2) (see also Fig. 5.3) are designed such that the resulting closed-loop system (5.2.2) has a very large bandwidth compared to the control system located at the next higher control level represented by (5.2.3) [105, 36, 111]. If this time-scale separation is followed in the design of the system (5.2.4), the first part of Assumption 5.2.4 can be mathematically formalized by invoking singular perturbation theory [91], [95]. The second part of Assumption 5.2.4 expresses the fact that the inner control system (5.2.2) is assumed to track the reference $v_{\mathrm{ref},i} = w_i(z_i, u_i)$ exactly, independently of the disturbance $i_{abc,i}$. Typical values for the bandwidth of (5.2.2) reported in [111, 122] are in the range of $400 - 600$ Hz, while those of (5.2.3) are in the range of $2 - 10$ Hz.

Assumption 5.2.5 implies that the dynamics of loads and grid-feeding units can be neglected. This assumption is also frequently employed in microgrid and power system stability studies, where loads are often modeled as either constant impedance (Z), constant current (I) or constant power loads (P) or a combination of them (ZIP) [96, 158]. Similarly, grid-feeding units with positive active power injection are represented by setting $a_{P,k} = a_{Q_k} = 0$ and $b_{P,k}$ or $c_{P,k}$ to negative values. The values for $b_{Q,k}$ and $c_{Q,k}$ should be chosen in dependency of the reactive power contribution of the unit.

Assumption 5.2.6 is standard in power system analysis [96, 62, 132, 7, 106, 59]. The usual justification of Assumption 5.2.6 is that the line dynamics evolve on a much faster time-scale than the dynamics of the generation sources. In the present case, Assumption 5.2.6 is justified whenever Assumption 5.2.4 is employed, since the line dynamics (5.2.13) are typically at least as fast as those of the internal inverter controls (5.2.2), see, *e.g.*, [122]. Again, Assumption 5.2.6 can be mathematically formalized by invoking singular perturbation arguments [91], [95].

Under Assumption 5.2.4, the model of each grid-forming inverter (5.2.4) reduces to

$$\begin{aligned} \gamma_i \dot{z}_i &= g_i(z_i, u_i), \\ v_{abc,i} &= w_i(z_i, u_i), \quad i \sim \mathcal{E}_F. \end{aligned} \tag{5.2.17}$$

The model (5.2.17) represents the inverter as an ac voltage source, the amplitude and frequency of which can be defined by the designer. The system (5.2.17) is a very commonly used model of a grid-forming inverter in microgrid control design and analysis [105, 63, 89, 136]. The model simplification from (5.2.4) to (5.2.17) is illustrated in Figure 5.5.

Furthermore, often a particular structure of (5.2.17) is used in the literature [144, 145, 134, 136, 4, 114]. As discussed in Subsection 2.2.2, a symmetric three-phase voltage can be completely described by its phase angle and its amplitude. In addition, it is usually preferred to control the frequency of the inverter output voltage, instead of the phase angle. Hence, a suitable model of the inverter at the i-th

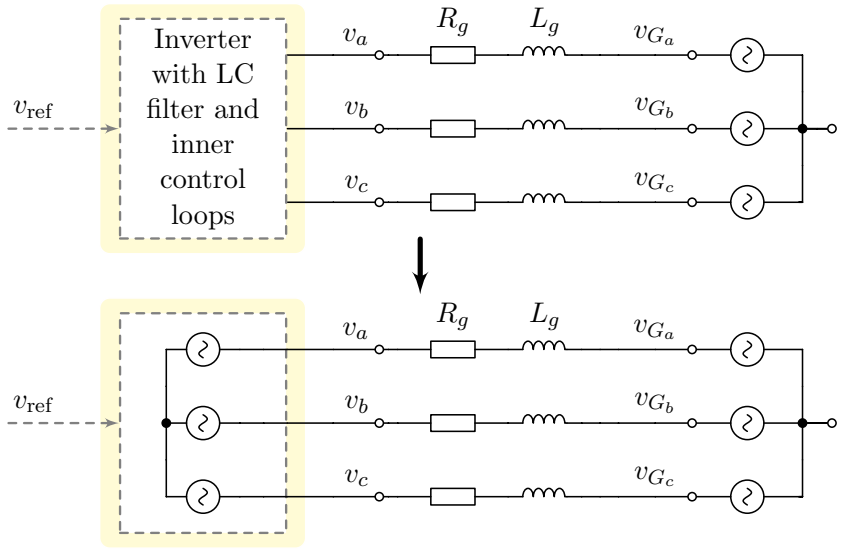

Figure 5.5: Simplified representation of an inverter operated in grid-forming mode as ideal controllable voltage source. Bold lines represent electrical connections, while dashed lines represent signal connections.

node is given by [136, 134]

$$\begin{aligned} \gamma_i \dot{\alpha}_i &= \omega_i = u_i^{\delta}, \\ V_i &= u_i^{\mathrm{V}}, \\ v_{abc,i} &= v_{abc,i}(\alpha_i, V_i), \end{aligned} \tag{5.2.18}$$

where $u_i^{\delta} : \mathbb{R}_+ \to \mathbb{R}$ and $u_i^{V} : \mathbb{R}_+ \to \mathbb{R}$ are control signals.

Usually, it is also assumed that the active and reactive power output is measured and processed through a filter to obtain the power components corresponding to the fundamental frequency [122, 36, 111]

$$\gamma_i \tau_{P_i} \dot{P}_i^m = -P_i^m + P_i, \qquad \gamma_i \tau_{P_i} \dot{Q}_i^m = -Q_i^m + Q_i. \tag{5.2.19}$$

Here, P_i and Q_i are the active and reactive power injections of the inverter, $P_i^m : \mathbb{R}_+ \to \mathbb{R}$ and $Q_i^m : \mathbb{R}_+ \to \mathbb{R}$ their measured values and $\tau_{P_i} \in \mathbb{R}_{>0}$ is the time constant of the low pass filter.

Note that whenever the particular form (5.2.18), (5.2.19) of (5.2.3) is considered and the measured and filtered power signals are used as feedback signals in the controls u_i^{δ}, respectively u_i^{V}, then the bandwidth of the overall control system is limited by the bandwidth of the measurement filter. Hence, if $\tau_{P_i} \gg \nu_i$, then Assumption 5.2.4 is justified.

With Assumption 5.2.5, (5.2.6) can be represented by the algebraic relation

$$P_k(\hat{v}_{dq,k}, \hat{i}_{dq,k}) = P_k^*(\|\hat{v}_{dq,k}\|_2), \quad Q_k(\hat{v}_{dq,k}, \hat{i}_{dq,k}) = Q_k^*(\|\hat{v}_{dq,k}\|_2), \quad k \sim \mathcal{E}_L. \tag{5.2.20}$$

Finally, under Assumption 5.2.6, the network interconnections (5.2.13) are also static and given by

$$\hat{i}_{dq} = \mathcal{B} \otimes \mathbb{I}_2 \left(R \otimes \mathbb{I}_2 - \mathcal{X}\right)^{-1} \mathcal{B}^{\top} \otimes \mathbb{I}_2 \hat{v}_{dq}. \tag{5.2.21}$$

In the following, a more compact representation of (5.2.18) - (5.2.21) is derived. To this end, it is

convenient to recall that α_i is the angle of the voltage at the i-th node with initial condition α_{0_i}, $i \sim \mathcal{N}$ and define

$$\delta_i := \alpha_{0_i} + \int_0^t (\dot{\alpha}_i - \omega^{\text{com}}) d\tau \in \mathbb{S}, \quad i \sim \mathcal{N}. \tag{5.2.22}$$

Let $\varpi : \mathbb{R}_+ \to \mathbb{S}$ and consider the mapping $T_\delta : \mathbb{S} \to \mathbb{R}^{2\times 2}$,

$$T_\delta(\varpi) := \begin{bmatrix} \cos(\varpi) & \sin(\varpi) \\ -\sin(\varpi) & \cos(\varpi) \end{bmatrix}. \tag{5.2.23}$$

which applied to any $x \in \mathbb{R}^2$ represents a rotational transformation. Note that, with δ_i defined in (5.2.22),

$$\alpha_i - \delta_i = \text{mod}_{2\pi}(\omega^{\text{com}} t) = \theta, \quad i \sim \mathcal{N},$$

and that straightforward algebraic manipulations yield

$$T_{dq}(\theta) = T_\delta(\delta_i) T_{dq}(\alpha_i).$$

Hence, by construction,

$$\hat{v}_{dq,i} = T_{dq}(\theta) v_{abc,i} = T_\delta(\delta_i) T_{dq}(\alpha_i) v_{abc,i} = T_\delta(\delta_i) V_i \begin{bmatrix} 0 \\ 1 \end{bmatrix}, \tag{5.2.24}$$

which makes it convenient to define

$$v_{dq,i} := \begin{bmatrix} V_{d,i} \\ V_{q,i} \end{bmatrix} = V_i \begin{bmatrix} 0 \\ 1 \end{bmatrix}, \quad i \sim \mathcal{N}. \tag{5.2.25}$$

The variables $v_{dq,i}$ are referred to as local dq-coordinates of $v_{abc,i}$ in the following. It is now convenient to represent (5.2.24) in the complex plane

$$\hat{V}_{qd,i} := \hat{V}_{q,i} + j\hat{V}_{d,i} = (\cos(\delta_i) + j\sin(\delta_i)) V_{qd,i} = e^{j\delta_i} V_{qd,i}, \tag{5.2.26}$$

where $V_{qd,i} = V_{q,i} + jV_{d,i}$, $i \sim \mathcal{N}$. Equivalently, let

$$\hat{I}_{qd,i} := \hat{I}_{q,i} + j\hat{I}_{d,i} = e^{j\delta_i} I_{qd,i} \tag{5.2.27}$$

and define

$$\begin{aligned} \hat{V}_{qd} :=& \hat{V}_q + j\hat{V}_d \in \mathbb{C}^{\mathsf{c}}, \quad \hat{I}_{qd} := \hat{I}_q + j\hat{I}_d \in \mathbb{C}^{\mathsf{c}}, \\ V_{qd} :=& V_q + jV_d \in \mathbb{C}^{\mathsf{c}}, \quad I_{qd} := I_q + jI_d \in \mathbb{C}^{\mathsf{c}}. \end{aligned} \tag{5.2.28}$$

Then, with $X := \text{diag}(X_i) = \text{diag}(L_i \omega^{\text{com}}) \in \mathbb{R}^{\mathsf{t}\times\mathsf{t}}$, we can rewrite (5.2.21) as

$$\hat{I}_{qd} = \mathcal{B} (R + jX)^{-1} \mathcal{B}^\top \hat{V}_{qd}. \tag{5.2.29}$$

Note that the reactances $X_i = L_i \omega^{\text{com}}$ are calculated at the frequency ω^{com}, which, under the made assumptions, should be chosen as the (constant) synchronous frequency of the network—denoted by $\omega^s \in \mathbb{R}$ in the following. Typically, $\omega^s \in 2\pi[45, 65]$ rad/s.

Remark 5.2.7. The form (5.2.28) is a very popular representation and these complex quantities are

often denoted as phasors [7, 178]. Furthermore, by using Euler's formula [75], (5.2.28) can also be rewritten in polar form. Note, however, that, unlike, *e.g.*, [7, 178], other authors define a phasor as a complex sinusoidal quantity with a constant frequency [59].

Define the admittance matrix of the electrical network by

$$\mathcal{Y} := \mathcal{B}\left(R + jX\right)^{-1}\mathcal{B}^{\top} \in \mathbb{C}^{\mathsf{c}\times\mathsf{c}} \tag{5.2.30}$$

and

$$G_{ii} :=\mathfrak{Re}(\mathcal{Y}_{ii}), \quad B_{ii} := \mathfrak{Im}(\mathcal{Y}_{ii}), \qquad Y_{ik} := G_{ik} + jB_{ik} := -\mathcal{Y}_{ik}, \quad i \neq k.$$

Moreover, it follows immediately that

$$\mathcal{Y}_{ik} = \begin{cases} 0 & \text{if nodes } i \text{ and } k \text{ are not connected} \\ -(R_i + jX_i)^{-1} & \text{if nodes } i \text{ and } k \text{ are connected by line } i \end{cases}$$

and

$$G_{ii} + jB_{ii} = \sum_{i\sim\mathcal{E}_{T,i}} (R_i + jX_i)^{-1},$$

where $\mathcal{E}_{T,i}$ denotes the set of transmission edges associated to node i. Inserting (5.2.26) and (5.2.27) into (5.2.29) yields

$$I_{qd} = \mathrm{diag}\left(e^{-j\delta_i}\right)\mathcal{Y}\mathrm{diag}\left(e^{j\delta_i}\right)V_{qd}. = \hat{\mathcal{Y}}(\delta)V_{qd}. \tag{5.2.31}$$

Recall that V_{qd} and I_{qd} defined in (5.2.28) are expressed in local dq-coordinates. By making use of (5.2.25) and (5.2.30), (5.2.31) can be written component-wise as

$$I_{qd,i} = I_{q,i} + jI_{d,i} \tag{5.2.32}$$

with:

$$\begin{aligned} I_{q,i} &= G_{ii}V_i - \sum_{k\sim\mathcal{N}_i} \left(G_{ik}\cos(\delta_{ik}) + B_{ik}\sin(\delta_{ik})\right)V_k, \\ I_{d,i} &= B_{ii}V_i - \sum_{k\sim\mathcal{N}_i} \left(B_{ik}\cos(\delta_{ik}) - G_{ik}\sin(\delta_{ik})\right)V_k, \end{aligned} \tag{5.2.33}$$

$i \sim \mathcal{N}$, where, for ease of notation, angle differences are written as $\delta_{ik} := \delta_i - \delta_k$. Furthermore, using the definition of power provided in Subsection 2.2.5, together with (5.2.25) and (5.2.33), the power flows in the network are given by

$$\begin{aligned} P_i &= V_i I_{q,i} = G_{ii}V_i^2 - \sum_{k\sim\mathcal{N}_i} \left(G_{ik}\cos(\delta_{ik}) + B_{ik}\sin(\delta_{ik})\right)V_k V_i \\ Q_i &= -V_i I_{d,i} = -B_{ii}V_i^2 + \sum_{k\sim\mathcal{N}_i} \left(B_{ik}\cos(\delta_{ik}) - G_{ik}\sin(\delta_{ik})\right)V_k V_i. \end{aligned} \tag{5.2.34}$$

The equations (5.2.34) are the standard power flow equations used in most recent work on microgrid stability analysis, *e.g.*, [144, 136, 4, 114].

Remark 5.2.8. Note that for any other choices of the transformation angle in local dq-coordinates $V_{d_i} \neq 0$. This is usually the case when modeling SGs, since the angle of the internal machine electromagnetic

force (EMF) is in general not known. Then, the equations (5.2.34) become slightly more involved, see [7].

Furthermore, in local dq-coordinates, the particular inverter model (5.2.18), (5.2.19), is given by

$$\begin{aligned} \gamma_i \dot{\delta}_i = \omega_i - \omega^{\text{com}} &= u_i^{\delta} - \omega^{\text{com}}, \\ \gamma_i \tau_{P_i} \dot{P}_i^m &= -P_i^m + P_i, \\ V_i &= u_i^V, \\ \gamma_i \tau_{P_i} \dot{Q}_i^m &= -Q_i^m + Q_i, \end{aligned} \tag{5.2.35}$$

with $V_{qd,i} = V_i$ (see (5.2.25)) and P_i and Q_i given by (5.2.34).

Recall (5.2.20) and note that

$$\|\hat{v}_{dq,k}\|_2 = \|\hat{V}_{qd,k}\|_2 = \|V_{qd,k}\|_2 = V_k, \quad k \in \mathcal{E}_L.$$

Defining the vectors

$$\begin{aligned} \delta_I :=& \text{col}(\delta_i) \in \mathbb{S}^{\mathsf{f}},\ V_I := \text{col}(V_i) \in \mathbb{R}^{\mathsf{f}}, \\ u^{\delta} :=& \text{col}(u_i^{\delta}) \in \mathbb{R}^{\mathsf{f}},\ u^V := \text{col}(u_i^V) \in \mathbb{R}^{\mathsf{f}}, \\ P_I :=& \text{col}(P_i) \in \mathbb{R}^{\mathsf{f}},\ Q_I := \text{col}(Q_i) \in \mathbb{R}^{\mathsf{f}}, \\ P_L :=& \text{col}(P_k) \in \mathbb{R}^{\mathsf{l}},\ Q_\ell := \text{col}(Q_k) \in \mathbb{R}^{\mathsf{l}}, \\ P_L^* :=& \text{col}(P_k^*(V_k)) \in \mathbb{R}^{\mathsf{l}},\ Q_L^* := \text{col}(Q_k^*(V_k)) \in \mathbb{R}^{\mathsf{l}}, \end{aligned}$$

with P_i, P_k, Q_i, and Q_k given by (5.2.34), as well as the matrix

$$T := \text{diag}(\tau_{P_i}) \in \mathbb{R}^{\mathsf{f}\times\mathsf{f}},$$

the system (5.2.18) - (5.2.21) can be written equivalently by means of (5.2.20), (5.2.35), (5.2.34) as

$$\begin{aligned} \Gamma \dot{\delta}_I &= u^{\delta} - \omega^{\text{com}} \mathbf{1}_{\mathsf{f}}, \\ \Gamma T \dot{P}^m &= -P^m + P_I, \\ V_I &= u^V, \\ \Gamma T \dot{Q}^m &= -Q^m + Q_I, \\ 0_{\mathsf{l}} &= P_L - P_L^*, \\ 0_{\mathsf{l}} &= Q_L - Q_L^*, \end{aligned} \tag{5.2.36}$$

where the last $2\mathsf{l}$ algebraic equations correspond to the power balances at nodes $k \sim \mathcal{E}_L$.

This section has illustrated the main modeling steps and assumptions, which lead from the detailed microgrid model (5.2.14), (5.2.15) to the model (5.2.36), (5.2.34). The model (5.2.36), (5.2.34) is frequently used in the analysis and control design of microgrids [144, 145, 24, 135, 136, 4, 114, 138, 139]. Some of the mentioned work is conducted under additional assumptions such as instantaneous power measurements [144, 4, 114], constant voltage amplitudes [144, 24, 4, 135] or small phase angle differences [145, 138, 139]. In addition, ideal clocks are usually assumed, *i.e.*, $\Gamma = \mathbb{I}_{\mathsf{f}}$.

5.3 Synchronous generator connected to a resistive load: analysis

5.3.1 Motivation & contributions

A typical power network consists of a large number of synchronous generators interconnected through transmission lines and supplying electrical power to loads. The stability of the entire network depends up on the ability of individual synchronous generators to reach their post-fault equilibria. The representation of synchronous generators by means of an appropriate mathematical model that, on one hand, capture the complicated nonlinear phenomena while, on the other hand, are amenable for analysis and control design is critical for power system stability analysis. With the latter objective in mind, power engineers have developed simplified, reduced order models for synchronous generators, that neglect some fast transients and losses. In particular, it is assumed that the electrical magnitudes can be represented via (first harmonic) phasors, and the dynamics is reduced to a second or third order model see [96]. These reductions "destroy" the physical structure of the system, leading to some approximate rationalizations of the new quantities, e.g., the concept of "voltage behind the reactance", and an awkward interpretation of basic physical concepts like energy and dissipation, which are introduced only for mathematical convenience see [58].

In this section — proceeding from a bond graph representation of the synchronous generators, a port–Hamiltonian, first–principles model of a synchronous generator connected to a load is derived, without the aforementioned simplifying assumptions (section 5.3.2). This leads to an energy–based description of the generation system, where all elements preserve their original physical interpretation, paving the road for the energy–based analysis. For, an appropriate dq–transformation is employed, allowing to rewrite the system equations in a more convenient form for stability analysis. A quotient system after this transformation and after eliminating rotor angle dynamics admit equilibria. The section is concluded with some preliminary results on stability analysis of equilibria using an energy shaping technique (Subsection 5.3.3).

5.3.2 Physical modeling

In this subsection a port-Hamiltonian representation of a three–phase synchronous generator connected to resistive loads is derived by applying energy–based modeling technique as in Chapter 3. The obtained model represents the trivial case for a generalized power system, where we have just one generator, no transmission lines and a static and linear load connected to the generator.

A synchronous generator can be defined as a multi–domain system characterized by both mechanical and electrical variables, *i.e* an electromechanical system. The model, derived starting from physical principles such as Maxwell equations and Newton's 2nd law, is basically the most direct way to describe dynamics in terms of certain specific physical quantities (magnetic flux and voltages, angles, momenta and torques). Nevertheless the complete model is given not only by ordinary differential equations (ODE) but also by algebraic constraints expressing flux-currents relations (DAE). The generator rotor circuit is formed by a field circuit and one amortisseur circuit, the last is divided in d and q axis circuits. The stator is formed by three-phase windings spatially distributed $\frac{2\pi}{3}$ mechanical radians in order to generate three-phase voltages at machine terminals. For convenience magnetic saturation effects are negligible. Therefore using bond graph modeling ([44]) a model of the synchronous generator connected to resistive loads can be obtained as in Fig. 5.6, where the higher part refer to the electrical dynamics

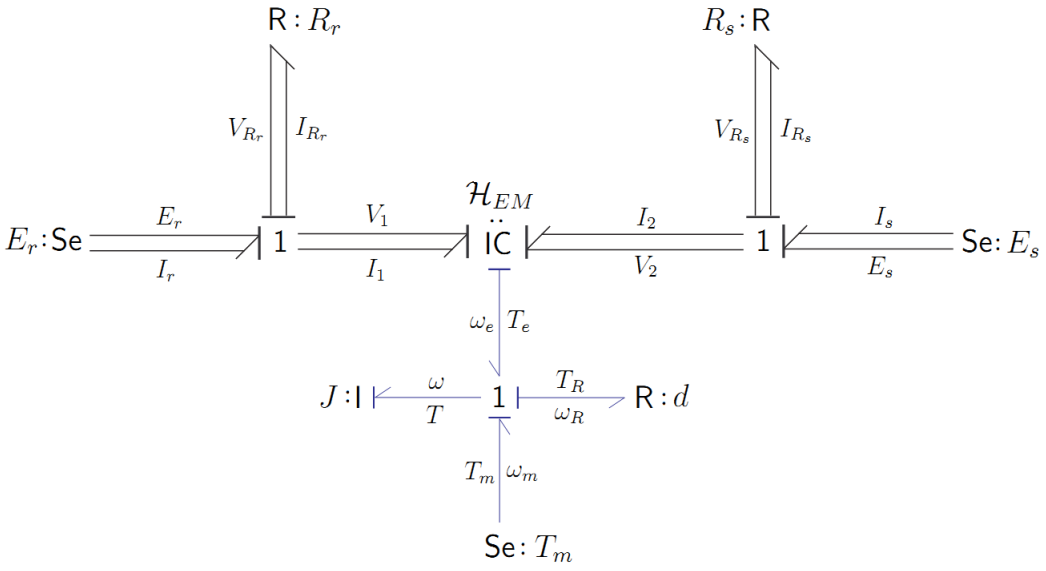

Figure 5.6: Bond graph model of a three-phase synchronous machine.

while the lower part to the mechanical one. Non standard element IC ensure then the electromechanical coupling.

By straightforward computations, the following equations (for the details see [96], [179]) can be easily derived:

$$\begin{bmatrix} \dot{\Psi}_s \\ \Psi_r \\ p \\ \theta \end{bmatrix} = \begin{bmatrix} -R_{s\ell} & 0 & 0 & 0 \\ 0 & -R_r & 0 & 0 \\ 0 & 0 & -d & -1 \\ 0 & 0 & 1 & 0 \end{bmatrix} \nabla\mathcal{H} + \begin{bmatrix} 0 & 0 \\ B_r & 0 \\ 0 & 1 \\ 0 & 0 \end{bmatrix} \begin{bmatrix} E_f \\ T_m \end{bmatrix}, \tag{5.3.1}$$

with associated energy function:

$$\mathcal{H}(x) = \frac{1}{2} \begin{bmatrix} \Psi_s & \Psi_r \end{bmatrix}^\top L^{-1}(\theta) \begin{bmatrix} \Psi_s & \Psi_r \end{bmatrix} + \frac{1}{2J} p^2. \tag{5.3.2}$$

where: $\Psi_s := \mathrm{col}(\psi_{s,a}, \psi_{s,b}, \psi_{s,c})$ and $\Psi_r := \mathrm{col}(\psi_{fd}, \psi_{kd}, \psi_{kq})$ represent three–phase stator and rotor flux linkages; $R_{s\ell} = R_s + R_\ell$, with $R_s = \mathrm{diag}(r_s, r_s, r_s)$ representing three–phase stator resistances and $R_{ell} = \mathrm{diag}(r_\ell, r_\ell, r_\ell)$ representing three–phase resistive loads; $R_r = \mathrm{diag}(r_{fd}, r_{kd}, r_{kq})$ represents resistances of rotor field and amortisseur windings; E_f represent the voltage applied across the rotor field winding; θ, ω and p represent angular displacement, angular velocity and momentum of rotor respectively with respective to stationary rotor reference frame axis; T_m represents the mechanical torque applied to the rotor; $\mathcal{H}$ is the total energy in the synchronous machine; J is the rotational inertia of the rotor,

$$L(\theta) := \begin{bmatrix} L_{ss} & L_{rs} \\ L_{rs}^\top & L_{rr} \end{bmatrix}, \qquad B_r := \begin{bmatrix} 1 & 0 & 0 \end{bmatrix}^\top, \tag{5.3.3}$$

where $L_{ss}(\theta)$, $L_{rs}(\theta)$, L_{rr} refer to stator and rotor self- and mutual inductances. For the structure of these self– and mutual dependencies and their explicit dependency on θ the reader is referred to [96].

In shorthand notation (5.3.1) can be written in standard port–Hamiltonian form as follows

$$\begin{aligned} \dot{x} &= [\mathcal{J}(x) - \mathcal{R}(x)]\nabla_x \mathcal{H}(x) + g(x)u \\ y &= g(x)^\top \nabla_x \mathcal{H}(x) \end{aligned} \tag{5.3.4}$$

where

$$\mathcal{J}(x) := \begin{bmatrix} 0 & 0 & 0 & 0 \\ 0 & 0 & 0 & 0 \\ 0 & 0 & 0 & -1 \\ 0 & 0 & 1 & 0 \end{bmatrix}, \quad \mathcal{R}(x) := \begin{bmatrix} R_{s\ell} & 0 & 0 & 0 \\ 0 & R_r & 0 & 0 \\ 0 & 0 & d & 0 \\ 0 & 0 & 0 & 0 \end{bmatrix}, \quad g(x) = \begin{bmatrix} 0 & 0 \\ B_r & 0 \\ 0 & 1 \\ 0 & 0 \end{bmatrix}. \tag{5.3.5}$$

It is evident from the equations above that the matrices $\mathcal{J}(x), \mathcal{R}(x), g(x)$ are independent of the state x. Nevertheless, it is easy to see that the inductances given in (5.3.3) depend upon θ and hence are functions of time t, which makes the analysis more difficult. To eliminate this dependency on time we refer the stator side electrical quantities to the rotor side by using the dq transformation introduced in Section 2.2, picking as transformation angle $\vartheta = \theta$. Hence we have:

$$x_{dq} := \mathcal{T}(x)x, \qquad \mathcal{T}(x) := \begin{bmatrix} T_{dq}(\theta) & 0 & 0 & 0 \\ 0 & \mathbb{I}_3 & 0 & 0 \\ 0 & 0 & 1 & 0 \\ 0 & 0 & 0 & 1 \end{bmatrix} \tag{5.3.6}$$

so that in the new coordinates the Hamiltonian energy function reads:

$$\mathcal{H}(x_{dq}) = \begin{bmatrix} \Psi_{dq}^\top & \Psi_r^\top \end{bmatrix}^\top L_{dq}^{-1} \begin{bmatrix} \Psi_{dq}^\top & \Psi_r^\top \end{bmatrix} + \frac{1}{2J}p^2 \tag{5.3.7}$$

with

$$L_{dq} := \begin{bmatrix} T_{dq}(\theta) & 0 \\ 0 & \mathbb{I}_3 \end{bmatrix} L(\theta) \begin{bmatrix} T_{dq}(\theta) & 0 \\ 0 & \mathbb{I}_3 \end{bmatrix}^\top = \begin{bmatrix} L_{dq} & L_{dqr} \\ L_{dqr}^\top & L_{rr} \end{bmatrix}.$$

From (5.3.6) we calculate the matrix

$$\mathcal{T}_x := \frac{\partial \mathcal{T}(x)}{\partial x}x + \mathcal{T}(x) = \begin{bmatrix} T_{dq}(\theta) & 0 & 0 & \frac{\partial T_{dq}(\theta)}{\partial \theta}\Psi_s \\ 0 & \mathbb{I}_3 & 0 & 0 \\ 0 & 0 & 1 & 0 \\ 0 & 0 & 0 & 1 \end{bmatrix} = \begin{bmatrix} T_{dq}(\theta) & 0 & 0 & -J_2\Psi_{dq} \\ 0 & \mathbb{I}_3 & 0 & 0 \\ 0 & 0 & 1 & 0 \\ 0 & 0 & 0 & 1 \end{bmatrix}, \tag{5.3.8}$$

where in the last equivalence we used:

$$\left[\frac{\partial T_{dq}(\theta)}{\partial \theta}\right]\Psi_s = \left[\frac{\partial T_{dq}(\theta)}{\partial \theta}\right] T_{dq}(\theta)\Psi_{dq} = -J_2\Psi_{dq}. \tag{5.3.9}$$

Therefore using (5.3.6) we have

$$\dot{x}_{dq} = \mathcal{T}_x\dot{x} = \mathcal{T}_x\left[(\mathcal{J} - \mathcal{R})\nabla_x\mathcal{H} + gu\right] = \mathcal{T}_x(\mathcal{J} - \mathcal{R})\mathcal{T}_x^\top \nabla_{x_{dq}}\mathcal{H}(x_{dq}) + \mathcal{T}_x g u.$$

Summarizing we have

$$\dot{x}_{dq} = [\bar{\mathcal{J}}(x_{dq}) - \bar{\mathcal{R}}]\nabla_{x_{dq}}\mathcal{H}(x_{dq}) + \bar{g}u \tag{5.3.10}$$

where

$$\hat{\mathcal{J}}(x_{dq}) = \mathcal{T}_x \mathcal{J} \mathcal{T}_x^\top = \begin{bmatrix} 0 & 0 & -J_2\Psi_{dq} & 0 \\ 0 & 0 & 0 & 0 \\ J_2\Psi_{dq} & 0 & 0 & -1 \\ 0 & 0 & 1 & 0 \end{bmatrix}, \tag{5.3.11}$$

and

$$\hat{\mathcal{R}} = \mathcal{T}_x \mathcal{R} \mathcal{T}_x^\top = \text{bdiag}(R_{s\ell}, R_r, d, 0) \quad \hat{g} = \mathcal{T}_x g = g \tag{5.3.12}$$

From (5.3.7) we have $\frac{\partial H(z)}{\partial \theta} = 0$ hence the right hand side of (5.3.10) is independent of θ. Therefore we can decompose the dynamics of the system in to the dynamics of $z = \text{col}(\Psi_d^\top, \Psi_r^\top, p)$ and θ as follows

$$\dot{z} = [\tilde{\mathcal{J}}(z) - \tilde{\mathcal{R}}]\nabla_z \mathcal{H}(z) + \tilde{g}u \tag{5.3.13}$$

$$\dot{\theta} = \frac{p}{J} \tag{5.3.14}$$

where

$$\tilde{\mathcal{J}}(z) := \begin{bmatrix} 0 & 0 & -J_2\Psi_{dq} \\ 0 & 0 & 0 \\ J_2\Psi_{dq} & 0 & 0 \end{bmatrix}, \quad \tilde{\mathcal{R}} := \begin{bmatrix} R_{s\ell} & 0 & 0 \\ 0 & R_r & 0 \\ 0 & 0 & d \end{bmatrix}, \quad \tilde{g} := \begin{bmatrix} 0 & 0 \\ B_r & 0 \\ 0 & 0 \end{bmatrix}. \tag{5.3.15}$$

Consider now the following quotient system after eliminating θ

$$\dot{z} = \left[\tilde{\mathcal{J}}(z) - \tilde{\mathcal{R}}\right] \nabla_z \mathcal{H}(z) + \tilde{g}u. \tag{5.3.16}$$

It can be easily seen that for a given constant input $u = \bar{u}$ the nonlinear system given by (5.3.16), in general, has more than one equilibrium points.

5.3.3 Stability analysis

Now consider the quotient system given by (5.3.16):

$$\dot{z} = \left[\tilde{\mathcal{J}}(z) - \tilde{\mathcal{R}}\right] \nabla_z \mathcal{H}(z) + \tilde{g}\bar{u}. \tag{5.3.17}$$

Note that this should verify the following power balance equation

$$\dot{\mathcal{H}}(z) = -\nabla_z \mathcal{H}(z)^\top \tilde{\mathcal{R}} \nabla_z \mathcal{H}(z) + \bar{u}^\top y \tag{5.3.18}$$

where $\bar{u}^\top y$ is the power externally supplied to the system and the first term on the right-hand side represents the energy dissipation due to the resistive elements in the system. The right hand side of (5.3.18) in general will not be nonpositive. Thus, in most cases, the Hamiltonian function ceases to act as a Lyapunov function for stability studies of a forced equilibrium. By means of energy shaping techniques under some conditions we can construct a Lyapunov function using Hamiltonian and external power supplied. In order to proceed we recall the following theorem from [110].

Theorem 5.3.1. *Consider the system with constant $u = \bar{u}$*

$$\dot{x} = [\mathcal{J}(x) - \mathcal{R}(x)]\nabla_x \mathcal{H}(x) + g(x)\bar{u} \tag{5.3.19}$$

with $\bar{x}$ is an equilibrium and $F := \mathcal{J}(x) - \mathcal{R}(x)$ is invertible. Assume the function $K(x) = -F^{-1}(x)g(x)$

satisfy

$$\frac{\partial K_{ij}}{\partial x_k} = \frac{\partial K_{kj}}{\partial x_i} \qquad \forall\ i,k \in \bar{n}, j \in \bar{m} \tag{5.3.20}$$

where n and m are cardinalities of x and $\bar{u}$, respectively. Then there exists locally smooth functions $C_1, \ldots, C_m$ satisfying

$$K_{ij}(x) = \frac{\partial C_j}{\partial x_i}(x) \qquad \forall i \in \bar{n}\ ,\ \ j \in \bar{m}. \tag{5.3.21}$$

The function $\mathcal{V}$ defined by

$$\mathcal{V}(x) := \mathcal{H}(x) - \Sigma_{j=1}^{m} \bar{u}_j C_j(x)$$

has an extremum at $\bar{x}$, and $\dot{V}(x) \leq 0$. If the function $\mathcal{V}(x)$ also has minimum at $\bar{x}$ then $\mathcal{V}$ qualifies as Lyapunov function. Further if the largest invariant set contained in $\{x \mid \dot{\mathcal{V}}(x) = 0\}$ is equal to $\{\bar{x}\}$ then $\bar{x}$ is locally asymptotically stable.

$\diamondsuit$

We now apply the above theorem to the quotient system (5.3.17). Define $\tilde{F} := \tilde{\mathcal{J}} - \tilde{\mathcal{R}}$, $r_m = r_s + r_\ell$, and assume $\bar{z}$ is an equilibrium of (5.3.17), *i.e.*

$$F(\bar{z})\nabla_z \mathcal{H}(\bar{z}) + \tilde{g}\bar{u} = 0. \tag{5.3.22}$$

As $F(z)$ is assumed to be invertible we have $\nabla_z \mathcal{H}(\bar{z}) + F^{-1}(\bar{z})\tilde{g}\bar{u} = 0$. Define

$$K := -F^{-1}\tilde{g}_1 = \begin{bmatrix} 0 & -\frac{1}{\Psi_d^2+\Psi_q^2+r_m d} J_2 \\ R_r B_r & 0 \\ 0 & \frac{r_m}{\Psi_d^2+\Psi_q^2+r_m d} \end{bmatrix} \in \mathbb{R}^{6\times 2}. \tag{5.3.23}$$

In order to construct a Lyapunov function using power balancing technique as described in [110] we need to express integral $\bar{u}^\top \int_0^t y(\tau)d\tau$ as a function of z_1 for which we need to satisfy following Poincare's condition

$$\frac{\partial K_{ij}}{\partial z_k} = \frac{\partial K_{kj}}{\partial z_i} \qquad \forall\ i,k \in \bar{n}, j \in \bar{m}. \tag{5.3.24}$$

From (5.3.23) we have :

$$\begin{aligned} &\frac{\partial K_{12}}{\partial z_2} = \frac{\partial K_{12}}{\partial \Psi_q} = \frac{-\Psi_d^2 + \Psi_q^2 - r_m d}{(\Psi_d^2 + \Psi_q^2 + r_m d)^2}, && \frac{\partial K_{22}}{\partial z_1} = \frac{\partial K_{12}}{\partial \Psi_s} = \frac{-\Psi_d^2 + \Psi_q^2 + r_m d}{(\Psi_d^2 + \Psi_q^2 + r_m d)^2} \\ &\frac{\partial K_{12}}{\partial z_6} = \frac{\partial K_{12}}{\partial p} = 0, && \frac{\partial K_{62}}{\partial z_1} = \frac{\partial K_{62}}{\partial \Psi_d} = \frac{-2\Psi_d r_m}{(\Psi_d^2 + \Psi_q^2 + r_m d)^2} \end{aligned} \tag{5.3.25}$$

From the above we have $\frac{\partial K_{12}}{\partial z_2} \neq \frac{\partial K_{22}}{\partial z_1}$ and $\frac{\partial K_{12}}{\partial z_7} \neq \frac{\partial K_{72}}{\partial z_1}$ which violates Poincare's condition (5.3.24). When we assume the resistance value $r_m = 0$ then the matrix K given by (5.3.23) does satisfy the Poincare's condition (5.3.24). and we can express $\bar{u}^\top \int_0^t y(\tau)d\tau$ as a function of z_1. With this assumption let

$$\tilde{K} = \begin{bmatrix} 0 & -J_2 \frac{1}{\Psi_d^2+\Psi_q^2} \\ R_r B_r & 0 \\ 0 & 0 \end{bmatrix}. \tag{5.3.26}$$

$$V(z_1) = H(z_1) - \Sigma_{j=1}^{2} \bar{u}_j C_j(z_1) \tag{5.3.27}$$

where Casimirs, C_js, are given by the equations satisfying

$$K_{ij}(z_1) = \frac{\partial C_j}{\partial z_i} \qquad \forall i \in \bar{n_1} \ \& \ j \in \bar{m} \tag{5.3.28}$$

Using (5.3.26), the C_js satisfying (5.3.28) are given by

$$C_1 = \frac{\Psi_f}{R_f}, \qquad C_2 = \tan^{-1}\left(\frac{\Psi_q}{\Psi_d}\right). \tag{5.3.29}$$

Let

$$\mathcal{V}(z) := \mathcal{H}(z) - \left[\frac{E_f \Psi_f}{R_f} + T_m \tan^{-1}\left(\frac{\Psi_q}{\Psi_d}\right)\right]. \tag{5.3.30}$$

From above $\mathcal{V}$ is bounded from below and by construction has extremum at all equilibrium points of the system given by (5.3.17) with $r_m = 0$. Let $\tilde{R}_1 = \{0, R_r, d\}$. We have

$$\begin{aligned}
\dot{\mathcal{V}}(z) &= \nabla_z V(z)\dot{z} = (\nabla_z H() - \tilde{K}\bar{u})^\top (F(z)\nabla_z H(z) + \tilde{g}\bar{u}) \\
&= \nabla_z \mathcal{H}(z)^\top F(z) \nabla_z \mathcal{H}(z) + \nabla_z \mathcal{H}(z)^\top \tilde{g}\bar{u} - (\tilde{K}\bar{u})^\top F(z)\nabla_z \mathcal{H}(z) - (\tilde{K}\bar{u})^\top (\tilde{g}\bar{u}) \\
&= -\nabla_z \mathcal{H}(z)^\top \tilde{R} \nabla_z \mathcal{H}(z) - \frac{E_f^2}{R_f} \leq 0
\end{aligned}$$

for all z. In above we used the facts that $\nabla_z \mathcal{V}(z) = \nabla_z \mathcal{H}(z) - \tilde{K}\bar{u}$, $(\tilde{K}\bar{u})^\top F(z) = g\bar{u}$ and $(K\bar{u})^\top (g\bar{u}) = \frac{E_f^2}{R_f}$. Further, if the largest invariant set contained in $\{z \mid \dot{\mathcal{V}}(z) = 0\}$ is equal to $\{\bar{z}\}$ then $\bar{z}$ is locally asymptotically stable.

Remark 5.3.2. *In the stability analysis we showed that it is necessary to assume $r_m = r_s + r_l = 0$ in order to satisfy Poincare's integrability condition and to apply the energy shaping technique given in [110]. The assumption $r_m = 0$ physically means that there are no losses in the stator winding and the stator terminals are short circuited. We assumed the existence of unique equilibrium for (5.3.17), but in general the system (5.3.17) might admit more than one equilibrium. Obtaining the stability results by lifting these assumptions is the topic of future research.*

Chapter 6

Conclusions

6.1 Summary

In the recent years we have witnessed notable changes in the power systems landscape, which require on one hand to rethink the overall system architecture, and on the other hand to revisit modeling, analysis and control techniques that better account for the high penetration of renewable energy sources. With this work, we aimed to contribute, if modestly, to bridge the gap between theory and applications, providing methods that allow a rigourous analysis of modern power systems architectures, yet preserving their physical characterization. Letting aside the preliminary notions introduced in Chapter 2, main contributions of this work were presented in two self–contained chapters, namely Chapter 3 and Chapter 4, while tangential contributions were provided in Chapter 5. Hence, brief discussions on the obtained results are presented separately.

A first contribution of this work —- developed in Chapter 3 — is thus the formulation of a generalized approach for the modeling of electric power systems. This is based on a suitably defined combination of port–Hamiltonian models of the single components and a graph description of the system topology. The proposed approach have the following unprecedented features: it preserves components identities and full nonlinear dynamics; it reveals explicit information about the energy properties of the system, through the port–Hamiltonian formulation; it allows to treat highly diversified components on an equal footing; it is suitable for *plug & play* operation of the components, which can be described by appropriate modification of the graph and, consequently, of the associated incidence matrix. The first two aspects are particularly relevant. Firstly, they pave the road to a rigourous stability analysis, based on Lyapunov's theory, in which Lyapunov's candidate can be chosen starting from physical motivations. Secondly, they make the model suitable for the construction of reduced models, where the underlying assumptions are well understood and physically justified. Last but not least, it should be noted that the proposed method applies *mutatis mutandi* to the case where the components are described by port (not necessarily Hamiltonian) nonlinear systems. Since port descriptions of most of the components of modern power systems are available in literature (as port–Hamiltonian as well), the proposed approach provides a simple modeling procedure that can be adopted by practitioners with no need of a deep knowledge of the port–Hamiltonian framework. The modeling procedure was applied to multi–terminal hvdc transmission system in Section 4.3, using the port–Hamiltonian framework, and to ac microgrids in Section 5.2, using a port description of the components.

The second part of this work — developed in Chapter 4 — is dedicated to multi–terminal hvdc

transmission systems. Starting from a full port–Hamiltonian model of the overall system, we provided a unified approach for modeling, analysis and control of these systems. After reviewing the traditional control architecture, analysis and design of two fundamental layers of control were carried out, namely for the inner–loop and primary control layers.

For what concern the inner–loop control different results were obtained. First of all, a new, decentralized PI controller, based on passivity arguments (PI–PBC), was presented as an alternative to standard control strategies based on vector control. The proposed controller ensures global asymptotic stability in nominal operating conditions for any positive gain. Unfortunately, there are some drawbacks: stability proof is not valid in perturbed conditions; the controller has clear performance limitations, which are determined by an *extremely* slow zero dynamics. A similar analysis was carried out with respect to the output employed by standard vector control strategies, showing that unappropriate choice of the gains may lead to instability of the controller, as well as of the uncontrolled variables, independently from the operating conditions. Hence a time–consuming and expensive procedure to tune the gains of the controller is required to complete the design. In order to overcome the performance limitations of the PI–PBC, we proposed to add an outer–loop, which, under the assumption of nominal operating condition, was shown to neatly improve time responses while inheriting the same stability properties of the PI–PBC. The mentioned results were validated by simulations. Although it is still unclear how the behavior of the PI–PBC plus outer–loop is affected by perturbed operating conditions (see Subsection 4.7.5 for more details), we believe that it should be considered a serious competitor of the standard vector control for the inner–loop control of hvdc transmission systems.

The problem of primary control was further addressed in this work. A first step towards the definition of this control problem is the construction of an appropriate, physically–motivated, reduced model of the inner–loop controlled hvdc transmission system. Under reasonable time–scale assumptions, a reduced *nonlinear* model was derived, which should be contrasted with the linear models usually adopted in literature. Main novelties in the obtained models are indeed the approximation of inner–loop PQ controlled units with constant power devices (instead of current sources) and the formulation of a generalized class of primary controllers — including the voltage droop control — which can be equivalently described by ZIP models. Finally, the inner–loop controlled system was reduced to a linear capacitive resistive circuit where at each node a constant power device is attached . Moving from this model, we established necessary conditions for the existence of equilibria and the fulfillment of the power sharing property, in terms of feasibility of linear matrix inequalities (LMIs). This allows to establish regions of controller parameters, for which it is impossible to have a constant steady state and an appropriate, pre–specified power distribution. In order to validate the obtained results, such regions were established, via numerical calculations, for a simple four–terminal benchmark.

Two additional contributions are contained in Chapter 5. Firstly, we addressed the problem of construction of a reduced model, suitable for primary control, of an ac microgrid. A full nonlinear model of an inner–loop controlled microgrid, obtained using the approach developed in Chapter 3, was obtained. Then, it was shown that — under reasonable time–scale assumptions — it is possible to recover the standard model employed in literature, which is typically presented without any reference to the reduction procedure, hampering the understanding of the physical phenomena behind it. A second contribution concerns the analysis of an extremely simplified model of an electric power system, that is constituted by a synchronous generator connected to a resistive load, and for which stability results were obtained starting from the port–Hamiltonian model.

6.2 Future works

In the same way that the main contributions to this work were presented in two self-contained chapters, future research guidelines are discussed separately below.

One of the main advantages of describing electric power system using a port–Hamiltonian representation is that information about energy properties of the system is explicitly revealed. A major interest is thus to establish stability properties of the full model of an electric power system, starting from its energy–based description. An application to a trivial power system model was presented in Section 5.3, where energy–based techniques were used to determine conditions for the stability of a synchronous generator connected to a resistive load. Although the presented model is not particularly interesting *per se*, it is the author's belief that it provides an insightful starting point for extending the methodology to more complex power systems. An analysis of a (reduced model) of a synchronous generator attached to an infinite bus is carried out in [115], where the problem of almost global asymptotic stability is analyzed. The proposed model is of particular interest for the analysis since it clearly outlines the problem of stability of a generator under sinusoidal excitations. An extension to generalized power system, based on synchronous generators, is tentatively proposed in [28]. Unfortunately, stability holds only under very strong assumptions, which are rarely verified in practice.

Before starting a discussion on future works and perspectives on multi–terminal hvdc transmission systems we find convenient to make the following considerations. Multi–terminal hvdc transmission systems are a relatively new option in the power systems scenario and there is no broad consensus on the control architecture to be adopted. However, a diffused approach is to mimick the control architecture employed for conventional (ac) power systems, based on synchronous generators. This leads to one of the main bedrock for the control of converter–based electric power systems: the time–scale separation induced by appropriate design of the different layers of control [46, 65, 131]. Roughly speaking, power converters are operated sufficiently fast by an inner–loop control so that a stable behavior is ensured and they can be seen as elementary electrical units from the higher level of control, that is the primary control. If stability and fast reponses are guaranteed, then the problems of inner–loop and primary control can be separated. However, it is rarely questioned whether this time–scale separation is necessary for a correct and safe operation of the system or, this is merely done to simplify the control design. Bearing in mind this preamble, we next discuss possible extensions of the results presented in this work, obviously starting from the lower level of control, that is the inner–loop control.

As already discussed, the behavior of the system controlled via the modified PI–PBC was proved fast and stable in case of nominal operating conditions, via Lyapunov's stability analysis. Hence, a Lyapunov function for the error system is known. Unfortunately, the behavior of the controlled system is still unclear in presence of perturbations. Performed simulations suggest that stability is always preserved, but yet the systems is unable to achieve fast transient responses. This obviously constitutes a serious drawback if we want to induce a time–scale separation by means of the inner–loop control, since responses are not fast enough. On the other hand, we proved that the standard vector controllers are characterized by fast responses independently from the operating conditions, but they may experience instability. Certainly, a question of interest is how to tune the gains of the modified PI–PBC or, eventually, how to modify once again the PI–PBC in order to ensure good performances of the system. Or viceversa, how to tune the gains of the vector controllers to ensure stability [150, 172]. Nevertheless, one

may question whether our interest should be focused on performances and stability of the inner–loop control and not on the problem of inner–loop and primary control as a whole. Moreover, it should be noted that in the case of the modified PI–PBC, a Lyapunov function is known for the error system (in nominal conditions), which is already a good starting point to formulate a modified Lyapunov function for the perturbed error system. A future extension of the modified PI–PBC is thus to determine a further modification of the controller and/or conditions for stability in the case of perturbed conditions. The inclusion of primary control objectives, *i.e.* power sharing and vicinity of the voltage near their nominal value, would be likely the next step.

Putting aside for a moment the discussion on control system architecture, let assume that the standard control design based on time–scale separation is followed, *e.g.* with appropriate tuning of the modified PI–PBC or of the vector controllers. Hence, as shown in Section 4.8, the inner–loop controlled system can be reduced to a linear capacitive resistive circuit where at each node a constant power device is attached. The existence and stability of equilibria for LTI circuit with constant power devices is an open problem in literature [9, 146, 113, 14, 97]. Noting that necessary conditions, in the form of LMIs feasibilities, were derived, it is of particular interest to understand in which measure these are affected by system parameters, among which: free controller parameters, line resistances (and eventually filters) and values of the absorbed and injected constant powers. When (local) stability can be proved, it is also of particular interest to determine an estimation of the region of attraction. Moreover, a possible extension of the proposed model is to account for a distributed primary control design, where exchange of information between different units is allowed [8]. Again, it would be of interest to verify how this design would affect conditions on existence of equilibria and power sharing. Further open challenges regard sufficiency of the conditions and inclusion of additional conditions for the vicinity of the voltages near the nominal value. It is also interesting to note that the same theory used to determine necessary conditions for existence of equilibria in hvdc systems has an equivalent characterization in ac circuits. Then, a further possibility is to investigate the problem of existence of equilibria in the case of ac grids.

Bibliography

[1] Ieee guide for planning dc links terminating at ac locations having low short-circuit capacities. *IEEE Std 1204-1997*, pages i–, 1997. 49

[2] A.M. Abbas and P.W. Lehn. PWM based VSC-HVDC systems – a review. In *Power Energy Society General Meeting, 2009. PES '09. IEEE*, pages 1–9, July 2009. 47, 48, 52

[3] Thomas Ackermann, Göran Andersson, and Lennart Söder. Distributed generation: a definition. *Electric power systems research*, 57(3):195–204, 2001. 90

[4] N. Ainsworth and S. Grijalva. A structure-preserving model and sufficient condition for frequency synchronization of lossless droop inverter-based AC networks. *IEEE Transactions on Power Systems*, 28(4):4310–4319, Nov 2013. 101, 104, 105

[5] H. Akagi. *Instantaneous Power Theory and Applications to Power Conditioning*. Wiley, Newark, 2007. 46, 64

[6] H. Akagi, E.H. Watanabe, and M. Aredes. *Instantaneous Power Theory and Applications to Power Conditioning*. IEEE Press Series on Power Engineering. Wiley, 2007. 29

[7] P.M. Anderson and A.A. Fouad. *Power system control and stability*. J.Wiley & Sons, 2002. 1, 8, 26, 32, 38, 57, 80, 90, 92, 101, 104, 105

[8] M. Andreasson, M. Nazari, D. V. Dimarogonas, H. Sandberg, K. H. Johansson, and M. Ghandhari. Distributed Voltage and Current Control of Multi-Terminal High-Voltage Direct Current Transmission Systems. *ArXiv e-prints*, November 2013. 46, 58, 80, 81, 84, 116

[9] N. Barabanov, R. Ortega, R. Grino, and B. Polyak. On existence and stability of equilibria of linear time-invariant systems with constant power loads. *Circuits and Systems I: Regular Papers, IEEE Transactions on*, PP(99):1–8, 2015. 46, 81, 116

[10] M. Barnes, J. Kondoh, H. Asano, J. Oyarzabal, G. Ventakaramanan, R. Lasseter, N. Hatziargyriou, and T. Green. Real-world microgrids-an overview. In *IEEE Int. Conf. on System of Systems Engineering, 2007. SoSE '07*, pages 1 –8, april 2007. 92

[11] C. Batlle and A. Dòria-Cerezo. Bond graph models of electromechanical systems. the ac generator case. In *Industrial Electronics, 2008. ISIE 2008. IEEE International Symposium on*, pages 1064–1069, June 2008. 36

[12] Carles Batlle, Arnau Dòria-Cerezo, and Romeo Ortega. Power flow control of a doubly-fed induction machine coupled to a flywheel. *European Journal of Control*, 11(3):209–221, 2005. 36

[13] Jef Beerten and Ronnie Belmans. Analysis of power sharing and voltage deviations in droop-controlled dc grids. *IEEE Transactions on Power Systems*, 28(4):4588 – 4597, 2013. 58, 80, 84

[14] M. Belkhayat, R. Cooley, and A. Witulski. Large signal stability criteria for distributed systems with constant power loads. In *Power Electronics Specialists Conference, 1995. PESC '95 Record., 26th Annual IEEE*, volume 2, pages 1333–1338 vol.2, Jun 1995. 46, 81, 116

[15] A. Benchaib. *Advanced Control of AC / DC Power Networks: System of Systems Approach Based on Spatio-temporal Scales*. Wiley, 2015. 57, 61

[16] A.R. Bergen and D.J. Hill. A structure preserving model for power system stability analysis. *IEEE Transactions on Power Apparatus and Systems*, PAS-100(1):25 –35, jan. 1981. 31

[17] R.E. Best. *Phase-Locked Loops*. Professional Engineering. Mcgraw-hill, 2003. 53

[18] F.D. Bianchi and O. Gomis-Bellmunt. Droop control design for multi-terminal vsc-hvdc grids based on lmi optimization. In *Decision and Control and European Control Conference (CDC-ECC), 2011 50th IEEE Conference on*, pages 4823–4828, Dec 2011. 58

[19] Frede Blaabjerg, Remus Teodorescu, Marco Liserre, and Adrian V Timbus. Overview of control and grid synchronization for distributed power generation systems. *IEEE Transactions on Industrial Electronics*, 53(5):1398–1409, 2006. 95

[20] V. Blasko and V. Kaura. A new mathematical model and control of a three-phase ac-dc voltage source converter. *Power Electronics, IEEE Transactions on*, 12(1):116–123, Jan 1997. 53, 61

[21] Bela Bollobas. *Modern Graph Theory*. Springer, 1998. 15

[22] S. Bolognani and S. Zampieri. A distributed control strategy for reactive power compensation in smart microgrids. *IEEE Transactions on Automatic Control*, 58(11):2818–2833, Nov 2013. 95

[23] Bimal K Bose. Global warming: Energy, environmental pollution, and the impact of power electronics. *Industrial Electronics Magazine, IEEE*, 4(1):6–17, 2010. 1, 7

[24] Hedi Bouattour, John W. Simpson-Porco, Florian Dörfler, and Francesco Bullo. Further results on distributed secondary control in microgrids. In *52nd Conference on Decision and Control*, pages 1514–1519, Dec 2013. 105

[25] Clare Breidenich, Daniel Magraw, Anne Rowley, and James W Rubin. The kyoto protocol to the united nations framework convention on climate change. *American Journal of International Law*, pages 315–331, 1998. 1, 8

[26] M.K. Bucher, R. Wiget, G. Andersson, and C.M. Franck. Multiterminal HVDC Networks – what is the preferred topology? *Power Delivery, IEEE Transactions on*, 29(1):406–413, Feb 2014. 49

[27] C.I. Byrnes, A. Isidori, and J.C. Willems. Passivity, feedback equivalence, and the global stabilization of minimum phase nonlinear systems. *Automatic Control, IEEE Transactions on*, 36(11):1228–1240, Nov 1991. 21, 22, 23, 46, 63

[28] S.Y. Caliskan and P. Tabuada. Compositional transient stability analysis of multimachine power networks. *IEEE Transactions on Control of Network Systems*, 1(1):4–14, March 2014. 115

[29] J.M. Carrasco, L.G. Franquelo, J.T. Bialasiewicz, E. Galvan, R.C.P. Guisado, Ma.A.M. Prats, J.I. Leon, and N. Moreno-Alfonso. Power-electronic systems for the grid integration of renewable energy sources: A survey. *Industrial Electronics, IEEE Transactions on*, 53(4):1002–1016, June 2006. 45

[30] Juan Manuel Carrasco, Leopoldo Garcia Franquelo, Jan T Bialasiewicz, Eduardo Galván, Ramón C Portillo Guisado, Ma Ángeles Martín Prats, José Ignacio León, and Narciso Moreno-Alfonso. Power-electronic systems for the grid integration of renewable energy sources: A survey. *IEEE Transactions on Industrial Electronics*, 53(4):1002–1016, 2006. 95

[31] S. Chatzivasileiadis, D. Ernst, and G. Andersson. The global grid. *CoRR*, abs/1207.4096, 2012. 2, 8, 45, 47

[32] H. Chen, Z. Xu, and F. Zhang. Nonlinear control for VSC based HVDC system. In *Power Engineering Society General Meeting, 2006. IEEE*, pages 5 pp.–, 2006. 61

[33] Y. Chen, J. Dai, G. Damm, and F. Lamnabhi-Lagarrigue. Nonlinear control design for a multi-terminal VSC-HVDC system. In *Control Conference (ECC), 2013 European*, pages 3536–3541, July 2013. 61

[34] S. Chiniforoosh, J. Jatskevich, A. Yazdani, V. Sood, V. Dinavahi, J.A. Martinez, and A. Ramirez. Definitions and applications of dynamic average models for analysis of power systems. *IEEE Transactions on Power Delivery*, 25(4):2655–2669, Oct 2010. 97

[35] Sunetra Chowdhury and Peter Crossley. *Microgrids and active distribution networks*. The Institution of Engineering and Technology, 2009. 90, 91

[36] E.A.A. Coelho, P.C. Cortizo, and P.F.D. Garcia. Small-signal stability for parallel-connected inverters in stand-alone AC supply systems. *IEEE Transactions on Industry Applications*, 38(2):533 –542, 2002. 90, 101, 102

[37] S. Cole and R. Belmans. A proposal for standard {VSC} {HVDC} dynamic models in power system stability studies. *Electric Power Systems Research*, 81(4):967 – 973, 2011. 49, 51

[38] Communication from the commission. Europe 2020 - a european strategy for smart, sustainable and inclusive growth (COM(2010) 2020). European Commission, 2010. 1, 8

[39] W. Dib, R. Ortega, A. Barabanov, and F. Lamnabhi-Lagarrigue. A globally convergent controller for multi-machine power systems using structure-preserving models. *IEEE Transactions on Automatic Control*, 54(9):2179 –2185, sept. 2009. 31

[40] R.C. Dorf. *The Electrical Engineering Handbook,Second Edition*. Electrical Engineering Handbook. Taylor & Francis, 1997. 25

[41] F. Dörfler and F. Bullo. Synchronization and transient stability in power networks and non-uniform Kuramoto oscillators. In *American Control Conference*, pages 930 –937, 30 2010-july 2 2010. 31

[42] F. Dorfler and F. Bullo. Kron reduction of graphs with applications to electrical networks. 60(1):150–163, 2013. 34, 50

[43] V. Duindam and al. *Modeling and control of complex physical systems: The port-Hamiltonian approach*. Springer-Verlag, Berlin, 2009. 16, 24, 35, 36, 38

[44] V. Duindam and al. *Modeling and control of complex physical systems: The port-hamiltonian approach*. Springer-Verlag, Berlin, 2009. 106

[45] A. Egea-Alvarez, J. Beerten, D. Van Hertem, and O. Gomis-Bellmunt. Primary and secondary power control of multiterminal hvdc grids. In *AC and DC Power Transmission (ACDC 2012), 10th IET International Conference on*, pages 1–6, Dec 2012. 58, 59

[46] Agustí Egea-Alvarez, Jef Beerten, Dirk Van Hertem, and Oriol Gomis-Bellmunt. Hierarchical power control of multiterminal HVDC grids. *Electric Power Systems Research*, 121:207 – 215, 2015. 57, 58, 59, 115

[47] Sustainable Energy. Choosing among options. *JW Tester*, 2005. 1, 7

[48] Robert W Erickson and Dragan Maksimovic. *Fundamentals of power electronics*. Springer, 2001. 60, 94, 97

[49] G. Escobar, A.J. Van Der Schaft, and R. Ortega. A Hamiltonian viewpoint in the modeling of switching power converters. *Automatica*, 35(3):445–452, March 1999. 36, 45, 54

[50] H. Farhangi. The path of the smart grid. *Power and Energy Magazine, IEEE*, 8(1):18–28, January 2010. 32, 45

[51] H. Farhangi. The path of the smart grid. *IEEE Power and Energy Magazine*, 8(1):18 –28, january-february 2010. 90

[52] S. Fiaz, D. Zonetti, R. Ortega, J.M.A. Scherpen, and A.J. van der Schaft. On port-hamiltonian modeling of the synchronous generator and ultimate boundedness of its solutions. In *4th IFAC Workshop on Lagrangian and Hamiltonian Methods for Non Linear Control Bertinoro, Italy*, August 2102. 12, 36, 89

[53] S Fiaz, D Zonetti, Romeo Ortega, JMA Scherpen, and AJ van der Schaft. A port-hamiltonian approach to power network modeling and analysis. *European Journal of Control*, 19(6):477–485, 2013. 12, 36, 38, 89

[54] N. Flourentzou, V.G. Agelidis, and G.D. Demetriades. VSC-based HVDC power transmission systems: An overview. *Power Electronics, IEEE Transactions on*, 24(3):592–602, Mar 2009. 47, 48, 49

[55] B.A. Francis and G. Zames. On H^{∞}-optimal sensitivity theory for siso feedback systems. *Automatic Control, IEEE Transactions on*, 29(1):9–16, Jan 1984. 65

[56] Shoji Fukuda and Takehito Yoda. A novel current-tracking method for active filters based on a sinusoidal internal model [for pwm invertors]. *IEEE Transactions on Industry Applications*, 37(3):888–895, 2001. 95

[57] C.W. Gellings. A globe spanning super grid. *Spectrum, IEEE*, 52(8):48–54, August 2015. 2, 8, 45, 47

[58] A. Giusto. *On some dynamics properties of electrical power systems*. PhD thesis, Universidad de la República, 2010. 106

[59] J Duncan Glover, Mulukutla S Sarma, and Thomas J Overbye. *Power system analysis and design*. Cengage Learning, 2011. 91, 92, 101, 104

[60] Chris Godsil and Gordon Royle. *Algebraic graph theory*, volume 207 of *Graduate Texts in Mathematics*. Springer-Verlag, New York, 2001. 15

[61] O. Gomis-Bellmunt, J. Liang, J. Ekanayake, R. King, and N. Jenkins. Topologies of multiterminal HVDC-VSC transmission for large offshore wind farms. *Electric Power Systems Research*, 81(2):271 – 281, 2011. 45, 47, 49

[62] John J Grainger and William D Stevenson. *Power system analysis*, volume 621. McGraw-Hill New York, 1994. 101

[63] T.C. Green and M. Prodanovic. Control of inverter-based micro-grids. *Electric Power Systems Research*, Vol. 77(9):1204–1213, july 2007. 2, 8, 90, 91, 92, 97, 101

[64] J Guerrero, P Loh, Mukul Chandorkar, and T Lee. Advanced control architectures for intelligent microgrids – part I: Decentralized and hierarchical control. *IEEE Transactions on Industrial Electronics*, 60(4):1254–1262, 2013. 97

[65] J.M. Guerrero, J.C. Vasquez, J. Matas, L.G. de Vicuña, and M. Castilla. Hierarchical control of droop-controlled ac and dc microgrids — a general approach toward standardization. *Industrial Electronics, IEEE Transactions on*, 58(1):158–172, Jan 2011. 46, 57, 58, 115

[66] J.M. Guerrero, J.C. Vasquez, J. Matas, L.G. de Vicuna, and M. Castilla. Hierarchical control of droop-controlled AC and DC microgrids; a general approach toward standardization. *IEEE Transactions on Industrial Electronics*, 58(1):158 –172, jan. 2011. 97

[67] Yi Guo and Wolfgang Gawlik. A survey of control strategies applied in worldwide microgrid projects. *Tagungsband ComForEn 2014*, page 47. 92

[68] Temesgen Mulugeta Haileselassie. Control, dynamics and operation of multi-terminal vsc-hvdc transmission systems. 2012. 62

[69] T.M. Haileselassie and K. Uhlen. Impact of dc line voltage drops on power flow of mtdc using droop control. *Power Systems, IEEE Transactions on*, 27(3):1441–1449, Aug 2012. 58, 74, 79

[70] T.M. Haileselassie, T. Undeland, and K. Uhlen. Multiterminal HVDC for offshore windfarms – control strategy. European Power Electronics and Drives Association, 2009. 46

[71] D.J. Hammerstrom. AC versus DC distribution systems — did we get it right? In *Power Engineering Society General Meeting, 2007. IEEE*, pages 1–5, June 2007. 45

[72] C. A. Hans, V. Nenchev, J Raisch, and C. Reincke-Collon. Minimax model predictive operation control of microgrids. To appear at 19th IFAC World Congress, Cape Town, South Africa, 2014. 95

[73] Jin Hao, Chen Chen, Libao Shi, and Jie Wang. Nonlinear decentralized disturbance attenuation excitation control for power systems with nonlinear loads based on the hamiltonian theory. *Energy Conversion, IEEE Transactions on*, 22(2):316–324, June 2007. 31

[74] N. Hatziargyriou, H. Asano, R. Iravani, and C. Marnay. Microgrids. *IEEE Power and Energy Magazine*, 5(4):78–94, 2007. 90, 91, 92

[75] Michiel Hazewinkel. *Encyclopaedia of Mathematics (9)*, volume 9. Springer, 1993. 104

[76] M. Hernandez-Gomez, R. Ortega, F. Lamnabhi-Lagarrigue, and G. Escobar. Adaptive PI stabilization of switched power converters. *Control Systems Technology, IEEE Transactions on*, 18(3):688–698, 2010. 45, 46, 62, 63, 64

[77] I.A. Hiskens and D.J. Hill. Energy functions, transient stability and voltage behaviour in power systems with nonlinear loads. *Power Systems, IEEE Transactions on*, 4(4):1525–1533, Nov 1989. 31

[78] D Grahame Holmes and Thomas A Lipo. *Pulse width modulation for power converters: principles and practice*, volume 18. John Wiley & Sons, 2003. 52

[79] T. Hornik and Q. Zhong. A current-control strategy for voltage-source inverters in microgrids based on and repetitive control. *IEEE Transactions on Power Electronics*, 26(3):943–952, 2011. 95

[80] A.Q. Huang, M.L. Crow, G.T. Heydt, J.P. Zheng, and S.J. Dale. The future renewable electric energy delivery and management (freedm) system: The energy internet. *Proceedings of the IEEE*, 99(1):133–148, Jan 2011. 45

[81] International Energy Agency. Topics: Renewables. http://www.iea.org/topics/renewables/, retrieved 04.05.2014. 1, 7

[82] A. Isidori. *Nonlinear Control Systems*. Springer-Verlag New York, Inc., Secaucus, NJ, USA, 3rd edition, 1995. 21, 22, 62

[83] A. Jager-Waldau. Photovoltaics and renewable energies in europe. *Renewable and Sustainable Energy Reviews*, 11(7):1414 – 1437, 2007. 45

[84] B. Jayawardhana, R. Ortega, E. Garcia-Canseco, and F. F. Castaños. Passivity of nonlinear incremental systems: Application to PI stabilization of nonlinear RLC circuits. In *Decision and Control, 2006 45th IEEE Conference on*, pages 3808–3812, 2006. 46, 62

[85] D. Jeltsema and J.M.A. Scherpen. Multidomain modeling of nonlinear networks and systems. *Control Systems, IEEE*, 29(4):28–59, Aug 2009. 24

[86] Hongbo Jiang and Ake Ekstrom. Multiterminal hvdc systems in urban areas of large cities. *Power Delivery, IEEE Transactions on*, 13(4):1278–1284, 1998. 45, 47

[87] Jackson John Justo, Francis Mwasilu, Ju Lee, and Jin-Woo Jung. Ac-microgrids versus dc-microgrids with distributed energy resources: A review. *Renewable and Sustainable Energy Reviews*, 24:387–405, 2013. 45

[88] F. Katiraei and M.R. Iravani. Power management strategies for a microgrid with multiple distributed generation units. *IEEE Transactions on Power Systems*, 21(4):1821 –1831, nov. 2006. 90

[89] Farid Katiraei, Reza Iravani, Nikos Hatziargyriou, and Aris Dimeas. Microgrids management. *IEEE Power and Energy Magazine*, 6(3):54–65, 2008. 90, 91, 94, 95, 101

[90] M.P. Kazmierkowski, R. Krishnan, F. Blaabjerg, and J.D. Irwin. *Control in Power Electronics: Selected Problems*. Academic Press Series in Engineering. Elsevier Science, 2002. 45, 57, 58, 60, 66

[91] Hassan K Khalil. *Nonlinear systems*, volume 3. Prentice Hall, 2002. 101

[92] H.K. Khalil. *Nonlinear Systems*. Pearson Education. Prentice Hall, 2002. 19, 77

[93] C.K. Kim, V.K. Sood, G.S. Jang, S.J. Lim, and S.J. Lee. *HVDC Transmission: Power Conversion Applications in Power Systems*. Wiley, 2009. 49

[94] NM Kirby, MJ Luckett, L Xu, and Werner Siepmann. HVDC transmission for large offshore windfarms. In *AC-DC Power Transmission, 2001. Seventh International Conference on (Conf. Publ. No. 485)*, pages 162–168. IET, 2001. 49

[95] Petar Kokotovic, Hassan K Khali, and John O'reilly. *Singular perturbation methods in control: analysis and design*, volume 25. Siam, 1999. 101

[96] P. Kundur. *Power system stability and control*. McGraw-Hill, 1994. 1, 8, 26, 32, 33, 37, 45, 49, 57, 90, 92, 98, 101, 106, 107

[97] Alexis Kwasinski and Chimaobi N Onwuchekwa. Dynamic behavior and stabilization of DC microgrids with instantaneous constant-power loads. *IEEE Transactions on Power Electronics*, 26(3):822–834, 2011. 46, 81, 116

[98] R.H. Lasseter. Microgrids. In *IEEE Power Engineering Society Winter Meeting, 2002*, volume 1, pages 305 – 308 vol.1, 2002. 2, 8, 90, 91

[99] Robert H Lasseter. Smart distribution: Coupled microgrids. *Proceedings of the IEEE*, 99(6):1074–1082, 2011. 90

[100] T. Lee. Input-output linearization and zero-dynamics control of three-phase AC/DC voltage-source converters. *Power Electronics, IEEE Transactions on*, 18(1):11–22, Jan 2003. 61

[101] Guangkai Li, Guopeng Ma, Chengyong Zhao, and Gengyin Li. Research of nonlinear control strategy for vsc-hvdc system based on lyapunov stability theory. In *Electric Utility Deregulation and Restructuring and Power Technologies, 2008. DRPT 2008. Third International Conference on*, pages 2187–2191, April 2008. 61

[102] Haifeng Liang, Gengyin Li, Guangkai Li, Peng Li, and Ming Yin. Analysis and design of H_∞ controller in vsc hvdc systems. In *Transmission and Distribution Conference and Exhibition: Asia and Pacific, 2005 IEEE/PES*, pages 1–6, Aug 2005. 61

[103] NWA Lidula and AD Rajapakse. Microgrids research: A review of experimental microgrids and test systems. *Renewable and Sustainable Energy Reviews*, 15(1):186–202, 2011. 91, 92

[104] Poh Chiang Loh and Donald Grahame Holmes. Analysis of multiloop control strategies for LC/CL/LCL-filtered voltage-source and current-source inverters. *IEEE Transactions on Industry Applications*, 41(2):644–654, 2005. 95

[105] J.A.P. Lopes, C.L. Moreira, and A.G. Madureira. Defining control strategies for microgrids islanded operation. *IEEE Transactions on Power Systems*, 21(2):916 – 924, may 2006. 94, 95, 97, 101

[106] J. Machowski, J.W. Bialek, and J.R Bumby. *Power system dynamics: stability and control*. J.Wiley & Sons, 2008. 90, 92, 101

[107] David MacKay. *Sustainable Energy-without the hot air*. UIT Cambridge, 2008. 1, 7

[108] N. Manjarekar, R. Banavar, and Roméo Ortega. Application of interconnection and damping assignment to the stabilization of a synchronous generator with a controllable series capacitor. *International journal of electrical Power & Energy Systems*, 32:63–70, 2010. 38

[109] G. Martinelli and M. Salerno. *Fondamenti di elettrotecnica I – Circuiti lineari e permanent*. Siderea, 1995. 16, 24, 25, 27, 28

[110] B. Maschke, R. Ortega, and A.J. Van der Schaft. Energy-based lyapunov functions for forced hamiltonian systems with dissipation. *Automatic Control, IEEE Transactions on*, 45(8):1498–1502, Aug 2000. 109, 110, 111

[111] Y. Mohamed and E.F. El-Saadany. Adaptive decentralized droop controller to preserve power sharing stability of paralleled inverters in distributed generation microgrids. *IEEE Transactions on Power Electronics*, 23(6):2806 –2816, nov. 2008. 90, 95, 97, 101, 102

[112] Ned Mohan and Tore M Undeland. *Power electronics: converters, applications, and design*. John Wiley & Sons, 2007. 60, 66, 94

[113] Nima Monshizadeh, Claudio De Persis, Arjan J van der Schaft, and Jacquelien Scherpen. A networked reduced model for electrical networks with constant power loads. *arXiv preprint arXiv:1512.08250*, 2015. 116

[114] Ulrich Münz and Michael Metzger. Voltage and angle stability reserve of power systems with renewable generation. In *19th IFAC World Congress*, pages 9075–9080, Cape Town, South Africa, 2014. 101, 104, 105

[115] Vivek Natarajan and George Weiss. A method for proving the global stability of a synchronous generator connected to an infinite bus. In *Electrical & Electronics Engineers in Israel (IEEEI), 2014 IEEE 28th Convention of*, pages 1–5. IEEE, 2014. 115

[116] M. Nazari, M. Baradar, M.R. Hesamzadeh, and M. Ghandhari. On-line control of multi-terminal hvdc systems connected to offshore wind farms using the opf-based multi-agent approarch. In *PowerTech, 2015 IEEE Eindhoven*, pages 1–6, June 2015. 58, 60

[117] Henk Nijmeijer and Arjan van der Schaft. *Nonlinear Dynamical Control Systems*. Springer-Verlag New York, Inc., New York, NY, USA, 1990. 22

[118] R.H. Park. Two-reaction theory of synchronous machines generalized method of analysis-part i. *American Institute of Electrical Engineers, Transactions of the*, 48(3):716–727, July 1929. 25

[119] M. Perez, R. Ortega, and J.R. Espinoza. Passivity-based PI control of switched power converters. *Control Systems Technology, IEEE Transactions on*, 12(6):881–890, 2004. 54, 62

[120] R.T. Pinto, S.F. Rodrigues, P. Bauer, and J. Pierik. Comparison of direct voltage control methods of multi-terminal dc (MTDC) networks through modular dynamic models. In *Power Electronics and Applications (EPE 2011), Proceedings of the 2011-14th European Conference on*, pages 1–10, Aug 2011. 58, 61

[121] Estefanía Planas, Asier Gil-de Muro, Jon Andreu, Iñigo Kortabarria, and Iñigo Martínez de Alegría. General aspects, hierarchical controls and droop methods in microgrids: A review. *Renewable and Sustainable Energy Reviews*, 17:147–159, 2013. 92

[122] N. Pogaku, M. Prodanovic, and T.C. Green. Modeling, analysis and testing of autonomous operation of an inverter-based microgrid. *IEEE Transactions on Power Electronics*, 22(2):613 –625, march 2007. 90, 91, 95, 97, 101, 102

[123] E. Prieto-Araujo, F.D. Bianchi, A. Junyent-Ferré, and O. Gomis-Bellmunt. Methodology for droop control dynamic analysis of multiterminal vsc-hvdc grids for offshore wind farms. *Power Delivery, IEEE Transactions on*, 26(4):2476–2485, Oct 2011. 46, 58, 79

[124] Milan Prodanovic and Timothy C Green. Control and filter design of three-phase inverters for high power quality grid connection. *IEEE Transactions on Power Electronics*, 18(1):373–380, 2003. 95

[125] L. Qiu and E. J. Davison. Performance limitations of non-minimum phase systems in the servomechanism problem. pages 337–349, 1993. 65

[126] H.S. Ramadan, H. Siguerdidjane, and M. Petit. A robust stabilizing nonlinear control design for vsc-hvdc systems: A comparative study. In *Industrial Technology, 2009. ICIT 2009. IEEE International Conference on*, pages 1–6, Feb 2009. 61

[127] Joan Rocabert, Alvaro Luna, Frede Blaabjerg, and Pedro Rodriguez. Control of power converters in AC microgrids. *IEEE Transactions on Power Electronics*, 27(11):4734–4749, Nov 2012. 94, 95, 96, 98

[128] Daniel Salomonsson. *Modeling, Control and Protection of Low-Voltage DC Microgrids.* PhD thesis, KTH, Electric Power Systems, 2008. 45

[129] S. Sanchez, R. Ortega, R. Gri no, G. Bergna, and M. Molinas-Cabrera. Conditions for existence of equilibrium points of systems with constant power loads. In *Decision and Control, 2013 52nd IEEE Conference on, Firenze, Italy*, 2013. 59, 60, 81

[130] S.R. Sanders and G.C. Verghese. Lyapunov-based control for switched power converters. *Power Electronics, IEEE Transactions on*, 7(1):17–24, Jan 1992. 45, 46

[131] P.W. Sauer. Time-scale features and their applications in electric power system dynamic modeling and analysis. In *American Control Conference (ACC), 2011*, pages 4155–4159, June 2011. 45, 80, 115

[132] P.W. Sauer and M.A. Pai. *Power system dynamics and stability.* Prentice Hall, 1998. 101

[133] Frank Schettler, Hartmut Huang, and Norbert Christl. Hvdc transmission systems using voltage sourced converters design and applications. In *Power Engineering Society Summer Meeting, 2000. IEEE*, volume 2, pages 715–720. IEEE, 2000. 49

[134] Johannes Schiffer, Adolfo Anta, Truong Duc Trung, Jörg Raisch, and Tevfik Sezi. On power sharing and stability in autonomous inverter-based microgrids. In *51st Conference on Decision and Control*, pages 1105–1110, Maui, HI, USA, 2012. 101, 102

[135] Johannes Schiffer, Darina Goldin, Jörg Raisch, and Tevfik Sezi. Synchronization of droop-controlled microgrids with distributed rotational and electronic generation. In *52nd Conference on Decision and Control*, pages 2334–2339, Florence, Italy, 2013. 105

[136] Johannes Schiffer, Romeo Ortega, Alessandro Astolfi, Jörg Raisch, and Tevfik Sezi. Conditions for stability of droop-controlled inverter-based microgrids. *Automatica*, 50(10):2457–2469, 2014. 101, 102, 104, 105

[137] Johannes Schiffer, Romeo Ortega, Christian Hans, and Jörg Raisch. Droop-controlled inverter-based microgrids are robust to clock drifts. *American Control Conference*, 2015. To appear. 97

[138] Johannes Schiffer, Thomas Seel, Jörg Raisch, and Tevfik Sezi. A consensus-based distributed voltage control for reactive power sharing in microgrids. In *13th European Control Conference*, pages 1299–1305, Strasbourg, France, 2014. 105

[139] Johannes Schiffer, Thomas Seel, Jörg Raisch, and Tevfik Sezi. Voltage stability and reactive power sharing in inverter-based microgrids with consensus-based distributed voltage control. *IEEE Transactions on Control Systems Technology*, 2014. Submitted. 105

[140] Johannes Schiffer, Daniele Zonetti, Romeo Ortega, Aleksandar M. Stankovic, Tevfik Sezi, and Jörg Raisch. Modeling of microgrids - from fundamental physics to phasors and voltage sources. *CoRR*, abs/1505.00136, 2015. 2, 8, 12, 25, 29, 77, 89

[141] M.M. Seron, J.H. Braslavsky, and G.C. Goodwin. *Fundamental Limitations in Filtering and Control*. Springer Publishing Company, Incorporated, 1st edition, 2011. 65

[142] S. Shah, R. Hassan, and J. Sun. HVDC transmission system architectures and control - a review. In *Control and Modeling for Power Electronics (COMPEL), 2013 IEEE 14th Workshop on*, pages 1–8, June 2013. 46, 58, 74, 79

[143] D. Shuai and X. Zhang. Input-output linearization and stabilization analysis of internal dynamics of three-phase AC/DC voltage-source converters. In *Electrical Machines and Systems (ICEMS), 2010 International Conference on*, pages 329–333, Oct 2010. 61

[144] J. W. Simpson-Porco, F. Dörfler, and F. Bullo. Synchronization and power sharing for droop-controlled inverters in islanded microgrids. *Automatica*, 49(9):2603 – 2611, 2013. 91, 101, 104, 105

[145] J. W. Simpson-Porco, F. Dörfler, and F. Bullo. Voltage stabilization in microgrids using quadratic droop control. In *52nd Conference on Decision and Control*, pages 7582–7589, Florence, Italy, 2013. 101, 105

[146] John W Simpson-Porco, Florian Dorfler, and Francesco Bullo. On resistive networks of constant-power devices. *Circuits and Systems II: Express Briefs, IEEE Transactions on*, 62(8):811–815, 2015. 116

[147] J.J.E. Slotine and W. Li. *Applied Nonlinear Control*. Prentice Hall, 1991. 19

[148] Cole Stijn. *Steady-state and dynamic modelling of VSC HVDC systems for power system Simulation*. PhD thesis, PhD dissertation, Katholieke University Leuven, Belgium, 2010. 58, 61

[149] Goran Strbac, Nikos Hatziargyriou, Joao Pecas Lopes, Carlos Moreira, Aris Dimeas, and Dimitrios Papadaskalopoulos. Microgrids: Enhancing the resilience of the European megagrid. *IEEE Power and Energy Magazine*, 13(3):35–43, 2015. 90, 91

[150] Jon Are Suul, Marta Molinas, Lars Norum, and Tore Undeland. Tuning of control loops for grid connected voltage source converters. In *Power and Energy Conference, 2008. PECon 2008. IEEE 2nd International*, pages 797–802. IEEE, 2008. 61, 72, 115

[151] Joshua Adam Taylor, Sairaj V. Dhople, and Duncan S. Callaway. Power systems without fuel. *CoRR*, abs/1506.04799, 2015. 2, 7, 9, 32, 45

[152] Rodrigo Teixeira Pinto. *Multi-Terminal DC Networks System Integration, Dynamics and Control*. PhD thesis, Delft University of Technology, 2014. 45, 47, 48, 49, 57, 58, 61

[153] Remus Teodorescu, Frede Blaabjerg, Marco Liserre, and P Chiang Loh. Proportional-resonant controllers and filters for grid-connected voltage-source converters. *IEE Proceedings-Electric Power Applications*, 153(5):750–762, 2006. 95

[154] Remus Teodorescu, Marco Liserre, and Pedro Rodriguez. *Grid converters for photovoltaic and wind power systems*, volume 29. John Wiley & Sons, 2011. 89, 90, 92, 95

[155] J.-L. Thomas, S. Poullain, and A. Benchaib. Analysis of a robust DC-bus voltage control system for a VSC transmission scheme. In *AC-DC Power Transmission, 2001. Seventh International Conference on (Conf. Publ. No. 485)*, pages 119–124, Nov 2001. 52, 61

[156] M.A. Torres. Estudio de un sistema VSC-HVDC y aplicación de método de control basado en pasividad. Master's thesis, Universidad de Concepción, Chile, March 2007. 51, 52

[157] N. Tsolas, A. Arapostathis, and P.P. Varaiya. A structure preserving energy function for power system transient stability analysis. *IEEE Transactions on Circuits and Systems*, 32(10):1041–1049, Oct 1985. 31

[158] Thierry Van Cutsem and Costas Vournas. *Voltage stability of electric power systems*, volume 441. Springer, 1998. 98, 101

[159] A.J. van der Schaft. *$\mathcal{L}_2$-gain and passivity techniques in nonlinear control*. Communications and control engineering. Springer, Berlin, 2000. 16, 22, 23, 46, 63

[160] Arjan van der Schaft. Characterization and partial synthesis of the behavior of resistive circuits at their terminals. *Systems & Control Letters*, 59(7):423 – 428, 2010. 34, 43, 50, 92

[161] Arjan van der Schaft and Dimitri Jeltsema. Port-hamiltonian systems theory: An introductory overview. *Foundations and Trends® in Systems and Control*, 1(2-3):173–378, 2014. 16

[162] Pravin Varaiya, Felix Fulih Wu, and Rong-Liang Chen. Direct methods for transient stability analysis of power systems: Recent results. *Proceedings of the IEEE*, 73(12):1703–1715, 1985. 31

[163] Pravin P Varaiya, Felix F Wu, and Janusz W Bialek. Smart operation of smart grid: Risk-limiting dispatch. *Proceedings of the IEEE*, 99(1):40–57, 2011. 90

[164] Til Kristian Vrana, Jef Beerten, Ronnie Belmans, and Olav Bjarte Fosso. A classification of {DC} node voltage control methods for {HVDC} grids. *Electric Power Systems Research*, 103:137 – 144, 2013. 58

[165] Peng Wang, L. Goel, Xiong Liu, and Fook Hoong Choo. Harmonizing AC and DC: A hybrid AC/DC future grid solution. *Power and Energy Magazine, IEEE*, 11(3):76–83, May 2013. 45

[166] Xiongfei Wang, Josep M Guerrero, Frede Blaabjerg, and Zhe Chen. A review of power electronics based microgrids. *Journal of Power Electronics*, 12(1):181–192, 2012. 94

[167] George Weiss, Qing-Chang Zhong, Tim C Green, and Jun Liang. $H\infty$ repetitive control of DC-AC converters in microgrids. *IEEE Transactions on Power Electronics*, 19(1):219–230, 2004. 95

[168] P.E. Wellstead. *Introduction to Physical System Modelling*. Mathematics in Science and Engineering series. Academic Press, 1979. 15, 16, 24

[169] JanC. Willems. Dissipative dynamical systems part i: General theory. *Archive for Rational Mechanics and Analysis*, 45(5):321–351, 1972. 22

[170] R. Wu, S.B. Dewan, and G.R. Slemon. Analysis of an ac-to-dc voltage source converter using pwm with phase and amplitude control. *Industry Applications, IEEE Transactions on*, 27(2):355–364, Mar 1991. 51, 52

[171] Lie Xu, B.R. Andersen, and P. Cartwright. Control of vsc transmission systems under unbalanced network conditions. In *Transmission and Distribution Conference and Exposition, 2003 IEEE PES*, volume 2, pages 626–632 vol.2, Sept 2003. 51, 58, 61

[172] Li Yaping, Yang Shengchun, Wang Ke, and Zeng Dan. Research on pi controller tuning for vsc-hvdc system. In *Advanced Power System Automation and Protection (APAP), 2011 International Conference on*, volume 1, pages 261–264, Oct 2011. 61, 72, 115

[173] A. Yazdani and R. Iravani. *Voltage–Sourced Controlled Power Converters – Modeling, Control and Applications*. Wiley IEEE, 2010. 47, 48, 52, 57, 58, 60, 66

[174] Hai-Sheng Yu, Ke-You Zhao, Lei Guo, and Hai-Liang Wang. Maximum torque per ampere control of pmsm based on port-controlled hamiltonian theory. In *Zhongguo Dianji Gongcheng Xuebao(Proceedings of the Chinese Society of Electrical Engineering)*, volume 26, pages 82–87, 2006. 36

[175] Lidong Zhang, Lennart Harnefors, and H.-P. Nee. Interconnection of two very weak ac systems by vsc-hvdc links using power-synchronization control. *Power Systems, IEEE Transactions on*, 26(1):344–355, Feb 2011. 49

[176] Lidong Zhang and H.-P. Nee. Multivariable feedback design of vsc-hvdc connected to weak ac systems. In *PowerTech, 2009 IEEE Bucharest*, pages 1–8, June 2009. 61

[177] J. Zhao and F. Dörfler. Distributed control and optimization in DC microgrids. *Automatica*, 61:18 – 26, 2015. 46, 58, 81

[178] Q. Zhong and T. Hornik. *Control of power inverters in renewable energy and smart grid integration*. John Wiley & Sons, 2012. 94, 95, 104

[179] D. Zonetti. An hamiltonian approach to power systems modeling. *Université de Paris-Sud XI*, 2011. 107

[180] D Zonetti, S Fiaz, Roméo Ortega, Arjan Van Der Schaft, D Langarica, and Jacquelien MA Scherpen. Du bond graph au modèle hamiltonien à ports d'un système de puissance. In *CIFA 2012*, pages 1–6, 2012. 12, 35, 89

[181] D. Zonetti, R. Ortega, and A. Benchaib. A globally asymptotically stable dencentralized PI controller for multi–terminal high–voltage DC transmission systems. In *Proceedings of the 13th European Control Conference on*, Jun 2014. 12, 49

[182] D. Zonetti, R. Ortega, and A. Benchaib. Modeling and control of HVDC transmission systems from theory to practice and back. *Control Engineering Practice*, 45:133 – 146, 2015. 12, 36

Modélisation de systèmes électriques de puissance avec propriétés de stabilité – Pour traiter les systèmes non linéaires, à grande échelle, multi–domaine tels que les systèmes électriques de puissance, nous avons remarqué dans les dernières années un intérêt croissant pour les techniques de modélisation, analyse et contrôle basées sur la notion d'énergie. L'énergie est en fait un concept fondamental en science et en ingénierie, où typiquement les systèmes dynamiques sont regardés comme des dispositifs de transformation d'énergie. Cette perspective est particulièrement utile pour étudier des systèmes non linéaires assez complexes, qui peuvent être décomposés en sous-systèmes plus simples, caractérisés au niveau énergétique, et qui, à travers leurs interconnexions, déterminent le comportement global du système tout entier. Il représente bien évidemment le langage le plus naturel et intuitif pour représenter les systèmes électriques de puissance. En particulier, l'utilisation de systèmes Hamiltoniens à Ports a eu un impact très fort dans différentes applications, plus précisément dans le cas de systèmes mécaniques, électriques et électromécaniques. Dans ce contexte alors, l'approche Hamiltonien à Ports représentent sans doute une base solide qui montre une nouvelle façon d'aborder les problèmes d'analyse et contrôle de systèmes électriques de puissance. Basée sur cette approche, la thèse est structurée en trois étapes fondamentales:

i) Modélisation d'une classe très générale de systèmes électriques de puissance, basée sur la théorie des graphes et la formulation en Systèmes Hamiltoniens à Ports des composantes.

ii) Modélisation, analyse et commande de systèmes de transmission de courant continu haute tension. Avec l'intention de construire un pont entre la théorie et les éventuelles applications, un des objectifs fondamentaux consiste à établir des relations évidentes entre les solutions adoptées dans la pratique et les solutions obtenues à travers une analyse mathématique précise.

iii) Travaux apparentés de l'auteur, dans différents domaines des systèmes électriques de puissance: systèmes ac conventionnels et micro réseaux.

Mots clés: systèmes électriques de puissance, passivité, systèmes port–Hamiltoniens, théorie des graphes, architectures de contrôle, contrôle PI, analyse non linéaire, systèmes multi–terminal de transmission hvdc.

Energy-based modeling and control of electric power systems with guaranteed stability properties – To deal with nonlinear, large scale, multi domain, systems, as power systems are, we have witnessed in the last few years an increasing interest in energy-–based modeling, analysis and controller design techniques. Energy is one of the fundamental concepts in science and engineering practice, where it is common to view dynamical systems as energy-transformation devices. This perspective is particularly useful in studying complex nonlinear systems by decomposing them into simpler subsystems which, upon interconnection, add up their energies to determine the full systems behavior. This is obviously the most natural and intuitive language to represent power systems. In particular, the use of port—Hamiltonian (pH) systems has been already proven highly successful in many applications, namely for mechanical, electrical and electromechanical systems. The port-Hamiltonian systems paradigm therefore provides a solid foundation, which suggests new ways to look at power systems analysis and control problems. Based on this framework, this thesis is structured in three main steps:

i) Modeling of a generalized class of electric power systems, based on graph theory and port-Hamiltonian representation of the individual components.

ii) Modeling, analysis and control of multi terminal hvdc transmission systems. With the intention to bridge the gap between theory and applications, one of the main concerns is to establish connections between existing engineering solutions, usually derived via ad hoc considerations, and the solutions stemming from theoretical analysis.

iii) Additional contributions of the author in other fields of electric power systems, including traditional ac power systems an microgrids.

Keywords: electric power systems, passivity, port–Hamiltonian systems, graph theory, control architectures, PI control, nonlinear analysis, multi–terminal hvdc transmission systems.